Synthesis and Characterization of Nanoporous Copolymers with Potential Gas Storage Applications

Xu Zhou

Dissertation submitted to the faculty of the Virginia Polytechnic Institute and State University in partial fulfillment of the requirements for the degree of

Doctor of Philosophy
In
Chemistry

S. Richard Turner, Chair
Alan R. Esker
Richard D. Gandour
Harry W. Gibson

August 28, 2013
Blacksburg, VA

Keywords: nanoporous polymer, semirigid alternating copolymer, gas sorption, surface area, functionalized stilbene, functionalized maleimide, hypercrosslinked polymer, suspension polymerization, free radical polymerization, mesoporous silica, CO_2 capture.

Synthesis and Characterization of Nanoporous Copolymers with Potential Gas Storage Applications

Xu Zhou

Abstract

Nanoporous organic polymers, including hypercrosslinked polymers (HCPs), covalent organic frameworks (COFs), polymers of intrinsic microporosity (PIMs), and conjugated microporous polymers (CMPs) etc., are considered good candidates for potential gas storage and gas separation applications.

Porosities and surface areas of a series of semirigid alternating copolymers, which contained *tert*-butyl carboxylate-functionalized stilbene or *tert*-butyl carboxylate-functionalized styrene, and maleic anhydride or *tert*-butyl carboxylate-functionalized phenyl maleimide, were investigated using nitrogen sorption/desorption isotherms at 77 K and molecular simulations. These alternating copolymers were found to have Brunauer-Emmett-Teller (BET) surface areas in the range of 20-40 m^2/g. Surface areas of these alternating copolymers increased as the steric crowding of the polymer backbone increased, which was the result of introducing extra phenyl rings and/or *N*-phenyl substituent maleimide units. Surface areas were found to increase as the persistence length increased.

A series of HCPs containing functionalized stilbene and *N*-substituted phenyl maleimide were synthesized via free radical suspension polymerization. The incorporation of these functionalized, chain stiffening, T_g enhancing comonomers raised the T_gs of precursor polymers before they were crosslinked. Surface areas of these HCPs, obtained from nitrogen adsorption/desorption isotherms at 77 K, were up to 1058 m^2/g. However, the surface areas of

these HCPs were systematically lower than the controls. The high rigidity of the polymer backbone, which was the result of incorporating T_g enhancing comonomer, likely affected the chain mobility of the precursor polymer, decreased the efficiency of post-crosslinking reactions, and thus resulted in lower surface areas.

Amine-functionalized styrene/stilbene polymers were prepared via free radical polymerization or post-modification. Amine-containing silica-based sorbents were prepared using the impregnation method. Sorption of CO_2 by these materials was tested using TGA and compared with control samples. Both high amine content and certain levels of surface area were found to be important for a sorbent to achieve high CO_2 uptake. Highest CO_2 uptake (12 wt%) under our testing condition in these materials was achieved by an amine-containing silica sorbent.

Dedication

I dedicate this dissertation to my family and friends,

who have continuously supported me,

especially to my loving grandparents, Lie Feng and Weifen Zheng,

my faithful and supportive parents, Hongbiao Zhou and Zefen Feng,

my sister Xuru Zhou and brother Xucheng Zhou.

Acknowledgements

First, I would like to take this chance to thank my advisor, Dr. S. Richard Turner, for the opportunity to work in his group. Through the past few years, we are on a "journey" of exploring a research area, which was unfamiliar to us. This journey would not have been possible without his trust, guidance, encouragement, and patience. I would like to acknowledge my advisory committee members, past and present, Dr. Alan R. Esker, Dr. Richard D. Gandour, Dr. Harry W. Gibson, and Dr. John Y. Walz, for their valuable advice and help. I would also like to thank the graduate program advisor, Dr. Paul A. Deck, for his guidance and support.

I would like to acknowledge Department of Chemistry at Virginia Tech, ICTAS through a Transformative Science & Technology Project Grant, and the National Science Foundation (NSF) under Grant DMR-0905231 and DMR-1206409 for financial supporting my graduate research.

I would like to express my gratitude to our collaborators, Dr. Frantisek Svec at Molecular Foundry, Lawrence Berkeley National Laboratory and Dr. Coray M. Colina, her students Mr. Kyle E. Hart, and Ms. Lauren J. Abbott at Penn State University for their measurements/simulations, efficient communications, and in-depth discussions. I would also like to thank Dr. Roe-Hoan Yoon and his students Jing Niu and Riddhika Jain of the Department of Mining and Minerals Engineering at Virginia Tech, Dr. Richard D. Gandour and Dr. Diego Troya of the Department of Chemistry for their efforts on the CO_2 capture project.

I would like to thank past and current members of Turner research group, Dr. Keiichi Osano, Dr. Yanchun Liu, Dr. Bin Zhang, Dr. Daiqiang Xu, Dr. Sneha S. Kelkar, Ms. Alice Savage, Mr. Zhengmian Chang, Ms. Jing Huang, Mr. Kevin W. Barr, and Ms. Jenny B. England for their

help, discussion, and friendship. Especially, I am grateful to Dr. LaShonda T. Cureton and Dr. Yi Li for their accompany, support, and precious friendship. I enjoyed our group lunches/dinners and group activities.

I am grateful to all assistance I have received from the research groups, staff members at Virginia Tech. I would like to thank Dr. Robert B. Moore for sharing instruments, Mr. Ninad Y. Dixit for his help with TGA, and Ms. Amanda G. Hudson for her help with FTIR. I would like to acknowledge Dr. Michael W. Ellis and Dr. Junbo Hou at Department of Mechanical Engineering for instrumentation, assistance, and helpful discussion. I would like to thank Mr. Steve McCartney of ICTAS Nanoscale Characterization and Fabrication Laboratory for his assistance on SEM. I am grateful to Ms. Teresa S. Dickerson, Ms. Tammy Jo Hiner, Mr. Thomas E. Bell, Ms. Joli Huynh for their assistance and sometime fixing the mistakes I made. I would like to thank Ms. Mary Jane Smith for her encouragement.

Finally, to my family and friends, thank you for your endless love and support, which make my life wonderful. Special thanks to my friend, Jing Li, who was extremely patient to proof read all the “boring” scientific sentences in this dissertation.

Attribution

Chapter 2 of this dissertation was co-authored with Dr. Yi Li, Mr. Kyle E. Hart, Ms. Lauren J. Abbott, Dr. Zhixing Lin, Dr. Frantisek Svec, Dr. Coray M. Colina, and Dr. S. Richard Turner. Dr. Colina is an associate professor of the Department of Materials Science and Engineering, The Penn State University. Mr. Hart and Ms. Abbott are graduate students in Dr. Colina's research group. Dr. Colina, Mr. Hart, and Ms. Abbott provided molecular simulations of the polymers, data analysis, and part of discussion for the publication. Dr. Svec is the facility director at The Molecular Foundry, Lawrence Berkeley National Laboratory and Dr. Lin is a researcher at Lawrence Berkeley National Laboratory. They provided BET surface area measurements and helpful discussion of gas sorption measurements. Dr. Turner is a research professor at Department of Chemistry, Virginia Tech. Dr. Li was a member in Dr. Turner's research group. Dr. Li provided samples of alternating copolymers. Dr. Turner served as the research advisor.

Ms. Jing Huang, Mr. Kevin W. Barr, Dr. Zhixing Lin, Dr. Frantisek Svec, and Dr. S. Richard Turner co-authored **Chapter 3**. Dr. Svec and Dr. Lin provided BET surface area measurements and discussion for this project. Ms. Huang and Mr. Barr are members in Dr. Turner's research group. Both of them provided part of the synthesis and thermal analysis of HCPs. Dr. Turner provided oversight for this project.

In **Chapter 4**, Dr. Richard D. Gandour is the principal investigator (PI), and Dr. S. Richard Turner, Dr. Diego Troya and Dr. Roe-Hoan Yoon are the co-PI of the project. They all provided guidance and valuable suggestions for this project. Both Dr. Gandour and Dr. Troya are faculty members in Department of Chemistry at Virginia Tech. Dr. Yoon is a professor at Department of

Mining and Minerals Engineering, Virginia Tech. Ms. Jing Niu was a graduate student in Dr. Yoon's research group. She provided most of CO_2 sorption measurements for this project. Dr. Robert B. Moore, a professor at Department of Chemistry, Virginia Tech, provided the assess to TGA instrument for CO_2 sorption test. Mr. Ninad Y. Dixit, a graduate student in Dr. Moore's group, provided help with setting up TGA and some measurements on CO_2 sorption properties.

Table of Contents

List of Figures

List of Tables

List of Schemes

Chapter 1. Review on Nanoporous Organic Polymers

1.1. Introduction

Nanoporous organic polymers contain pores which are smaller than 100 nm.[1,2] They have been intensively investigated in the past few decades for numerous applications, including chromatographic separations,[3-7] catalysis,[8,9] biomedical applications,[10-13] and potential gas storage applications.[14-16] There are several subclasses of nanoporous organic polymers including hypercrosslinked polymers (HCPs) pioneered by Davankov,[17-19] covalent organic frameworks (COFs) pioneered by Yaghi,[20-22] polymers of intrinsic microporosity (PIMs) introduced by McKeown and Budd,[23-26] conjugated microporous polymers (CMPs) introduced by Cooper,[27,28] porous aromatic frameworks (PAFs) introduced by Qiu,[29,30] porous polymer networks (PPNs) reported by Zhou,[31,32] etc.

This chapter discusses the synthetic approaches and general structure-porous property relationships of nanoporous organic polymers. It also presents the characterization of porous polymers including gas sorption properties, porosity analysis, and molecular simulations. Finally, potential applications of nanoporous polymers for gas storage and separation are discussed.

1.2. Synthesis

1.2.1. Polymers of Intrinsic Microporosity (PIMs)

Intrinsic microporosity in polymers is defined as "a continuous network of interconnected intermolecular microcavities."[33] PIMs are a class of amorphous microporous organic materials which contain highly rigid and contorted molecular structures that pack space inefficiently in the solid state (**Figure 1-1**).[24,26] Because of barriers to structural relaxation, the "awkward" molecular structures from PIMs cannot rearrange their conformations, resulting in microporosity.

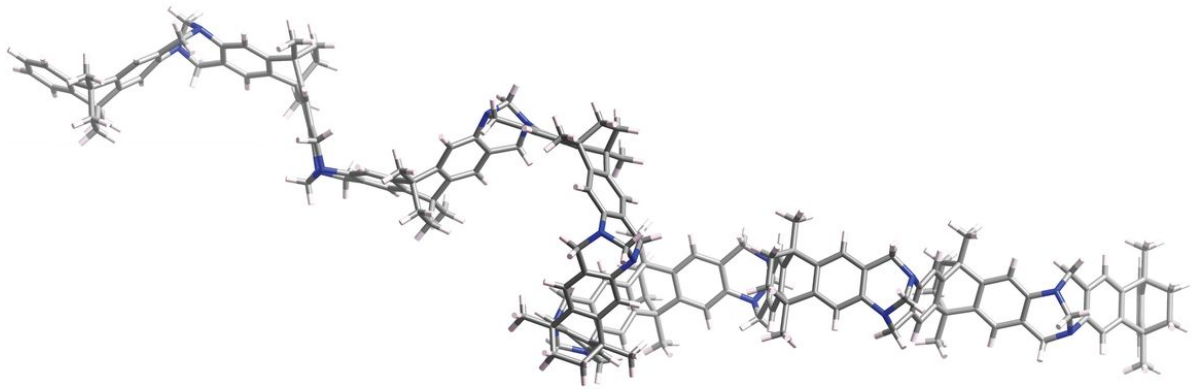

Figure 1-1. A molecular model of PIM-EA-TB showing its rigid and contorted structure. (From [34]. Reprinted with permission from AAAS.)

McKeown and Budd first developed PIMs.[35] Initial work involved the incorporation of aromatic macrocycles – phthalocyanines to form rigid polymer networks in order to mimic the graphene sheets of activated carbons for catalytic applications.[36] However, due to the noncovalent interactions between macrocycles, the first generation of phthalocyanine containing networks exhibited insignificant porosity. In their later work on phthalocyanine-based polymers, the incorporation of rigid and nonlinear units (A1 in **Figure 1-2**) between phthalocyanines resulted in polymer networks with large microporosity and high Brunauer-Emmett-Teller (BET) surface areas (500 – 1000 m^2/g) (**Table 1-1**) (see **§1.3.5** for the definition of BET surface area).[37,38] The rigid and nonlinear units are crucial for achieving large microporosity, because they interrupt the noncovalent interactions between macrocycles, inhibit the rotation along the polymer chain, and consequently frustrate efficient space packing.[23] Since these early studies, a large variety of microporous network polymers have been synthesized and studied. **Table 1-1** shows some examples of network PIMs.

PIMs can be prepared by different bond-forming reactions including ether bond formation between aromatic rings (dibenzodioxin), imide formation, amide formation, etc. (**Figure 1-2**). Most PIMs are synthesized using catechol containing monomers (e.g., A1-5 in **Table 1-1**) and

halide based monomers (e.g., B1-4 in **Table 1-1**) via aromatic nucleophilic substitutions (**Figure 1-2**, a).[35] In such reaction, two monomers and K_2CO_3 are mixed in DMF and heated at 50-60 ºC over 24 hours.[35,39] The concentration of monomers is important, because high concentration yields crosslinked products while low concentration leads to the formation of cyclic oligomers (**Figure 1-4**).[40-42] Optimum monomer concentration was found to be 0.2-0.3 M for a successful synthesis of linear PIMs.[26]

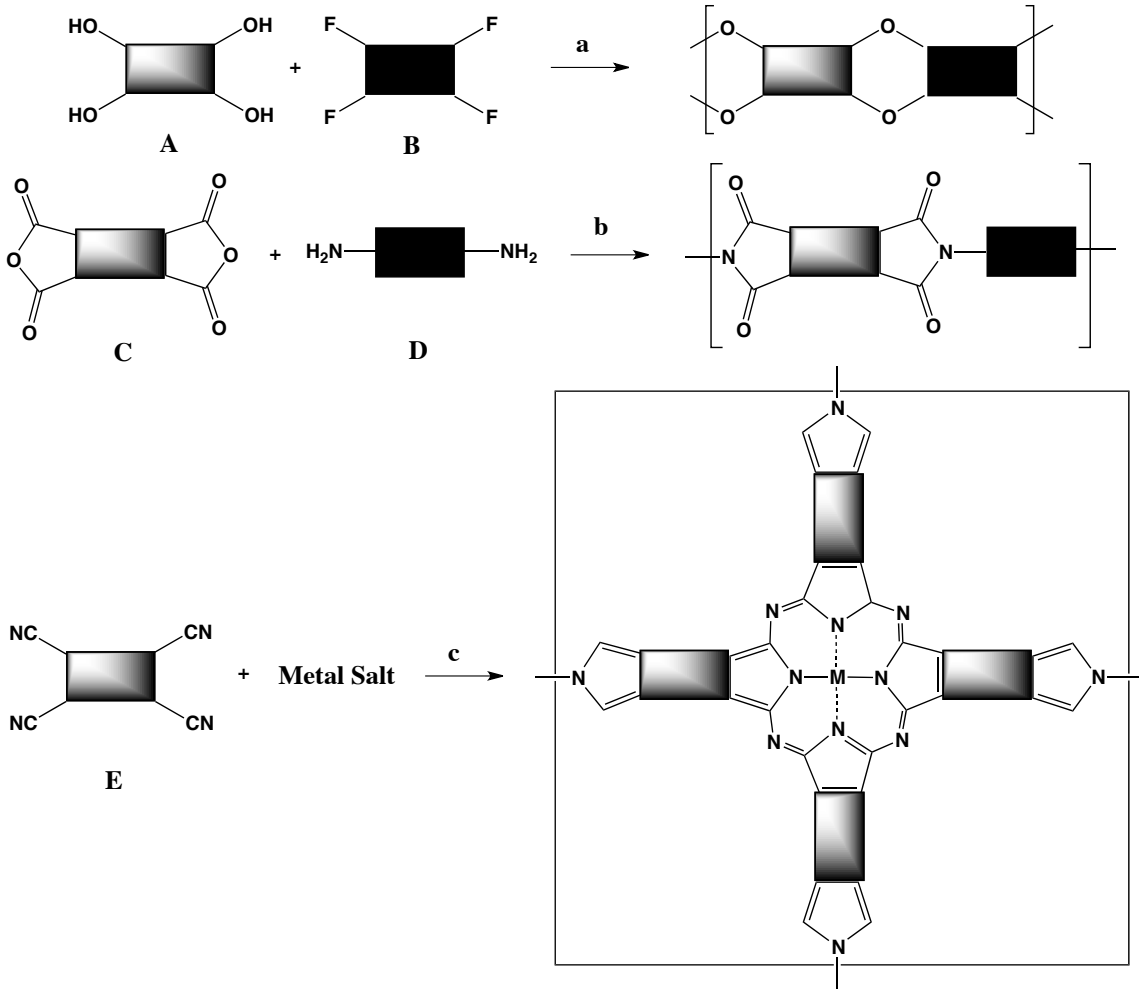

Figure 1-2. Reactions to form rigid linkages between rigid monomers (see A, B, C D, and E in **Figure 1-3**) to prepare PIMs (see **Table 1-1**): (a) base-mediated aromatic nucleophilic substitution; (b) imide formation; (c) metal ion-mediated phthalocyanine formation.[25]

Table 1-1. PIMs derived from rigid monomers.

Monomers[a]	Synthesis[b]	Type of PIMs	Name	BET Surface area (m^2/g)	Ref.
A1 + B1	a	Network	Por-PIM	980	43
A1 + B2	a	Network	HATN-PIM	775	44
A2 + B3	a	Network	CTC-PIM	830	45
A3 + B3	a	Network	Trip-PIM	1760	46,47
E1	c	Network	Pc-PIM	650-750	38,48
A1 + B3	a	Non-network	PIM-1	760-850	35,39
A4 + B4	a	Non-network	Cardo-PIM-1	621	49
A5 + B3	a	Non-network	PIM-CO-100	630	50
C1 + D1	b	Non-network	PIM-PI-1	680	51,52
C2 + D2	b	Non-network	P4	551	53
C2 + D3	b	Non-network	PIM-6FDA-OH	225	54

[a]See **Figure 1-3**. [b]See **Figure 1-2**.

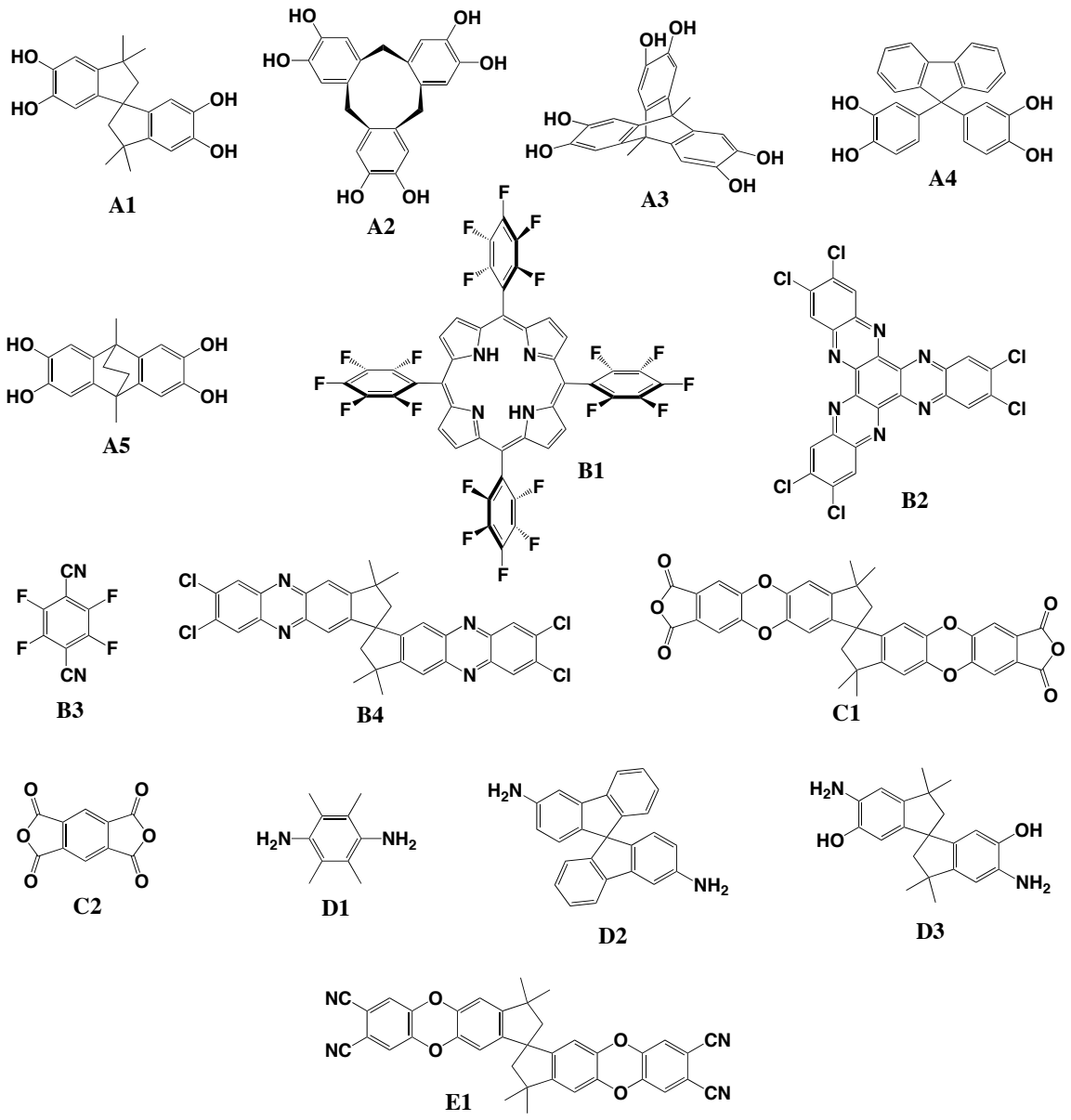

Figure 1-3. Rigid monomers for the synthesis of PIMs.

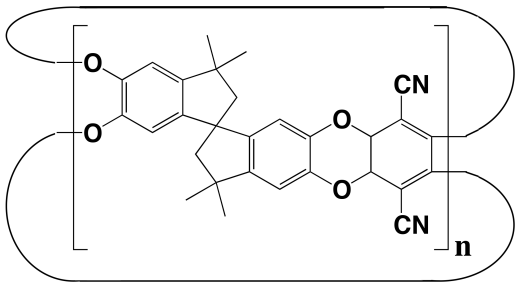

Figure 1-4. An example of cyclic oligomer synthesized at low monomer concentration.[42]

The study of the efficiency of double aromatic nucleophilic substitution reactions of network PIMs led to the discovery of non-network PIMs. A soluble polymer, known as PIM-1 (**Figure 1-5**), was synthesized from spirocyclic biscatechol (A1 in **Table 1-1**) and 2,3,5,6-tetrafluoroterephthalonitrile (B4 in **Table 1-1**), and was found to have high microporosity with BET surface area up to 850 m^2/g.[35,39] Since then, non-network PIMs have been intensively studied (summarized in **Table 1-1**).

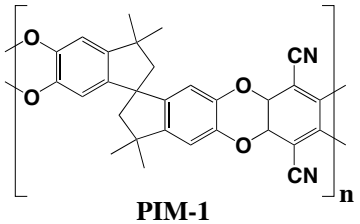

PIM-1

Figure 1-5. Chemical structure of PIM-1.[35,39]

Due to the solution processability, non-network PIMs can be cast into films and membranes for a number of applications such as gas separation.[55-57] **Figure 1-6** shows an example of a solution-cast film of PIM-EA-TB. Mechanical property measurements on film sample of PIM-1 give a tensile strength of 47-48 MPa and a strain of 10-11% at break.[40,58]

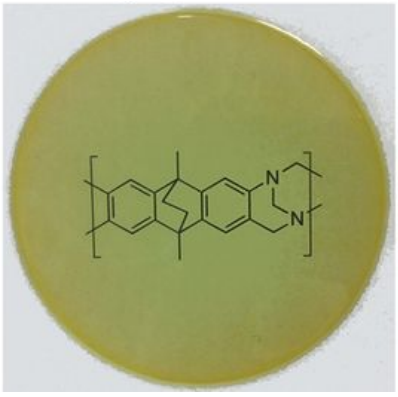

Figure 1-6. A solution-cast film of PIM-EA-TB. (From [34]. Reprinted with permission from AAAS.)

PIMs exhibit microporosity and their surface areas can be calculated from nitrogen adsorption isotherms at 77 K using the BET equation (see §**1.3.5**).[59] In nitrogen adsorption/desorption measurements, PIMs typically show type I isotherms (see §**1.3.2**) and a characteristic of high gas uptake at low relative pressure ($P/P_o < 0.01$, see §**1.3.5** for definition of P/P_o).[23] Also, some isotherms of PIMs have a continuous increase in gas uptake as pressure increases at moderate relative pressure, and low pressure hysteresis, which is the lack of convergence of desorption branch and adsorption branch at $P/P_o < 0.4$. These two features are believed to be associated with the "swelling" effect of the non-rigid polymers.[26,60] An example of isotherm (N_2, 77 K) for PIM-1 with BET surface area of 850 m^2/g is shown in **Figure 1-7**.[35] PIMs have been found to have high BET surface areas in the range of 300 - 1760 m^2/g (**Table 1-1**).[24,25,46,47,61] A triptycene-based network PIM, Trip-PIM, which was synthesized from monomers A3 and B4 (**Figure 1-3**), has the highest surface area of PIMs (1760 m^2/g).[46,47]

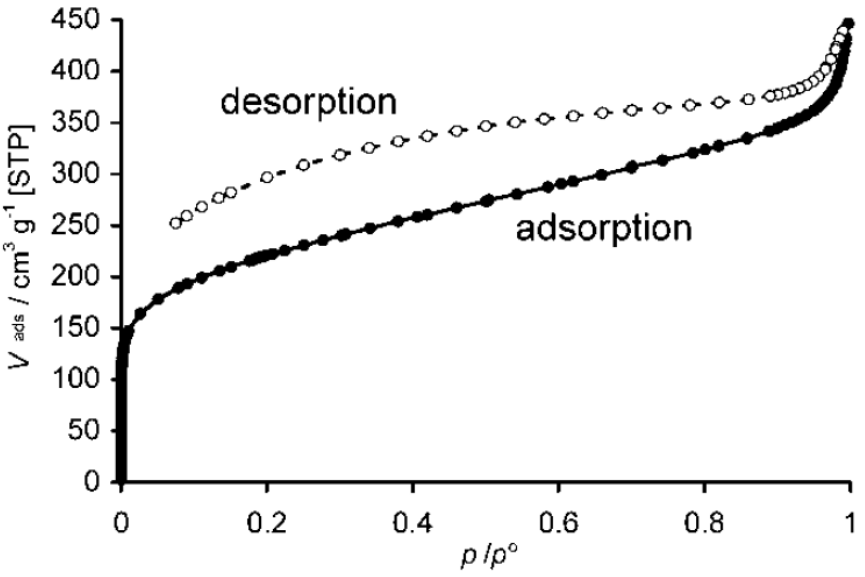

Figure 1-7. Nitrogen adsorption/desorption isotherm for PIM-1 (Reproduced with permission from [35] Copyright © 2004 WILEY-VCH Verlag GmbH & Co. KGaA, Weinheim.)

1.2.2. Hypercrosslinked Polymers (HCPs)

Hypercrosslinked polymers (HCPs) were first introduced by Davankov and Tsyurupa in the 1970s.[62] The hypercrosslinked polystyrene networks, also known as "Davankov resins," with high permeability and low swelling or deswelling abilities, were initially designed for column packing materials.[63,64] Hypercrosslinked polystyrene networks have been found to have large microporosity, high surface areas (in excess of 2000 m^2/g by the BET method),[65] and unique swelling properties,[18] thus have been intensively studied over the past few decades.[18,66-72]

The unique properties of HCPs are derived from highly crosslinked structures. In general, linear polymers or lightly crosslinked polymer precursors are firstly dissolved or highly swollen in a thermodynamically good solvent to form free volume between polymer chains. In the following post-crosslinking step, a large number of rigid bridges are formed rapidly via efficient Friedel-Crafts reactions and "lock" the networks, preventing them from collapsing upon the removal of the solvent. This process results in large microporosity in the dry state (**Figure 1-8**).[18]

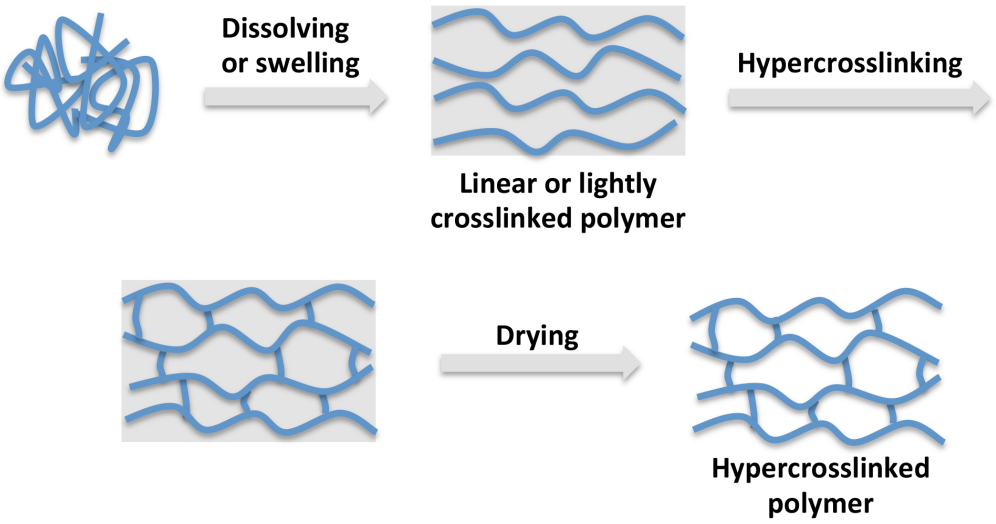

Figure 1-8. Scheme illustrating the general approach to prepare HCPs.[73]

The initial synthesis approach proposed by Davankov and coworkers involved the introduction of external electrophiles (crosslinkers) for post crosslinking. Aromatic compounds containing chloromethyl groups, such as: 1,4-bis-(chloromethyl)-diphenyl (CMDP),[74] *p*-xylylene dichloride (XDC),[75,76] 1,4-bis-(*p*-chloromethylphenyl)-butane (DPB),[77] 1,3,5-tris-(chloromethyl)-mesitylene (CMM),[77] and monochlorodimethyl ether (MCDE),[62,78] were found to be good candidates (**Figure 1-9**).

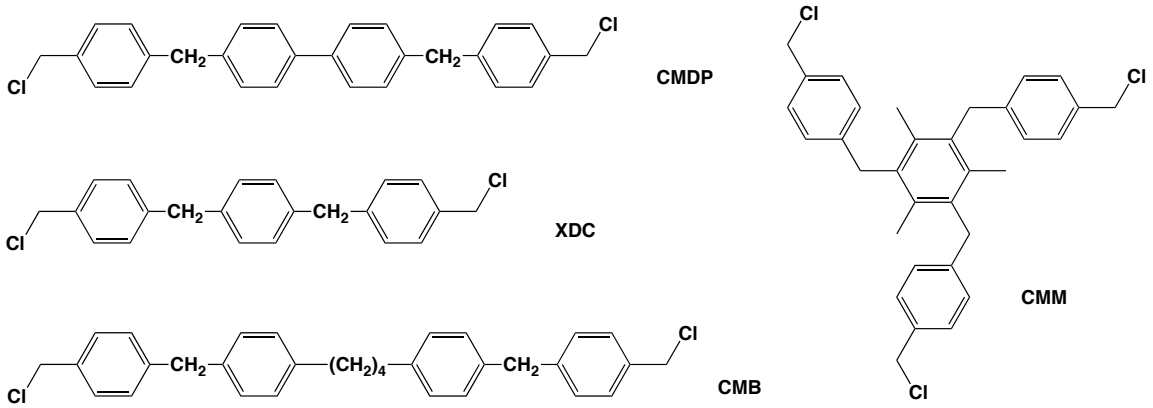

Figure 1-9. Crosslinkers used in preparation of HCPs.[63]

Veverka and Jerabek proposed a synthetic approach for HCPs without introducing external crosslinkers.[79,80] They used chloromethylated gel-type styrene-divinylbenzene resins and post-crosslinked them via Friedel-Crafts reactions. The resulting hypercrosslinked networks showed lower surface areas (up to 1000 m^2/g) compared to HCPs prepared by the traditional method. It is believed that during post-crosslinking, the conversion of chloromethyl group into methylene bridges decreases as the rigidity of the networks increases, resulting in unavailability of the neighboring phenyl rings to the chloromethyl groups. This reduction in mobility is well known in vitrifying networks to slow the hypercrosslinking reactions.[81,82]

In 2006, Sherrington and coworkers successfully synthesized Davankov-type HCPs without any external crosslinkers using a modified preparation method.[65] Firstly divinylbenzene-*co*-

vinylbenzyl chloride (DVB-VBC) gel–type resins (precursors) were synthesized using free radical suspension polymerization. The resins were then swollen in 1,2-dichloroethane (DCE) and post-crosslinked via Friedel-Crafts reactions, resulting in HCPs with surface areas up to 2000 m^2/g. VBC serves as an internal electrophile that allows the polymer precursors to crosslink without the introduction of external crosslinkers (**Scheme 1-1**). In this study, they varied the percentage of VBC by adding various amounts of styrene and found that the surface area of HCPs increases as VBC increases. They compared two series of HCPs with 2% or 20% DVB and found that at similar level of VBC mol%, HCPs containing 20% DVB showed lower surface area than HCPs with 2% DVB. The higher degree of crosslinking in the initial precursor likely inhibited the uniform swelling of precursor (evidenced by small swelling ratio) and decreased the accessibility of chloromethyl groups for post-crosslinking. The work also compared the activities of different Lewis acids ($FeCl_3$, $AlCl_3$, and $SnCl_4$). $FeCl_3$ was found to be the most active catalyst.

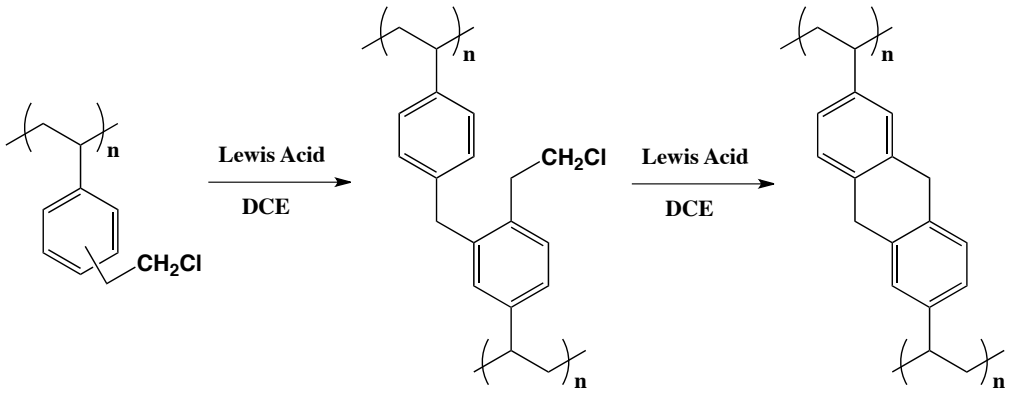

Scheme 1-1. Hypercrosslinking reaction of DVB-VBC precursors without external electrophile.[65]

Friedel-Crafts catalyzed polycondensation of bis(chloromethyl) monomers was utilized to prepare HCPs by Cooper and coworkers in 2007. The resulting HCPs exhibit BET surface areas up to 1904 m^2/g.[70] Monomers used to prepare HCPs were dichloroxylene (DCX) (including *o*-,

m-, *p*-isomers), 4,4'-bis(chloromethyl)-1,1'-biphenyl (BCMBP) and bis(chloromethyl)anthracene (BCMA) (**Figure 1-10**). In this study, they synthesized HCPs with various ratios of monomers and studied their porous properties and gas storage capabilities. HCPs containing *m*-DCX or *p*-DCX exhibit higher surface areas than *o*-DCX containing HCPs. HCPs prepared from BCMBP have the highest surface area among all HCPs in this work.

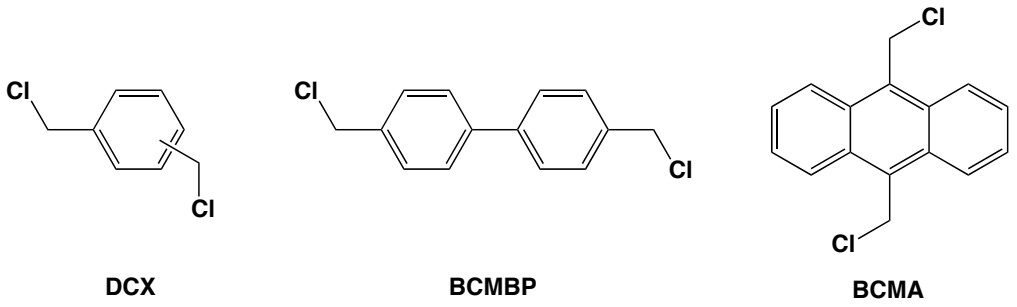

Figure 1-10. Bis(chloromethyl) monomers used to prepare HCPs via polycondensation.[70]

In general, HCPs can be prepared from reactions that allow intensive crosslinking to form rigid bridges and yield microporosity. Beside hypercrosslinked polystyrene, numbers of other types of HCPs have been synthesized.

Hypercrosslinked polysulfones were prepared by crosslinking of bromomethylated polysulfones via Friedel-Crafts reactions (**Scheme 1-2**).[18] However, due to the flexibility of the polymer chains and less efficient crosslinking, these hypercrosslinked polysulfones exhibited low surface areas (less than 100 m^2/g).

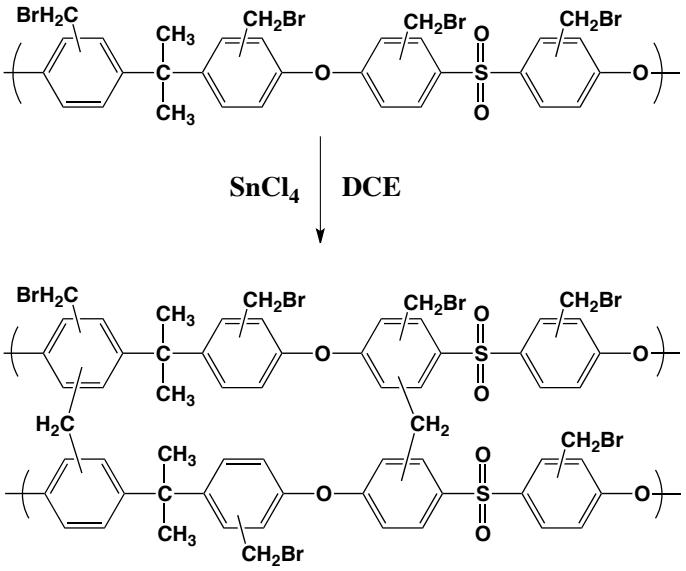

Scheme 1-2. Synthesis of hypercrosslinked polysulfones.[18]

Svec and coworkers prepared hypercrosslinked polyanilines by introducing bifunctional crosslinking agents into diluted linear polyaniline solution (**Scheme 1-3**).[73] The resulting hypercrosslinked polyanilines have BET surface area over 600 m^2/g. In this study, they varied the lengths of crosslinkers and found that polyanilines prepared from longer and more flexible crosslinkers have lower surface areas. These long crosslinkers were proposed to be insufficiently rigid to maintain the pore structure when solvent was removed from the network. Therefore, the rigidity of the crosslinkers is important for achieving high surface areas in polymers. Similar to the preparation of hypercrosslinked polyanilines, hypercrosslinked polypyrrols were synthesized with short crosslinkers and exhibited high surface areas (up to 700 m^2/g) (**Scheme 1-4**).[83]

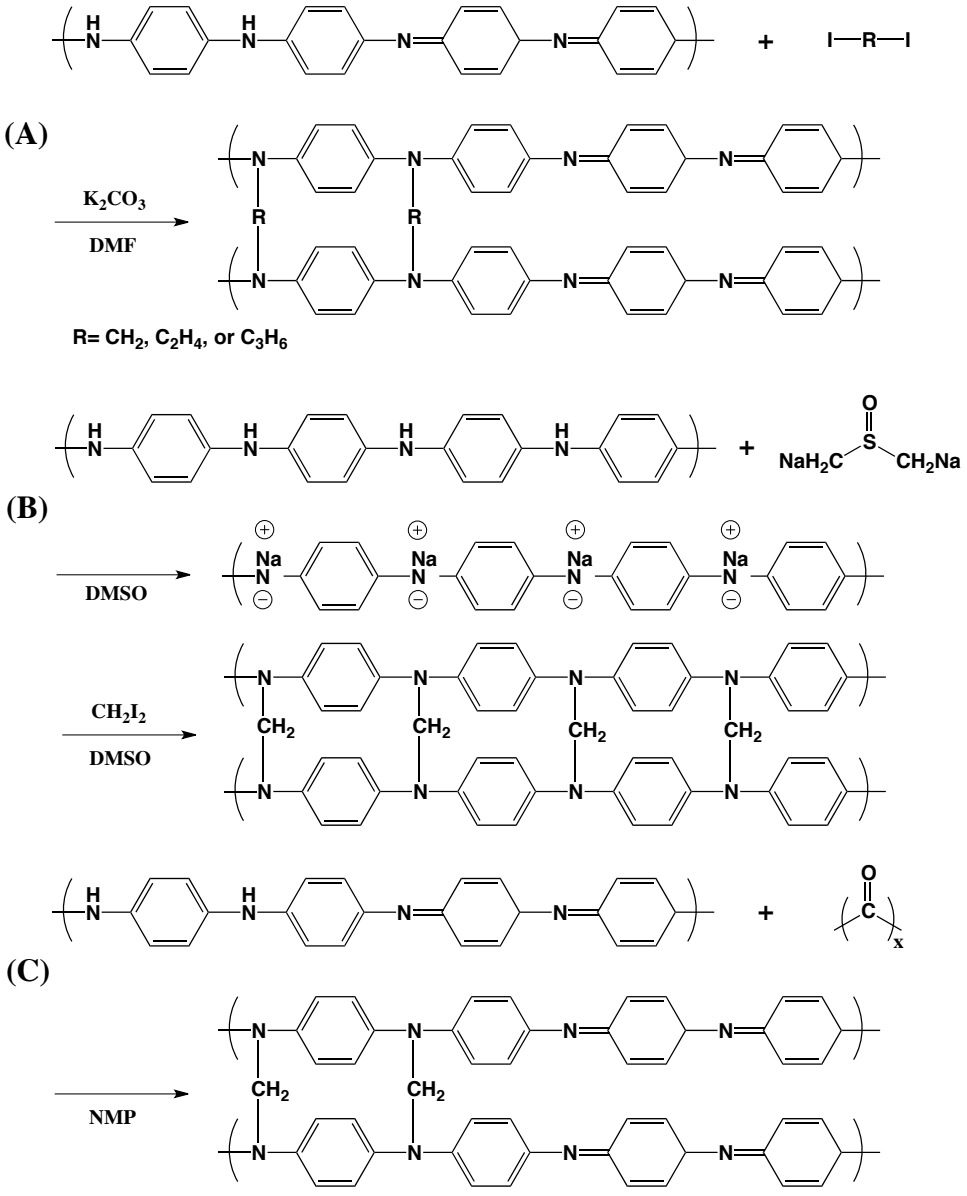

Scheme 1-3. Synthesis of hypercrosslinked polyanilines.[73]

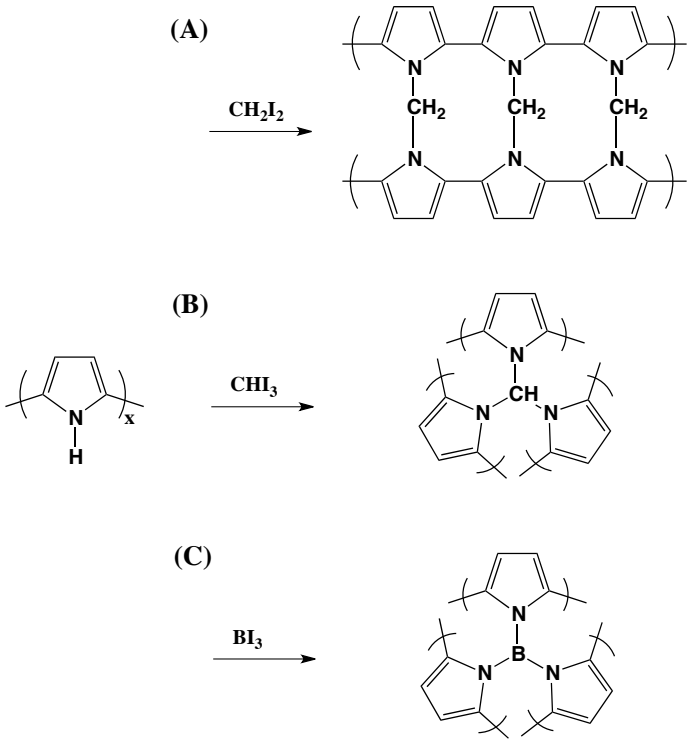

Scheme 1-4. Synthesis of hypercrosslinked polypyrrols.[83]

In 2011, Tan and coworkers reported a versatile, one-step synthetic strategy to prepare HCPs.[19,84] The approach involves "knitting" aromatic monomers with formaldehyde dimethyl acetal (FDA) as an external crosslinker via Friedel-Crafts reaction (**Scheme 1-5**). The resulting HCPs from this "knitting" method exhibited BET surface area up to 1391 m^2/g. Later, Tan's group successfully synthesized heterocyclic HCPs with BET surface area up to 726 m^2/g using FDA and heterocyclic monomers via the "knitting" approach (**Scheme 1-6**).[72] In 2012, Adams and coworkers extended the "knitting" approach to the synthesis of alcohol-containing HCPs and aniline containing HCPs for gas capture and separation applications.[85,86] In 2013, instead of using FDA as an external crosslinker, Tan's group prepared HCPs via self-condensation of hydroxymethyl monomers (**Scheme 1-7**).[87] In this study, they synthesized HCPs using bifunctional monomers or monofunctional monomers via "knitting" strategy. The success of

synthesizing HCPs using solely monofunctional monomers allows many synthetic possibilities for preparing porous materials based upon monofunctional monomers.

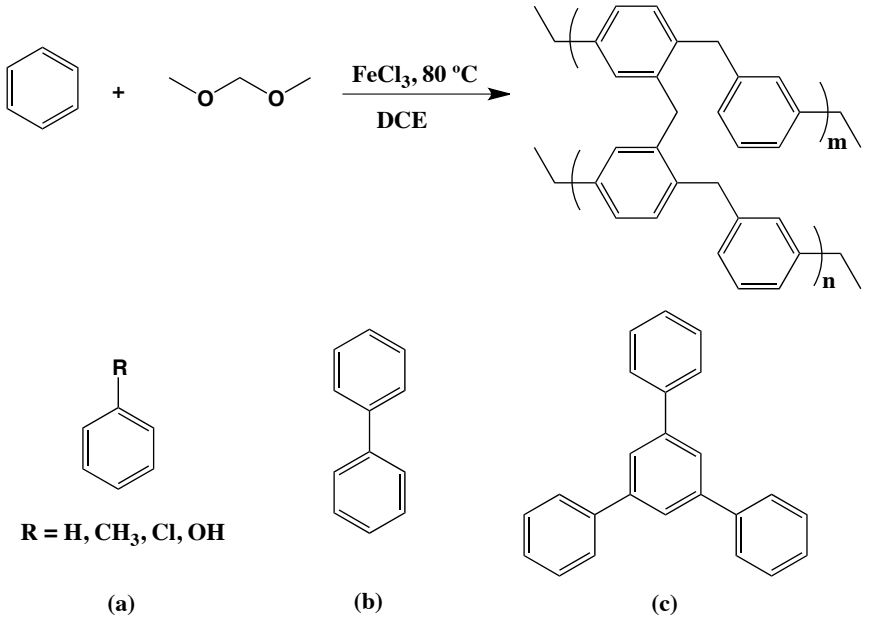

Scheme 1-5. Synthesis of HCPs via "knitting" approach; a-c are molecular structures of building blocks.[84]

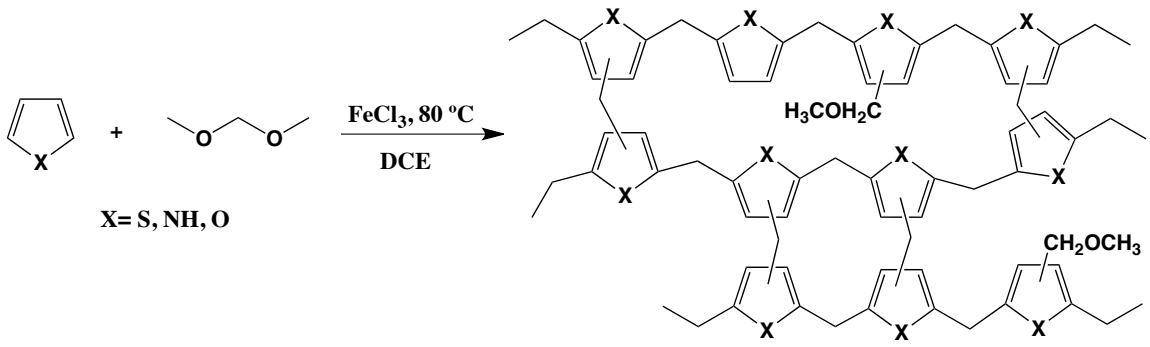

Scheme 1-6. Synthesis of aromatic heterocyclic HCPs.[72]

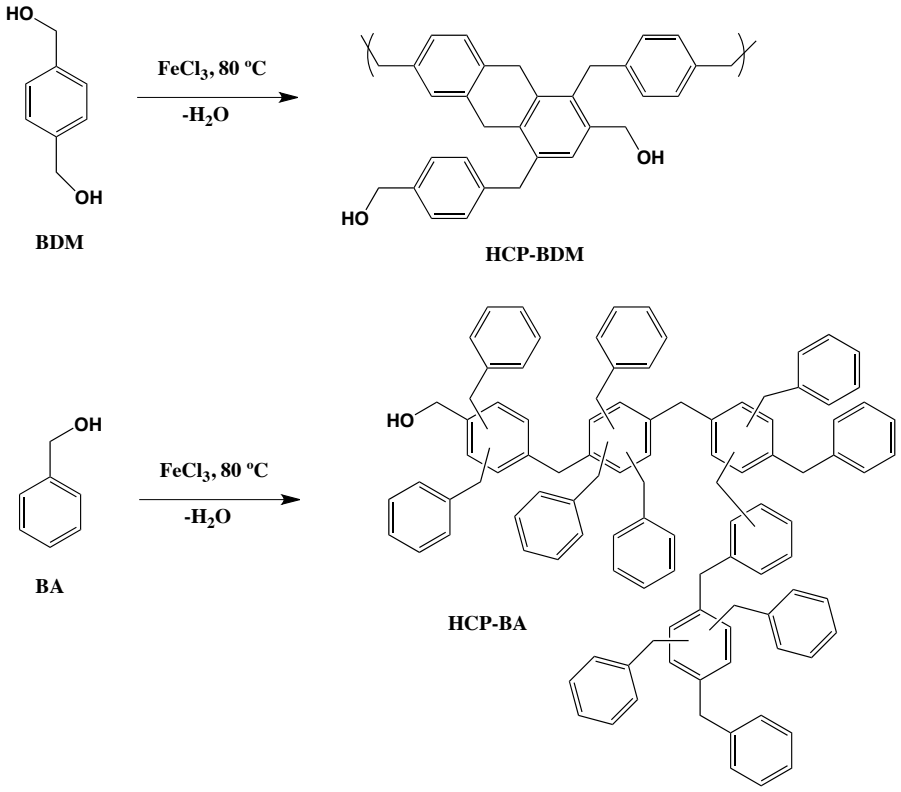

Scheme 1-7. Synthesis of HCPs by Friedel-Crafts catalyzed self-condensation.[87]

1.2.3. Covalent Organic Frameworks (COFs)

Covalent organic frameworks (COFs) are a class of covalently linked, porous, and crystalline polymers. COFs possess low mass densities, good thermal stabilities, and large microporosity.[22] In 2005, Yaghi and coworkers pioneered the work of COFs and successfully synthesized COFs using condensation reactions to link covalent bonds and form rigid porous architectures (**Scheme 1-8** and **Figure 1-11**).[88] The first COFs, COF-1 and COF-5, exhibit surface areas of 700 and 1600 m^2/g, respectively. In 2006, Lavigne and coworkers reported the synthesis of COF-18Å using condensation reactions with high yields (up to 95%).[89]

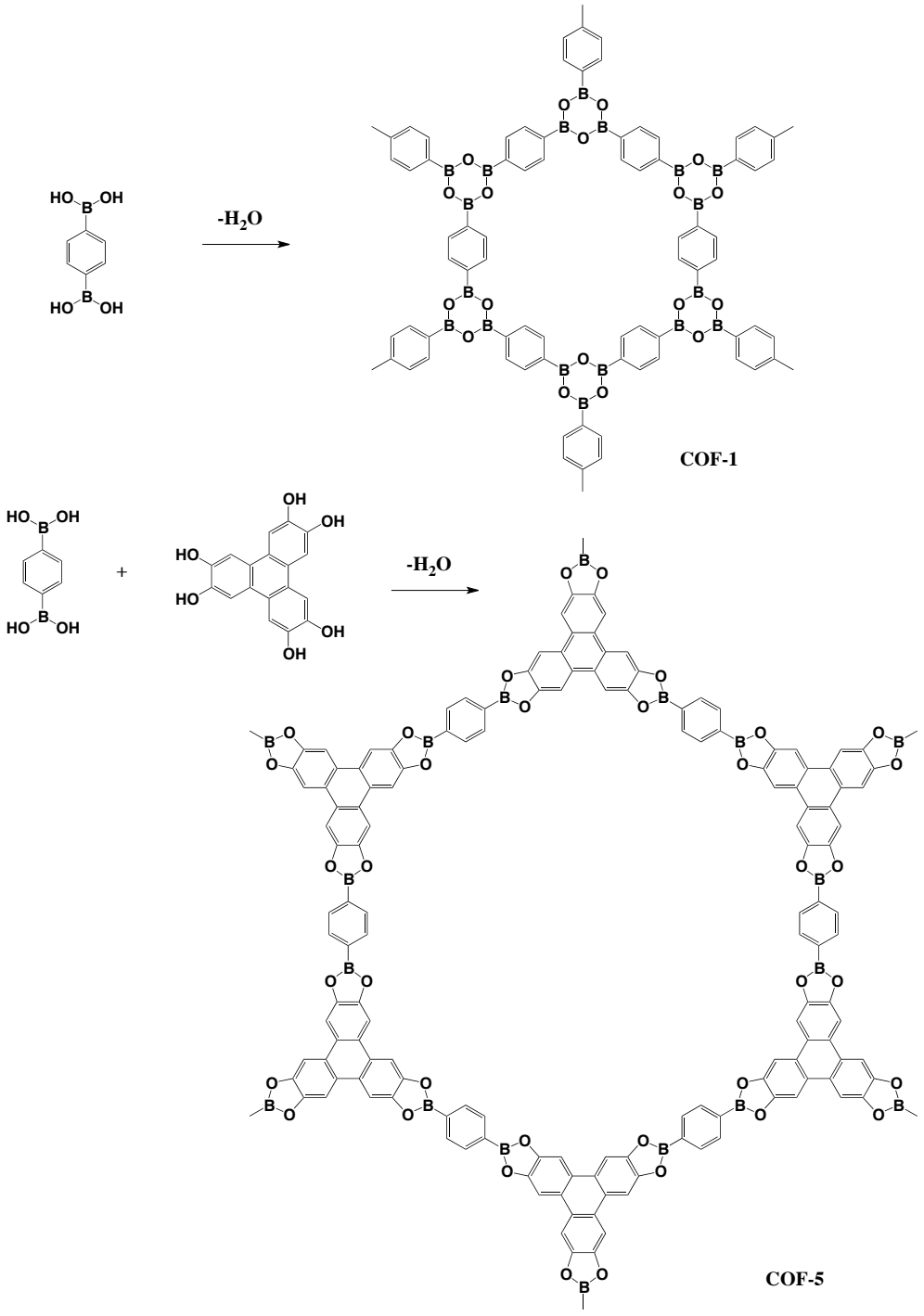

Scheme 1-8. Synthesis of COF-1 and COF-5.[88]

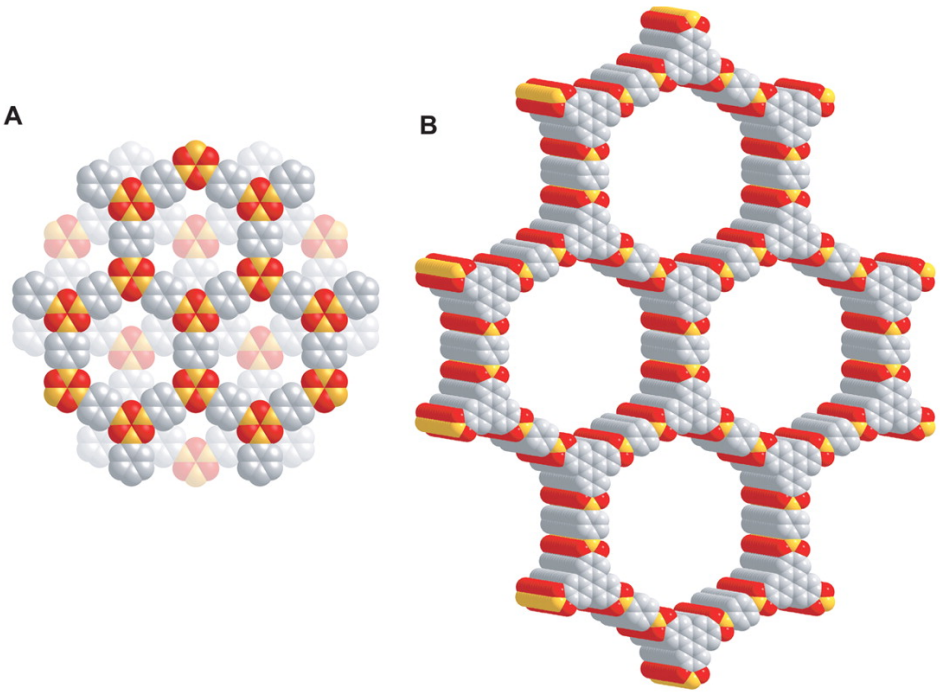

Figure 1-11. Structural representations of (A) COF-1 and (B) COF-5, illustrating the stacking of 2D porous sheets. Carbon, boron, and oxygen are represented as gray, orange, and red spheres, respectively. (H atoms are omitted) (From [88]. Adapted with permission from AAAS.)

In 2007, Yaghi and coworkers reported the synthesis of three-dimensional (3D) COFs with surface area up to 4200 m^2g, using condensation reactions of rigid building blocks.[90] Differing from 2D COFs which have layered structures as a result of the stacking of 2D porous sheets (**Figure 1-11**), 3D COFs have covalently linked structures with extended three-dimensionality.[22]

For successful synthesis of highly ordered crystalline COFs, one of the key requirements is to use reversible reactions.[20] Reversible reactions allow the formation of thermodynamically favored structures and self-correction of any structural defects.[91] **Figure 1-12** summarizes reversible reactions used for COFs preparation.

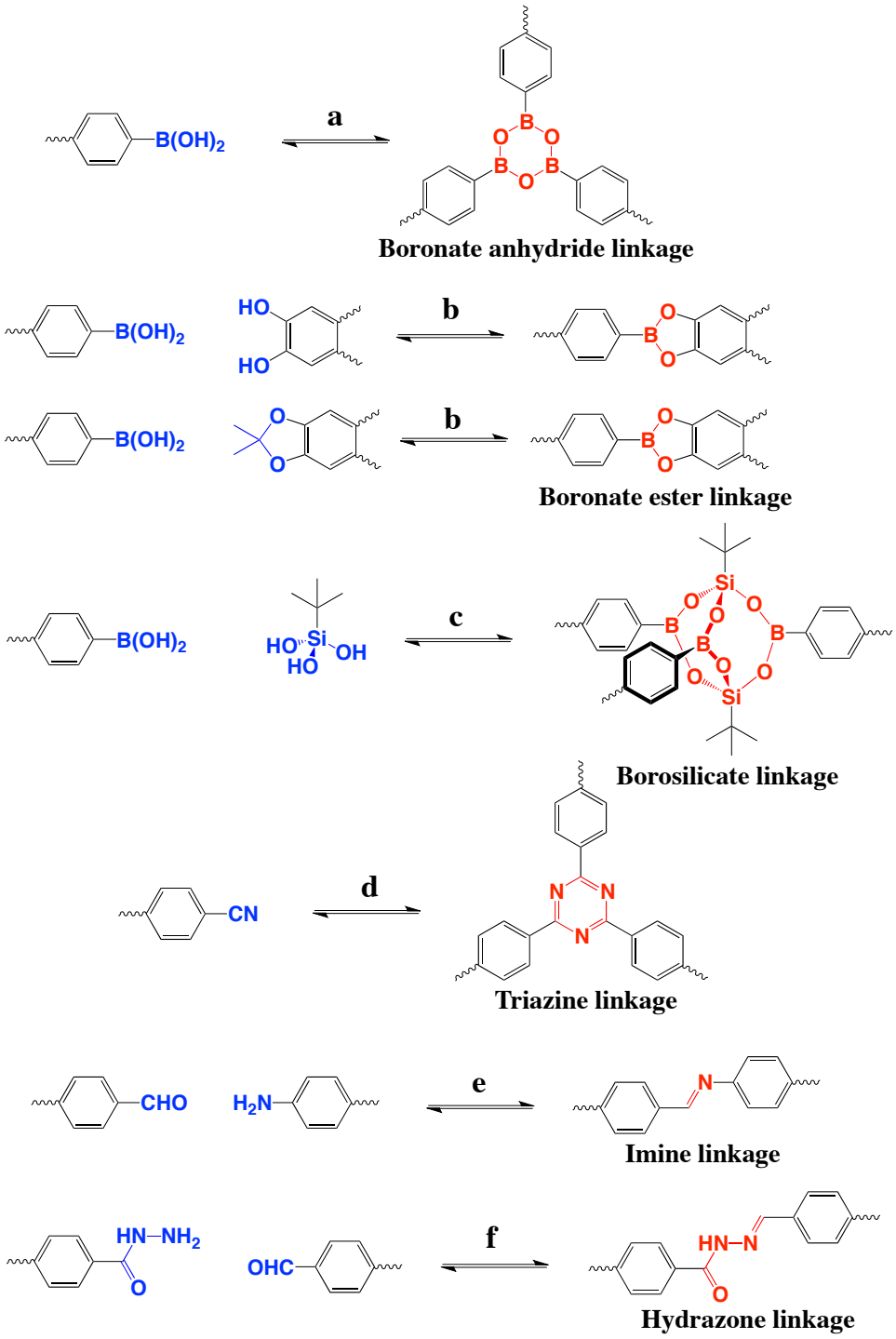

Figure 1-12. Reversible reactions (a-f) for the preparation of COFs, showing functional groups (in blue) from monomers (see **Figure 1-21**), and the covalent linkages (in red) formed after reactions.[20,22]

The multifunctional monomers (building blocks) used to prepare COFs are important factors. They are required to contain functional groups that form covalent linkages by reversible reactions. They also need to be rigid and with discrete bond formation directions.[22] The architecture of COFs can be tuned by varying combinations of the building blocks. Topology of the porous structure and pore size are greatly affected by the building blocks.[20] Examples of building blocks are shown in **Figure 1-13**.

Table 1-2. COFs derived from rigid building blocks.

Building Blocks[a]	Synthesis[b]	Type	Name	BET Surface Area (m^2/g)	Ref.
1	a	2D	COF-1	711	92
9	a	3D	COF-102	3472	90
10	a	3D	COF-103	4210	90
2 + 3	b	2D	COF-18Å	1263	93
4 + 9	c	3D	COF-202	2690	94
5	d	2D	CTF-1	791	95
6 + 11	e	3D	COF-300	1360	96
7 + 8	f	2D	COF-42	710	97
7 +12	f	2D	COF-43	620	97

[a]See **Figure 1-13**. [b]See **Figure 1-12**.

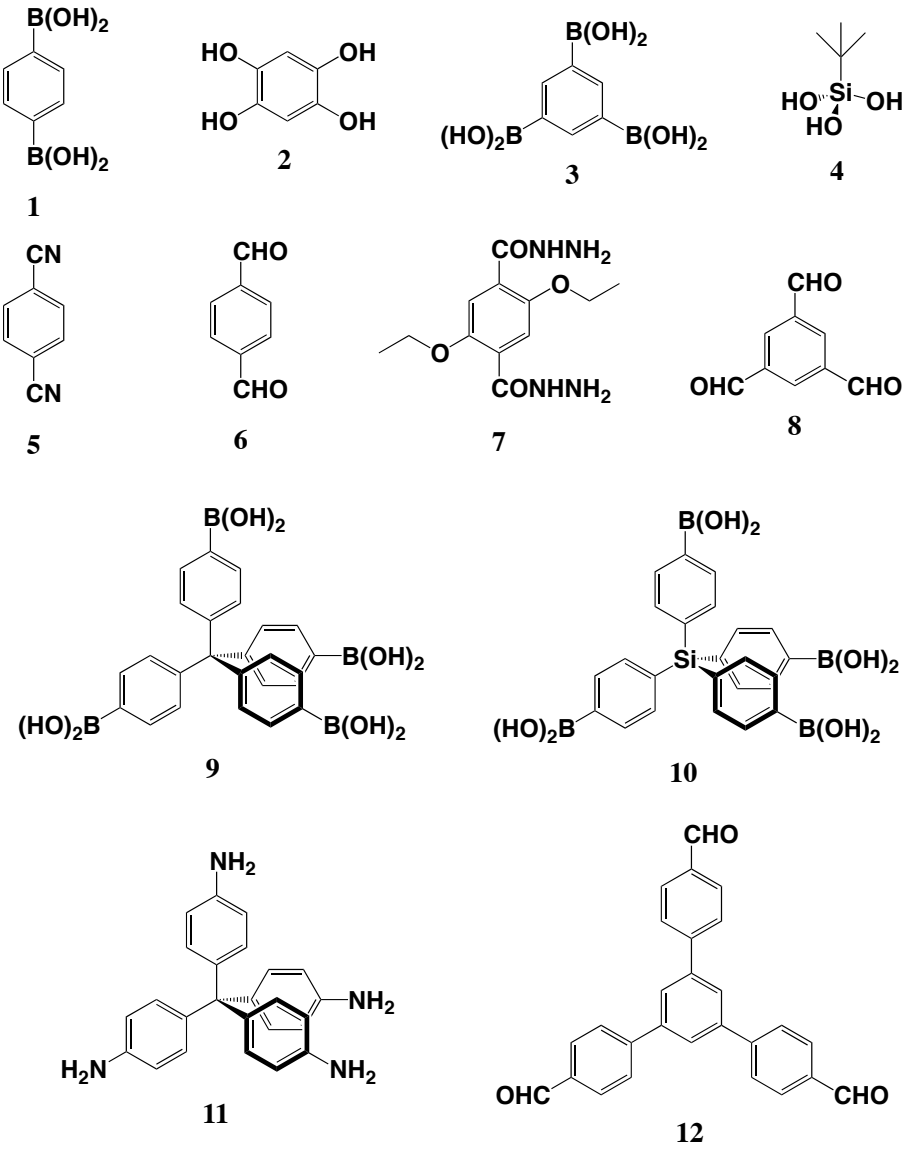

Figure 1-13. Rigid building blocks used to prepare COFs.

1.2.4. Conjugated Microporous Polymers (CMPs) and Analogues

1.2.4.1. Conjugated Microporous Polymers (CMPs)

Conjugated microporous polymers (CMPs) are a class of amorphous and three-dimensional networks containing microporosity and conjugation.[2,98] In 2007, Cooper and coworkers first reported the synthesis of a series of conjugated poly(aryleneethynylene) (PAE) networks (CMP-1, CMP-2, CMP-3, and CMP-4, see **Table 1-3**) using the palladium-catalyzed Sonogashira-

Hagihara coupling reaction between alkyne monomers and halogen monomers (**Figure 1-14**).[99] Example of the molecular structures and simulated structures of CMPs are shown in **Figure 1-15** and **1-16**. In their later work in 2008, CMP-0 and CMP-5 were synthesized (**Table 1-3**).[100] In the systematic study on these CMPs, they found that the pore structures of PAE networks were tunable by changing the length of monomer strut. CMP-0 with the shortest struts exhibits the highest surface areas (1018 m^2/g) among these PAE networks.

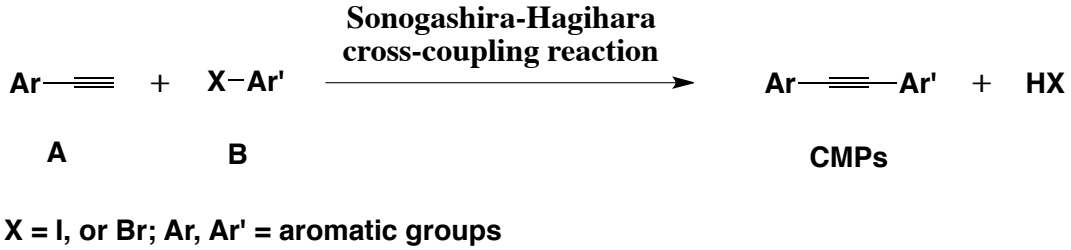

Figure 1-14. Synthesis of CMPs (see **Table 1-3**) from a ethynyl monomer (A, see **Figure 1-17**) and a halogen monomer (B, see **Figure 1-17**).

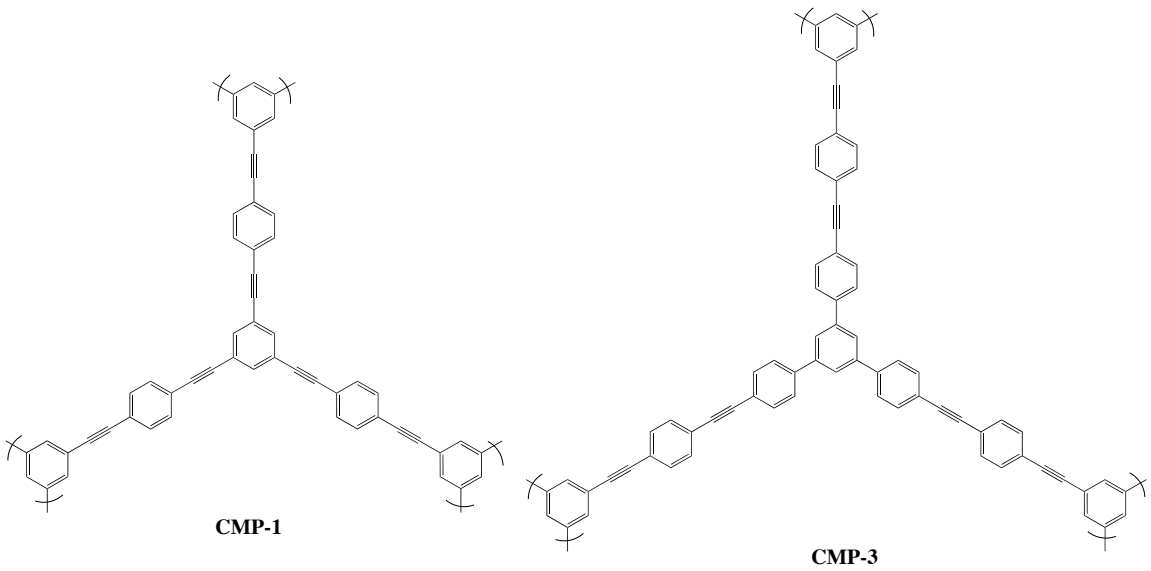

Figure 1-15. Molecular structures for networks CMP-1 and CMP-3.[100]

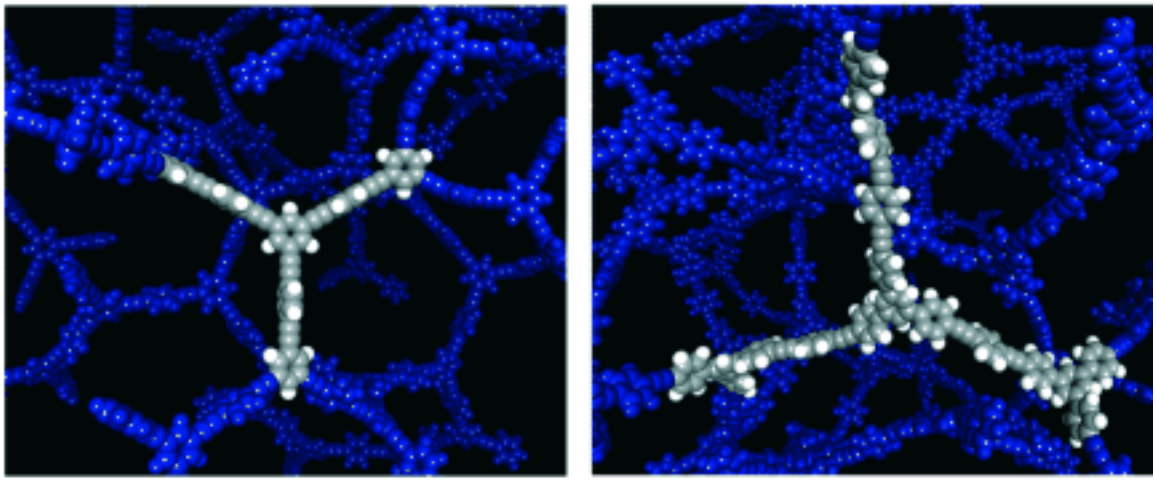

Figure 1-16. Simulated network fragments for CMP-1 (left) and CMP-3 (right), illustrating node-strut topology: 1,3,5-connected benzene node connecting three other nodes via rigid struts (highlighted). Reproduced from [99] with permission. Copyright © 2007 WILEY-VCH Verlag GmbH & Co. KGaA, Weinheim.)

A series of CMPs with high surface area up to 1631 m^2/g were synthesized from spiro-biphenylenedioxythiophene using Sonogashira-Hagihara coupling (see **Table 1-3**).[101] Weber and coworkers introduced spirobiflororene groups in the preparation of CMPs via Suzuki polycondensation (**Scheme 1-9**).[102] The resulting CMPs exhibit surface areas up to 870 m^2/g. Band gap energies of these CMPs obtained from UV/Vis spectra were found to be tunable by varying monomer compositions.

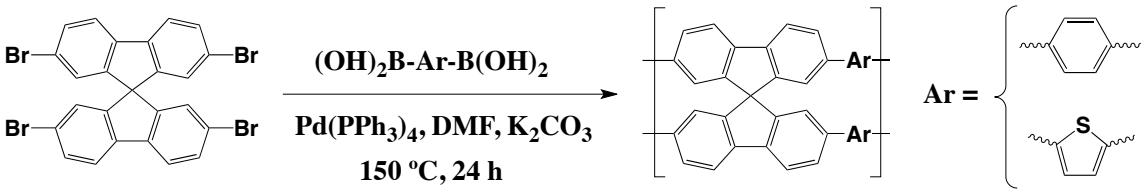

Scheme 1-9. Synthesis of spirobifluorene based CMPs.[102]

Table 1-3. CMPs prepared from ethynyl and halogen monomers (see **Figure 1-17**).

Name	Ethynyl monomer (A)	Halogen monomer (B)	BET Surface Area (m^2/g)	Ref.
CMP-0	A1	B1	1018	100
CMP-1	A1	B2	834	99
CMP-2	A2	B3	634	99
CMP-3	A2	B1	522	99
CMP-5	A3	B1	512	100
2	A1	B5	867	103
3	A1	B6	682	103
7	A1	B7	690	103
8	A1	B8	761	103
19	A1	B9	880	103
TCMP-0	A1	B4	963	104
TNCMP-2	A4	B4	995	104
TCMP-3	A2	B4	691	104
TCMP-5	A3	B4	494	104
SPT-CMP1	A2	B10	1631	101
SPT-CMP2	A1	B10	1601	101
SPT-CMP3	A5	B10	1334	101

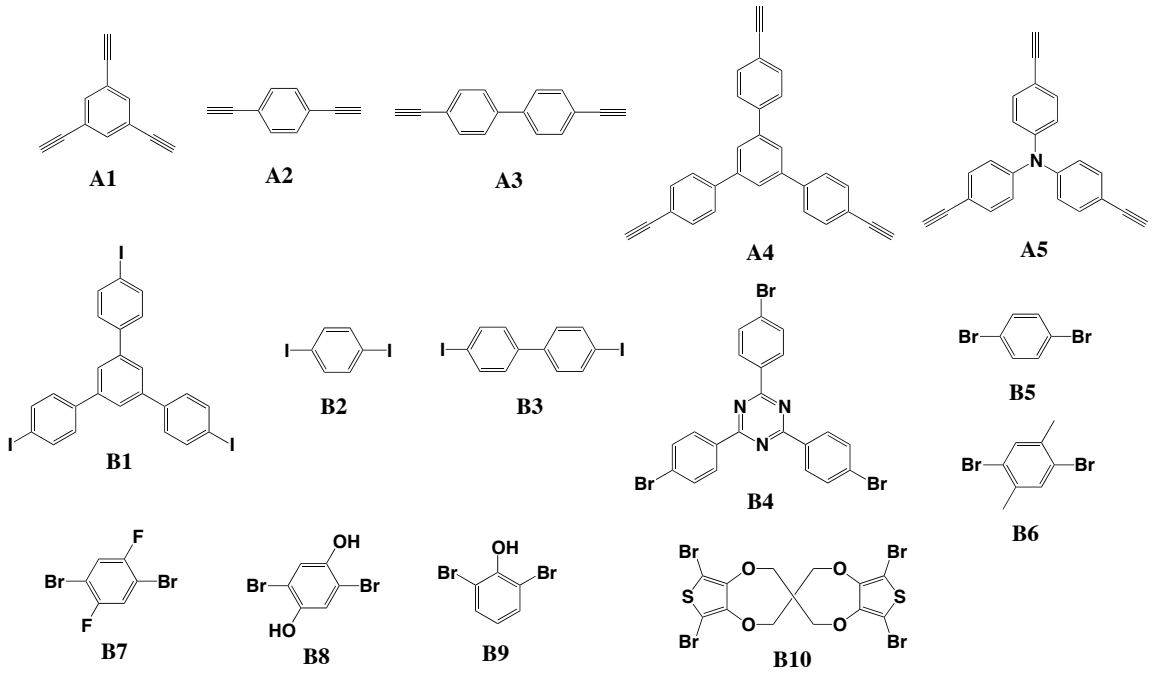

Figure 1-17. Monomers used to prepare CMPs.

In 2009, functionalized PAE networks were synthesized using functionalized dibromobezenes.[103] The hydrophobicity of these PAEs can be tuned by varying the functionality of the monomers. **Figure 1-18** shows the difference in contact angle with water for networks containing different functional groups. CMPs containing electron-withdrawing groups (1,3,5-triazine) were reported by Cooper and coworkers.[104] These 1,3,5-triazine group containing CMPs show comparable surface areas with their CMP analogs while having higher CO_2 uptakes. Among these polymers, TNCMP-2 exhibits the highest surface area (995 m^2/g) (**Table 1-3**). Post-modification of CMP was reported by Weber and coworkers.[105] In their work, CMP-1 was modified by aliphatic alcohols via radical thiol-yne chemistry (**Scheme 1-10**).

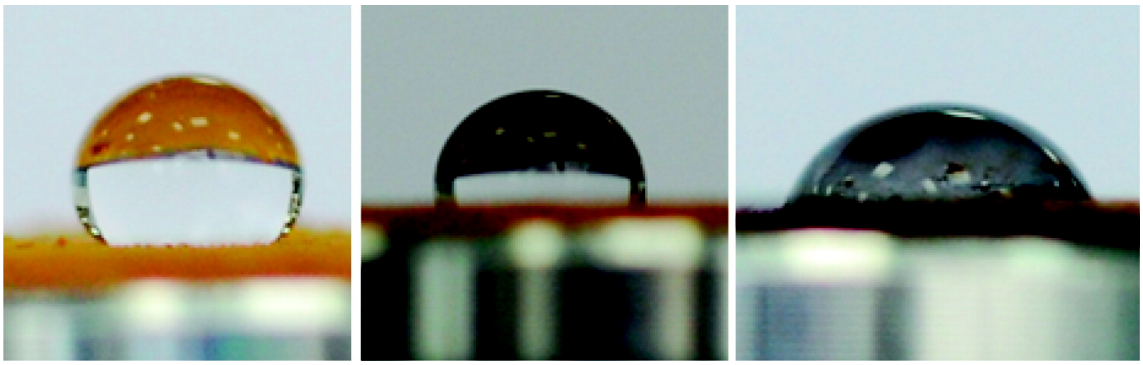

Figure 1-18. Contact angle images for network 7 (left), 2 (middle), and 3 (right) with water, with contact angle of 120, 90, and 96, respectively. (Reprinted with permission from [103]. Copyright 2009 American Chemical Society.)

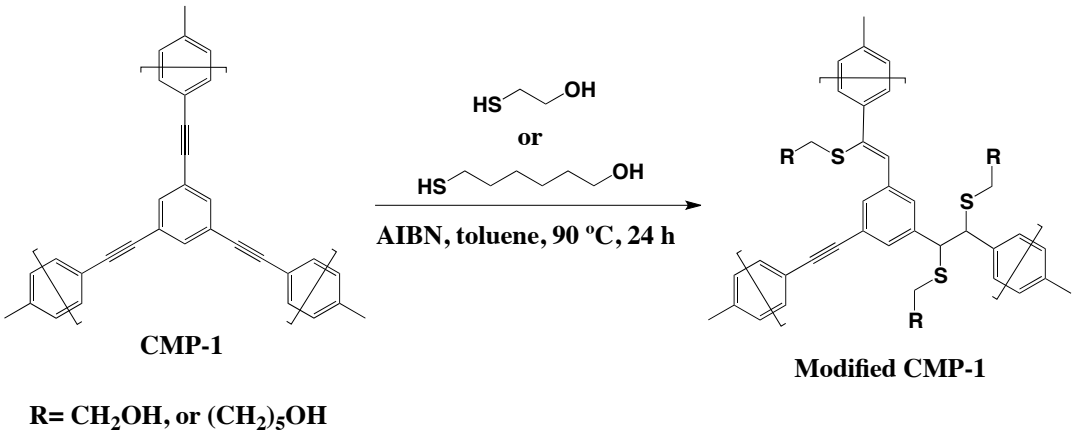

Scheme 1-10. Post-modification of CMP-1.[105]

1.2.4.2. Porous Aromatic Frameworks (PAFs) and Porous Polymer Networks (PPNs)

In 2009, Qiu and coworkers synthesized the first porous aromatic frameworks, PAF-1, using nickel(0)-catalyzed Yamamoto-type Ullmann coupling of tetrahedral monomers in DMF at 80 ºC for 1 h (**Figure 1-19**).[29] PAF-1 exhibits ultrahigh surface area (5640 m^2/g by BET method) and excellent thermal and hydrothermal stabilities. The approach to achieve high porosity was to connect tetrahedral carbons with rigid phenyl groups to form a diamond-like architecture. In 2011, poly(*p*-tetraphenylene)silane (PAF-3) and poly(*p*-tetraphenylene)germane (PAF-4) were

synthesized via same synthetic approach as PAF-1 and exhibit BET surface areas of 2932 and 2246 m^2/g, respectively (**Figure 1-19**).[30]

Zhou and coworkers reported a series of porous polymer networks (PPNs), which were synthesized via optimized the Yamamoto homo-coupling reaction (**Figure 1-19**).[31] The resulting PPNs, especially PPN-4 exhibit exceptionally high surface area (up to 6461 m^2/g by the BET method).

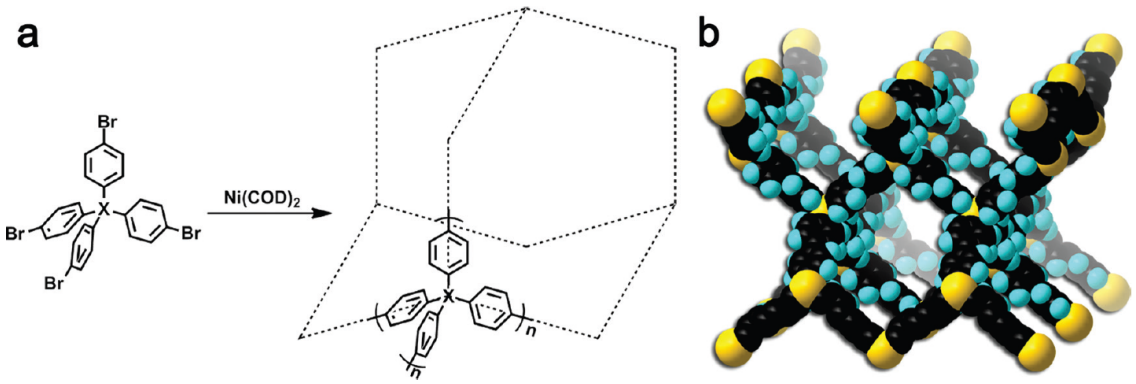

Figure 1-19. (a) Synthetic route for PAF-1 or PPN-6 (X: C), PPN-3 (X: Adamantane), PAF-3 or PPN-4 (X:Si), and PAF-4 or PPN-5 (X: Ge). (b) The default noninterpenerated diamondoid network of PPN-4 (black, C; pale grey, H; grey, Si). (Reproduced from [31] with permission. Copyright © 2011 WILEY-VCH Verlag GmbH & Co. KGaA, Weinheim.)

1.3. Characterization: Physisorption and Simulation

1.3.1. Introduction

Porous properties, such as specific surface area, average pore size, and pore size distribution, are important parameters for the evaluation of porous materials.[106] Gas adsorption is a widely used technique for determining porous properties.[107-115] Adsorption is defined as "the enrichment of one or more components in an interfacial layer." There are two types of sorption, physisorption and chemisorption. Chemisorption involves the formation of chemical bonds to the surface. Physisorption occurs whenever a gas (the adsorbate) is brought into contact with the

surface of a solid (the adsorbent). The major forces involved in physisorption are van-der Waals forces.[60,116]

According to the recommendation by the International Union of Pure and Applied Chemistry (IUPAC), pores can be classified by their pore widths as micropores (widths < 2 nm), mesopores (widths between 2 nm and 50 nm), and macropores (widths > 50 nm).[60,117] Pores can also be classified by their availability to external gases or liquids as 1) closed pores, which are totally isolated (e.g., a in **Figure 1-20**); and 2) open pores, which have continuing channels connected to external surface (e.g., b, c, d, e, and f in **Figure 1-20**).[106] Some open pores may open at one end (blind, e.g., b and f), at two ends (through pore, e.g., c), or open around (e.g., e). According to their shapes, pores can be described as cylindrical (open (c), or blind (f)), ink-bottle shaped (b), funnel shaped (d), or slit-shaped.[106]

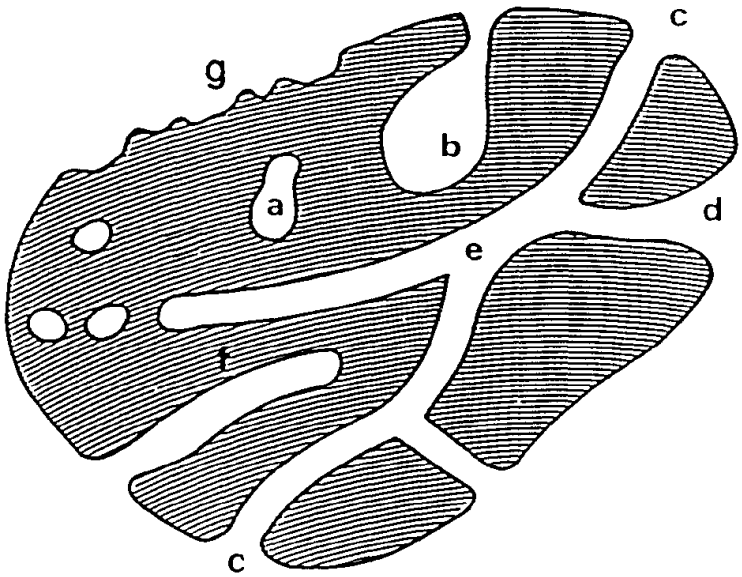

Figure 1-20. Schematic cross-section of a porous solid.[106]

1.3.2. Adsorption Isotherms

Adsorption isotherms are obtained by measuring the amount of gas adsorbed (n) over a range of relative pressures (P/P_o) at a constant temperature. For comparison of adsorption data, adsorption isotherms are usually in a graphical form of n versus P/P_o. According to the classification published by IUPAC, there are six types of adsorption isotherms (**Figure 1-21**).[60]

Type I isotherms are usually obtained for microporous solids. Type I isotherms show a knee at low relative pressure and a characteristic plateau.[107] In most cases, adsorption isotherms from non-porous solids are Type II. Type II isotherms often show a rather long linear region at moderate relative pressure. The beginning point of the linear region is called "point B", which indicates the completion of the monolayer and the beginning of multilayer adsorption.[60,107] Both Type III and Type V isotherms are convex to the relative pressure and do not exhibit point B. The Type III isotherms show convexity over the entire pressure range while Type V exhibit a plateau at high relative pressure ($P/P_o \geq 0.5$). Both types of isotherms indicate weak gas-solid interactions. A type III isotherm is given by a non-porous or macroporous solid while Type V isotherm is given by a mesoporous or microporous solid.[107] The type IV isotherms correspond to mesoporous solids (such as inorganic oxide xerogels). They feature a point B (as shown in **Figure 1-21**) at low relative pressure, a characteristic hysteresis loop, and a plateau at high relative pressure.[107] Stepwise multilayer adsorption leads to a Type VI isotherm. The plateau of each step is related to the monolayer capacity for each adsorbed layer.[60]

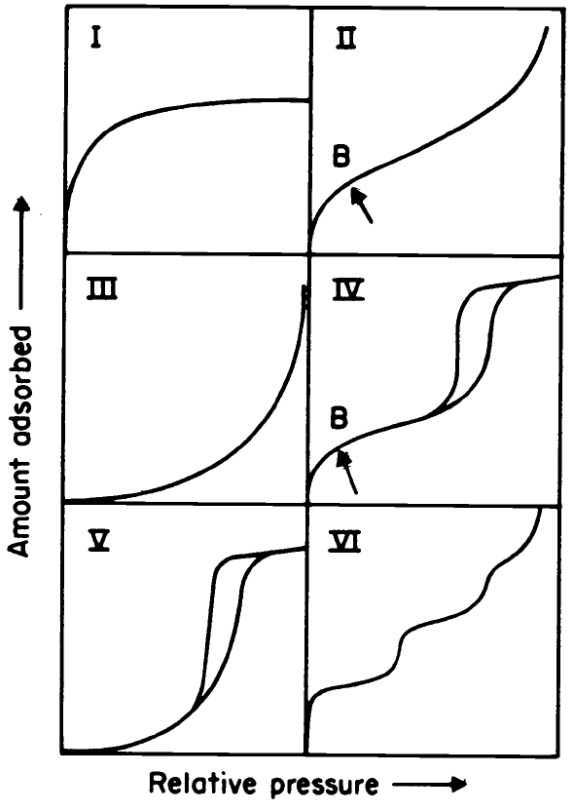

Figure 1-21. Classification of physisorption isotherms by IUPAC.[60]

1.3.3. Adsorption Mechanism

Physisorption mechanisms include monolayer-multilayer adsorption, capillary condensation, and micropore filling.[109] In micropores, sorption is governed by sorbent-adsorbate interactions, which are the interactions between gas molecules and pore walls.[116] The filling of micropores continuously occurs at low relative pressures ($P/P_o < 0.01$) and is termed primary micropore filling. In mesopores, sorption is also affected by the interaction between gas molecules and thus leads to multilayer adsorption and capillary condensation (at $P/P_o \geq 0.2$).[116]

1.3.4. Adsorption Hysteresis

Hysteresis, which is often caused by capillary condensation, provides information about the pore structure of porous materials.[116] The mechanism of adsorption hysteresis in porous

materials has been intensively investigated.[118-124] The shape of hysteresis loop is usually related to the pore structure of the adsorbent. IUPAC has classified 4 types of hysteresis loops (**Figure 1-22**). A Type H1 loop is often associated with porous materials containing fairly uniform pore structures with narrow distributions of pore size. A Type H2 loop is usually caused by porous adsorbents with large pore size distributions and non-uniform pore structures, and therefore is hard to interpret. A Type H3 loop is related to slit-shaped pores generated by plate-like particles. Type H4 is associated with narrow slit-like pore structures.[60]

The desorption and adsorption branches in isotherms usually approach a limiting relative pressure, which depends only on the nature of the adsorptive. For example, for nitrogen isotherms, desorption and adsorption branches usually coincide at the boiling point of nitrogen at $P/P_o \approx 0.42$. Low pressure hysteresis, which is the lack of convergence at low relative pressure ($P/P_o < 0.42$ for nitrogen isotherm), may be observed (shown in the dashed line in **Figure 1-22**). This phenomenon may be attributed to the swelling of non-rigid materials.[60]

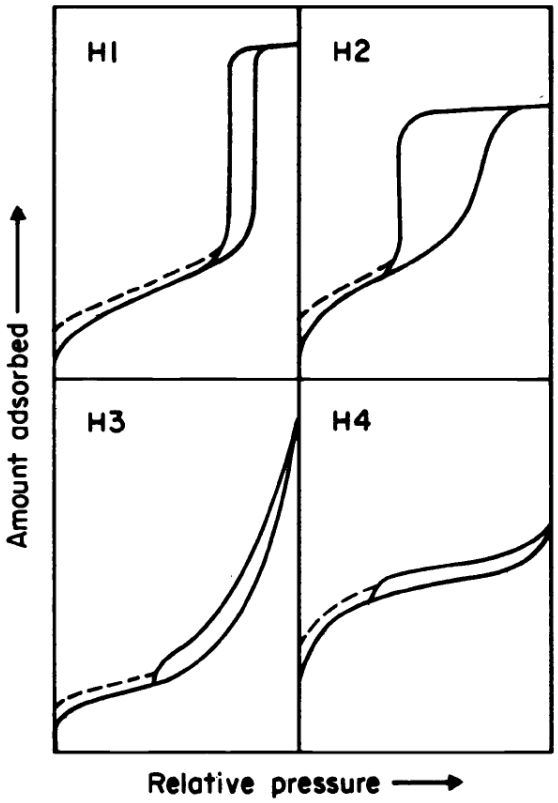

Figure 1-22. Classification of hysteresis loops by IUPAC.[60]

1.3.5. Surface Area - BET Method

Surface area is one of the important parameters for the evaluation of porous materials. The Brunauer-Emmett-Teller (BET) method is the most widely used procedure to calculate specific surface areas of solid materials from adsorption isotherms by using the BET equation.[59] The linear form of the BET equation is:

$$\frac{P/P_0}{n(1-P/P_0)} = \frac{1}{n_m C} + \frac{C-1}{n_m C}\frac{P}{P_0} \qquad \textbf{Equation 1-1}$$

where relative pressure, P/P_o, is the ratio of absolute pressure, P, to the saturated vapor pressure, P_o; P_o is the pressure at which a gas liquefies at a given temperature; n is the absorbed amount of gas; n_m is the monolayer capacity; and C is an empirical constant, which is an indicative of the magnitude of the adsorbent-adsorbate interaction energy. Adsorption isotherm data can be

transformed into a BET plot of $(P/P_o)/[n(1- P/P_o)]$ versus P/P_o, which gives a straight line at a low relative pressure range (approximately 0.05-0.3). For this linear region, the slope s = $(C-1)/n_mC$ and the intercept i = $1/n_mC$. Two parameters, C and n_m can be solved by equations:

$$n_m = 1/(s+i) \qquad \textbf{Equation 1-2}$$

and

$$C=(s/i)+1 \qquad \textbf{Equation 1-3}$$

The specific surface area (SA_{BET}) can be calculated from the equation:

$$SA_{BET} = n_m N_a \sigma \qquad \textbf{Equation 1-4}$$

Where N_a is Avogadro's constant and σ is the cross-sectional area. Nitrogen at 77 K is considered to be the standard adsorptive for surface area measurements, giving σ (N_2, 77 K)= 0.162 nm^2.[60]

For microporous materials, the selection of the relative pressure range of the linear region in a BET plot is crucial and may lead to large variation (30%). Rouquerol and coworkers have suggested several criteria for the selection of an appropriate relative pressure range: a) the intercept of the linear region is positive, b) the C value is positive, and c) the term $n^a(P/P_0)$ increases continuously with P/P_0.[125]

1.3.6. Pore Volume and Pore Size Distribution

Total pore volume can be calculated from the amount of gas uptake n_s at saturation (p/p^o close to 1) and the molar volume of adsorbate at operational temperature using the Gurvich rule, which states that the adsorbed liquid volume at saturation is constant.[107,126-128] For mesoporous materials, if isotherms (Type IV or Type V) have a distinctive horizontal plateau, the amount absorbed at the plateau can be converted into a volume of the adsorbate and is equal to the total

mesopore volume.[113] For microporous materials with Type I isotherms which have a long, horizontal plateau, the uptake at the plateau can be converted to a liquid volume of the adsorbate and is approximately equal to the micropore volume.[107,126]

Initial computational methods for determining pore size distribution from gas adsorption are based on the application of the Kelvin equation (**Equation 1-5**), which describes the relationship between the pore size and the relative pressure during capillary condensation.[110,112,114]

$$ln\frac{P}{P_0} = -\frac{2\gamma V_m}{r_K RT} \qquad \textbf{Equation 1-5}$$

where P/P_0 is the relative pressure of vapor in equilibrium with a meniscus having a radius of curvature r_K, γ is the surface tension of the liquid adsorptive, V_m is the molar volume of the liquid adsorptive, R is the gas constant, and T is the temperature.

Among these initial computational methods, regarded as "classical" approaches, the Barrett-Joyner-Halenda (BJH) method is the most widely used procedure to analyze mesoporous materials.[109,129] The BJH method assumes the desorption process is governed by both physical adsorption and capillary condensation, and relates the surface tension to capillary radius and the physical properties of adsorbent.[130] However, the BJH method is not applicable for micropore analysis, and was found to underestimate the pore size by up to 20-30% for small pores (less than 10 nm).[1,116]

For micropore analysis, the Horvath-Kawazoe (HK) method, which is a semi-empirical, analytical method, can be used to calculate pore size distributions of microporous materials from nitrogen isotherms.[114,131] The HK method is based upon the direct relationship between micropore filling of a given size and shape, and the adsorbent–adsorbate interaction energy. However, it is not applicable for mesopore analysis.[114]

Compared to classical, macroscopic methods discussed above, microscopic methods including the Grand Canonical Monte Carlo simulation (GCMC)[132,133] and Non-Local-Density-Functional Theory (NLDFT)[134-136] provide more accurate pore size analysis over a wider pore size range.[114,137] These two methods are considered to be the most advanced and accurate methods, which allow pore size analysis over the complete size range (micropore and mesopore size).[114,116]

1.3.7. Molecular Simulations

Many studies have focused on the investigation of gas adsorption and separation in porous materials using different simulation techniques such as *ab initio* and density functional theory (DFT) calculations, GCMC simulations, and molecular dynamics (MD) simulations. These simulation techniques are powerful tools for understanding porous properties (pore size, pore volume, surface area, etc.) of the materials and interaction between gas molecules and materials (e.g., specific adsorption sites, binding mechanism, and interaction energies).[138,139]

Gas adsorption and separation properties of MOFs have been intensively investigated using molecular simulations.[138,140-148] Similar to MOFs, COFs are crystalline porous materials and studies of gas sorption properties using molecular simulations were also reported.[149-157] Single gas (Ar, H_2, CH_4, CO_2, etc.) adsorption in COFs was simulated using GCMC simulations by a number of groups.[149,158-161] Assfour and Seifert studied the mechanical properties, adsorption energy, and favorable H_2 adsorption site in 2D and 3D COFs via MD simulations.[153] They found that the phenyl groups in the organic linkers are the most favored H_2 adsorption site, and the adsorption interaction energy for COFs is about 3.0 kJ/mol. Mendoza-Cortes and coworkers designed a series of COFs for methane storage and calculated their methane uptake using

GCMC.[155] They found two new COFs are good candidates as their calculated methane uptake exceeded the DOE target for methane storage. They also found that compared to H substituents, alkyl substituents on the phenyl rings do not increase the binding energies. Beside single gas sorption, gas mixture sorption in COFs was simulated by Liu et al. using GCMC simulations,[162] and by Keskin using GCMC and equilibrium molecular dynamics (EMD) simulations.[154]

Ben and Qiu employed first-principles calculations and GCMC simulations to predict the porosity of PAFs.[29,163] Based on the structure of diamond, they calculated the porosities of networks (P1, P2 and P3), which have various numbers of (1-3) phenyl rings between two carbons (circled in **Figure 1-23**) in the central C-C bond. P2, which has two phenyl rings added to a C-C bond (c in **Figure 1-23**), was predicted to exhibit the largest microporosity. PAF-1 was synthesized based on the structure of P2 and the resulting polymer shows a surface area of 7100 m^2/g.

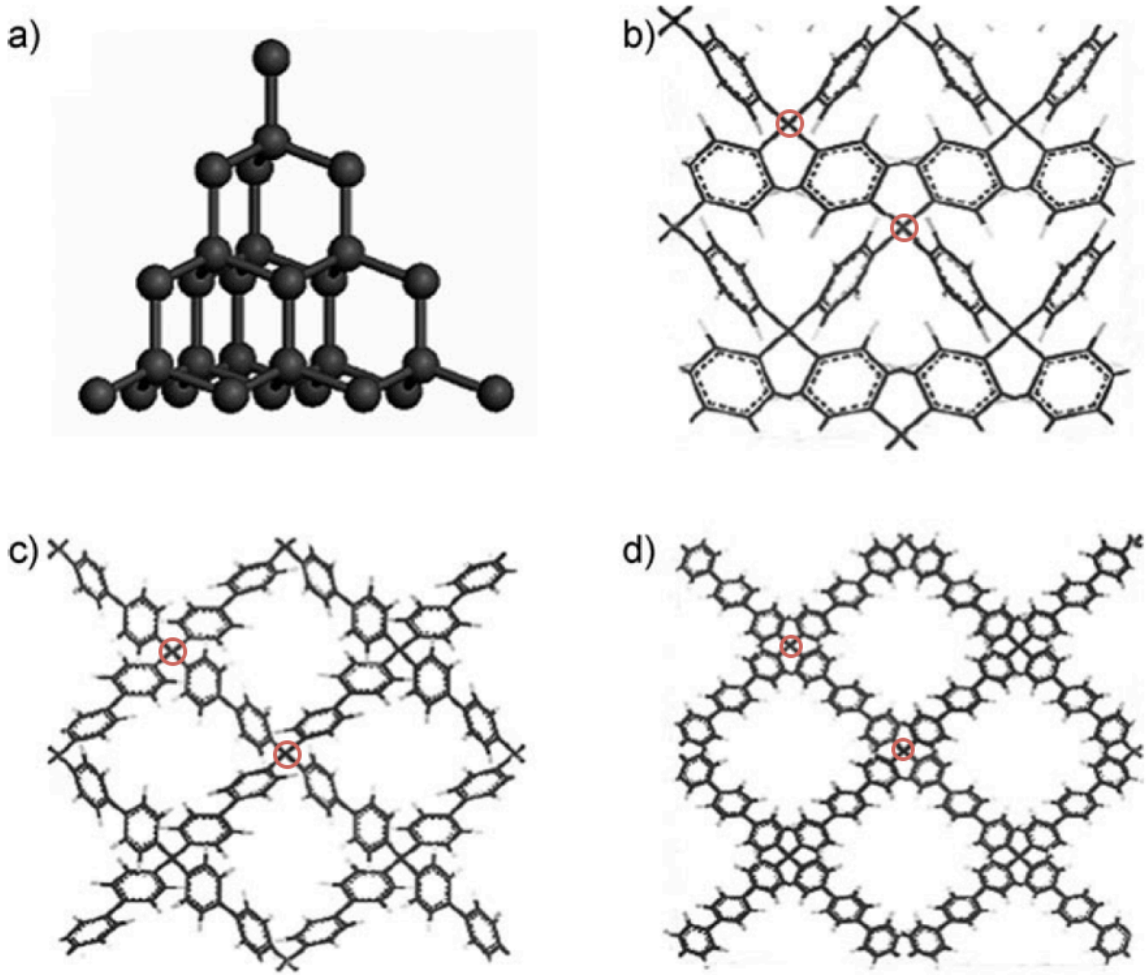

Figure 1-23. Structure of diamond (a) and structure model of P1 (b), P2 (c), and P3 (d). (Adapted from [29] with permission. Copyright © 2009 WILEY-VCH Verlag GmbH & Co. KGaA, Weinheim.)

Unlike the simulation of crystalline materials, simulations of amorphous materials are quite challenging due to the complexity of the structure and limited information for the nature of the pore structure.[70,164] Many works on molecular simulations of amorphous polymers (networks) were reported.[165-174] Cooper and coworkers employed atomistic simulations to investigate the porous properties and H_2 sorption properties of a HCP (poly(*p*-DCX)).[70] **Figure 1-24** allows visualization of the simulated poly(*p*-DCX) network (a-c) and H_2 sorption in the network. By comparing experimental and simulated data, they found that absolute density, bulk density, and

micropore volume were fairly well predicted by simulations. However, the simulated density are slightly lower, while the simulated micropore volume data are slightly higher. The shape of isotherm and isosteric heat of H_2 adsorption were predicted well, but the value of H_2 uptake was overestimated by the simulations due to the inaccessible porosity to gas sorption measurement. Later, the same HCPs were simulated by Colina's group using a new procedure for generating atomistic structures for simulation.[164,175] In this work, gas adsorption properties of hydrogen and methane were obtained using GCMC simulations and compared with experimental data (**Figure 1-25**). Also, they found that both the crosslinking degree and the density of the system during crosslinking are important to achieve polymers with microporosity.

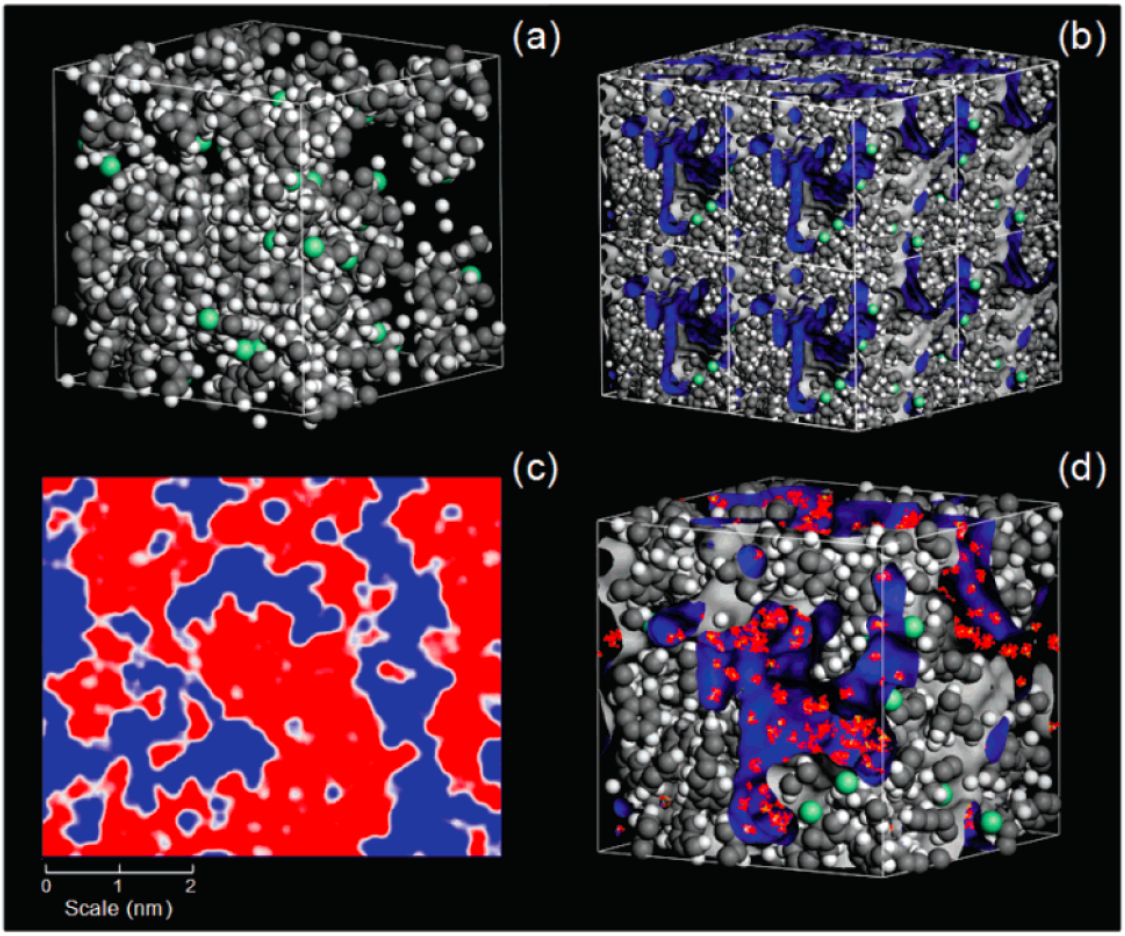

Figure 1-24. Molecular simulation of *p*-DCX: (a) a simulation box; (b) three-dimensional array of eight amorphous cells, A Connolly surface (molecular surface) is blue/gray; (c) two-dimensional "slice" through an array of amorphous cells, occupied and unoccupied volumes are in red and blue, respectively; and H_2 sorption properties (d), H_2 molecules are in red/orange. (Reprinted from [70] with permission. Copyright 2007 American Chemical Society.)

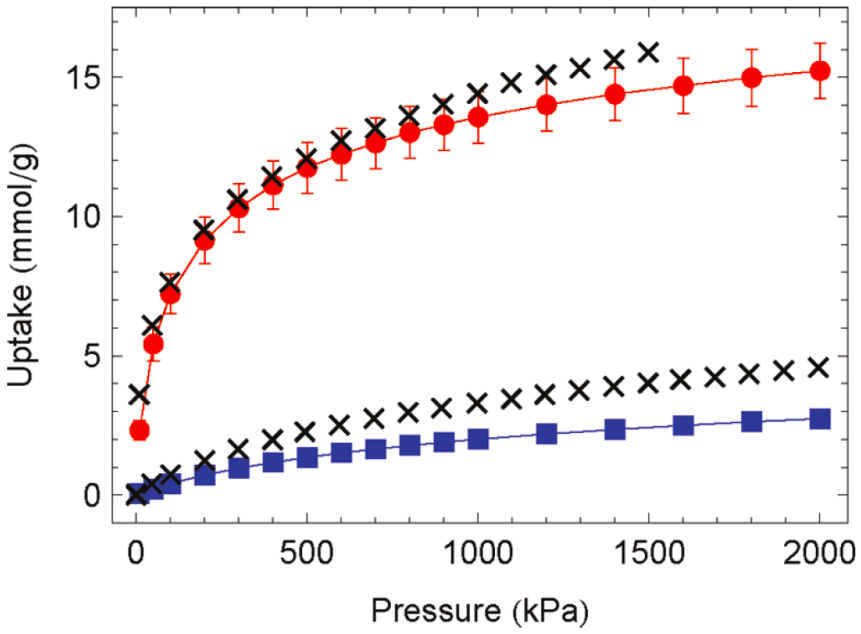

Figure 1-25. Hydrogen (●) and methane (■) adsorption isotherms calculated at 77 and 200 K, respectively, as compared to experimental data[70,176] (×). (Reprinted from [139] with permission. Copyright 2011 American Chemical Society.)

Jiang's group reported simulation of PIMs using Monte Carlo (MC) and MD simulations in 2010.[169] Simulated results of PIM-1 and PIM-7, including solubility, diffusivity, and permeation selectivities, show good agreement with experimental data. Later, they combined molecular simulations and *ab initio* calculations to study gas permeation and separation properties of PIMs with various functional groups.[171] Colina's group reported the molecular simulation of PIM-1 and analogs in 2011.[139] Pore size distributions, surface areas, structure factors, and gas adsorption properties of PIMs were simulated. Adsorption isotherms of methane of these PIMs were simulated and show good qualitative and quantitative agreement with experimental data. In 2012, they analyzed the force field for the simulation of PIMs and found that the combination of generalized amber force field (GAFF) (for bonded interactions) and united atom transferable potential for phase equilibria (TraPPE-UA) (for non-boned interactions) led to the best simulated results which showed good agreement with experimental data.[177]

1.4. Applications: Gas Storage and Separation

1.4.1. Hydrogen Storage

Hydrogen is clean and renewable and is considered to be a good alternative to replace fossil fuel and other carbon-rich fuels in order to reduce the dependency on fossil fuel and carbon dioxide emission to the atmosphere.[178] Although hydrogen has high gravimetric energy density, its volumetric energy density is quite low, which makes the storage of hydrogen challenging.[130] The United State Department of Energy (DOE) established targets for hydrogen storage systems to be able to store 5.5 wt% hydrogen gravimetrically and 40 g/L volumetrically in 2015.[179]

Nanoporous organic polymers as sorbents for hydrogen storage have the advantages of light weight, tunable functionality, and scalable synthesis.[70] A large number of nanoporous organic polymers have been designed and tested for their hydrogen storage properties. Most hydrogen uptakes for nanoporous polymers were measured at 77.3 K.

Svec and coworkers initiated the study of nanoporous polymers for hydrogen storage applications in 2006.[67] They screened hydrogen uptakes for commercially available porous polymers and hypercrosslinked polystyrene synthesized from lightly crosslinked precursors. These porous polystyrenes have BET surface area in the range of 370 - 1900 m^2/g, and exhibited H_2 storage capacity of up to 1.55 wt% at 77.3 K and 0.12 MPa. The enthalpy of hydrogen adsorption of the hypercrosslinked polystyrene, which reflects the magnitude of the interaction energy between hydrogen and adsorbent,[180] was found to be 6.6 kJ/mol. They also found that hydrogen uptake did not directly correlate with surface area, although high surface area is an important factor for effective hydrogen adsorption.

Later, Cooper and coworkers measured the hydrogen uptake of a series of HCPs, which were prepared by polycondensation of bis(chloromethyl) monomers (see §**1.2.2**) and have surface

areas in the range of 600 – 1900 m^2/g.[70] They found hydrogen uptake increases as a function of surface area, although the correlation for BET surface areas was fairly weak (**Figure 1-26**). HCPs synthesized by Cooper's group have an adsorption enthalpy of 7.5 kJ/mol.

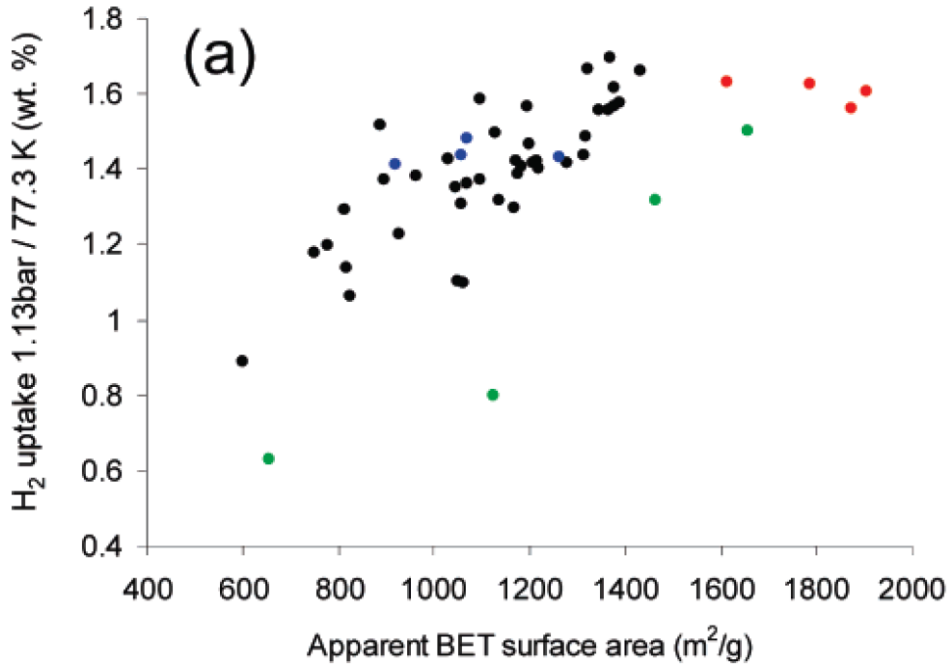

Figure 1-26. Hydrogen uptake at 1.13 bar/77.3 K as a function of BET surface area as a for a series of hypercrosslinked polymers: DCX networks (black symbols)), BCMBP networks (red symbols), BCMA networks (blue symbols) (see **Figure 1-10**), and hypercrosslinked poly(vinylbenzyl chloride) "Davankov resins" (green symbols). (Adapted from [70] with permission. Copyright 2007 American Chemical Society.)

For adsorption at higher temperature (such as room temperature), higher enthalpy of adsorption is required. Enthalpies of adsorption of 15-20 kJ/mol are suggested for hydrogen storage at room temperature.[130,181] It is believed that in the absence of metal, aromatic rings are the major adsorption sites in the materials.[182,183] It is also suggested that the incorporation of electron-donating groups to the aromatic rings may increase H_2-polymer interaction.[184] Svec's group compared hydrogen uptakes of hypercrosslinked polyaniline containing electron-donating groups with its analog which contains electron-withdrawing groups.[73] Unprotonated polyaniline

containing electron-donating groups exhibited much higher hydrogen uptake than protonated polyaniline. An adsorption enthalpy of 9.3 kJ/mol was achieved by unprotonated polyaniline. Later, polyanilines with small pore size were synthesized by Svec's group and achieved an enthalpy of adsorption of 18 kJ/mol, which makes hydrogen adsorption at room temperature possible.[185]

Hydrogen storage capabilities of PIMs are also reported.[45,46,186-188] McKeown and coworkers reported that PIMs show H_2 uptake up to 1.4 wt% (77 K, 1 bar) and 1.7 % (77 K, 10 bar) even with relative low BET surface areas (750-850 m^2/g) compared to surface areas of HCPs (up to 2000 m^2/g).[45] It is believed that a greater predominance of ultramicropores (pore width < 0.7 nm) from these PIMs enhances H_2 adsorption. Later, a triptycene-based PIM was found to have H_2 uptake of 1.61 wt% (77 K, 1 bar) and 2.7 % (77 K, 10 bar).[46] Polyimide and polyamide networks which were synthesized by Thomas' group, and showed H_2 adsorption capacities up to 1.15 wt% at 1 bar.[188] One of the polyamides, PA1, exhibits H_2 uptake of 0.52 wt% even with very low N_2 uptake. COFs, CMPs and analogs showed exceptional high H_2 uptake due to their extremely high surface areas. Some of the examples are summarized in **Table 1-4**. To date, all nanoporous polymers available fall far short of the specification for application for hydrogen storage.

Table 1-4. Nanoporous organic polymers for hydrogen storage.

	Name[a]	SA_{BET}[b] (m^2/g)	H_2 uptake[c] (wt%)	Pressure (MPa)	Ref.
HCP	Hypersol-Macronet MN200	840	1.3	0.1	67
	HCP-PSTR	1930	1.55	0.1	67
	(DCX)25(BCMBP)75	1904	1.61 3.68	0.1 1.5	70
	Polyanilines-diiodomethane	632	0.96	0.1	73
	Polypyrroles-CH_2	732	1.60	0.1	83
PIM	CTC-network-PIM	830	1.43 1.70	0.1 1.0	45
	Tri-PIM	1050	1.63 2.71	0.1 1.0	46
	PA1	50	0.52	0.1	188
	PI1	982	1.15	0.1	188
COF	COF-10	1760	3.92	0.1	189
	COF-102	3620	7.24	0.1	189,190
CMP and analogs	SPT-CMP1	1631	1.72	0.1	101
	SPT-CMP2	1601	1.57	0.1	101
	PAF-1	5640	10.7	4.8	29
	PAF-3	2932	2.07	0.1	30
	PPN-3	2840	1.58 4.28	0.1 4.2	191
	PPN-4	6461	9.1	5.5	31

[a]See Appendix for description of polymers. [b]BET surface area. [c]All measurements were performed at 77.3 K.

1.4.2. Carbon Dioxide Capture

Most electricity is generated via the combustion of fossil fuels. However, combustion of fossil fuels results in large quantities of CO_2 emission, which contributes to global climate change.[192] In order to reduce CO_2 emission, carbon dioxide capture and storage (CCS) is a critical technology. CCS is a process of separation and capture of CO_2 from large scale point sources such as coal-based power plants, transportation, and long-term isolation from the atmosphere.[192] CCS generally consists of 4 steps: CO_2 capture, compression, transportation, and storage.[193] For CO_2 capture, there are three main methods: post-combustion capture, oxy-combustion capture, and pre-combustion capture (**Figure 1-27**).[194] Post-combustion capture involves separation of CO_2 from flue gas, which comes from the power generation unit. An oxy-combustion capture system uses O_2 diluted with recycled flue gas to combust fuel in order to yield a flue gas with a high concentration of CO_2. Pre-combustion involves the separation of CO_2 from synthesis gas, which contains primarily CO and H_2, before combustion of fuel.[194,195]

The CCS target, set by the National Energy Technology Laboratory (NETL)/DOE, is to achieve 90% CO_2 capture at less than 10% increase in cost of energy (COE) for pre-combustion capture and less than a 35% increase in COE for post-combustion and oxy-combustion capture.[193] The challenges and scale of implementation of the CCS process are enormous and viable methods have to be identified and developed.

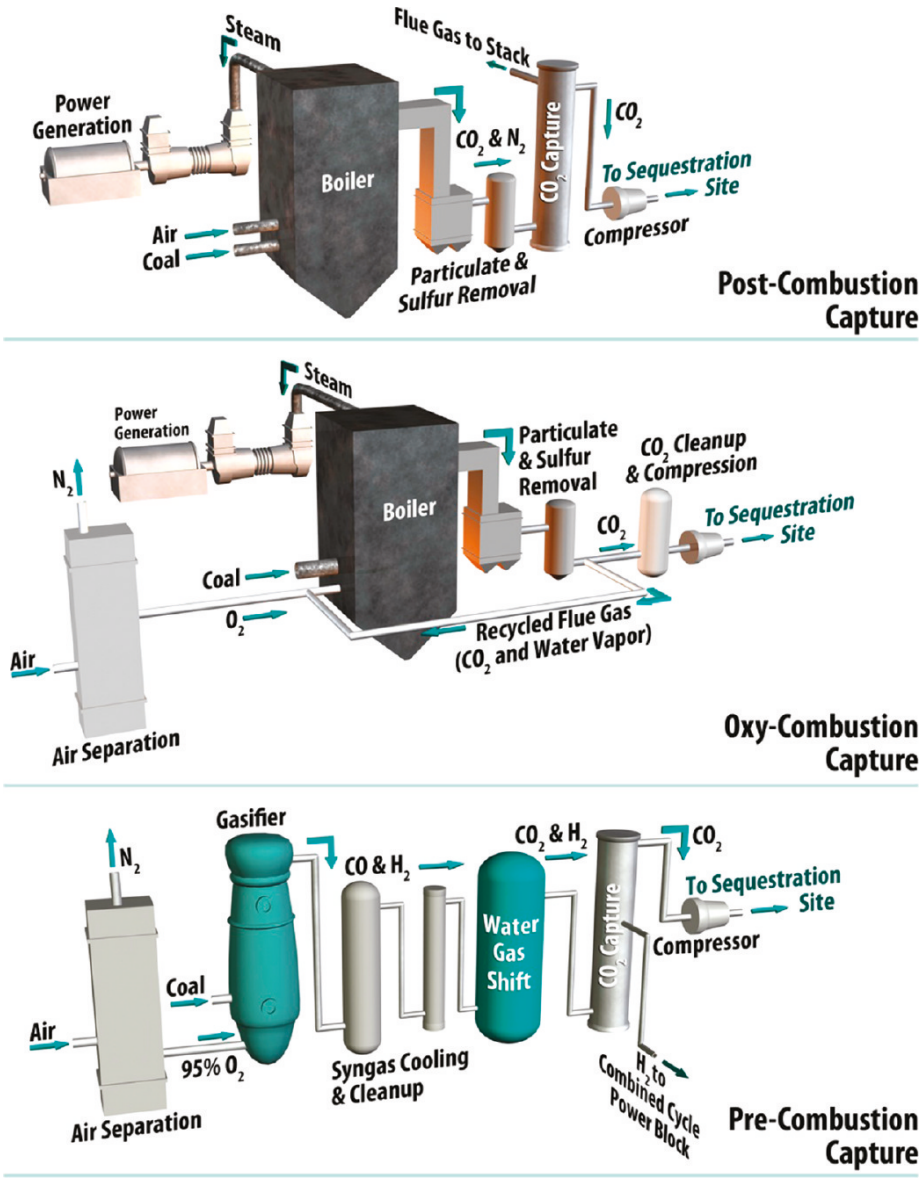

Figure 1-27. Post-, oxy-, and pre-combustion concepts and separation system integration into power plants. (Reproduced from [194] with permission. Copyright 2011 American Chemical Society.)

Conventional CO_2 capture systems integrated in power plants are post-combustion methods using liquid amine solvents such as monoethanolamine (MEA).[196] In these processes, gas mixture containing CO_2 is passed through MEA solution where CO_2 reacts with MEA to form the carbamate. The carbamate is transported to a desorption unit, where it is heated to regenerate

MEA and CO_2. The disadvantages of these systems are high regeneration energy, subsequently high COE, equipment corrosion, and solvent degradation.[197-199] Loss of MEA during the CO_2 recovery process is also a significant problem.[197-199] Solid sorbents are good candidates for CO_2 capture and exhibit several advantages over aqueous amine-based processes: lower regeneration energy, lower heat capacity, and wider operating temperature range.[200,201] In order to meet the CCS targets, solid sorbents are required to have high adsorption capacity, high CO_2 selectivity, fast adsorption/desorption kinetics, suitable isosteric heats of sorption, low sorbent cost, robust durability etc.[200,202,203] Solid sorbents, including carbon based sorbents,[204-206] zeolites,[207-209] amine-based solid sorbents,[210-214] metal organic frameworks,[144,215-218] etc., have been intensively studied for CO_2 capture. CO_2 sorption capacities of nanoporous organic polymers have been investigated recently. Some of the examples are shown in **Table 1-5**.

Yaghi and coworkers pioneered the study of gas storage properties of COFs in 2009.[189] 2D COF exhibits CO_2 uptake up to 1010 mg/g at 5.5 MPa, 298 K. A 3D COF, COF-102, has the highest CO_2 uptake among COFs, which is 1200 mg/g at 5.5 MPa, 298 K. These values exceeded some of active carbon, zeolites, and MOFs. A strong correlation between intrinsic surface area/pore volume and gas storage capacity was found. COFs containing primarily micropores yields a more linear correlation between pore volume and gas uptake, compared to COFs with lower percentages of micropores. Recent work from Cao's group on covalent-organic polymers showed the importance of small pore size on adsorption selectivity.[21,219] In this study, adsorption selectivities of a binary gas mixture (CO_2 and N_2) were predicted based on pure gas adsorption isotherms using the dual-site Langmuir-Freundlich (DSLF) adsorption model[220] – based IAST theory[221]. COP-1, which contains small pore size, exhibits very high adsorption selectivity of CO_2 over N_2 (91 at 298 K and 0.1 MPa).

In 2009, Ben et al. studied the gas properties of PAFs.[30] PAF-1 with ultrahigh surface area shows an exceptionally high CO_2 uptake, which is 1300 mg/g at 298 K and 4 MPa.[29] Later, they found that PAF-3 had the highest CO_2 uptake and selectivity (87) among the PAFs.[30] Zhou and coworkers investigated the CO_2 adsorption capacity of PPNs.[31,32,191,222] PPN-3 and PPN-4 show high CO_2 uptake (2121 mg/g at 295 K and 5 MPa).[31,191] Sulfonate-modified PPNs, PPN-6-SO_3H and PPN-6-SO_3Li, were modified from PPN-6 (also known as PAF-1) (**Scheme 1-11**).[222] Compared to PPN-6, these sulfonate-modified PPNs show much higher CO_2 uptake and exceptionally high CO_2 selectivity over N_2 (up to 414). It is believed that at low pressures, CO_2 uptake is greatly affected by the CO_2-pore surface interaction while at higher pressure the surface area plays a major role in the CO_2 uptake capacity.[222] Later, Zhou's group introduced amine groups in PPN-6 and studied the CO_2 capture properties of these polyamine-tethered PPNs.[32] They found that PPN-6-CH_2DETA (containing $–CH_2(NHCH_2CH_2)_2NH_2$ groups) exhibits the highest CO_2 uptake among all polyamine-tethered PPNs, even though it has the lowest surface area. This result indicates a strong correlation between amine loading and CO_2 uptake.

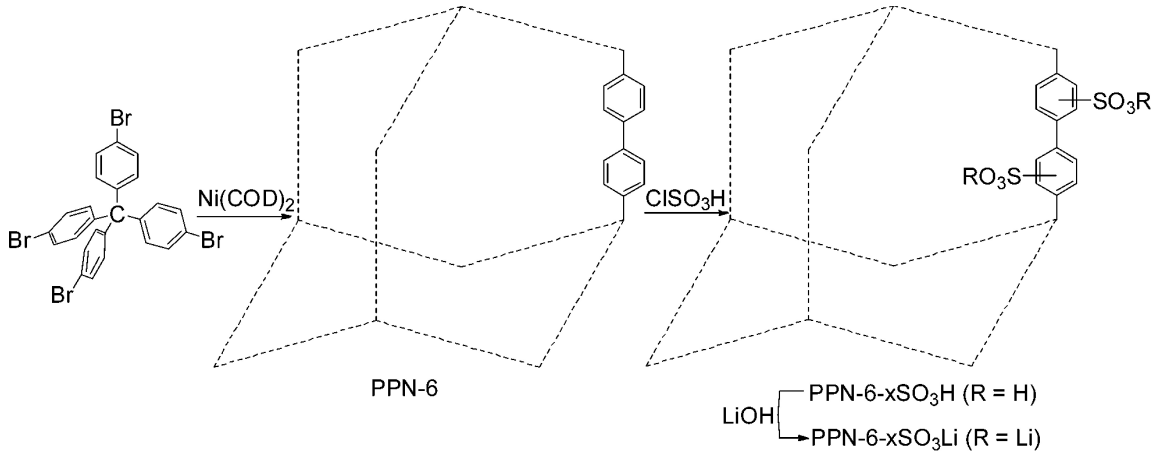

Scheme 1-11. Synthesis and modification of PPN-6. (Reproduced from [222] with permission. Copyright 2011 American Chemical Society.)

Cooper and coworkers studied the CO_2 sorption properties of CMPs with various functionalities.[202] Carboxylic acid functionalized CMP shows higher isosteric heat of sorption for CO_2 than its amine containing analog. The isosteric heats are in the following order: COOH > $(OH)_2$ > NH_2 > H > $(CH_3)_2$. Later, triazine-based CMPs synthesized by Cooper's group showed CO_2 uptake up to 63.8 mg/g at 298 K and 0.1 MPa.[104]

CO_2 sorption properties of HCPs were investigated by several research groups.[72,84-86,223] Dawson et al. found that in the present of water vapor, CO_2 uptakes of a series of alcohol-containing HCPs are much lower than their hydrophobic analogs.[85] They also studied a series of HCPs prepared from aniline and benzene.[86] They found that the increase in aniline content leads to HCPs with higher CO_2/N_2 selectivity. Aromatic heterocyclic HCPs developed by Tan's group show high CO_2 uptake due to the dipole-dipole interactions between CO_2 and the lone pair electrons from heteroatoms.[72] These HCPs also show high CO_2/N_2 selectivity (up to 117) because heteroatoms favorably interact with CO_2, which contains a larger quadruple moment.

Table 1-5. Nanoporous organic polymers for CO_2 capture.

	Name[a]	SA_{BET}[b] (m^2/g)	CO_2 uptake (mg/g)	Condition	Ref.
HCP	1	1391	135	273 K, 0.1 MPa	84
	3	1059	159	273 K, 0.1 MPa	84
	HCP 1	1646	585	298 K, 3.0 MPa	223
	Py-1	437	119	273 K, 0.1 MPa	72
COF	COF-10	1760	1010	298 K, 5.5 MPa	189
	COF-102	3620	1200	298 K, 5.5 MPa	189
CMP and analogs	CMP-1-COOH	552	70.4	273 K, 0.1 MPa	202
	TNCMP-2	995	63.8	298 K, 0.1 MPa	104
	PAF-1	5640	1300 153	298 K, 4.0 MPa 273 K, 0.1 MPa	29, 30
	PAF-3	2932	107	273 K, 0.1 MPa	30
	PPN-3	2840	1113	295 K, 5.8 MPa	191
	PPN-4	6461	2121	295 K, 5.0 MPa	31
	PPN-6-SO_3H	1254	1310	295 K, 0.1 MPa	222
	PPN-6-SO_3Li	1186	1350	295 K, 0.1 MPa	222
	PPN-6-CH_2DETA	555	1580	295 K, 0.1 MPa	32

[a]See Appendix for description of polymers. [b]BET surface area.

1.4.3. Membranes for Gas Separation

Membrane gas separation has been commercialized since 1970s and became a competitive technology with the advantage of low energy cost.[224-226] Commercial gas separation membranes are most widely used for hydrogen separation (e.g., from ammonia production) and nitrogen separation from air.[226] The key to a good membrane for gas separation is to achieve both high permeability and high selectivity. However, membranes with high gas selectivity usually have low permeability, which lead to slow separation processes.[227] Membranes with high permeability generally suffer from poor selectivity. It is well known that there is a tradeoff relationship between gas permeability and selectivity.[224,225,228] Robeson demonstrated the empirical upper bound relationship in 1999 and updated it in 2008; most experimental data points are within the upper bound in the selectivity-permeability plot for many gas pairs (**Figure 1-28**).[224,225] In these plots, materials with data points exceeding the upper bound and sitting on the upper right corner would be desirable. Freeman in 1999 provided a fundamental theory for the observation of upper bound relationship.[228] The theory shows good agreement with experimental data for many gas pairs. Membranes for gas separation were recently the subject of a thorough review.[229] This section will focus only on the literature for PIMs.

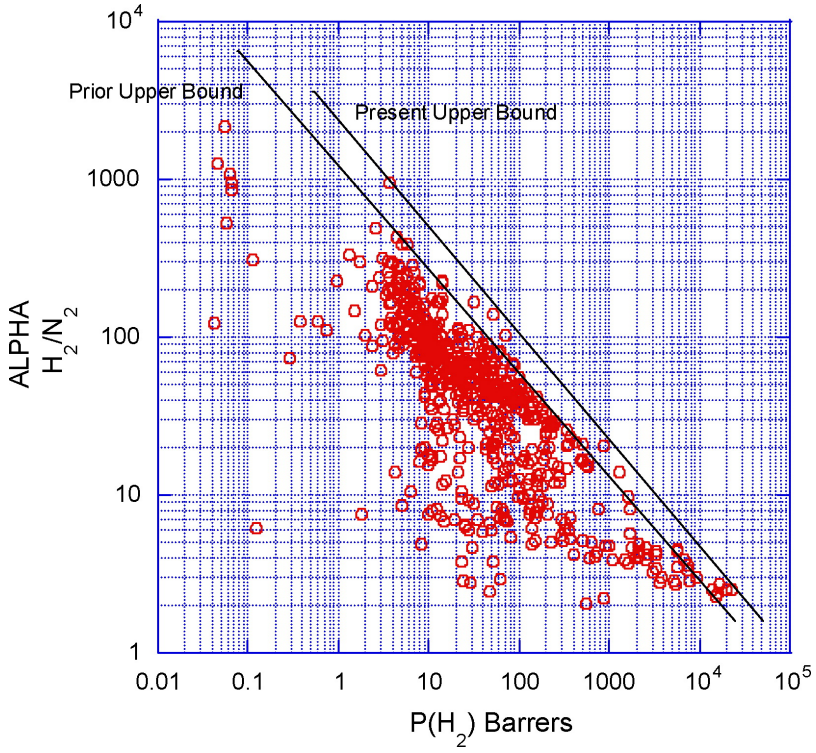

Figure 1-28. Upper bound correlation for H_2/N_2 separation. (Reprinted from [225] Copyright 2008, with permission from Elsevier.)

Non-network PIMs, which have good solubility and processability, and are considered good candidates for membrane gas separation.[23,24,34,51,55,57,58,61,172,230-235] In 2005, Budd et al. reported the gas permeability of PIM-1 (**Figure 1-5**) and PIM-7 (**Figure 1-29**).[235] They found that both PIM-1 and PIM-7 show higher selectivities than other polymers with similar permeability for the O_2/N_2 gas pair, exceeding Robeson's 1991 upper bound, where the top right side of the plot is desirable.[23]

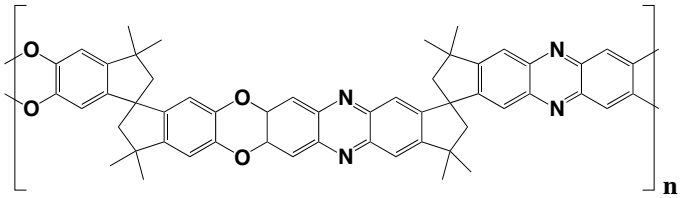

PIM-7

Figure 1-29. Molecular structure of PIM-7.[23]

Guiver and coworkers synthesized a series of PIMs, which contained trifluoromethyl and phenylsulfone groups.[230] The gas permeabilities and selectivities of these PIMs (TFMPSPIM1-4) and PIM-1 were studied. They found that TFMPSPIM1-4 polymers show much higher selectivity than PIM-1 while maintaining high permeability, which make them exceed the Robeson upper bound (**Figure 1-30**). The result suggests that the $-CF_3$ and $-SO_2C_6H_5$ side groups increase the selectivity by affecting the chain rigidity and chain packing, and thus improve the gas separation properties.

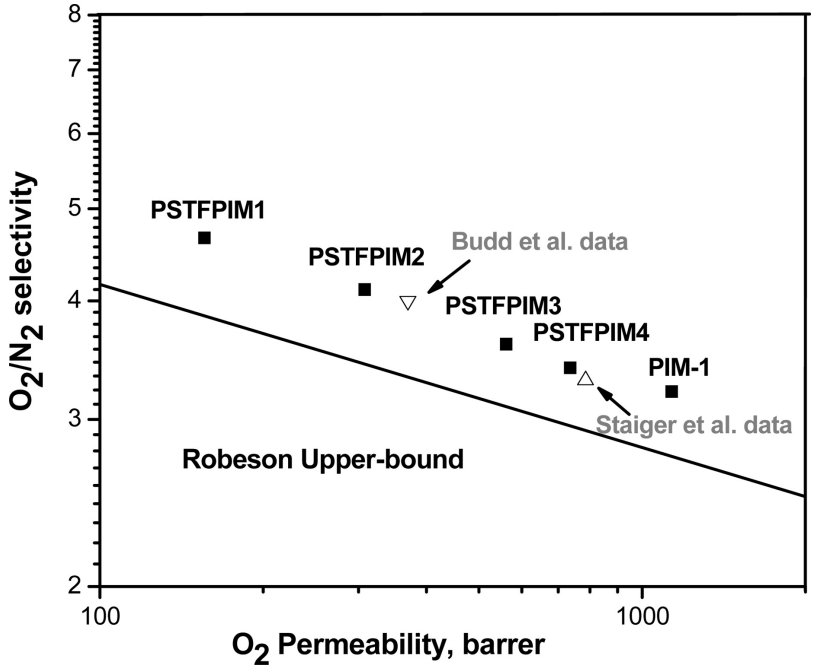

Figure 1-30. Trade-off between O_2 permeability and O_2/N_2 selctivity of PIM-1 and TFMPSPIM1-4 membranes relative to the Robeson upper bound line. Triangles are data points of PIM-1 measured by Budd et al.[235] and Staiger et al.,[231] respectively. (Reproduced from [230] with permission. Copyright 2008 American Chemical Society).

In 2008, McKeown, Budd, and coworkers reported a series of PIM-polyimides, PIM-PI-1, PIM-PI-3, and PIM-PI-8.[51] They found the permeability for these PIM-polyimides increases in the order of $N_2 < CH_4 < O_2 < He < H_2 < CO_2$. For each gas, permeabilities increase in the order

of PIM-PI-3 < PIM-PI-1 < PIM-PI-8, which are strongly correlated to their surface areas. PIM-PI-8 exhibits the highest permeabilities and exceeds the Robeson's 1991 upper bound.

Recently, McKeown and coworkers found that the incorporation of more rigid spirobifluorene units to PIMs improved the performance of gas separation.[232] PIM-SBF reported in this work lies above the Robeson's 2008 upper bound for several gas pairs, and shows significantly higher selectivities for CO_2/N_2 and CH_4/N_2 gas pairs. The result suggests that the rigidity of polymer backbones is important for PIMs to achieve high gas selectivities. McKeown and coworkers incorporated inflexible bridged bicyclic units into PIMs.[34] The resulting polymer, PIM-EA-TB (**Figure 1-31**), which contains both bridged EA and TB units, exhibits remarkably high gas selectivities and good permeability, and surpasses Robeson's 2008 upper bound for several gas pairs (**Figure 1-32**).

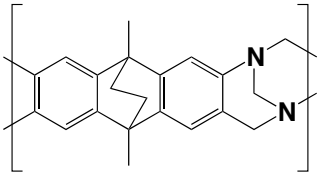

PIM-EA-TB

Figure 1-31. Molecular structures of PIM-SBI-TB.[34]

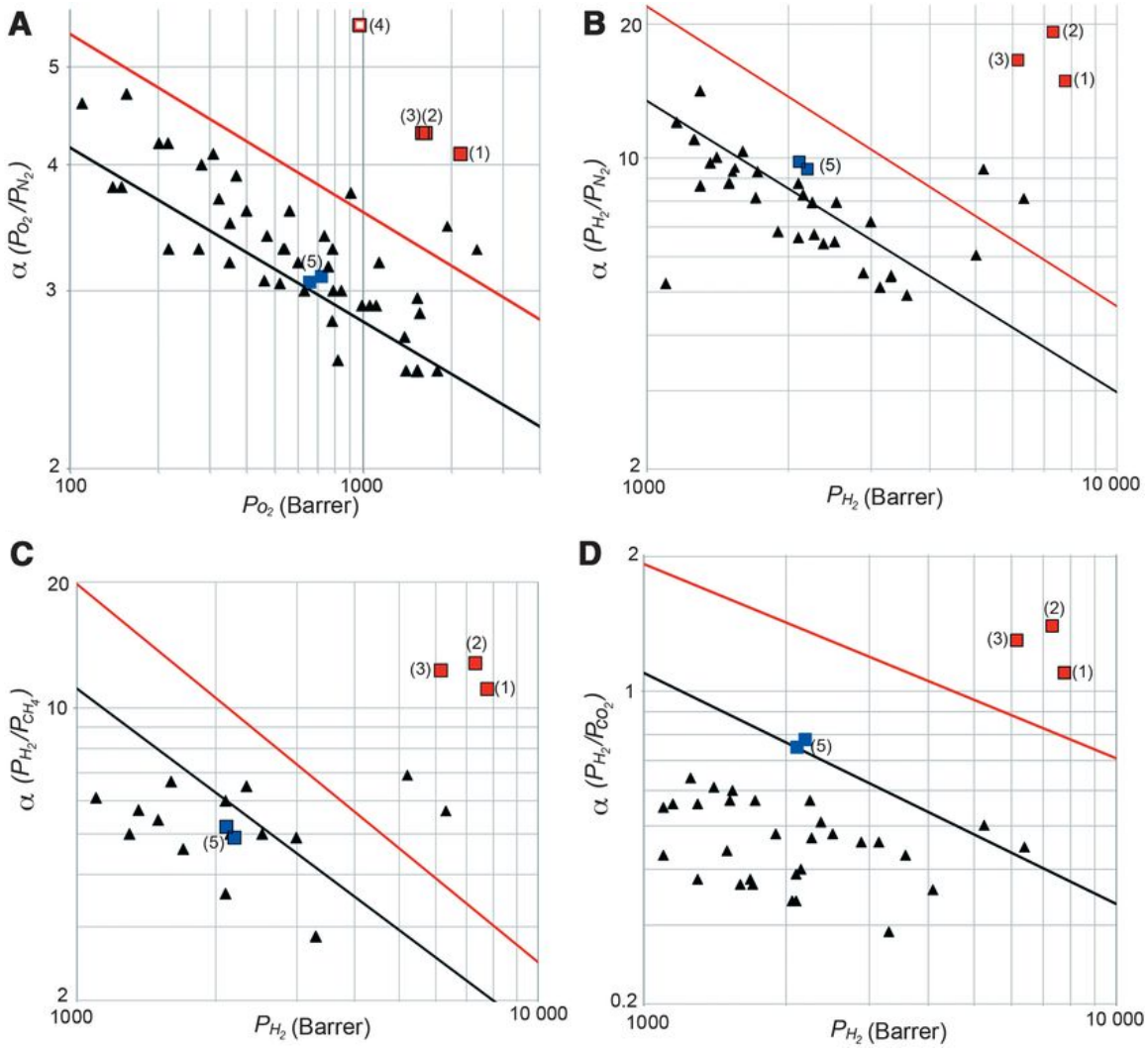

Figure 1-32. Portions of Robeson plots for (A) O_2/N_2; (B) O_2/N_2; (C) O_2/N_2; (D) O_2/N_2 gas pairs for PIM-EA-TB, with data points: 1) 181-μm film; 2) 95-μm film; 3) 181-μm film after aging for 24 h; 4) average value; 5) 157- and 128-μm films of PIM-SBI-TB. Other data points (black triangle) represent PIMs and other highly permeable polymers reported since 2008. The black and red lines are Robeson's upper bound in 1991 and 2008, respectively. (From [34]. Reprinted with permission from AAAS.)

1.5. Conclusions

In this chapter, we described several subclasses of nanoporous organic polymers: PIMs, HCPs, COFs, and CMPs and analogs (PAFs and PPNs). The synthesis and structure-porosity relationship of these polymers were discussed in **§1.2**. **Table 1-6** summarizes the properties of subclasses of nanoporous polymers (surface area) and the mechanisms of the formation of high porosity. In **§1.3**, we presented the fundamental knowledge of porosity characterization via gas sorption measurement and recent development on molecular simulations of gas sorption and separation properties. **§1.4** discussed potential applications such as hydrogen storage, CO_2 capture, and gas separation.

Table 1-6. Properties and pore forming mechanisms of nanoporous organic polymers.

Subclass of nanoporous polymers	Type of polymers	Formation of porosity	BET Surface areas (m^2/g)
PIMs	Amorphous	Inefficient chain packing of rigid, contorted polymer chains in the solid state	300-1700
HCPs	Amorphous	Highly crosslinking from external or internal crosslinkers	400-2000
COFs	Crystalline	Formation of rigid linkages between rigid monomers to yield 2D or 3D architectures	600-4000
CMPs	Amorphous	Metal catalyzed coupling of alkyne and halogen monomers to form 3D, conjugated networks	500-1600
PAFs	Amorphous	Metal catalyzed Yamamoto coupling of tetrahedral monomers	500-6500
PPNs	Amorphous		

The development of nanoporous polymers leads to a large variety of synthetic routes and the ease of incorporation of various functionalities, making these polymers strong candidates for potential gas storage and separation applications. Also, these polymers have high surface area and good thermal stability, which are important in gas storage and separation applications.

However, there are some challenges of these materials for their potential gas storage and separation applications.[2,21] Most of these materials are amorphous (except COFs) and insoluble (except linear PIMs), thus making the available characterization techniques limited. Furthermore, the lack of processability (except linear PIMs) and high cost of synthesis (of some of the networks) due to the expensive monomers or reagents prevent these materials from being scaled up. Therefore, making cost-efficient polymers with good gas storage/separation properties that meet the requirements established by DOE is still very challenging.

1.6. Appendix to Chapter 1

Description of polymers in **Table 1-4** and **1-5**

	Name	Description
HCP	Hypersol-Macronet MN200	Commercial porous hypercrosslinked polystyrene beads (Purolite Company, Philadelphia, PA)
	HCP-PSTR	Hypercrosslinked polymer prepared from gel poly (chloromethylstyrene-*co*-divinylbenzene), See **Scheme 1-1**
	(DCX)25(BCMBP)75	Hypercrosslinked polymer network prepared from 25% DCX and 75% BCMBP via polycondensation (see **Figure 1-10**)
	Polyanilines-diiodomethane	See **Scheme 1-3** (A), R=CH_2.
	Polypyrroles-CH_2	See **Scheme 1-4** (A)
	1	See **Scheme 1-5** (a), R=H
	3	See **Scheme 1-5** (c)
	HCP 1	Poly(BCMBP) (see **Figure 1-10**)
	Py-1	See **Scheme 1-6**, X=NH
PIM	CTC-network-PIM	See **Table 1-1**
	Tri-PIM	See **Table 1-1**
	PA1	Poly(amide) network synthesized from tetrafunctionalized spirobifluorene monomer
	PI1	Poly(imide) network synthesized from tetrafunctionalized spirobifluorene monomer
COF	COF-10	A 2D COF[236]
	COF-102	A 3D COF, see **Table 1-2**
CMP and analogs	SPT-CMP1	See **Table 1-3**
	SPT-CMP2	
	PAF-1	See **Figure 1-19**
	PAF-3	
	PPN-3	
	PPN-4	
	PPN-6-SO_3H	See **Scheme 1-11**
	PPN-6-SO_3Li	
	PPN-6-CH_2DETA	$–CH_2(NHCH_2CH_2)_2NH_2$ group containing PPN-6
	CMP-1-COOH	-COOH group containing CMP-1
	TNCMP-2	See **Table 1-3**

References

(1) Lu, G. Q. Zhao, X. S. *Nanoporous Materials: Science and Engineering*; Imperial College Press, 2004; Vol. 4.

(2) Dawson, R.; Cooper, A. I.; Adams, D. J. *Prog. Polym. Sci.* **2012**, *37*, 530.

(3) Svec, F.; Frechet, J. M. J. *Ind. Eng. Chem. Res.* **1999**, *38*, 34.

(4) Hilder, E. F.; Svec, F.; Frechet, J. M. *J. Chromatogr. A* **2004**, *1044*, 3.

(5) Penner, N. A.; Nesterenko, P. N.; Ilyin, M. M.; Tsyurupa, M. P.; Davankov, V. A. *Chromatographia* **1999**, *50*, 611.

(6) Davankov, V.; Tsyurupa, M.; Ilyin, M.; Pavlova, L. *J. Chromatogr. A* **2002**, *965*, 65.

(7) Urban, J.; Jandera, P. *Anal. Bioanal. Chem.* **2013**, *405*, 2123.

(8) Kaur, P.; Hupp, J. T.; Nguyen, S. T. *ACS Catal.* **2011**, *1*, 819.

(9) Zhang, Y. G.; Riduan, S. N. *Chem. Soc. Rev.* **2012**, *41*, 2083.

(10) Hou, Q. P.; Grijpma, D. W.; Feijen, J. *Biomaterials* **2003**, *24*, 1937.

(11) Hentze, H.-P.; Antonietti, M. *Rev. Mol. Biotechnol.* **2002**, *90*, 27.

(12) Rezwan, K.; Chen, Q. Z.; Blaker, J. J.; Boccaccini, A. R. *Biomaterials* **2006**, *27*, 3413.

(13) Maquet, V.; Jerome, R. *Porous Mater. Sci. Forum* **1997**, *250*, 15.

(14) Thomas, A.; Kuhn, P.; Weber, J.; Titirici, M. M.; Antonietti, M. *Macromol. Rapid Comm.* **2009**, *30*, 221.

(15) Vilela, F.; Zhang, K.; Antonietti, M. *Energ. Environ. Sci.* **2012**, *5*, 7819.

(16) Morris, R. E.; Wheatley, P. S. *Angew. Chem. Int. Ed.* **2008**, *47*, 4966.

(17) Davankov, V. A.; Tsyurupa, M. P. *React. Polym.* **1990**, *13*, 27.

(18) Tsyurupa, M. P.; Davankov, V. A. *React. Funct. Polym.* **2002**, *53*, 193.

(19) Xu, S.; Luo, Y.; Tan, B. *Macromol. Rapid Commun.* **2013**, *34*, 471.

(20) Ding, S. Y.; Wang, W. *Chem. Soc. Rev.* **2013**, *42*, 548.

(21) Xiang, Z. H.; Cao, D. P. *J. Mater. Chem. A* **2013**, *1*, 2691.

(22) Feng, X.; Ding, X. S.; Jiang, D. L. *Chem. Soc. Rev.* **2012**, *41*, 6010.

(23) McKeown, N. B.; Budd, P. M.; Msayib, K. J.; Ghanem, B. S.; Kingston, H. J.; Tattershall, C. E.; Makhseed, S.; Reynolds, K. J.; Fritsch, D. *Chem. Eur. J.* **2005**, *11*, 2610.

(24) McKeown, N. B.; Budd, P. M. *Chem. Soc. Rev.* **2006**, *35*, 675.

(25) McKeown, N. B.; Budd, P. M. *Macromolecules* **2010**, *43*, 5163.

(26) McKeown, N. B. *ISRN Mater. Sci.* **2012**, *2012*, 16.

(27) Weder, C. *Angew. Chem. Int. Ed.* **2008**, *47*, 448.

(28) Cooper, A. I. *Adv. Mater.* **2009**, *21*, 1291.

(29) Ben, T.; Ren, H.; Ma, S. Q.; Cao, D. P.; Lan, J. H.; Jing, X. F.; Wang, W. C.; Xu, J.; Deng, F.; Simmons, J. M.; Qiu, S. L.; Zhu, G. S. *Angew. Chem. Int. Ed.* **2009**, *48*, 9457.

(30) Ben, T.; Pei, C. Y.; Zhang, D. L.; Xu, J.; Deng, F.; Jing, X. F.; Qiu, S. L. *Energ. Environ. Sci.* **2011**, *4*, 3991.

(31) Yuan, D. Q.; Lu, W. G.; Zhao, D.; Zhou, H. C. *Adv. Mater.* **2011**, *23*, 3723.

(32) Lu, W. G.; Sculley, J. P.; Yuan, D. Q.; Krishna, R.; Wei, Z. W.; Zhou, H. C. *Angew. Chem. Int. Edit.* **2012**, *51*, 7480.

(33) Ilinitch, O. M.; Fenelonov, V. B.; Lapkin, A. A.; Okkel, L. G.; Terskikh, V. V.; Zamaraev, K. I. *Micropor. Mesopor. Mat.* **1999**, *31*, 97.

(34) Carta, M.; Malpass-Evans, R.; Croad, M.; Rogan, Y.; Jansen, J. C.; Bernardo, P.; Bazzarelli, F.; McKeown, N. B. *Science* **2013**, *339*, 303.

(35) Budd, P. M.; Ghanem, B. S.; Makhseed, S.; McKeown, N. B.; Msayib, K. J.; Tattershall, C. E. *Chem. Commun.* **2004**, 230.

(36) McKeown, N. B. *J. Mater. Chem.* **2000**, *10*, 1979.

(37) Makhseed, S.; McKeown, N. B.; Msayib, K.; Bumajdad, A. *J. Mater. Chem.* **2005**, *15*, 1865.

(38) McKeown, N. B.; Makhseed, S.; Budd, P. M. *Chem. Commun.* **2002**, 2780.

(39) Budd, P. M.; Elabas, E. S.; Ghanem, B. S.; Makhseed, S.; McKeown, N. B.; Msayib, K. J.; Tattershall, C. E.; Wang, D. *Adv. Mater.* **2004**, *16*, 456.

(40) Song, J.; Du, N.; Dai, Y.; Robertson, G. P.; Guiver, M. D.; Thomas, S.; Pinnau, I. *Macromolecules* **2008**, *41*, 7411.

(41) Kricheldorf, H. R.; Fritsch, D.; Vakhtangishvili, L.; Lomadze, N.; Schwarz, G. *Macromolecules* **2006**, *39*, 4990.

(42) Kricheldorf, H. R.; Lomadze, N.; Fritsch, D.; Schwarz, G. *J. Polym. Sci. Polym. Chem.* **2006**, *44*, 5344.

(43) McKeown, N. B.; Hanif, S.; Msayib, K.; Tattershall, C. E.; Budd, P. M. *Chem. Commun.* **2002**, 2782.

(44) Budd, P. M.; Ghanem, B.; Msayib, K.; McKeown, N. B.; Tattershall, C. *J. Mater. Chem.* **2003**, *13*, 2721.

(45) McKeown, N. B.; Gahnem, B.; Msayib, K. J.; Budd, P. M.; Tattershall, C. E.; Mahmood, K.; Tan, S.; Book, D.; Langmi, H. W.; Walton, A. *Angew. Chem. Int. Ed.* **2006**, *45*, 1804.

(46) Ghanem, B. S.; Msayib, K. J.; McKeown, N. B.; Harris, K. D. M.; Pan, Z.; Budd, P. M.; Butler, A.; Selbie, J.; Book, D.; Walton, A. *Chem. Commun.* **2007**, 67.

(47) Ghanem, B. S.; Hashem, M.; Harris, K. D. M.; Msayib, K. J.; Xu, M. C.; Budd, P. M.; Chaukura, N.; Book, D.; Tedds, S.; Walton, A.; McKeown, N. B. *Macromolecules* **2010**, *43*, 5287.

(48) Maffei, A. V.; Budd, P. M.; McKeown, N. B. *Langmuir* **2006**, *22*, 4225.

(49) Ghanem, B. S.; McKeown, N. B.; Budd, P. M.; Fritsch, D. *Macromolecules* **2008**, *41*, 1640.

(50) Emmler, T.; Heinrich, K.; Fritsch, D.; Budd, P. M.; Chaukura, N.; Ehlers, D.; Ratzke, K.; Faupel, F. *Macromolecules* **2010**, *43*, 6075.

(51) Ghanem, B. S.; McKeown, N. B.; Budd, P. M.; Selbie, J. D.; Fritsch, D. *Adv. Mater.* **2008**, *20*, 2766.

(52) Ghanem, B. S.; McKeown, N. B.; Budd, P. M.; Al-Harbi, N. M.; Fritsch, D.; Heinrich, K.; Starannikova, L.; Tokarev, A.; Yampolskii, Y. *Macromolecules* **2009**, *42*, 7881.

(53) Weber, J.; Su, O.; Antonietti, M.; Thomas, A. *Macromol. Rapid Comm.* **2007**, *28*, 1871.

(54) Ma, X. H.; Swaidan, R.; Belmabkhout, Y.; Zhu, Y. H.; Litwiller, E.; Jouiad, M.; Pinnau, I.; Han, Y. *Macromolecules* **2012**, *45*, 3841.

(55) Budd, P. M.; McKeown, N. B.; Ghanem, B. S.; Msayib, K. J.; Fritsch, D.; Starannikova, L.; Belov, N.; Sanfirova, O.; Yampolskii, Y.; Shantarovich, V. *J. Membrane Sci.* **2008**, *325*, 851.

(56) Du, N. Y.; Robertson, G. P.; Pinnau, I.; Guiver, M. D. *Macromolecules* **2009**, *42*, 6023.

(57) Du, N. Y.; Robertson, G. P.; Song, J. S.; Pinnau, I.; Guiver, M. D. *Macromolecules* **2009**, *42*, 6038.

(58) Du, N. Y.; Robertson, G. P.; Pinnau, I.; Guiver, M. D. *Macromolecules* **2010**, *43*, 8580.

(59) Brunauer, S.; Emmett, P. H.; Teller, E. *J. Am. Chem. Soc.* **1938**, *60*.

(60) Sing, K. S. W.; Everett, D. H.; Haul, R. A. W.; Moscou, L.; Pierotti, R. A.; Rouquerol, J.; Siemieniewska, T. *Pure Appl. Chem.* **1985**, *57*, 603.

(61) Silverstein, M. S.; Cameron, N. R.; Hillmyer, M. A. *Porous Polymers*; John Wiley & Sons, Inc. **2011**.

(62) Davankov, V. A.; Rogozhin, S. V.; Tsyurupa, M. P.; *USSR Pat.* 299165, **1969**. US *Pat. 3729457*, **1973**. Chem. Abstr. **1971**, 75, 6841B.

(63) Davankov, V. A.; Tsyurupa, M. P. *Hypercrosslinked Polymeric Networks and Adsorbing Materials*; Elsevier, **2011**; Vol. 56.

(64) Davankov, V.; Sychov, C. S.; Ilyin, M. M.; Sochilina, K. O. *J. Chromatogr. A* **2003**, *987*, 67.

(65) Ahn, J.-H.; Jang, J.-E.; Oh, C.-G.; Ihm, S.-K.; Cortez, J.; Sherrington, D. C. *Macromolecules* **2006**, *39*, 627.

(66) Pastukhov, A. V.; Tsyurupa, M. P.; Davankov, V. A. *J. Polym. Sci. Polym. Phys.* **1999**, *37*, 2324.

(67) Germain, J.; Hradil, J.; Frechet, J. M. J.; Svec, F. *Chem. Mater.* **2006**, *18*, 4430.

(68) Lee, J.-Y.; Wood Colin, D.; Bradshaw, D.; Rosseinsky Matthew, J.; Cooper Andrew, I. *Chem. Commun.* **2006**, 2670.

(69) Tsyurupa, M. P.; Davankov, V. A. *React. Funct. Polym.* **2006**, *66*, 768.

(70) Wood, C. D.; Tan, B.; Trewin, A.; Niu, H.; Bradshaw, D.; Rosseinsky, M. J.; Khimyak, Y. Z.; Campbell, N. L.; Kirk, R.; Stoeckel, E.; Cooper, A. I. *Chem. Mater.* **2007**, *19*, 2034.

(71) Li, B. Y.; Gong, R. N.; Luo, Y. L.; Tan, B. E. *Soft. Matter.* **2011**, *7*, 10910.

(72) Luo, Y. L.; Li, B. Y.; Wang, W.; Wu, K. B.; Tan, B. *Adv. Mater.* **2012**, *24*, 5703.

(73) Germain, J.; Frechet, J. M. J.; Svec, F. *J. Mater. Chem.* **2007**, *17*, 4989.

(74) Davankov, V. A.; Rogozhin, S. V.; Tsyurupa, M. P. *Vysokomol. Soedin.* **1973**, *B15*, 95.

(75) Grassie, N.; Gilks, J. *J. Polym. Sci.: Polym. Chem. Ed.* **1973**, *11*, 1531.

(76) Krauss, D.; Popov, G.; Schwachula, G. *Plaste Kautsch.* **1979**, *26*, 214.

(77) Tsyurupa, M. P.; Lalaev, V. V.; Davankov, V. A. *Dokl. AN SSSR* **1984**, *279*, 156.

(78) Popov, G.; Krauss, D.; Feistel, L.; Schwachula, G. In *Patent DRR* 150218, **1981**.

(79) Veverka, P.; Jerabek, K. *React. Funct. Polym.* **1999**, *41*, 21.

(80) Veverka, P.; Jerabek, K. *React. Funct. Polym.* **2004**, *59*, 71.

(81) Turi, E. A. *Thermal Characterization of Polymeric Materials*; 2nd ed.; Academic Press, **1997**.

(82) Pascault, J. P.; Sautereau, H.; Verdu, J.; Williams, J. J. R. *Thermosetting Polymers*; Marcel Dekke, **2001**.

(83) Germain, J.; Frechet, J. M. J.; Svec, F. *Chem. Commun.* **2009**, 1526.

(84) Li, B. Y.; Gong, R. N.; Wang, W.; Huang, X.; Zhang, W.; Li, H. M.; Hu, C. X.; Tan, B. E. *Macromolecules* **2011**, *44*, 2410.

(85) Dawson, R.; Stevens, L. A.; Drage, T. C.; Snape, C. E.; Smith, M. W.; Adams, D. J.; Cooper, A. L. *J. Am. Chem. Soc.* **2012**, *134*, 10741.

(86) Dawson, R.; Ratvijitvech, T.; Corker, M.; Laybourn, A.; Khimyak, Y. Z.; Cooper, A. I.; Adams, D. J. *Polym. Chem-Uk* **2012**, *3*, 2034.

(87) Luo, Y. L.; Zhang, S. C.; Ma, Y. X.; Wang, W.; Tan, B. *Polym. Chem-Uk* **2013**, *4*, 1126.

(88) Cote, A. P.; Benin, A. I.; Ockwig, N. W.; O'Keeffe, M.; Matzger, A. J.; Yaghi, O. M. *Science* **2005**, *310*, 1166.

(89) Tilford, R. W.; Gemmill, W. R.; zur Loye, H. C.; Lavigne, J. J. *Chem. Mater.* **2006**, *18*, 5296.

(90) El-Kaderi, H. M.; Hunt, J. R.; Mendoza-Cortes, J. L.; Cote, A. P.; Taylor, R. E.; O'Keeffe, M.; Yaghi, O. M. *Science* **2007**, *316*, 268.

(91) Rowan, S. J.; Cantrill, S. J.; Cousins, G. R. L.; Sanders, J. K. M.; Stoddart, J. F. *Angew. Chem. Int. Ed.* **2002**, *41*, 898.

(92) Cote, A. P.; Benin, A. I.; Ockwig, N. W.; O'Keeffe, M.; Matzger, A. J.; Yaghi, O. M. *Science* **2005**, *310*, 1166.

(93) Tilford, R. W.; Mugavero, S. J.; Pellechia, P. J.; Lavigne, J. J. *Adv. Mater.* **2008**, *20*, 2741.

(94) Hunt, J. R.; Doonan, C. J.; LeVangie, J. D.; Cote, A. P.; Yaghi, O. M. *J. Am. Chem. Soc.* **2008**, *130*, 11872.

(95) Kuhn, P.; Antonietti, M.; Thomas, A. *Angew. Chem. Int. Ed.* **2008**, *47*, 3450.

(96) Uribe-Romo, F. J.; Hunt, J. R.; Furukawa, H.; Klock, C.; O'Keeffe, M.; Yaghi, O. M. *J. Am. Chem. Soc.* **2009**, *131*, 4570.

(97) Uribe-Romo, F. J.; Doonan, C. J.; Furukawa, H.; Oisaki, K.; Yaghi, O. M. *J. Am. Chem. Soc.* **2011**, *133*, 11478.

(98) Chen, L.; Honsho, Y.; Seki, S.; Jiang, D. L. *J. Am. Chem. Soc.* **2010**, *132*, 6742.

(99) Jiang, J. X.; Su, F.; Trewin, A.; Wood, C. D.; Campbell, N. L.; Niu, H.; Dickinson, C.; Ganin, A. Y.; Rosseinsky, M. J.; Khimyak, Y. Z.; Cooper, A. I. *Angew. Chem. Int. Ed.* **2007**, *46*, 8574.

(100) Jiang, J. X.; Su, F.; Trewin, A.; Wood, C. D.; Niu, H.; Jones, J. T. A.; Khimyak, Y. Z.; Cooper, A. I. *J. Am. Chem. Soc.* **2008**, *130*, 7710.

(101) Jiang, J. X.; Laybourn, A.; Clowes, R.; Khimyak, Y. Z.; Bacsa, J.; Higgins, S. J.; Adams, D. J.; Cooper, A. I. *Macromolecules* **2010**, *43*, 7577.

(102) Brandt, J.; Schmidt, J.; Thomas, A.; Epping, J. D.; Weber, J. *Polym. Chem-Uk* **2011**, *2*, 1950.

(103) Dawson, R.; Laybourn, A.; Clowes, R.; Khimyak, Y. Z.; Adams, D. J.; Cooper, A. I. *Macromolecules* **2009**, *42*, 8809.

(104) Ren, S.; Dawson, R.; Laybourn, A.; Jiang, J. X.; Khimyak, Y.; Adams, D. J.; Cooper, A. I. *Polym. Chem-Uk* **2012**, *3*, 928.

(105) Kiskan, B.; Weber, J. *ACS Macro Letters* **2012**, *1*, 37.

(106) Rouquerol, J.; Avnir, D.; Fairbridge, C. W.; Everett, D. H.; Haynes, J. H.; Pernicone, N.; Ramsay, J. D. F.; Sing, K. S. W.; Unger, K. K. *Pure Appl. Chem.* **1994**, *66*, 1739.

(107) Gregg, S. J.; Sing, K. S. W. *Adsorption, surface area, and porosity*; 2nd ed.; Academic Press, **1982**.

(108) Gregg, S. J.; Sing, K. S. W. *Adsorption, surface area, and porosity*; Academic Press, **1967**.

(109) Sing, K. S. W. *J. Porous Mat*. **1995**, *2*, 5.

(110) Sing, K. S. W. *Adv. Colloid Interf. Sci.* **1998**, *76*, 3.

(111) Sing, K. *Colloid Surf. A* **2001**, *187*, 3.

(112) Sing, K. S. W. *Colloid Surf. A* **2004**, *241*, 3.

(113) Rouquerol, F.; Rouquerol, J.; Sing, K. *Adsorption by Powders and Porous Solids: Principles, Methodology and Applications*; Academic Press, **1999**.

(114) Lowell, S.; Shields, J. E.; Thomas, M. A.; Thommes, M. *Characterization of Porous Solids and Poweders: Surface Area, Pore Size and Density*; Kluwer Academic Publishers, **2004**.

(115) Kaufmann, E. N., *Characterization of Materials*; 2nd ed.; John Wiley and Sons, **2012**.

(116) Thommes, M. *Chem. Ing. Tech.* **2010**, *82*, 1059.

(117) Rouquerol, J.; Avnir, D.; Fairbridge, C. W.; Everett, D. H.; Haynes, J. H.; Pernicone, N.; Ramsay, J. D. F.; Sing, K. S. W.; Unger, K. K. *Pure Appl. Chem.* **1994**, *66*, 1739.

(118) Mason, G. *P Roy. Soc. Lond. A Mat.* **1988**, *415*, 453.

(119) Burgess, C. G. V.; Everett, D. H.; Nuttall, S. *Pure Appl. Chem.* **1989**, *61*, 1845.

(120) Efremov, D. K.; Fenelonov, V. B. *React. Kinet. Catal. Lett.* **1989**, *40*, 177.

(121) Donohue, M. D.; Aranovich, G. L. *J. Colloid Interf. Sci.* **1998**, *205*, 121.

(122) Woo, H. J.; Sarkisov, L.; Monson, P. A. *Characterization of Porous Solids VI* **2002**, *144*, 155.

(123) Kikkinides, E. S.; Kainourgiakis, M. E.; Stubos, A. K. *Langmuir* **2003**, *19*, 3338.

(124) Ramirez, A.; Sierra, L.; Mesa, M.; Restrepo, J. *Chem. Eng. Sci.* **2005**, *60*, 4702.

(125) Rouquerol, J.; Llewellyn, P.; Rouquerol, F. *Stud. Surf. Sci. Catal.* **2007**, *160*, 49.

(126) Rouquerol, F.; Rouquerol, J.; Sing, K. *Adsorption by Powders and Porous Solids: Principles, Methodology and Applications*; Academic Press, **1998**.

(127) Hirscher, M. *Micropor. Mesopor. Mat.* **2010**, *135*, 209.

(128) Moellmer, J.; Celer, E. B.; Luebke, R.; Cairns, A. J.; Staudt, R.; Eddaoudi, M.; Thommes, M. *Micropor. Mesopor. Mat.* **2010**, *129*, 345.

(129) Barrett, E. P.; Joyner, L. G.; Halenda, P. P. *J. Am. Chem. Soc.* **1951**, *73*.

(130) Germain, J.; Frechet, J. M. J.; Svec, F. *Small* **2009**, *5*, 1098.

(131) Horvath, G.; Kawazoe, K. *J. Chem. Eng. Jpn.* **1983**, *16*, 470.

(132) Samios, S.; Stubos, A. K.; Kanellopoulos, N. K.; Cracknell, R. F.; Papadopoulos, G. K.; Nicholson, D. *Langmuir* **1997**, *13*, 2795.

(133) Lastoskie, C.; Gubbins, K. E.; Quirke, N. *Characterization of Porous Solids III* **1994**, *87*, 51.

(134) Ravikovitch, P. I.; Neimark, A. V. *Langmuir* **2002**, *18*, 1550.

(135) Ravikovitch, P. I.; Neimark, A. V. *J. Phys. Chem. B* **2001**, *105*, 6817.

(136) Ravikovitch, P. I.; Haller, G. L.; Neimark, A. V. *Adv. Colloid Interf. Sci.* **1998**, *76*, 203.

(137) Olivier, J. P. *Carbon* **1998**, *36*, 1469.

(138) Li, J. R.; Ma, Y. G.; McCarthy, M. C.; Sculley, J.; Yu, J. M.; Jeong, H. K.; Balbuena, P. B.; Zhou, H. C. *Coordin. Chem. Rev.* **2011**, *255*, 1791.

(139) Larsen, G. S.; Lin, P.; Hart, K. E.; Colina, C. M. *Macromolecules* **2011**, *44*, 6944.

(140) Garberoglio, G.; Skoulidas, A. I.; Johnson, J. K. *J. Phys. Chem. B* **2005**, *109*, 13094.

(141) Skoulidas, A. I.; Sholl, D. S. *J. Phys. Chem. B* **2005**, *109*, 15760.

(142) Babarao, R.; Jiang, J. W. *Langmuir* **2008**, *24*, 6270.

(143) Li, J. R.; Kuppler, R. J.; Zhou, H. C. *Chem. Soc. Rev.* **2009**, *38*, 1477.

(144) Yazaydin, A. O.; Snurr, R. Q.; Park, T. H.; Koh, K.; Liu, J.; LeVan, M. D.; Benin, A. I.; Jakubczak, P.; Lanuza, M.; Galloway, D. B.; Low, J. J.; Willis, R. R. *J. Am. Chem. Soc.* **2009**, *131*, 18198.

(145) Tafipolsky, M.; Amirjalayer, S.; Schmid, R. *Micropor. Mesopor. Mat.* **2010**, *129*, 304.

(146) Wilmer, C. E.; Snurr, R. Q. *Chem. Eng. J.* **2011**, *171*, 775.

(147) Getman, R. B.; Bae, Y. S.; Wilmer, C. E.; Snurr, R. Q. *Chem. Rev.* **2012**, *112*, 703.

(148) Numaguchi, R.; Tanaka, H.; Watanabe, S.; Miyahara, M. T. *J. Chem. Phys.* **2013**, *138*.

(149) Yang, Q. Y.; Zhong, C. L. *Langmuir* **2009**, *25*, 2302.

(150) Srepusharawoot, P.; Scheicher, R. H.; Araujo, C. M.; Blomqvist, A.; Pinsook, U.; Ahuja, R. *J. Phys. Chem. C* **2009**, *113*, 8498.

(151) Han, S. S.; Mendoza-Cortes, J. L.; Goddard, W. A. *Chem. Soc. Rev.* **2009**, *38*, 1460.

(152) Lan, J. H.; Cao, D. P.; Wang, W. C.; Smit, B. *ACS Nano* **2010**, *4*, 4225.

(153) Assfour, B.; Seifert, G. *Chem. Phys. Lett.* **2010**, *489*, 86.

(154) Keskin, S. *J. Phys. Chem. C* **2012**, *116*, 1772.

(155) Mendoza-Cortes, J. L.; Pascal, T. A.; Goddard, W. A. *J. Phys. Chem. A* **2011**, *115*, 13852.

(156) Krishna, R.; van Baten, J. M. *Ind. Eng. Chem. Res.* **2011**, *50*, 7083.

(157) Garberoglio, G. *Langmuir* **2007**, *23*, 12154.

(158) Babarao, R.; Jiang, J. W. *Energ. Environ. Sci.* **2008**, *1*, 139.

(159) Han, S. S.; Furukawa, H.; Yaghi, O. M.; Goddard, W. A. *J. Am. Chem. Soc.* **2008**, *130*, 11580.

(160) Assfour, B.; Seifert, G. *Micropor. Mesopor. Mat.* **2010**, *133*, 59.

(161) Mendoza-Cortes, J. L.; Han, S. S.; Furukawa, H.; Yaghi, O. M.; Goddard, W. A. *J. Phys. Chem. A* **2010**, *114*, 10824.

(162) Liu, Y. H.; Liu, D. H.; Yang, Q. Y.; Zhong, C. L.; Mi, J. G. *Ind. Eng. Chem. Res.* **2010**, *49*, 2902.

(163) Ben, T.; Qiu, S. L. *CrystEngComm* **2013**, *15*, 17.

(164) Abbott, L. J.; Colina, C. M. *Macromolecules* **2011**, *44*, 4511.

(165) Cuthbert, T. R.; Wagner, N. J.; Paulaitis, M. E. *Macromolecules* **1997**, *30*, 3058.

(166) Lyulin, A. V.; Balabaev, N. K.; Mazo, M. A.; Michels, M. A. J. *Macromolecules* **2004**, *37*, 8785.

(167) Neyertz, S.; Brown, D. *Macromolecules* **2009**, *42*, 8521.

(168) Arnold, J. C. *Eur. Polym. J.* **2010**, *46*, 1131.

(169) Fang, W. J.; Zhang, L. L.; Jiang, J. W. *Mol. Simulat.* **2010**, *36*, 992.

(170) Pandiyan, S.; Brown, D.; Neyertz, S.; van der Vegt, N. F. A. *Macromolecules* **2010**, *43*, 2605.

(171) Fang, W. J.; Zhang, L. L.; Jiang, J. W. *J. Phys. Chem. C* **2011**, *115*, 14123.

(172) Mason, C. R.; Maynard-Atem, L.; Al-Harbi, N. M.; Budd, P. M.; Bernardo, P.; Bazzarelli, F.; Clarizia, G.; Jansen, J. C. *Macromolecules* **2011**, *44*, 6471.

(173) Ferrante, F.; Lo Celso, F.; Duca, D. *Colloid Polym. Sci.* **2012**, *290*, 1443.

(174) Holck, O.; Bohning, M.; Heuchel, M.; Siegert, M. R.; Hofmann, D. *J. Membrane Sci.* **2013**, *428*, 523.

(175) Abbott, L. J.; Hart, K. E.; Colina, C. M. *Theor. Chem. Acc.* **2013**, *132*, 1.

(176) Wood, C. D.; Tan, B.; Trewin, A.; Su, F.; Rosseinsky, M. J.; Bradshaw, D.; Sun, Y.; Zhou, L.; Cooper, A. I. *Adv. Mater.* **2008**, *20*, 1916.

(177) Hart, K. E.; Abbott, L. J.; Colina, C. M. *Mol. Simul.* **2012**, *39*, 397.

(178) van den Berg, A. W. C.; Arean, C. O. *Chem. Commun.* **2008**, 668.

(179) Targets for Onboard Hydrogen Storage Systems for Light-Duty Vehicles, *US Department of Energy,* **2009**. http://www1.eere.energy.gov/hydrogenandfuelcells/storage/pdfs/targets_onboard_hydro_storage_explanation.pdf.

(180) Arean, C. O.; Bonelli, B.; Delgado, M. R.; Garrone, E. *Turk. J. Chem.* **2009**, *33*, 599.

(181) Bhatia, S. K.; Myers, A. L. *Langmuir* **2006**, *22*, 1688.

(182) Buda, C.; Dunietz, B. D. *J. Phys. Chem. B* **2006**, *110*, 10479.

(183) Rowsell, J. L. C.; Eckert, J.; Yaghi, O. M. *J. Am. Chem. Soc*. **2005**, *127*, 14904.

(184) Lochan, R. C.; Head-Gordon, M. *Phys. Chem. Chem. Phys.* **2006**, *8*, 1357.

(185) Germain, J.; Svec, F.; Frechet, J. M. J. *Chem. Mater.* **2008**, *20*, 7069.

(186) McKeown, N. B.; Budd, P. M.; Book, D. *Macromol. Rapid Comm.* **2007**, *28*, 995.

(187) Budd, P. M.; Butler, A.; Selbie, J.; Mahmood, K.; McKeown, N. B.; Ghanem, B.; Msayib, K.; Book, D.; Walton, A. *Phys. Chem. Chem. Phys.* **2007**, *9*, 1802.

(188) Weber, J.; Antonietti, M.; Thomas, A. *Macromolecules* **2008**, *41*, 2880.

(189) Furukawa, H.; Yaghi, O. M. *J. Am. Chem. Soc.* **2009**, *131*, 8875.

(190) Han, S. S.; Furukawa, H.; Yaghi, O. M.; Goddard, W. A., III *J. Am. Chem. Soc.* **2008**, *130*, 11580.

(191) Lu, W. G.; Yuan, D. Q.; Zhao, D.; Schilling, C. I.; Plietzsch, O.; Muller, T.; Brase, S.; Guenther, J.; Blumel, J.; Krishna, R.; Li, Z.; Zhou, H. C. *Chem. Mater.* **2010**, *22*, 5964.

(192) *IPCC Special Report on Carbon Dioxide Capture and Storage*, **2005**. In http://www.ipcc.ch/pdf/special-reports/srccs/srccs_wholereport.pdf.

(193) *Carbon Dioxide Capture and Storage RD&D Roadmap*, National Energy Technology Laboratory, Department of Energy, **2010**.

(194) Stauffer, P. H.; Keating, G. N.; Middleton, R. S.; Viswanathan, H. S.; Berchtod, K. A.; Singh, R. P.; Pawar, R. J.; Mancino, A. *Environ. Sci. Technol.* **2011**, *45*, 8597.

(195) Mondal, M. K.; Balsora, H. K.; Varshney, P. *Energy* **2012**, *46*, 431.

(196) Rochelle, G. T. *Science* **2009**, *325*, 1652.

(197) D'alessandro, D. M.; McDonald, T. *Pure Appl. Chem.* **2011**, *83*, 57.

(198) D'alessandro, D. M.; Smit, B.; Long, J. R. *Angew. Chem. Int. Ed.* **2010**, *49*, 6058.

(199) Olajire, A. A. *Energy* **2010**, *35*, 2610.

(200) Samanta, A.; Zhao, A.; Shimizu, G. K. H.; Sarkar, P.; Gupta, R. *Ind. Eng. Chem. Res.* **2012**, *51*, 1438.

(201) Wang, Q. A.; Luo, J. Z.; Zhong, Z. Y.; Borgna, A. *Energ. Environ. Sci.* **2011**, *4*, 42.

(202) Dawson, R.; Adams, D. J.; Cooper, A. I. *Chem. Sci*. **2011**, *2*, 1173.

(203) Drage, T. C.; Snape, C. E.; Stevens, L. A.; Wood, J.; Wang, J. W.; Cooper, A. I.; Dawson, R.; Guo, X.; Satterley, C.; Irons, R. *J. Mater. Chem.* **2012**, *22*, 2815.

(204) Su, F. S.; Lu, C. S.; Cnen, W. F.; Bai, H. L.; Hwang, J. F. *Sci. Total Environ.* **2009**, *407*, 3017.

(205) Plaza, M. G.; Pevida, C.; Arenillas, A.; Rubiera, F.; Pis, J. J. *Fuel* **2007**, *86*, 2204.

(206) Pevida, C.; Plaza, M. G.; Arias, B.; Fermoso, J.; Rubiera, F.; Pis, J. J. *Appl. Surf. Sci.* **2008**, *254*, 7165.

(207) Phan, A.; Doonan, C. J.; Uribe-Romo, F. J.; Knobler, C. B.; O'Keeffe, M.; Yaghi, O. M. *Acc. Chem. Res.* **2010**, *43*, 58.

(208) Xiao, P.; Zhang, J.; Webley, P.; Li, G.; Singh, R.; Todd, R. *Adsorption* **2008**, *14*, 575.

(209) Zhang, J.; Singh, R.; Webley, P. A. *Micropor. Mesopor. Mat.* **2008**, *111*, 478.

(210) Ebner, A. D.; Gray, M. L.; Chisholm, N. G.; Black, Q. T.; Mumford, D. D.; Nicholson, M. A.; Ritter, J. A. *Ind. Eng. Chem. Res.* **2011**, *50*, 5634.

(211) Song, C. S.; Xu, X. C.; Andresen, J. M.; Miller, B. G.; Scaroni, A. W. *Stud. Surf. Sci. Catal.* **2004**, *153*, 411.

(212) Song, C. S.; Xu, X. C.; Andresen, J. M.; Miller, B. G.; Scaroni, A. W. *Micropor. Mesopor. Mat.* **2003**, *62*, 29.

(213) Xu, X. C.; Andresen, J. M.; Song, C. S.; Miller, B. G.; Scaroni, A. W. *Abstr. Pap. Am. Chem. Soc.* **2002**, *223*, U573.

(214) Zhao, H. L.; Hu, J.; Wang, J. J.; Zhou, L. H.; Liu, H. L. *Acta. Phys-Chim Sin.* **2007**, *23*, 801.

(215) Sumida, K.; Rogow, D. L.; Mason, J. A.; McDonald, T. M.; Bloch, E. D.; Herm, Z. R.; Bae, T. H.; Long, J. R. *Chem. Rev.* **2012**, *112*, 724.

(216) Britt, D.; Furukawa, H.; Wang, B.; Glover, T. G.; Yaghi, O. M. *Proc. Natl. Acad. Sci. USA* **2009**, *106*, 20637.

(217) Demessence, A.; D'Alessandro, D. M.; Foo, M. L.; Long, J. R. *J. Am. Chem. Soc.* **2009**, *131*, 8784.

(218) Liu, J.; Thallapally, P. K.; McGrail, B. P.; Brown, D. R.; Liu, J. *Chem. Soc. Rev.* **2012**, *41*, 2308.

(219) Xiang, Z. H.; Zhou, X.; Zhou, C. H.; Zhong, S.; He, X.; Qin, C. P.; Cao, D. P. *J. Mater. Chem.* **2012**, *22*, 22663.

(220) Ruthven, D. M. *Principles of Adsorption and Adsorption Processes*; Wiley, **1984**.

(221) Myers, A. L.; Prausnitz, J. M. *AIChE J.* **1965**, *11*, 121.

(222) Lu, W. G.; Yuan, D. Q.; Sculley, J. L.; Zhao, D.; Krishna, R.; Zhou, H. C. *J. Am. Chem. Soc.* **2011**, *133*, 18126.

(223) Martin, C. F.; Stockel, E.; Clowes, R.; Adams, D. J.; Cooper, A. I.; Pis, J. J.; Rubiera, F.; Pevida, C. *J. Mater. Chem.* **2011**, *21*, 5475.

(224) Robeson, L. M. *J. Membrane Sci.* **1991**, *62*, 165.

(225) Robeson, L. M. *J. Membrane Sci.* **2008**, *320*, 390.

(226) Bernardo, P.; Drioli, E.; Golemme, G. *Ind. Eng. Chem. Res.* **2009**, *48*, 4638.

(227) Guiver, M. D.; Lee, Y. M. *Science* **2013**, *339*, 284.

(228) Freeman, B. D. *Macromolecules* **1999**, *32*, 375.

(229) Sanders, D. F.; Smith, Z. P.; Guo, R.; Robeson, L. M.; McGrath, J. E.; Paul, D. R.; Freeman, B. D. Energy Efficient Polymeric Gas Separation Membranes for a Sustainable Future: A Review, *Polymer* **2013**, DOI: 10.1016/j.polymer.2013.05.075.

(230) Du, N. Y.; Robertson, G. P.; Song, J. S.; Pinnau, I.; Thomas, S.; Guiver, M. D. *Macromolecules* **2008**, *41*, 9656.

(231) Staiger, C. L.; Pas, S. J.; Hill, A. J.; Cornelius, C. J. *Chem. Mater.* **2008**, *20*, 2606.

(232) Bezzu, C. G.; Carta, M.; Tonkins, A.; Jansen, J. C.; Bernardo, P.; Bazzarelli, F.; McKeown, N. B. *Adv. Mater.* **2012**, *24*, 5930.

(233) Du, N. Y.; Park, H. B.; Robertson, G. P.; Dal-Cin, M. M.; Visser, T.; Scoles, L.; Guiver, M. D. *Nat. Mater.* **2011**, *10*, 372.

(234) Guiver, M. D.; Du, N. Y.; Song, J. S.; Robertson, G. P.; Pinnau, I.; Thomas, S. *Abstr. Pap. Am. Chem. Soc.* **2009**, *237*.

(235) Budd, P. M.; Msayib, K. J.; Tattershall, C. E.; Ghanem, B. S.; Reynolds, K. J.; McKeown, N. B.; Fritsch, D. *J. Membrane Sci.* **2005**, *251*, 263.

(236) Doonan, C. J.; Tranchemontagne, D. J.; Glover, T. G.; Hunt, J. R.; Yaghi, O. M. *Nat. Chem.* **2010**, *2*, 235.

Chapter 2. Nanoporous Structure of Semirigid Alternating Copolymers via Nitrogen Sorption and Molecular Simulation

2.1. Manuscript Published in Macromolecules

(Xu Zhou, Yi Li, Kyle E. Hart, Lauren J. Abbott, Zhixing Lin, Frantisek Svec, Coray M. Colina, and S. Richard Turner; *Macromolecules* **2013**, *46*, 5968. Adapted with permission. Copyright 2013 American Chemical Society.)

2.1.1. Abstract

Surface area and porosity of a series of semirigid alternating copolymers consisting of *tert*-butyl carboxylate-functionalized stilbene or *tert*-butyl carboxylate-functionalized styrene, and maleic anhydride or *tert*-butyl carboxylate-functionalized *N*-phenylmaleimide were investigated using nitrogen adsorption/desorption isotherms at 77 K and atomistic molecular simulations. Surface areas from experiments using the Brunauer-Emmett-Teller (BET) theory and geometric surface areas of molecular simulations show good correlation. It is shown here that the stilbene copolymers have higher surface areas than their styrene analogues. It is also found that BET surface areas increase as the persistence length (chain stiffness) increases for these alternating copolymers.

2.1.2. Introduction

Nanoporous organic polymers are a class of materials with pore sizes in the range of 1-100 nm.[1,2] They have numerous applications in separation media and are proposed for use as gas storage materials.[3-6] Three major subclasses of nanoporous organic polymers include hyper-

cross-linked polymers (HCPs) introduced by Davankov et al.,[7,8] networked polymer frameworks (e.g., covalent organic frameworks (COFs),[9,10] conjugated microporous polymers (CMPs),[11,12] porous organic polymers (POPs),[13,14] porous aromatic frameworks (PAFs)),[15,16] and linear polymers of intrinsic microporosity (PIMs) developed by McKeown and Budd.[17-19] The primary difference among these three classes of nanoporous materials is how the porosity is formed within the materials, where the pore volume is either formed as a result of the solvent, networked 3-dimensionality with rigid spacers, or inefficiently packed linear chains, which correspond to HCPs, networked polymer frameworks, and PIMs, respectively.

We have found that radically prepared sterically congested stilbene containing alternating copolymers manifest unique properties because of the steric crowding along the backbone.[20-26] Tolerance of radical polymerization to functional groups makes it possible to incorporate highly functional monomers with controlled density of functionality into the polymer backbones. These copolymers have excellent thermal stability as evidenced by no thermal decompositions below 350 ºC in TGA experiments and no observable glass transition temperatures in DSC experiments.[20] The steric crowding of extra phenyl groups from the enchained stilbene units yields interesting optical properties.[24]

A series of *tert*-butyl carboxylate group containing stilbene and styrenic alternating copolymers was synthesized and their chain stiffnesses were studied by small-angle X-ray scattering (SAXS) and size exclusion chromatography (SEC).[25,26] Persistence length data, which are indicative of chain stiffness, show these copolymers are semirigid. Persistence length measurements also indicate that the added phenyl group enhances chain stiffness in the backbone of the polymer.[26]

In this study, we expand the concept of PIMs to stilbene and styrenic alternating copolymers. Porous properties of these copolymers were explored using gas sorption measurements and molecular simulations. Increasing steric crowding leads to inefficient chain packing and consequently increases surface area. Moreover, we have found that the surface areas of these alternating copolymers increase as persistence length (chain stiffness) increases, providing quantitative evidence of the effect of chain rigidity on porosity in PIMs type materials.

2.1.3. Experimental Section

Materials. *tert*-Butyl carboxylate group containing alternating copolymers were synthesized and characterized, as previously reported, and their chemical structures are shown in **Figure 2-1**.[25] Preparation, molecular weights, and thermal properties of copolymer I-IV and polystyrene (PS) are reported in the Supporting Information (see **§2.2**).

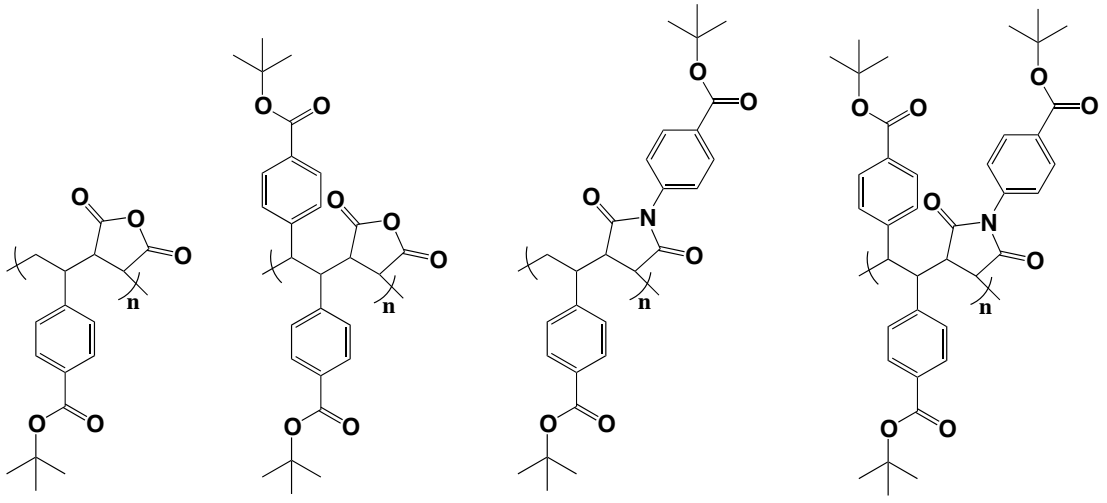

Copolymer I **Copolymer II** **Copolymer III** **Copolymer IV**

Figure 2-1. Chemical structures of copolymer I, II, III, and IV.[25]

Instrumentation. The surface areas were calculated using the Brunauer-Emmett-Teller (BET) equation and data from nitrogen adsorption/desorption isotherms at 77 K obtained with a TriStar II 3020 surface area analyzer (Micromeritics, Norcross, GA). Approximately 0.5 g of sample was used. Prior to analysis, the samples were heated at elevated temperature (55 °C for PS, 140 °C for copolymers) under N_2 overnight.

Simulation Method. The simulation models of all polymers in this work were generated using the open source *Polymatic* simulated polymerization code.[27,28] By this approach, polymer chains were generated by artificially bonding together repeat units within a periodic simulation cell using the polymer consistent force field,[29] with specialized charges calculated from a restrained electrostatic potential charge fitting procedure from ab initio calculations at the HF/6-31G* level of theory. The repeat units were designed in such a way that the resulting polymer was accurate but did not necessarily mimic the synthetic route. Bonds were formed in cycles along with energy minimization and molecular dynamics steps performed in LAMMPS[30,31] to produce a well-relaxed initial structure of the polymeric materials at a low density. After the simulated polymerization, the structures were compressed and equilibrated using a 21-step molecular dynamics protocol,[27,32] which has been utilized for effective structure generation of a wide variety of amorphous materials.[33-35] Simulations of polystyrene were taken from previous work,[27] which were generated using the same approach as was taken for the copolymer presented here, and the porosity is examined here for comparison. All properties were calculated as the average and standard deviation of five independently generated simulation samples. Further simulation details can be found in the Supporting Information.

2.1.4. Results and Discussion

Surface Area and Porosity Characterization. Polystyrene (PS) and alternating copolymers were characterized by nitrogen sorption measurements at 77 K. According to the classification given by the International Union of Pure and Applied Chemistry (IUPAC), nitrogen sorption isotherms of copolymers I-IV (**Figure 2-2**) are type III isotherms.[36] Surface areas were calculated using the Brunauer-Emmett-Teller (BET) equation.[37] The relative pressure (P/P_0) range for the linear region in the BET plot was kept between 0.05 and 0.2 according to the recommendations for microporous samples.[38] The relative pressure range was chosen such that (a) the intercept of the straight portion is positive, (b) the C value is positive, (c) the term $n^a(P/P_0)$ increases with P/P_0.

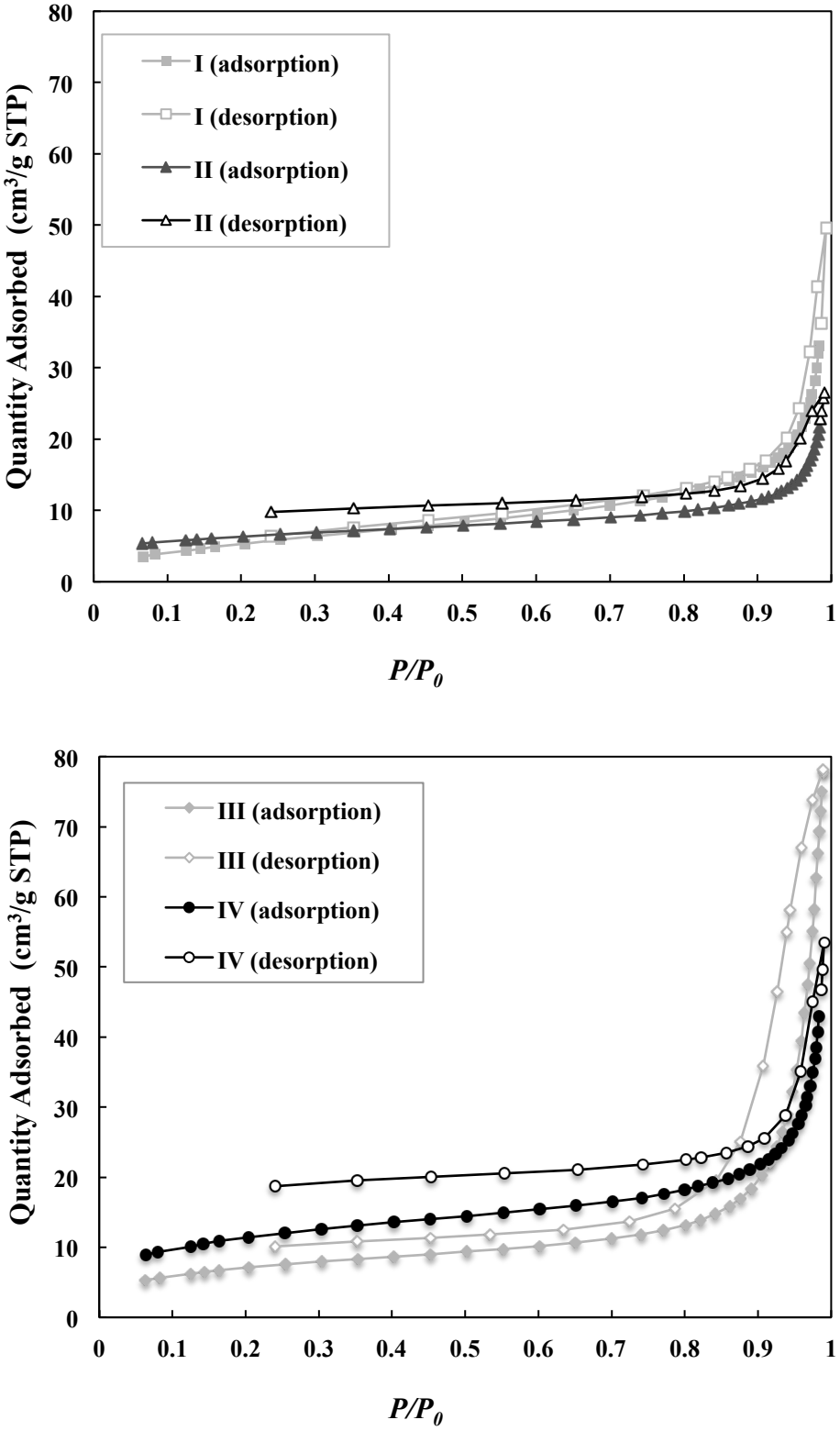

Figure 2-2. Nitrogen adsorption/desorption isotherms for copolymers I, II, III, and IV.

In addition, PS and the four copolymers were simulated. Once a simulated sample was generated from the knowledge of only the chemical repeat unit, i.e. **Figure 2-1**, using the available *Polymatic* simulated polymerization algorithm,[27,28] the pore topology of the polymer was measured. The surface areas of the simulated samples were measured by systematically rolling a N_2-sized probe molecule (d = 3.681 Å) over the van der Waals surface of all the framework atoms; the surface outlined by the center of the probe not overlapping any atom of the polymer matrix is referred to as the geometrically accessible surface area.[39-41] An example of simulated copolymer IV is shown in **Figure 2-3** highlighting the polymer backbone and void volume present.

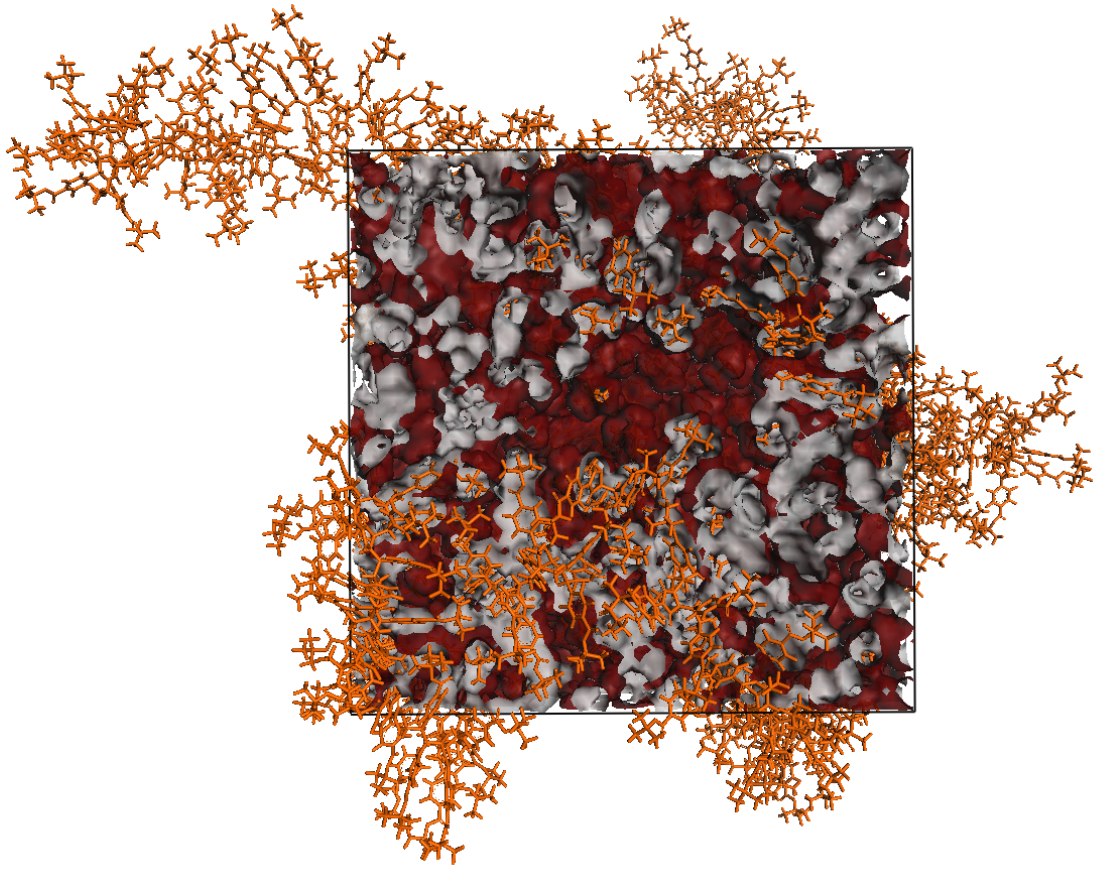

Figure 2-3. A simulation box of copolymer IV illustrating the polymer framework (orange) and pore volume (maroon).

The results of the nitrogen sorption measurements and molecular simulations are summarized in **Table 2-1**. The experimental BET surface areas of PS and the alternating copolymers are in the range of 9-41 m^2/g while geometric surface areas from simulations are from 11 to 91 m^2/g. Although, it has been recently shown that geometric surface areas and BET surface areas may not yield equivalent absolute values for intrinsically microporous materials,[33] it is shown here that there is a good correlation in the trends between the simulated and experimental measured surface areas.

For microporosity, the values obtained from experiments (SA_{exp}, V_p^{exp}) and simulations (SA_{sim}, V_p^{sim}) are slightly different. This is because experiments and simulations are measuring two fundamentally different concepts of porosity. In the experiments, the volume of nitrogen adsorbed is used to determine the amount of microporosity accessible to the gas, either pore volume or surface area. As a result, the calculated pore volume and surface area are inherently connected to the process of adsorbing and the implications entailed. Thus, the experiments are calculating the apparent porosity that is present during adsorption. In the atomistic simulations, porosity is calculated from the amount of unoccupied volume, which is inherently created by the glassy nature of the polymer. A polymer sample will have porosity present as a result of only the molecular structure and polymer packing arrangement. Therefore, simulations are characterizing the intrinsic microporosity of the polymer sample.

In general, according to both experimental and simulated values of porosity, stilbene containing copolymers have higher surface areas than styrenic copolymers as shown by comparing the surface area of copolymer II to its analogue, copolymer I, or copolymer IV to its analogue, copolymer III. Moreover, copolymers with maleimide units have higher surface area than their analogues containing maleic anhydride units, by comparing surface area of copolymer

III to copolymer I, or copolymer IV to copolymer II. Similar trends are observed in experimental and simulated micropore volumes of these alternating copolymers. Therefore, steric crowding of the polymer backbone by introducing extra phenyl rings and/or *N*-phenyl-substituted maleimide units was found to increase the surface area and the micropore volume of these alternating copolymers.

Table 2-1. Persistence length and porous properties of PS and copolymers I-IV from experiments and simulations.

Polymer	l_p (nm)[a]	SA_{exp}[b] (m^2/g)	SA_{sim} (m^2/g)	V_p^{exp}[c] (cm^3/g)	V_p^{sim}[d] (cm^3/g)	FFV[e] (%)	$V_p^{exp, total}$[f] (cm^3/g)	P_{bulk}[g] (g/cm^3)
PS	0.9[42]	8.8±0.1	5±2	0.0035	0.0022	15.0±0.7	0.0114	0.977±0.008
Copolymer I	2.6	20.9±0.3	18±6	0.0076	0.0080	14.3±0.3	0.0463	1.162±0.004
Copolymer II	3.0	22.2±0.2	44±26	0.0094	0.0163	16.6±0.4	0.0302	1.100±0.004
Copolymer III	4.3	26.0±0.2	51±32	0.0104	0.0181	17.2±1.1	0.0971	1.074±0.015
Copolymer IV	6.1	41.1±0.3	9 ±15	0.0168	0.0386	19.3±0.3	0.0596	1.039±0.005

[a]From Li et al.[26]; [b]Error bars represent deviation from fitting linear region in the BET calculation. [c]Microporosity can be estimated from gas uptake at low relative pressure ($P/P_0 < 0.2$) in adsorption isotherm.[43] Here, nitrogen uptakes at $P/P_0 = 0.16$ were used to determine micropore volumes; [d]The V_p^{sim} reported is a geometric measure of the amount of void space which is larger than that of a nitrogen-molecule-sized probe ($2^{1/6}\sigma_{N2}$; σ_{N2} = 3.681 Å), calculated as the integral of the PSD function of all larger probe sizes; [e]The fractional free volume (FFV) = $1 - 1.3\ V_w/V_{sp}$, where the specific volume (V_{sp}) is the reciprocal bulk density, and the van der Waals volume (V_w) is the total amount of volume occupied by the van der Waals spheres of the polymer in the simulated samples; [f]Total pore volumes were determined from nitrogen adsorption isotherm at P/P_0=0.98. [g]The bulk density (ρ_{bulk}) is determined as the density of the simulated sample including all pore volume.

Correlation Between Porosity and Chain Stiffness. In order to probe the effect of chain stiffness on the porosity of these polymers, surface areas and micropore volumes of PS and copolymers I-IV were compared with their persistence length data.[26,42] **Figure 2-4** illustrates that both surface area and micropore volume increase as a function of increasing persistence length. We used the persistence length data from SEC for comparison, but persistence lengths from SAXS also give similar results. These semirigid alternating copolymers do not pack well in the solid state, exemplified by the absence of melting points observed in previous studies.[25] The increase in chain stiffness confirmed by SAXS and SEC measurements due to anhydride/maleimide groups and the steric crowding of the extra phenyl groups from the stilbene comonomers leads to the frustration of chain packing, and thus results in nanopore formation.

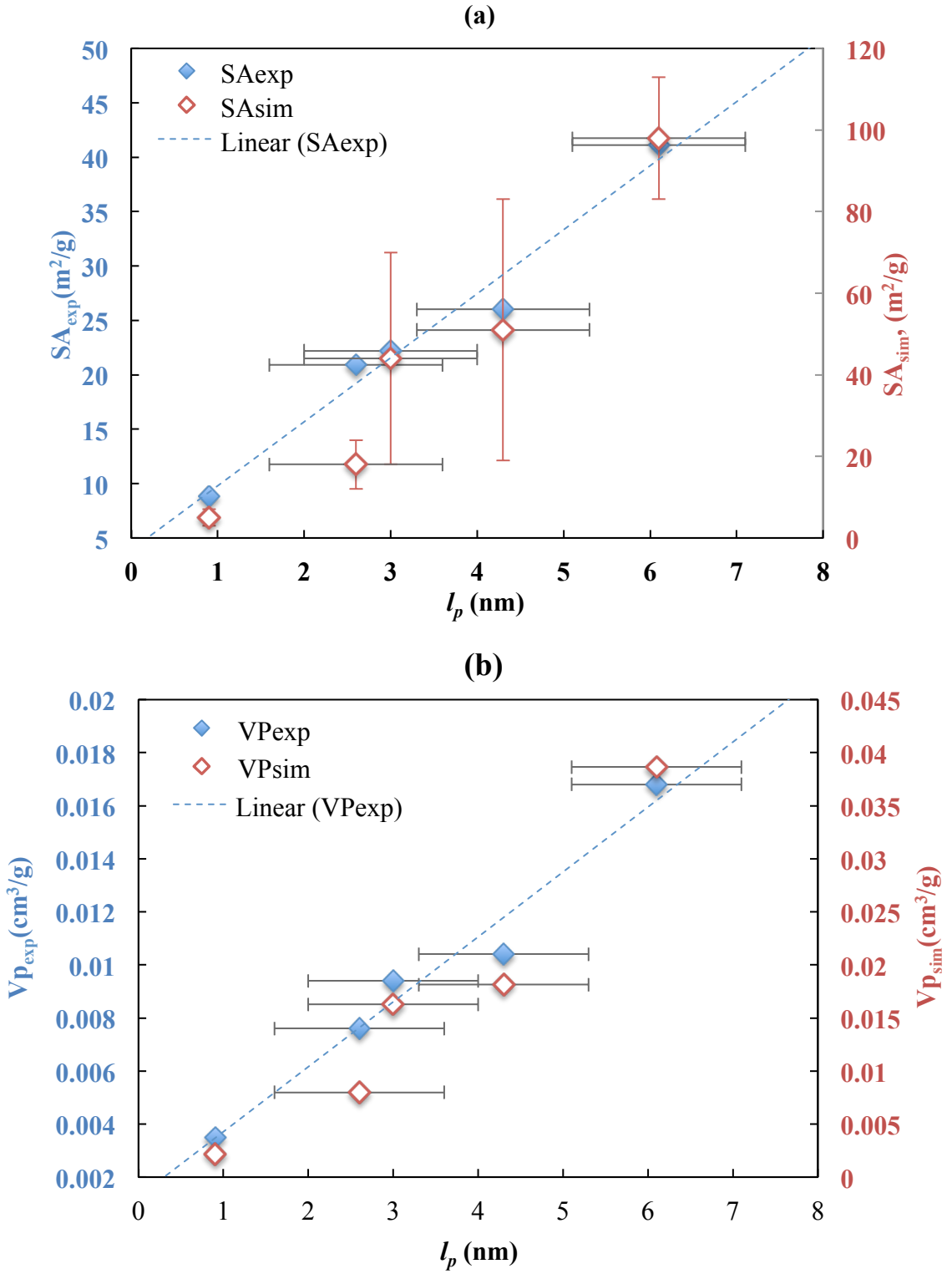

Figure 2-4. Surface area (a) and micropore volume (b) as a function of SEC persistence length for both experiments and simulations with best fit line.

A continuing increase in gas uptake with increasing relative pressure was observed in all of the isotherms of the polymers studied here (PS in **Figure 2-6**, Supporting Information, and I-IV in **Figure 2-2**). However, low-pressure hysteresis, which is the lack of convergence of the adsorption and desorption branches at low relative pressures ($P/P_0 < 0.4$), was only observed in the more rigid copolymers (II-IV). These two features are common in low-temperature nitrogen isotherms of PIMs and are possibly associated with "swelling" effects due to the dissolution of gas into the polymer matrix, which can lead to microstructural changes during the sorption process (i.e., sorption-induced plasticization).[36,44-46] The dissolution process can be described in terms of the dual mode sorption model used for gas sorption in membranes. First, there is gas filling of micropores in the polymeric materials followed by swelling of the polymer as gas pressure increases (Henry sorption).[45,47] By comparing the amount of nitrogen adsorbed and desorbed in the polymers at low relative pressure, the degree of hysteresis was found to be similar for copolymers II and III, but distinctly higher for copolymer IV, while no low-pressure hysteresis was observed in PS or copolymer I. As such, the amount of low-pressure hysteresis correlates well with the calculated persistence length of these polymers. This gives valuable insight into the behavior of the polymers during adsorption. Initially, all polymers exhibited Henry sorption and thus displayed some degree of swelling. However, PS and copolymer I, which did not exhibit low pressure hysteresis, swelled only reversibly. On the other hand, the more rigid copolymers underwent sorption-induced plasticization of the matrix, through which the amount of available porosity increased and resulted in a higher desorption capacity.

Additionally, the atomistic detail of the molecular simulations allows for further insight into the pore size distribution (PSD) of the apparent porosity.[48] The PSD calculations of the atomistic simulated samples were carried out using the Poreblazer code,[41] which calculates the fraction of

pore volume that can be covered by spherical probes of radius r or smaller, $V_p(r)$. The numerical derivative, $-dV_p(r)/dr$, is the PSD function and is shown in **Figure 2-5** for PS and copolymers I-IV. As noted previously, the simulations are able to capture the intrinsic microporosity of the system, and **Figure 2-5** illustrates that a significant amount of void volume is inaccessible to a nitrogen molecule. In addition, it is shown that the distribution of void volume and the apparent pore volume, which is calculated as the area under the curve past a specific probe diameter, increases as the persistence length of the copolymer increases. As such, copolymer IV, which has the longest persistence length, also has the highest amount of pore volume and a higher distribution of volume accessible to an adsorbing nitrogen molecule. It seems that as the persistence length increases from copolymer I to copolymer IV, the PSD also shifts to slightly larger pores, but all copolymers have substantial void volume accessible only to probe sizes smaller than 2 Å. It is important to note that these PSDs are of snapshots of a polymer without absorbed gas near mechanical equilibrium. The PSD curve of the experimental sample during adsorption could be shifted to larger probe sizes due to local elastic dilations making most of the total free volume accessible to the adsorbing nitrogen molecules. However, the simulations presented here give insight on the intrinsic differences of the materials porosity before the adsorption occurs.

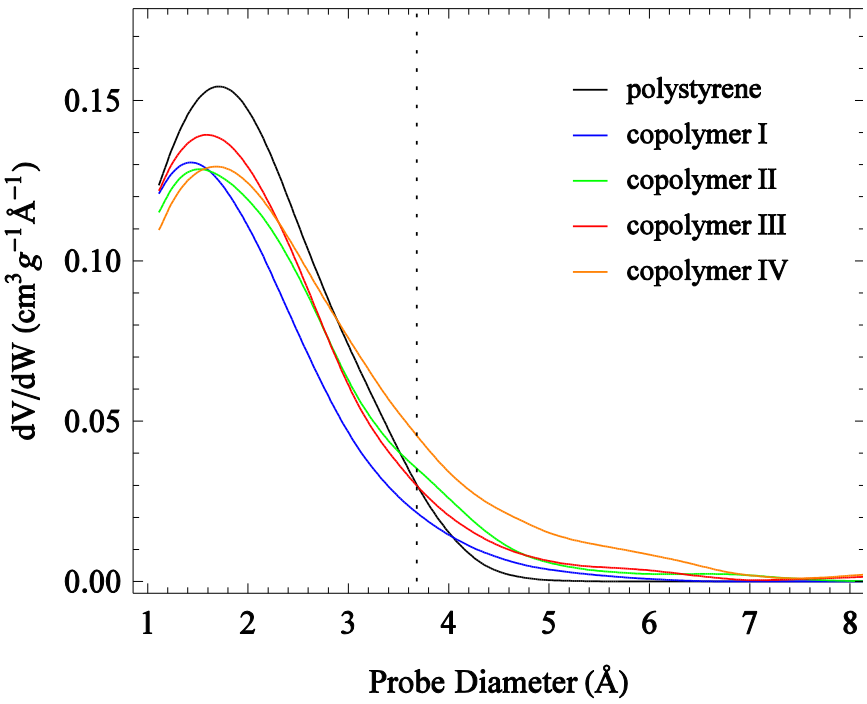

Figure 2-5. Pore size distribution of the molecular simulations of polystyrene (black), copolymer I (blue), copolymer II (green), copolymer III (red), and copolymer IV (orange) and the probe diameter of a nitrogen molecule (dashed).

2.1.5. Summary

In this study, semirigid alternating copolymers consisting of *tert*-butyl carboxylate-functionalized stilbene or *tert*-butyl carboxylate-functionalized styrene, and maleic anhydride or *tert*-butyl carboxylate-functionalized *N*- phenylmaleimide were found to have BET surface areas in the range of 20-40 m^2/g. Surface areas of these alternating copolymers were increased by the sterical crowding of the polymer backbones as the result of introducing extra phenyl rings and/or *N*-phenyl-substituted maleimide units. Geometric surface areas obtained from molecular simulations showed similar trends as observed in BET surface area measurements. The BET surface areas of these alternating copolymers were found to increase as a function of increasing

persistence length, giving quantitative evidence of the effect on chain stiffness on the porosity for these alternating copolymers.

2.1.6. Associated Content

Supporting Information (See §2.2)

Synthesis, molecular weights, thermal properties, and nitrogen isotherms. Additional details of the structure generation for the simulation samples.

2.1.7. Acknowledgements

This work was supported by the National Science Foundation (NSF) under grant numbers DMR-0905231**,** DMR-1206409, and DMR-0908781, and the Department of Chemistry at Virginia Tech. The specific surface area measurements were performed at the Molecular Foundry, Lawrence Berkeley National Laboratory. This work as well as F. Svec were supported by the Office of Science, Office of Basic Energy Sciences, Scientific User Facilities Division of the U.S. Department of Energy, under Contract No. DE-AC02-05CH11231. Computational resources were supported in part by the Materials Simulation Center of the Materials Research Institute, the Research Computing and Cyberinfrastructure unit of Information Technology Services and Penn-State Center for Nanoscale Science, and were supported in part through instrumentation funded by the National Science Foundation through grant OCI–0821527. We also would like to acknowledge Dr. Michael W. Ellis, Dr. Junbo Hou at Institute for Critical Technology and Applied Science for help with BET surface area measurements.

2.1.8. References

(1) Lu, G. Q. Zhao, X. S. *Nanoporous Materials: Science and Engineering*; Imperial College Press: London, 2004; Vol. 4.

(2) Dawson, R.; Cooper, A. I.; Adams, D. J. *Prog. Polym. Sci.* **2012**, *37*, 530.

(3) Furukawa, H.; Yaghi, O. M. *J. Am. Chem. Soc.* **2009**, *131*, 8875.

(4) Wood, C. D.; Tan, B.; Trewin, A.; Su, F.; Rosseinsky, M. J.; Bradshaw, D.; Sun, Y.; Zhou, L.; Cooper, A. I. *Adv. Mater.* **2008**, *20*, 1916.

(5) Lu, W. G.; Yuan, D. Q.; Zhao, D.; Schilling, C. I.; Plietzsch, O.; Muller, T.; Brase, S.; Guenther, J.; Blumel, J.; Krishna, R.; Li, Z.; Zhou, H. C. *Chem. Mater.* **2010**, *22*, 5964.

(6) Martin, C. F.; Stockel, E.; Clowes, R.; Adams, D. J.; Cooper, A. I.; Pis, J. J.; Rubiera, F.; Pevida, C. *J. Mater. Chem.* **2011**, *21*, 5475.

(7) Davankov, V. A.; Rogozhin, S. V.; Tsyurupa, M. P.; USSR Pat. 299165, **1969**. US Pat. 3729457, **1973**; *Chem. Abstr.* **1971**, 75, 6841B.

(8) Tsyurupa, M. P.; Davankov, V. A. *React. Funct. Polym.* **2006**, *66*, 768.

(9) Cote, A. P.; Benin, A. I.; Ockwig, N. W.; O'Keeffe, M.; Matzger, A. J.; Yaghi, O. M. *Science* **2005**, *310*, 1166.

(10) Feng, X.; Ding, X. S.; Jiang, D. L. *Chem. Soc. Rev.* **2012**, *41*, 6010.

(11) Jiang, J. X.; Su, F.; Trewin, A.; Wood, C. D.; Campbell, N. L.; Niu, H.; Dickinson, C.; Ganin, A. Y.; Rosseinsky, M. J.; Khimyak, Y. Z.; Cooper, A. I. *Angew. Chem. Int. Ed.* **2007**, *46*, 8574.

(12) Cooper, A. I. *Adv. Mater.* **2009**, *21*, 1291.

(13) Farha, O. K.; Bae, Y. S.; Hauser, B. G.; Spokoyny, A. M.; Snurr, R. Q.; Mirkin, C. A.; Hupp, J. T. *Chem. Commun.* **2010**, *46*, 1056.

(14) Farha, O. K.; Spokoyny, A. M.; Hauser, B. G.; Bae, Y. S.; Brown, S. E.; Snurr, R. Q.; Mirkin, C. A.; Hupp, J. T. *Chem. Mater.* **2009**, *21*, 3033.

(15) Ben, T.; Ren, H.; Ma, S. Q.; Cao, D. P.; Lan, J. H.; Jing, X. F.; Wang, W. C.; Xu, J.; Deng, F.; Simmons, J. M.; Qiu, S. L.; Zhu, G. S. *Angew. Chem. Int. Ed.* **2009**, *48*, 9457.

(16) Ben, T.; Pei, C. Y.; Zhang, D. L.; Xu, J.; Deng, F.; Jing, X. F.; Qiu, S. L. *Energ. Environ. Sci.* **2011**, *4*, 3991.

(17) Budd, P. M.; Ghanem, B. S.; Makhseed, S.; McKeown, N. B.; Msayib, K. J.; Tattershall, C. E. *Chem. Commun.* **2004**, 230.

(18) McKeown, N. B.; Budd, P. M. *Chem. Soc. Rev.* **2006**, *35*, 675.

(19) McKeown, N. B.; Budd, P. M. *Macromolecules* **2010**, *43*, 5163.

(20) Mao, M.; Turner, S. R. *Polymer* **2006**, *47*, 8101.

(21) Mao, M.; Turner, S. R. *J. Am. Chem. Soc.* **2007**, *129*, 3832.

(22) Mao, M.; Kim, C.; Wi, S.; Turner, S. R. *Macromolecules* **2008**, *41*, 387.

(23) Li, Y.; Turner, S. R. *Eur. Polym. J.* **2010**, *46*, 821.

(24) Mao, M.; England, J.; Turner, S. R. *Polymer* **2011**, *52*.

(25) Li, Y.; Mao, M.; Matolyak, L. E.; Turner, S. R. *ACS Macro Lett.* **2012**, *1*, 257.

(26) Li, Y.; Zhang, M. Q.; Mao, M.; Turner, S. R.; Moore, R. B.; Mourey, T. H.; Slater, L. A.; Hauenstein, J. R. *Macromolecules* **2012**, *45*, 1595.

(27) Abbott, L. J.; Hart, K. E.; Colina, C. M. *Theor. Chem. Acc.* **2013**, *132*, 1334.

(28) Abbott, L. J. Polymatic, v. 1.0; **2013**. http://nanohub.org/resources/17278.

(29) Sun, H. *J Comput. Chem.* **1994**, *15*, 752.

(30) Plimpton, S. *J. Comput. Phys.* **1995**, *117*, 1.

(31) Plimpton, S.; Thompson, A.; Crozier, P. Large-scale Atomic/Molecular Massively Parallel Simulator (LAMMPS); **2012**. http://lammps.sandia.gov/.

(32) Larsen, G. S.; Lin, P.; Hart, K. E.; Colina, C. M. *Macromolecules* **2011**, *44*, 6944.

(33) Hart, K. E.; Abbott, L. J.; Colina, C. M. *Mol. Simul.* **2012**, *39*, 397.

(34) Abbott, L. J.; McDermott, A. G.; Del Regno, A.; Taylor, R. G. D.; Bezzu, C. G.; Msayib, K. J.; McKeown, N. B.; Siperstein, F. R.; Runt, J.; Colina, C. M. *J. Phys. Chem. B*, **2013**, *117*, 355.

(35) Hart, K. E.; Abbott, L. J.; McKeown, N. B.; Colina, C. M. *Macromolecules* **2013**, *46*, 5371.

(36) Sing, K. S. W.; Everett, D. H.; Haul, R. A. W.; Moscou, L.; Pierotti, R. A.; Rouquerol, J.; Siemieniewska, T. *Pure Appl. Chem.* **1985**, *57*, 603.

(37) Brunauer, S.; Emmett, P. H.; Teller, E. *J. Am. Chem. Soc.* **1938**, *60*, 309.

(38) Rouquerol, J.; Llewellyn, P.; Rouquerol, F. *Stud. Surf. Sci. Catal.* **2007**, *160*, 49.

(39) Duren, T.; Millange, F.; Ferey, G.; Walton, K. S.; Snurr, R. Q. *J. Phys. Chem. C* **2007**, *111*, 15350.

(40) Furukawa, H.; Ko, N.; Go, Y. B.; Aratani, N.; Choi, S. B.; Choi, E.; Yazaydin, A. O.; Snurr, R. Q.; O'Keeffe, M.; Kim, J.; Yaghi, O. M. *Science* **2010**, *329*, 424.

(41) Sarkisov, L.; Harrison, A. *Mol. Simul.* **2011**, *37*, 1248.

(42) Fetters, L. J.; Lohse, D. J.; Colby, R. H. *Physical Properties of Polymers Handbook*, 2nd ed.; Springer: Berlin, **2007**.

(43) Weber, J.; Su, O.; Antonietti, M.; Thomas, A. *Macromol. Rapid Commun.* **2007**, *28*, 1871.

(44) McKeown, N. B. *ISRN Mater. Sci.* **2012**, *2012*, 16.

(45) Weber, J.; Antonietti, M.; Thomas, A. *Macromolecules* **2008**, *41*, 2880.

(46) Vieth, W. R.; Tam, P. M.; Michaels, A. S. *J. Colloid Interface Sci.* **1966**, *22*, 360.

(47) Tsujita, Y. *Prog. Polym. Sci.* **2003**, *28*, 1377.

(48) Gelb, L. D.; Gubbins, K. E. *Langmuir* **1999**, *15*, 305.

2.2. Supporting Information for Chapter 2

(This material is available at http://pubs.acs.org/doi/suppl/10.1021/ma4006582)

2.2.1. Synthesis

tert-Butyl carboxylate group containing alternating copolymers were synthesized via free radical polymerization, as previously reported.[1] Copolymers I and III were prepared at 60 ºC with AIBN as initiator and tetrahydrofuran (THF) as solvent for 4 h. Copolymers II and IV were prepared at 110 ºC with dicumyl peroxide (DCP) as initiator and chlorobenzene as solvent for 24 h. Copolymers were precipitated from THF or chlorobenzene into hexanes (volume ratio 1:20) twice, Soxhlet extracted with hexanes, and dried under vacuum at 60 ºC overnight.

Linear polystyrene was synthesized using the same synthetic method. A mixture of styrene (2.01 g), AIBN (0.010 g, 0.5 wt%), and THF (9.0 mL, 20 wt%) was sealed in a septum sealed glass bottle and degassed by purging with N_2 for 15 min and polymerized at 60 ºC for 24 h. Then the polymer was precipitated in 200 mL methanol, filtered and vacuum dried for 24 h at 50 ºC to yield a white powder (0.66 g, 33%).

2.2.2. Characterization

Molecular weights of the polymers (except copolymer III) were determined using a size exclusion chromatograph equipped with a Waters HR 0.5+ HR 2+ HR 3+ HR 4+ styragel column set, a viscosity detector, and a laser refractometer detector in chloroform at 30 ºC. The molecular weight of copolymer III was determined using a size exclusion chromatograph equipped with PLGel 5μm Mixed-C columns, a differential refractive index detector, and a laser light scattering detector in THF at 35 ºC.

Table 2-2. Molecular weights of PS and copolymer I-IV.

Polymer	M_n (kg/mol)	M_w/M_n
PS	17.0	1.63
Copolymer I	85.7	1.35
Copolymer II	111	1.53
Copolymer III	93.8	1.89
Copolymer IV	77.2	1.69

No glass transition temperature (T_g) nor crystalline melting temperature (T_m) was observed in differential scanning calorimetry (DSC) analysis for copolymers I-IV under their corresponding degradation temperatures.

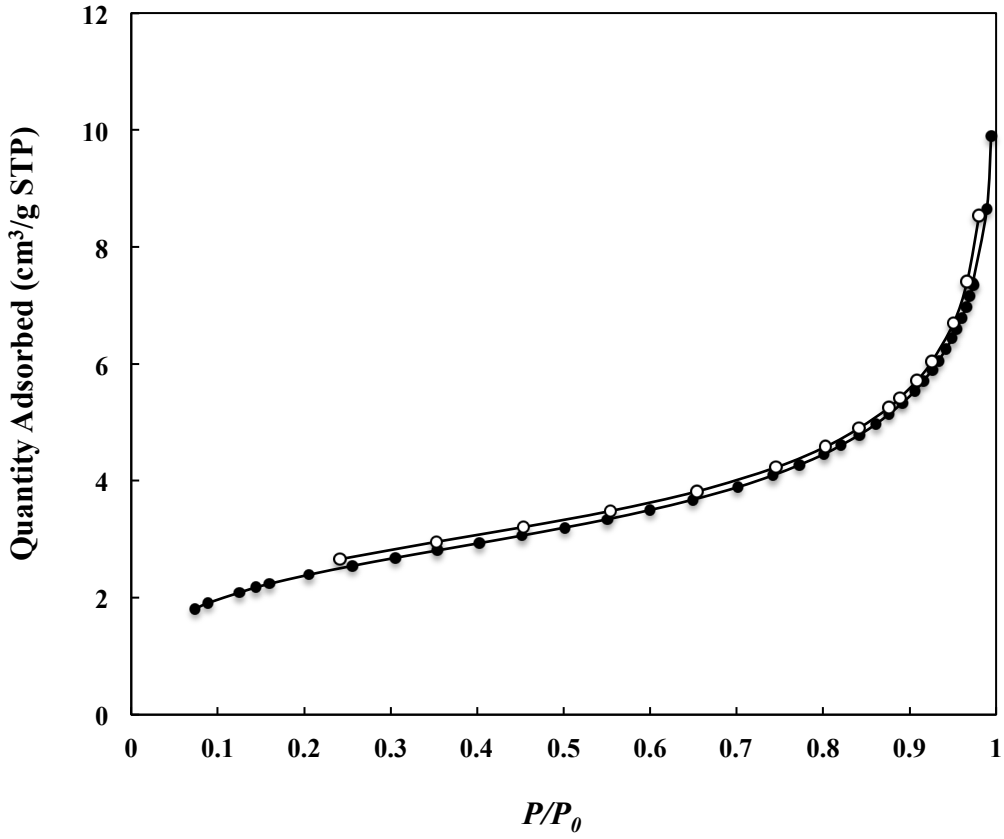

Figure 2-6. Nitrogen adsorption desorption isotherms of polystyrene (solid symbol: adsorption; open symbol: desorption).

2.2.3. Simulation Details

The polymers analyzed in this work used an atomistic definition with all bonded and non-bonded parameters taken from the polymer consistent force field (PCFF).[2] To generate the simulation samples, 200 copolymer repeat units (A-B) were packed into a three-dimensionally periodic cubic simulation box at a low density (0.2–0.4 g cm^{-3}). To "polymerize" the monomers, the available code *Polymatic*[3] was used—further details of the implementation of *Polymatic* can be found in Abbott et al.[4] The bonding criteria used was a cutoff length of 6.5 Å, with artificial charges of ± 0.3 *e* on the bonding-capable ends. After polymerization was completed, the 21-step compression and relaxation scheme[5] was used to compress the simulation samples to an

experimental-like density, using P_{max}=5x10^4 bar; P_{final}=1 bar; T_{max}=600 K; and T_{final}=300 K. A sample LAMMPS input script to run the 21-step MD compression and relaxation scheme can be found in Abbott et al.[4] As a result, the total number of atoms in the polymer samples were 3200, 8000, 13000, 13200, and 18200 and the box lengths were 32.8, 44.2, 52.5, 52.8, and 59.3 Å for polystyrene, copolymer I, copolymer II, copolymer III, and copolymer IV, respectively.

2.2.4. References

(1) Li, Y.; Mao, M.; Matolyak, L. E.; Turner, S. R. *ACS Macro Letters* **2012**, *1*, 257.

(2) Sun, H. *J Comput. Chem.* **1994**, *15*, 752.

(3) Abbott, L. J. *Polymatic*, v. 1.0; **2013**. http://nanohub.org/resources/17278.

(4) Abbott, L. J.; Hart, K. E.; Colina, C. M. *Theor. Chem. Acc.* **2013**, *132*, 1334.

(5) Larsen, G. S.; Lin, P.; Hart, K. E.; Colina, C. M. *Macromolecules* **2011**, *44*, 6944.

2.3. Appendix to Chapter 2

SEM micrographs of copolymers I-IV and PS are shown in **Figure 2-7** to **2-10**. Under high magnification, porous structures were observed for alternating copolymers while spherical structures were observed for PS. Since observation of nanopores (with pore width in 1-100 nm) in these polymers is difficult under such magnification, porous structures in SEM pictures have no direct correlation with surface area and porosity of the polymers.

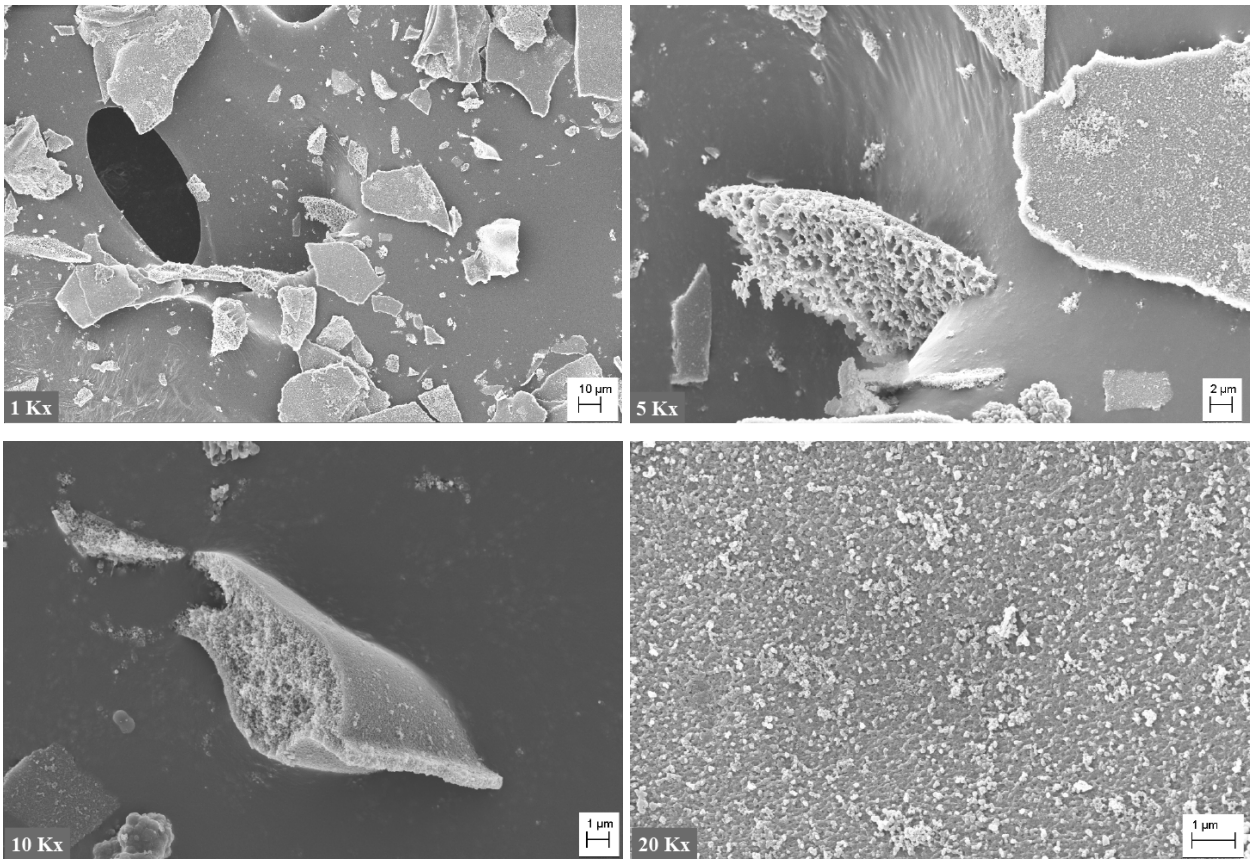

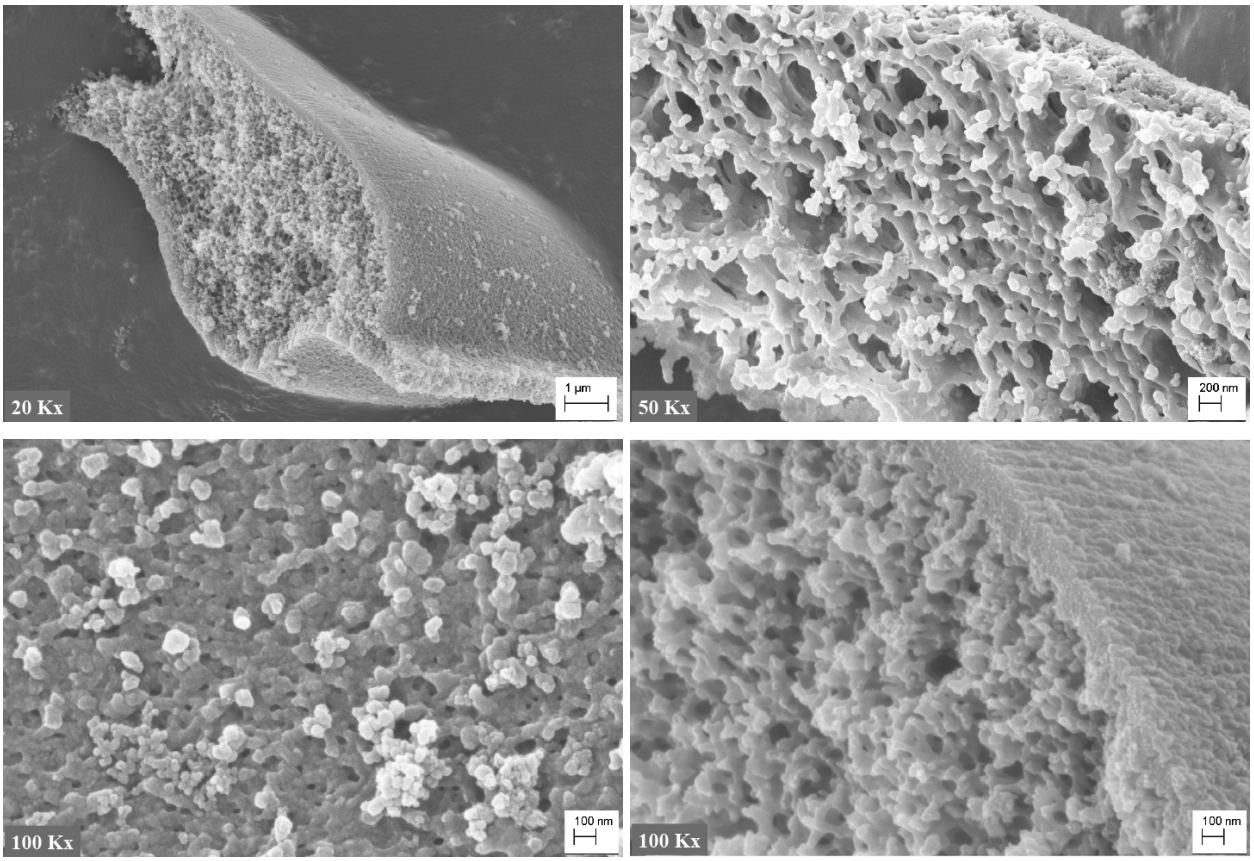

Figure 2-7. SEM pictures of copolymer I.

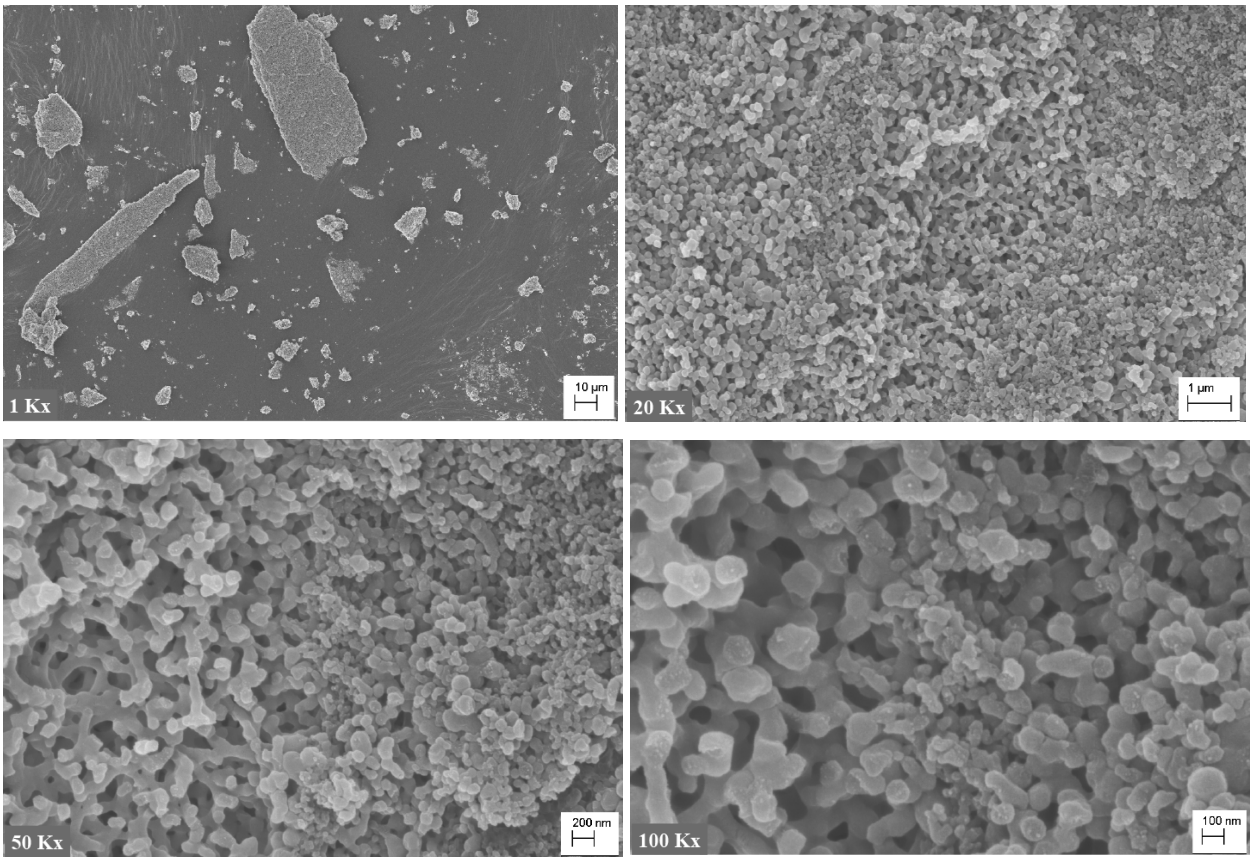

Figure 2-8. SEM pictures of copolymer II.

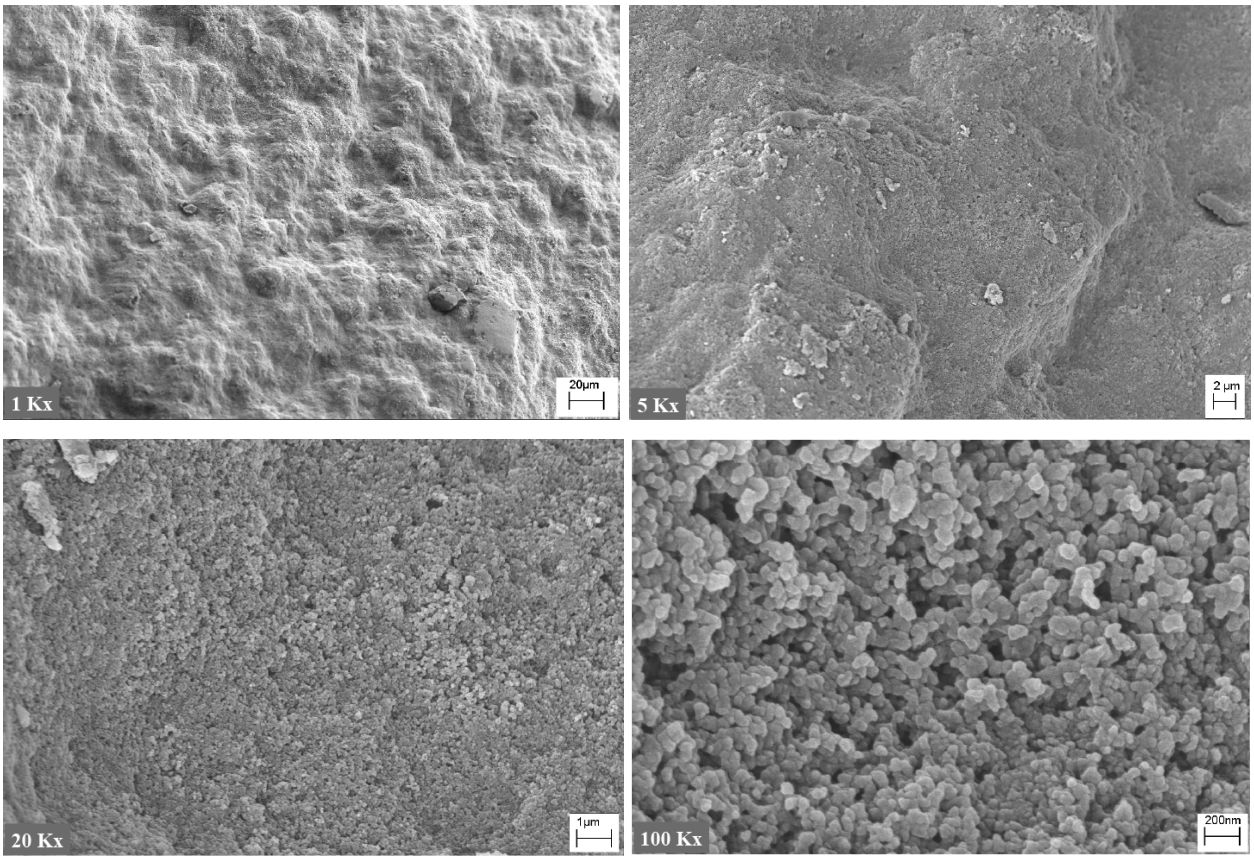

Figure 2-9. SEM pictures of copolymer III.

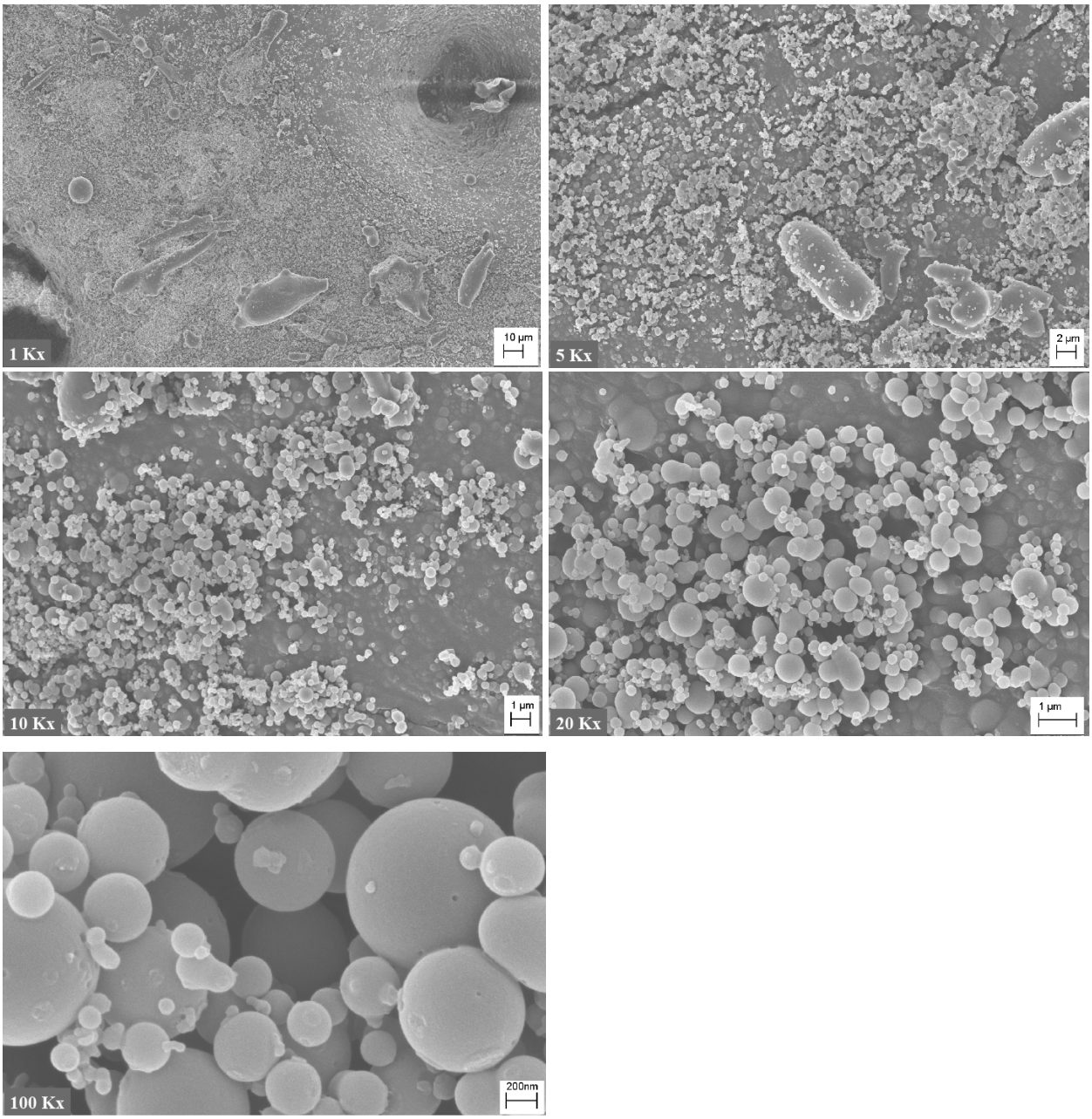

Figure 2-10. SEM pictures of polystyrene.

Chapter 3. Nanoporous Hypercrosslinked Polymers Containing T_g Enhancing Comonomers

3.1. Abstract

Hypercrosslinked polymers containing functionalized stilbene and *N*-substituted maleimide were synthesized. These comonomers showed enhancement of the rigidity of the polymer backbone, evidenced by the raised glass transition temperatures of precursors particles before post-crosslinking reaction. The surface area and porosity of hypercrosslinked polymers were investigated using nitrogen adsorption/desorption isotherms at 77 K. These hypercrosslinked polymers exhibit BET surface areas up to 1058 m^2/g. The correlation between rigidity and porosity was discussed in this chapter.

3.2. Introduction

Nanoporous organic polymers, which are defined as materials with pore sizes of 1-100 nm,[1,2] include hypercrosslinked polymers (HCPs),[3-5] covalent organic frameworks (COFs),[6-9] and polymers of intrinsic microporosity (PIMs)[10-13] etc. In the 1970s, Davankov and Tsyurupa proposed an approach to synthesize hypercrosslinked polymers termed "Davankov-type resin".[14] Since then, hypercrosslinked polymers have been intensively studied and have been suggested for applications in numerous areas such as chromatography, gas storage etc.[5,15-18] The preparation of hypercrosslinked polymers typically involves the suspension polymerization of vinylbenzyl chloride and divinylbenzene, followed by post-crosslinking reaction via Lewis acid catalyzed Friedel-Crafts alkylation.[16,18] These hypercrosslinked polymers exhibit BET surface areas up to 2000 m^2/g.[16]

Frechet, Svec, and coworker systematically studied a series hypercrosslinked polyanilines as another type of network systems.[19] They found that the rigidity of the polymer backbone is crucial to maintain high surface area, because longer and more flexible crosslinkers used in the synthesis resulted in lower surface areas.[19] These results suggested that decreasing the flexibility could hinder the collapse of pore structures and therefore lead to higher surface area materials.[17,19]

Sterically congested alternating copolymers containing stilbene and maleic anhydride or maleimide have been investigated in our group.[20-26] Functionalities of these alternating copolymers can be precisely controlled by incorporating various substituted stilbene and maleimide monomers. The steric congestion of extra phenyl groups from the stilbene units yields unique properties. Persistence length measurements by small-angle X-ray scattering (SAXS) and size exclusion chromatography (SEC) on a series of stilbene and styrenic alternating copolymers showed that these copolymers are semi-rigid and adding extra phenyl groups enhanced the chain stiffness.[25,26] Solution studies also reveal the semi-rigid structure in polyanions.[27] The porous properties of these copolymers showed that the addition of phenyl rings to the polymer backbone increased surface areas.[28]

In this paper, we enchained T_g enhancing comonomers, functionalized stilbene and *N*-substituted maleimide, into the Davankov-type hypercrosslinked systems in order to increase the rigidity of the polymer backbones. These T_g enhancing monomers also present opportunities to incorporate various functional groups in precise location along the backbone. We report the synthesis of hypercrosslinked polymers containing various levels of functionalized stilbene and *N*-substituted maleimides. We investigated the rigidity of polymer backbones using thermal

analysis of precursor particles before the hypercrosslinking reactions. Surface area and porosity of hypercrosslinked polymers were explored and correlated to the rigidity of polymer backbones.

3.3. Experimental Section

Materials. 4-Methylbenzyl chloride (Aldrich, 98%), triethyl phosphite (Aldrich, 98%), benzaldehyde (Aldrich, ≥99%), ^{t}BuOK (Aldrich, 1.0 M solution in THF), maleic anhydride (Aldrich, 99%), toluene (Fisher, certified ACS), *m*-toluidine (Aldrich, 99%), acetic anhydride (Aldrich, 98%), sodium acetate (Aldrich, anhydrous), methanol (Fisher, HPLC grade), 1,2-dichloroethane (Aldrich, ≥99%), $FeCl_3$ (Aldrich, 97%), poly(vinyl alcohol) (Aldrich, 87-89% hydrolyzed), sodium chloride (Fisher, certified ACS crystalline) were used as purchased. AIBN was recrystallized from methanol.

Instrumental Characterization. Proton nuclear magnetic resonance (^{1}H NMR) was utilized to confirm the chemical composition of the monomers and non-crosslinked polymers. $CDCl_3$-d and $DMSO_{d6}$ were used as the solvents. ^{1}H NMR was obtained on Varian Utility 400 MHz or JOEL EclipsePlus 500 MHz spectrometers at 25 ºC. Infrared analysis, using a Midac FTIR spectrometer, was used to confirm the incorporation of *N*-substituted maleimide. Thermogravimetric Analysis (TGA) was employed to study the thermal stability of polymer precursors and hypercrosslinked polymers using TA instrument model Q5000. Samples were heated from 30 to 600 ºC at a heating rate of 10 ºC/min under nitrogen. Thermal transitions such as glass transition temperatures (T_gs) were obtained by Differential Scanning Calorimetry (DSC) using a TA instrument model Q1000. Samples were measured using heat/cool/heat method at heating and cooling rate of 20 ºC under nitrogen. SEM micrographs were obtained using a LEO (Zeiss) 1550 field emission scanning electron microscope. The surface areas were calculated

using the Brunauer-Emmett-Teller (BET) equation and data from nitrogen adsorption/desorption isotherms at 77 K obtained with a TriStar II 3020 surface area analyzer (Micromeritics, Norcross, GA). Prior to analysis, the sample were heated at 140 °C under nitrogen overnight.

Monomer Synthesis.

(*E*)-4-Methylstilbene (4MSTB). (*E*)-4-Methylstilbene was synthesized via the Wittig-Horner reaction using 4-methylbenzyl(diethylphosphonate) and benzaldehyde (**Scheme 3-1**).[23] To synthesize 4-methylbenzyl(diethylphosphonate), 4-methylbenzylchloride (15.0 g, 107 mmol) and triethyl phosphite (70.9 g, 427 mmol) were stirred in a 250 ml flask and heated to 160 ºC for 24 h. The remaining triethyl phosphite was removed by vacuum distillation at 80 ºC under 0.2 mmHg to afford a colorless liquid (27.1 g, 100%). 4-Methylbenzyl(diethylphosphonate) (27.1 g, 112 mmol) and benzaldehyde (11.9 g, 112 mmol) in dry THF (60 ml) were stirred in a 250 ml round bottom flask cooled in an ice bath. ^{t}BuOK (1.0 M in THF, 120 mL) was then added dropwise. The solution formed was stirred at room temperature for an additional 24 hours after which it was poured into water (500 ml). The product was precipitated from the solution, filtered and washed with water and vacuum dried overnight to yield (*E*)-4-methylstilbene (white solid, 18.7 g, 86%). ^{1}H NMR ($CDCl_3$, 500 MHz) δ ppm: 7.52 – 7.08 (m, 11H), 2.37 (s, 3H). Melting point: 117 – 118 ºC (lit.[29]:118 – 120 ºC).

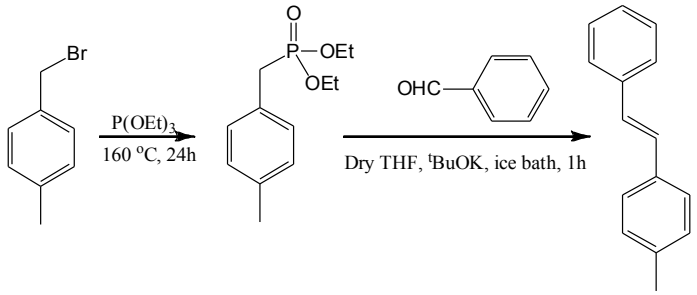

Scheme 3-1. Synthesis of (*E*)-4-methylstilbene.

***N*-(3-Methylphenyl)maleimide (3MPMI).** *N*-(3-Methylphenyl)maleimide was synthesized by a two step reaction (Scheme 2). The second step of the reaction used a modified literature method.[30] To synthesize *N*-(3-methylphenyl)maleamic acid, maleic anhydride (10.0 g, 102 mmol) and toluene (8 ml) were stirring in a 100 ml flask. *m*-Toluidine (11.1 g, 102 mmol) was added dropwise. During the addition, 15 ml toluene was added to maintain a good slurry consistency, after which the mixture was refluxed for 15 minutes. The product precipitated from solution was filtered warm and vacuum dried for 24 h to afford light yellow solid (19.63 g, 94%). ^{1}H NMR (DMSO, 400 MHz) δ ppm: 10.27 (s, 1H), 7.43 – 6.87 (m, 4H), 6.42 (d, 1H), 6.26 (d, 1H), 2.23 (s, 3H). A mixture of *N*-(3-methylphenyl)maleamic acid (17.6 g, 85.9 mmol), acetic anhydride (43.8 g, 429 mmol) and anhydrous sodium acetate (3.52 g, 42.9 mmol) was heated at 100 ºC for 6 h. The reaction mixture was cooled and poured into ice water. The crude product was then washed with ice water and vacuum distilled (62 ºC, 0.2 mmHg) to afford *N*-(3-methylphenyl)maleimide (yellow liquid, 15.1 g, 94%). The crude product was purified by column chromatography (silica gel, hexane-ethyl acetate = 5:1). The first band afforded pure product as a yellow liquid (6.19, 41%) (lit.[31] 78%) ^{1}H NMR (DMSO, 500 MHz) δ ppm: 7.36 (m, 1H), 7.22 - 7.10 (m, 5H), 2.34 (t, 3H).

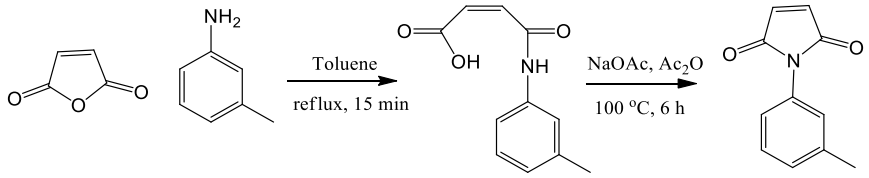

Scheme 3-2. Synthesis of *N*-(3-methylphenyl)maleimide.

Hypercrosslinked Copolymers. Hypercrosslinked copolymers **HCP1-16** were prepared following a modified literature procedure (**Scheme 3-3** to **3-5**).[16,18] For preparation of **HCP12**, (*E*)-4-methylstilbene (4MSTB) (0.519 g, 2.67 mmol), *N*-(3-methylphenyl)maleimide (3MPMI)

(0.500 g, 2.67 mmol), vinylbenzyl chloride (VBC) (2.446 g, 16.04 mmol) and divinylbenzene (DVB) (0.071 g, 0.44 mmol) were added to a three-neck, 250 ml round bottom flask equipped with a mechanical stirrer, gas inlet, and condenser. Additionally, to the mixture, poly(vinyl alcohol) (0.332 g, 9.4 wt%), sodium chloride (1.462 g, 41.4 wt%), and DI water (45 ml) were added. The polymerization was initiated with 2,2'-azobis(isobutyronitrile) (0.018 g, 0.5 wt%). The mixture was stirred under N_2 at 80 ºC for 6 h. The polymer beads were filtered, extracted with methanol and diethyl ether via Soxhlet extraction, and dried under vacuum at 50 ºC for 24 h to yield a white solid (2.063 g, 58%). The precursor **P12** (1.913 g) was swollen in 1,2-dichloroethane (30 ml) for 2 h. Then $FeCl_3$ (1.997 g) was added and the mixture was heated at 80 ºC for 18 h. The hypercrosslinked polymer was extracted with THF to remove any uncrosslinked polymer and vacuum dried at 50 ºC for 24 h to afford a brown powder (1.319 g).

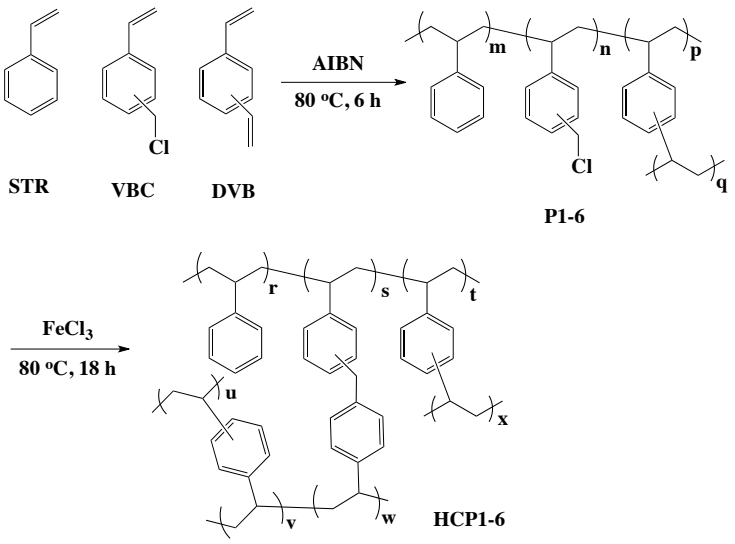

Scheme 3-3. Synthesis of styrenic hypercrosslinked copolymers (**HCP1-6**).

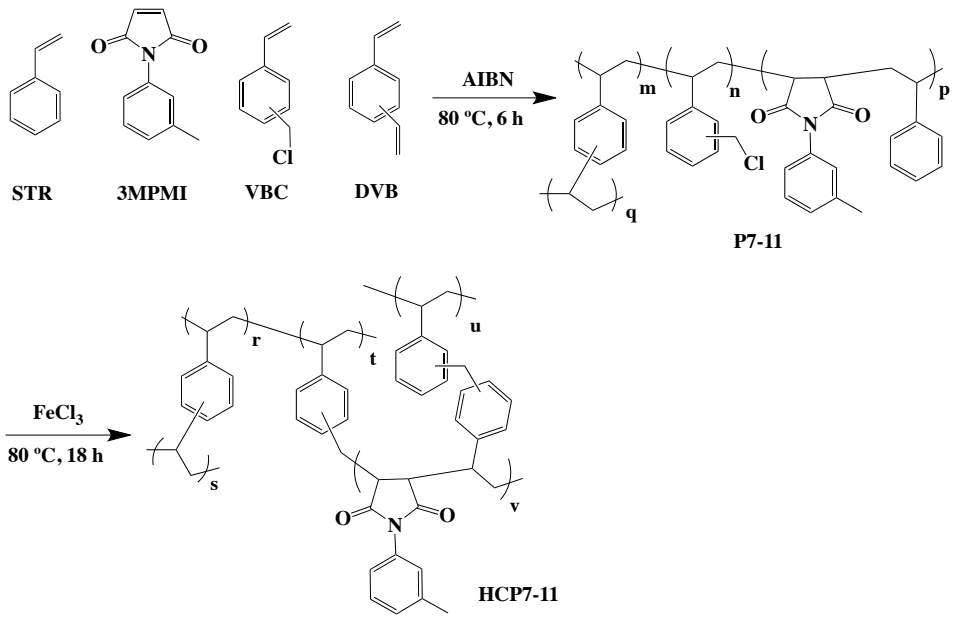

Scheme 3-4. Synthesis of hypercrosslinked copolymers STR-3MPMI-VBC-DVB (**HCP7-11**).

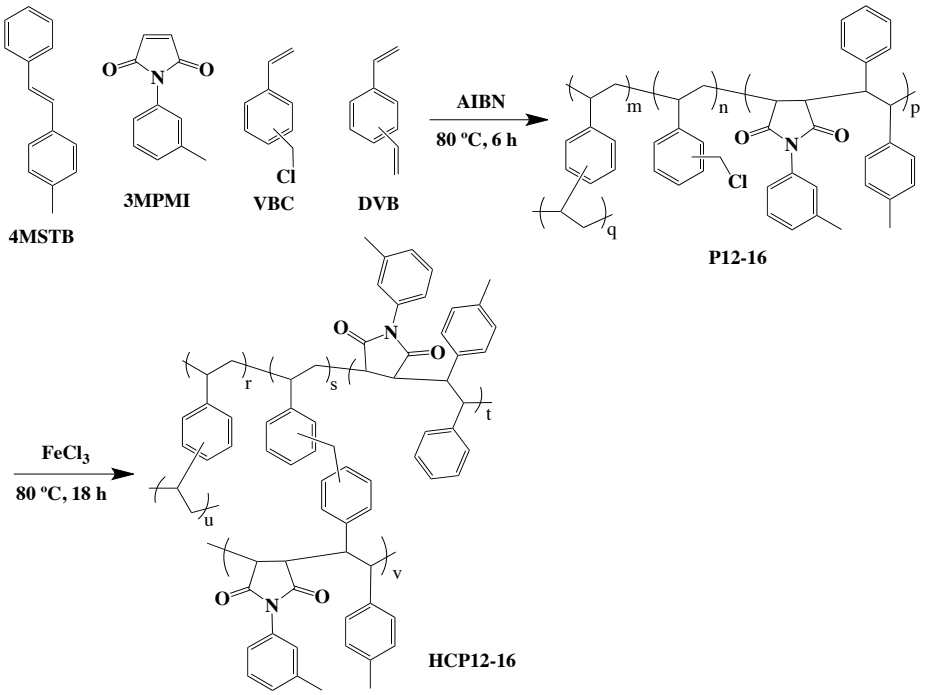

Scheme 3-5. Synthesis of hypercrosslinked copolymers 4MSTB-3MPMI-VBC-DVB (**HCP12-16**).

FT-IR was used to confirm incorporation of 3MPMI into the precursor particles. Stretching adsorption bands of the carbonyl group were observed around 1700 cm^{-1} for precursor particles containing 3MPMI monomer. Elemental analysis showed that **HCP7-16** contained 1.7-3.9 wt% N, indicating the successful incorporation of maleimide monomers into these hypercrosslinked networks.

3.4. Results and Discussion

Thermal Properties. Thermal properties of precursors (**P1-16**) before crosslinking reactions and hypercrosslinked polymers (**HCP1-16**) were investigated by differential scanning calorimetry (DSC). Glass transition temperatures (T_gs) of **P1-16** are in the range of 90-230 ºC, and are shown in **Table 3-1**. No T_g was observed in any of the hypercrosslinked polymers (**HCP1-16**), probably due to the high degree of crosslinking that inhibited the chain mobility. Precursors **P1-P6** exhibit T_gs of 90-105 ºC. The T_g of poly(vinyl benzyl chloride) (PVBC) is reported as 73 ºC[32] while the T_g of polystyrene is 100 ºC.[33] Although **P1** contained 98 mol% of VBC, it showed a higher T_g than PVBC. The low degree of crosslinking introduced by 2 mol% of DVB, likely decreases the chain mobility, and thus raises the T_g of **P1**. T_gs modestly increase from **P1** to **P6** as the amount of STR increases. Poly(styrene-*alt*-*N*-phenyl maleimide) exhibits a T_g of 223 ºC,[34] which is much higher than the T_g of the styrenic polymers. The incorporation of 3MPMI raised the T_gs of precursors (**P7-11**) to 121-189 ºC. From **P7** to **P11**, T_gs increase as the STR-3MPMI mol% increases; the trend is shown in **Figure 3-1**.

Functionalized stilbene and *N*-substituted phenyl maleimide alternating copolymers have excellent thermal stability and have no observable T_gs in DSC experiments under decomposition temperature (> 350 ºC).[20] **P12-16,** which contain both 4MSTB and 3MPMI units, exhibit higher T_gs (up to 225 ºC) compared to the T_gs of **P1-6** and **P7-11** at comparative compositions (**Figure**

3-1). Therefore, the incorporation of T_g enhancing comonomer pairs into backbone accomplished the goal of raising the rigidity of the polymer backbone in the lightly crosslinked polymer precursors.

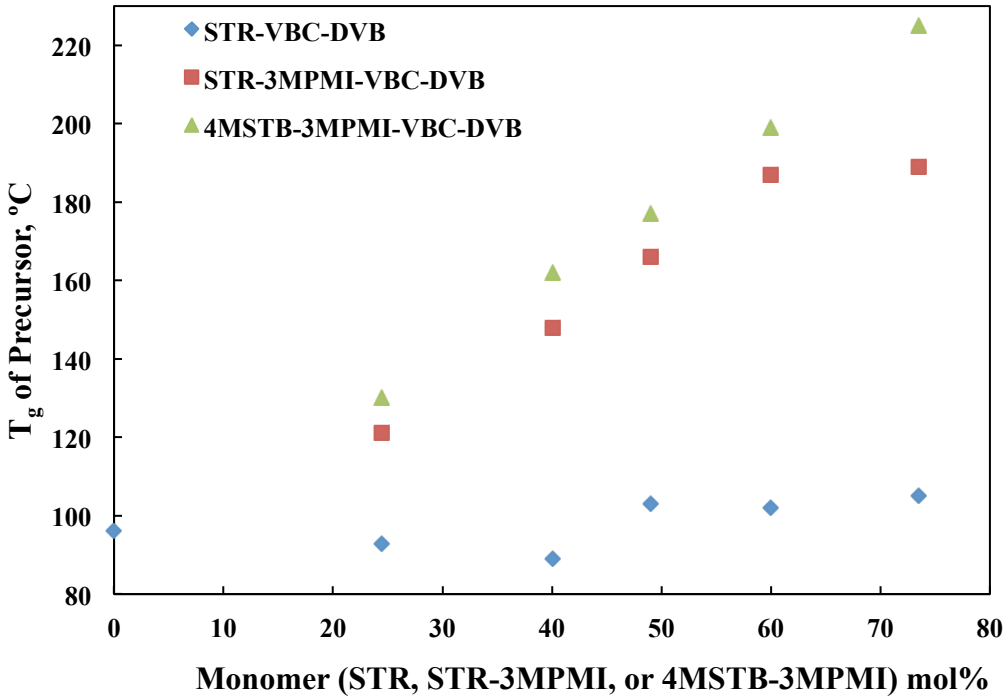

Figure 3-1. Glass transition temperatures of **P1-16** as a function of monomer concentration.

Table 3-1. Glass transition temperatures of precursors and porous properties of hypercrosslinked polymers.

	STR (mol%)	STR-3MPMI (mol%)	4MSTB-3MPMI (mol%)	VBC (mol%)	DVB (mol%)	Precursors	Hypercrosslinked Polymers		
						T_g (ºC)	SA_{BET} (m^2/g)[a]	$V_{p,}^{micro}$ (cm^3/g)[b]	V_p^{total} (cm^3/g)[c]
1	0	0	0	98.0	2.0	96	1577±11	0.628	1.039
2	24.5	0	0	73.5	2.0	93	1342±12	0.540	0.900
3	40.0	0	0	58.0	2.0	89	1263±23	0.583	1.022
4	49.0	0	0	49.0	2.0	103	908±13	0.368	0.613
5	60.0	0	0	38.0	2.0	102	878±17	0.359	0.591
6	73.5	0	0	24.5	2.0	105	508±6	0.209	0.350
7	0	24.5	0	73.5	2.0	121	1058±12	0.436	0.660
8	0	40.0	0	58.0	2.0	148	318±8	0.130	0.173
9	0	49.0	0	49.0	2.0	166	256±5	0.106	0.148
10	0	60.0	0	38.0	2.0	187	0	0	0
11	0	73.5	0	24.5	2.0	189	0	0	0
12	0	0	24.5	73.5	2.0	130	940±10	0.385	0.560
13	0	0	40.0	58.0	2.0	162	774±16	0.318	0.455
14	0	0	49.0	49.0	2.0	177	552±7	0.226	0.343
15	0	0	60.0	38.0	2.0	199	0	0	0
16	0	0	73.5	24.5	2.0	225	0	0	0

[a]BET surface area; error bars represent deviation from fitting linear region in the BET calculation. SA of HCP1, 7, 9, 12, and 14 are the average values of two measurements with ±2% error. [b]Micropore volumes determined from nitrogen adsorption isotherm at $P/P_0 = 0.14$; [c]Total pore volumes determined from nitrogen adsorption isotherm at $P/P_0 = 0.98$.

Porosity and Surface Area. Under SEM, spherical structures were observed for precursor particles, which are typical for the products of suspension polymerization due to the nature of the

synthetic method (**Figure 3-2a**). Porous structures were observed for hypercrosslinked polymers (**Figure 3-2b**), although micropores (with pore widths < 2 nm) are too small to be observed under such magnification.

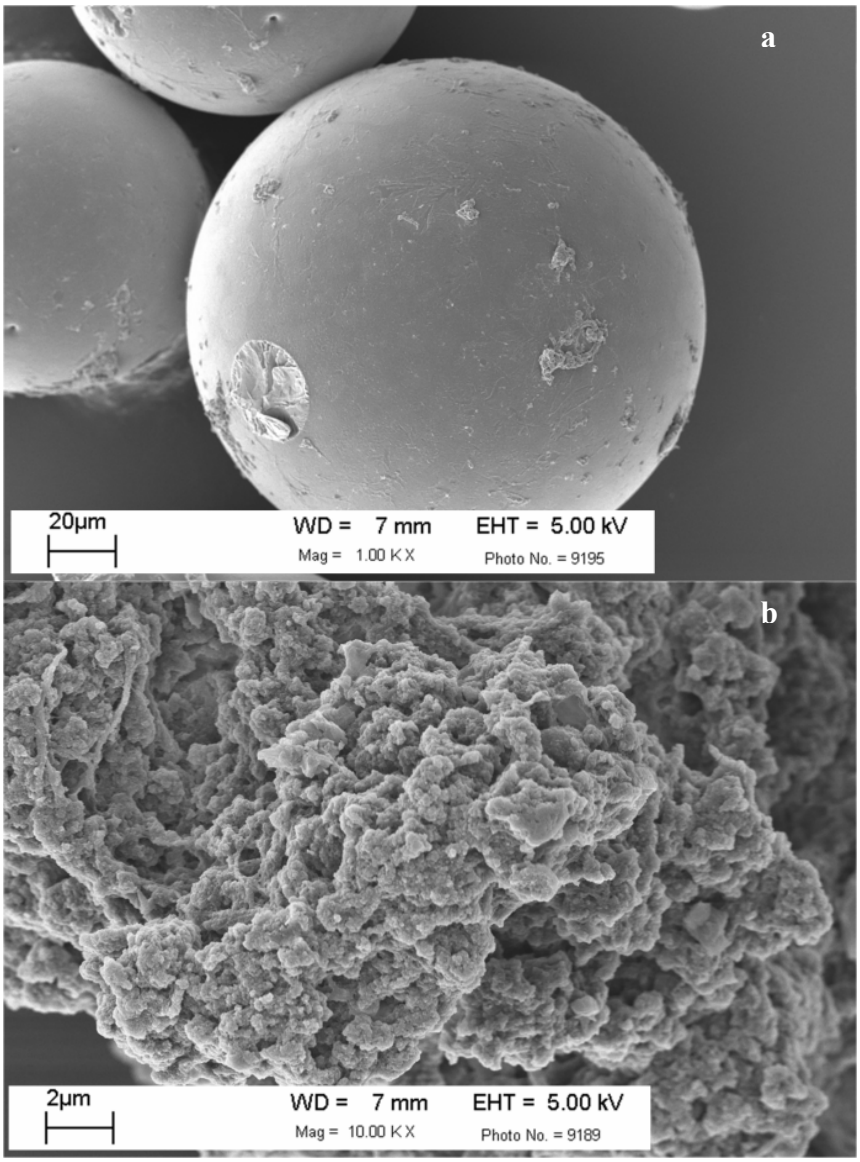

Figure 3-2. SEM micrographs of **P12** (a) and **HCP12** (b).

Nitrogen adsorption/desorption isotherms of these hypercrosslinked polymers were obtained at 77 K. Figure 3 shows adsorption/desorption isotherms of **HCP7-9** and **HCP12-14**. Type I isotherms were observed for these copolymers according to the classification given by

International Union of Pure and Applied Chemistry (IUPAC).[35] High nitrogen uptakes at low relative pressure ($P/P_0 < 0.2$) indicate that these copolymers possess micropores (with pore widths < 2 nm). Surface areas were calculated using the BET equation.[36] The relative pressure (P/P_0) for the linear region of BET plot was chosen in the range of 0.05-0.16 based on the recommendations for microporous samples.[37] BET surface areas, micropore volumes and total pore volumes **HCP1-16** are summarized in **Table 3-2**.

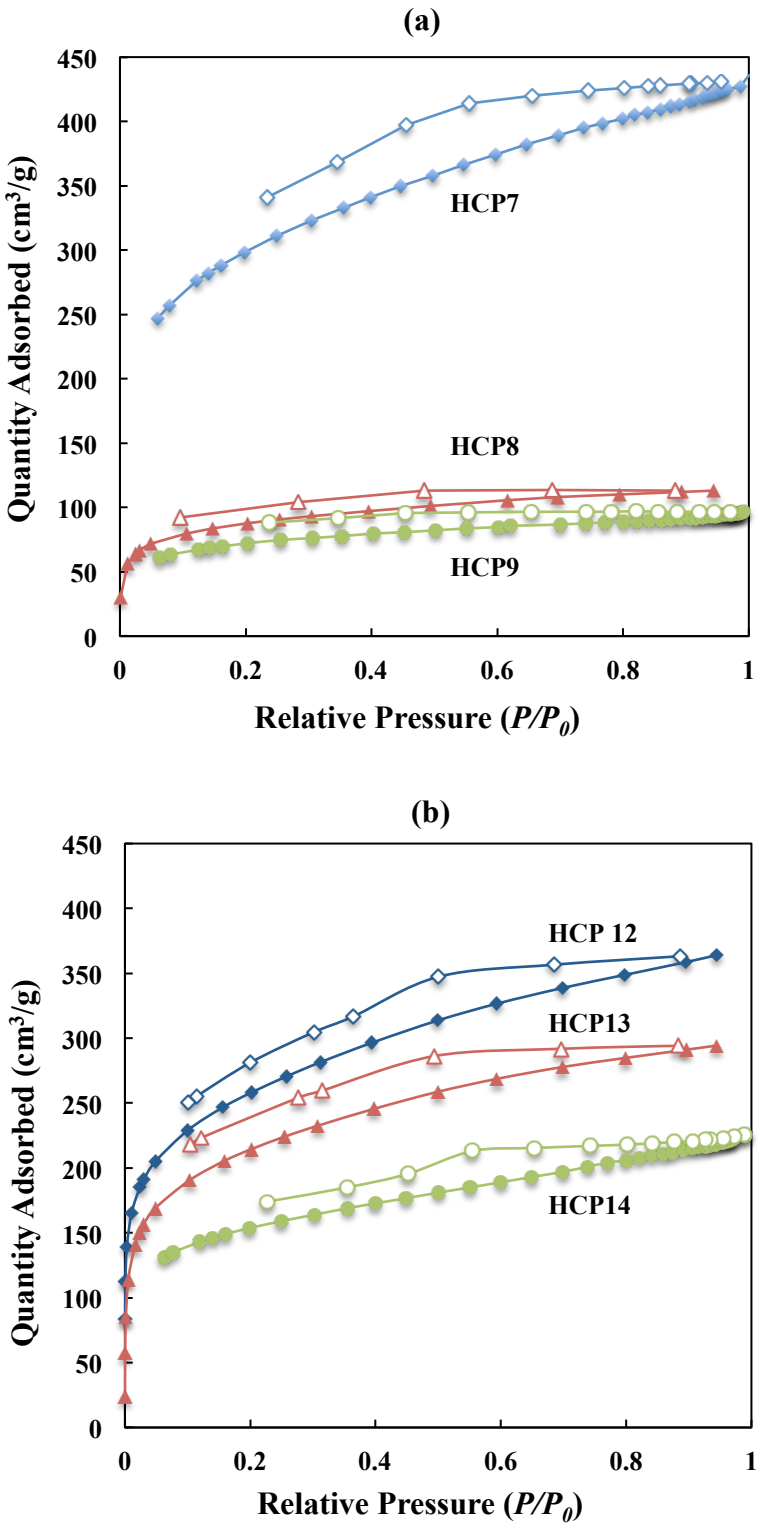

Figure 3-3. Nitrogen adsorption (closed symbol)/desorption (open symbol) isotherms at 77 K for **HCP7-9** (a) and **HCP12-14** (b).

Styrenic hypercrosslinked copolymers **HCP1-6** were used as controls. A systematic decrease in surface areas from 1577 to 508 m^2/g was observed when the mole percentage of STR increased from 0 to 75% (**Figure 3-4**). This observation is consistent with previous research reported by Sherrington and coworkers.[15] The decrease in surface areas is likely due to the dilution of VBC units, which served as the crosslinkers in the post-crosslinking reaction. Therefore, maintaining a high level of chloromethyl groups is crucial in preparing high surface area polymers.

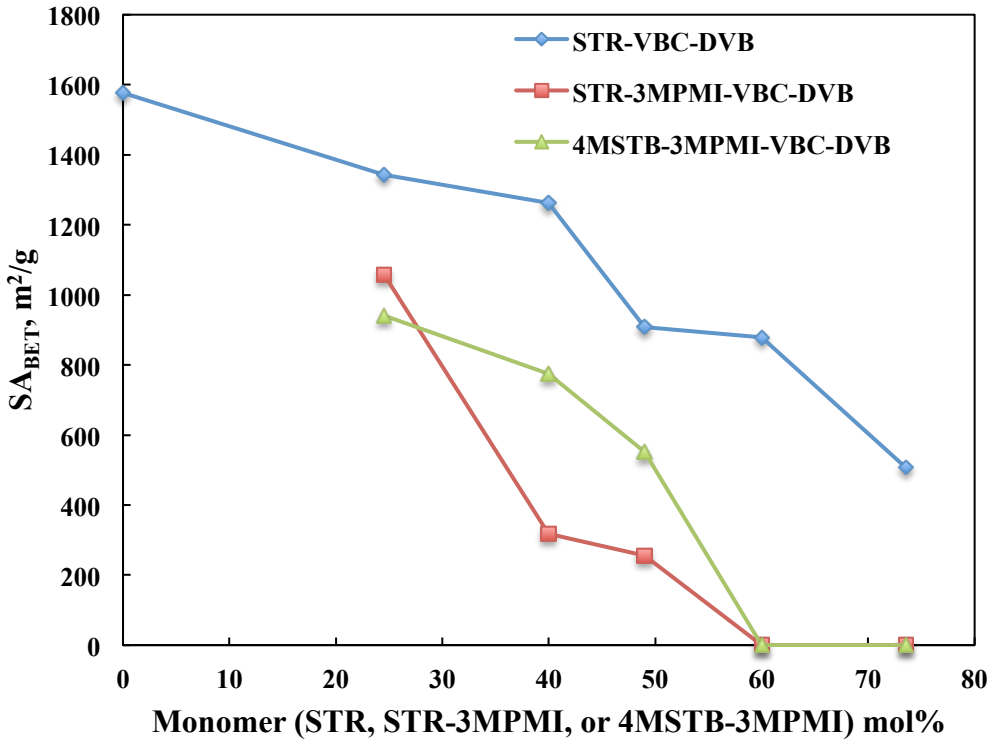

Figure 3-4. Surface areas of **HCP1-16** (see **Table 3-1**) as a function of monomer concentration.

The T_g enhancing comonomer containing hypercrosslinked copolymers **HCP7-11** and **HCP12-16** exhibit surface areas up to 1058 m^2/g. Similar decreasing trends in surface areas as monomer (STR-3MPMI or 4MSTB-3MPMI) concentration increased were also observed. However, no porosity was observed in hypercrosslinked copolymers containing more than 60%

STR-3MPMI or 4MSTB-3MPMI. Surface areas of these copolymers showed systematic decreases (280-380 m^2/g) compared to their controls (**HCP2-6**).

Correlation Between Rigidity and Porosity. As discussed in the previous section, a high concentration of crosslinker (VBC in our case) in the post-crosslinking reaction is important for the formation of high porosity. The concentration of DVB, which is the crosslinker in the first step to form lightly crosslinked precursor polymer, is believed to be another important factor. Sherrington compared hypercrosslinked STR-VBC-DVB polymers with 2% DVB to their analog with 20% DVB.[15] They found that even at similar concentration of chloromethyl groups, hypercrosslinked polymers with 2% DVB had much higher surface areas than the 20% DVB analogs. It is suggested that chloromethyl group precursors with 20% DVB potentially limited accessibility in the post-crosslinking reaction. A more systematic comparison among hypercrosslinked polymers with varying DVB concentration was done by Davankov and coworkers.[5] In this study, STR-DVB precursors were crosslinked with a bifunctional external crosslinker. As the percentage of DVB increased, the degree of crosslinking required to form porous polymers increased. Also, at different degrees of crosslinking, the optimum DVB concentration that led to highest surface area varied. In our study, DVB concentration was kept at 2%. However, since 3 series of hypercrosslinked polymers contain different comonomers, the optimum DVB concentration for highest surface area may vary.

Furthermore, the incorporation of stiffening units into the polymer backbone can decrease the chain mobility, resulting in a decrease in crosslinking efficiency in the post-crosslinking reaction, and thus lead to a decrease in surface area. Both reasons mentioned above may lead to the

systematic lower surface area of T_g enhanced hypercrosslinked polymers compared to the controls.

3.5. Conclusions

Incorporation of functionalized, chain stiffening, T_g enhancing comonomers into hypercrosslinked polymers is reported in this chapter. The thermal analysis of polymer precursors indicates that the incorporation of these comonomers, which have semi-rigid characteristics, leads to precursor polymers with enhanced T_gs. Nitrogen sorption measurements showed these hypercrosslinked polymers contains micropores and have BET surface areas up to 1058 m^2/g. However, the surface areas of these hypercrosslinked polymers are systematically lower than the controls. As the concentration of T_g enhancing comonomer increases, the high rigidity of the polymer backbones affects the chain mobility of the precursors and decreases the efficiency of post-crosslinking reactions. Future research will include optimization of DVB content to achieve higher surface areas, and incorporation of various functional groups into hypercrosslinked systems.

3.6. Acknowledgements

This work was supported by the National Science Foundation (NSF) under grant number DMR-0905231 and DMR-1206409, and the Department of Chemistry at Virginia Tech. The specific surface area measurements were performed at the Molecular Foundry, Lawrence Berkeley National Laboratory. This work as well as F. Svec were supported by the Office of Science, Office of Basic Energy Sciences, Scientific User Facilities Division of the U.S. Department of Energy, under Contract No. DE-AC02-05CH11231. We would like to

acknowledge Dr. Michael W. Ellis, Dr. Junbo Hou at Institute for Critical Technology and Applied Science for the help with BET surface area measurements. We thank Dr. James E. McGrath's group for assistance with TGA and DSC instruments, and Steve McCartney for assistance with SEM.

3.7. References

(1) Lu, G. Q. Zhao, X. S. *Nanoporous Materials: Science and Engineering*; Imperial College Press, 2004; Vol. 4.

(2) Dawson, R.; Cooper, A. I.; Adams, D. J. *Prog. Polym. Sci.* **2012**, *37*, 530.

(3) Pastukhov, A. V.; Tsyurupa, M. P.; Davankov, V. A. *J. Polym. Sci. Pol. Phys.* **1999**, *37*, 2324.

(4) Tsyurupa, M. P.; Davankov, V. A. *React. Funct. Polym.* **2002**, *53*, 193.

(5) Tsyurupa, M. P.; Davankov, V. A. *React. Funct. Polym.* **2006**, *66*, 768.

(6) Cote, A. P.; Benin, A. I.; Ockwig, N. W.; O'Keeffe, M.; Matzger, A. J.; Yaghi, O. M. *Science* **2005**, *310*, 1166.

(7) Cooper, A. I. *Adv. Mater.* **2009**, *21*, 1291.

(8) Feng, X.; Ding, X. S.; Jiang, D. L. *Chem. Soc. Rev.* **2012**, *41*, 6010.

(9) Ding, S. Y.; Wang, W. *Chem. Soc. Rev.* **2013**, *42*, 548.

(10) Budd, P. M.; Ghanem, B. S.; Makhseed, S.; McKeown, N. B.; Msayib, K. J.; Tattershall, C. E. *Chem. Commun.* **2004**, 230.

(11) McKeown, N. B.; Budd, P. M. *Chem. Soc. Rev.* **2006**, *35*, 675.

(12) McKeown, N. B.; Budd, P. M. *Macromolecules* **2010**, *43*, 5163.

(13) McKeown, N. B. *ISRN Mater. Sci.* **2012**, *2012*, 16.

(14) Davankov, V. A.; Rogozhin, S. V.; Tsyurupa, M. P.; USSR Pat. 299165, **1969**. US Pat. 3729457, **1973**; *Chem. Abstr.* **1971**, 75, 6841B.

(15) Ahn, J.-H.; Jang, J.-E.; Oh, C.-G.; Ihm, S.-K.; Cortez, J.; Sherrington, D. C. *Macromolecules* **2006**, *39*, 627.

(16) Germain, J.; Hradil, J.; Frechet, J. M. J.; Svec, F. *Chem. Mater.* **2006**, *18*, 4430.

(17) Germain, J.; Frechet, J. M. J.; Svec, F. *Small* **2009**, *5*, 1098.

(18) Wood, C. D.; Tan, B.; Trewin, A.; Niu, H.; Bradshaw, D.; Rosseinsky, M. J.; Khimyak, Y. Z.; Campbell, N. L.; Kirk, R.; Stoeckel, E.; Cooper, A. I. *Chem. Mater.* **2007**, *19*, 2034.

(19) Germain, J.; Frechet, J. M. J.; Svec, F. *J. Mater. Chem.* **2007**, *17*, 4989.

(20) Mao, M.; Turner, S. R. *Polymer* **2006**, *47*, 8101.

(21) Mao, M.; Turner, S. R. *J. Am. Chem. Soc.* **2007**, *129*, 3832.

(22) Mao, M.; Kim, C.; Wi, S.; Turner, S. R. *Macromolecules* **2008**, *41*, 387.

(23) Li, Y.; Turner, S. R. *Eur. Polym. J.* **2010**, *46*, 821.

(24) Mao, M.; England, J.; Turner, S. R. *Polymer* **2011**, *52*.

(25) Li, Y.; Mao, M.; Matolyak, L. E.; Turner, S. R. *ACS Macro Lett.* **2012**, *1*, 257.

(26) Li, Y.; Zhang, M. Q.; Mao, M.; Turner, S. R.; Moore, R. B.; Mourey, T. H.; Slater, L. A.; Hauenstein, J. R. *Macromolecules* **2012**, *45*, 1595.

(27) Li, Y.; Savage, A. M.; Zhou, X.; Turner, S. R.; Davis, R. M. *J. Polym. Sci., Part B: Polym. Phys.* **2013** in press.

(28) Zhou, X.; Li, Y.; Hart, K. E.; Abbott, L. J.; Lin, Z.; Svec, F.; Colina, C. M.; Turner, S. R. *Macromolecules* **2013**, *46*, 5968.

(29) Sugihara, T.; Satoh, T.; Miura, M.; Nomura, M. *Angew. Chem. Int. Ed.* **2003**, *42*, 4672.

(30) Cava, M. P.; Deana, A. A.; Muth, K.; Mitchell, M. J. *N-Phenylmaleimide*; John Wiley & Sons, Inc., 2008; Vol. 41.

(31) Matuszak, N.; Muccioli, G. G.; Labar, G.; Lambert, D. M. *J. Med. Chem.* **2009**, *52*, 7410.

(32) http://www.polymersource.com/dataSheet/P1362-VBC.pdf

(33) Mark, J. E. *Polymerdata Handbook*; 2nd ed.; Oxford University Press, 2009.

(34) Dean, B. D. *J. Appl. Polym. Sci.* **1987**, *33*, 2259.

(35) Sing, K. S. W.; Everett, D. H.; Haul, R. A. W.; Moscou, L.; Pierotti, R. A.; Rouquerol, J.; Siemieniewska, T. *Pure Appl. Chem.* **1985**, *57*, 603.

(36) Brunauer, S.; Emmett, P. H.; Teller, E. *J. Am. Chem. Soc.* **1938**, *60*.

(37) Rouquerol, J.; Llewellyn, P.; Rouquerol, F. *Stud. Surf. Sci. Catal.* **2007**, *160*, 49.

3.8. Supporting Information

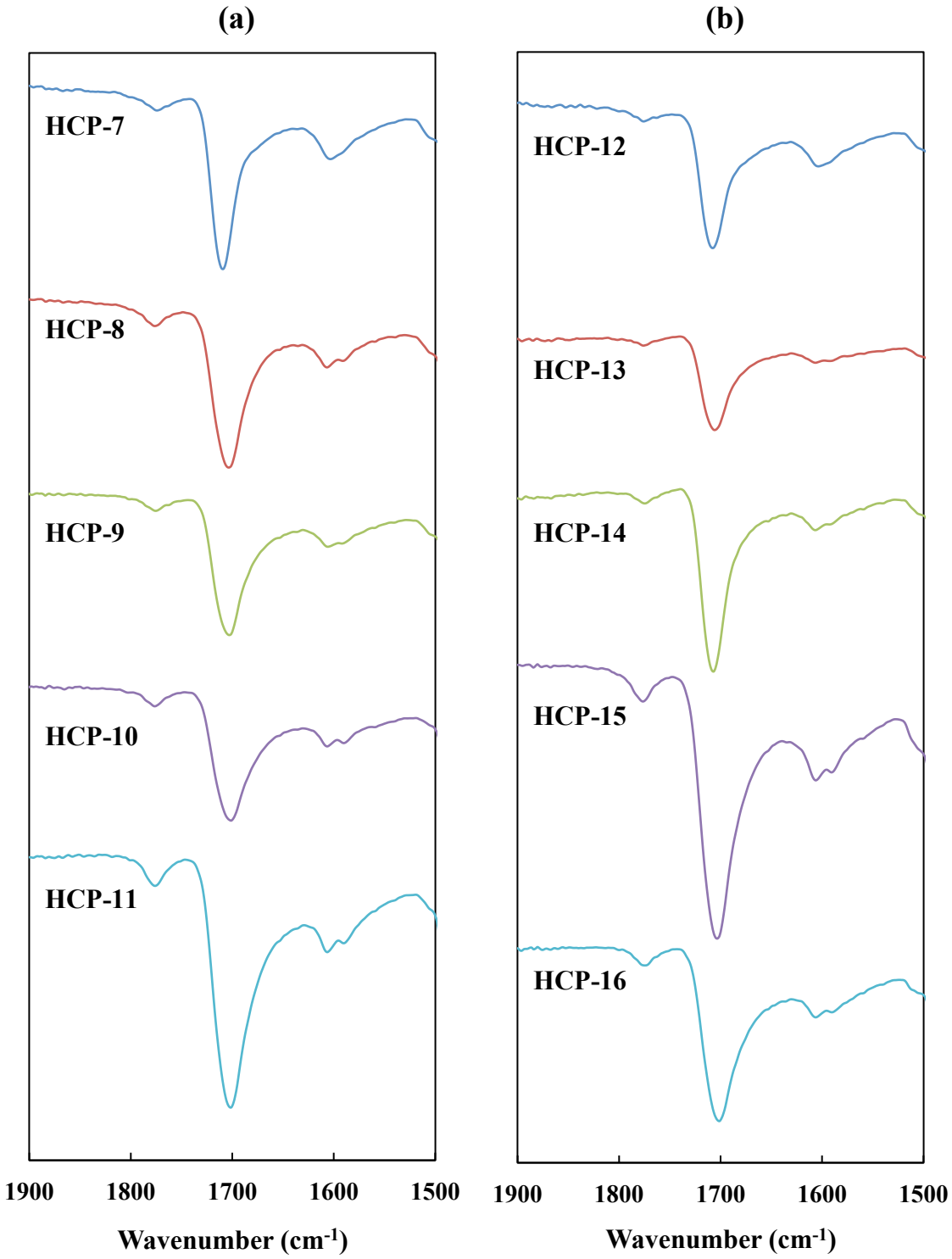

Figure 3-5. IR spectra of **HCP-7** to **HCP-16** showing peaks at around 1700 cm^{-1}, which are associated with C=O groups from incorporated maleimides.

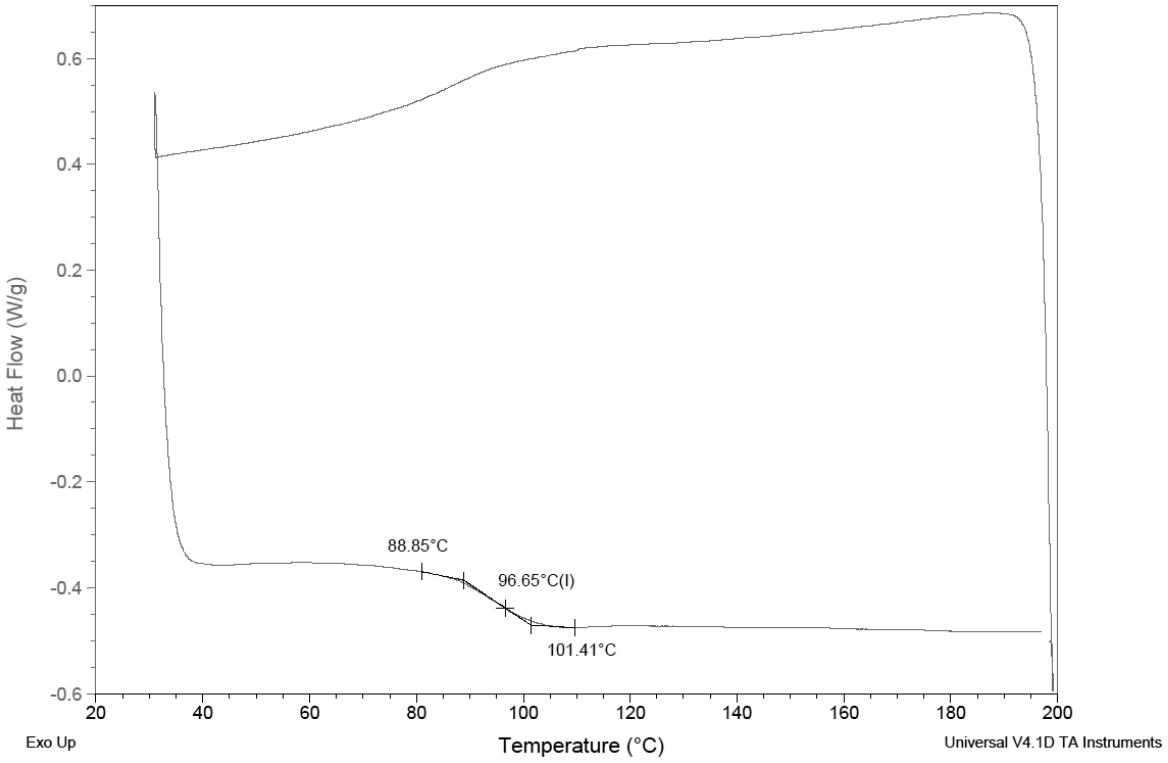

Figure 3-6. DSC curve of **P1** with a T_g of 97 ºC.

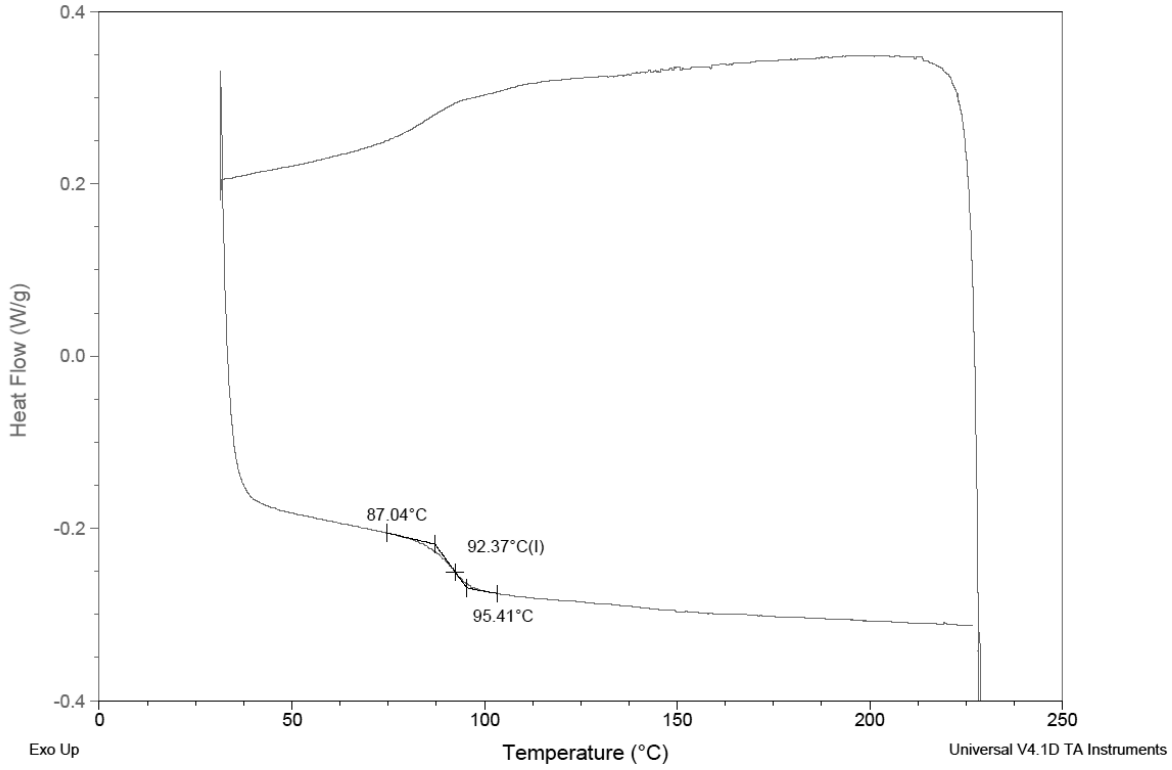

Figure 3-7. DSC curve of **P2** with a T_g of 92 ºC.

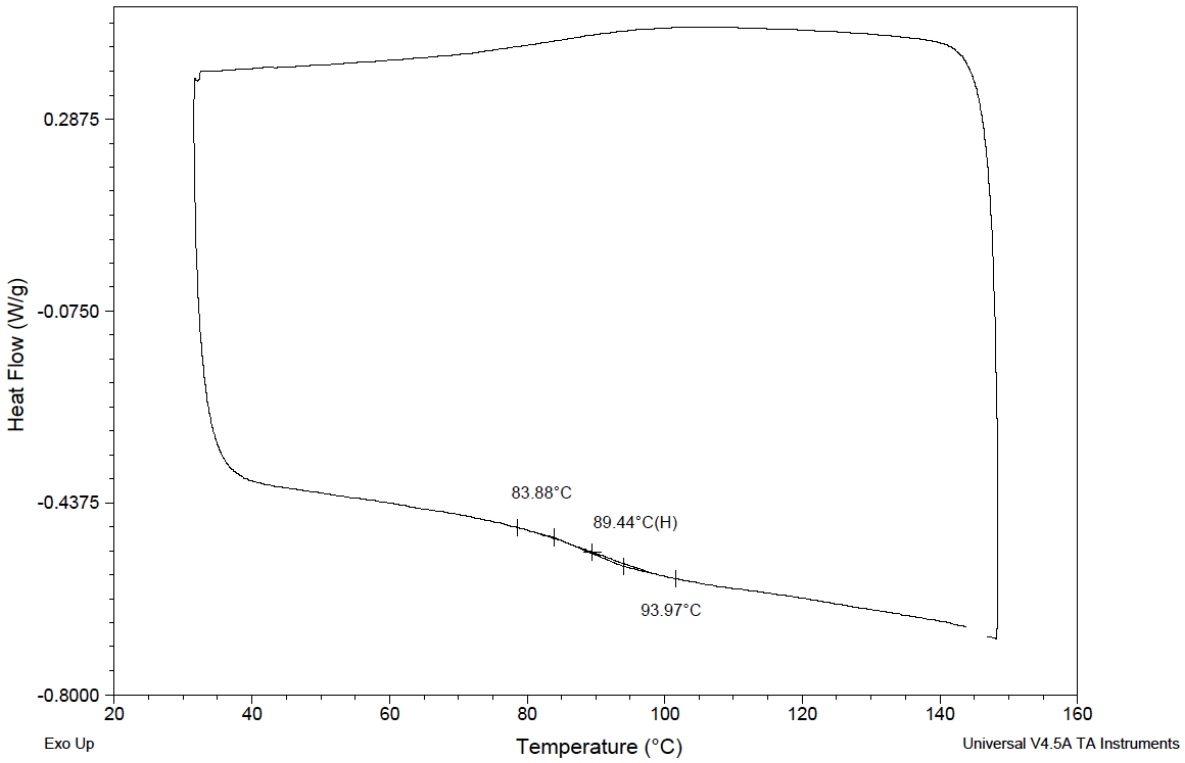

Figure 3-8. DSC curve of **P3** with a T_g of 89 ºC.

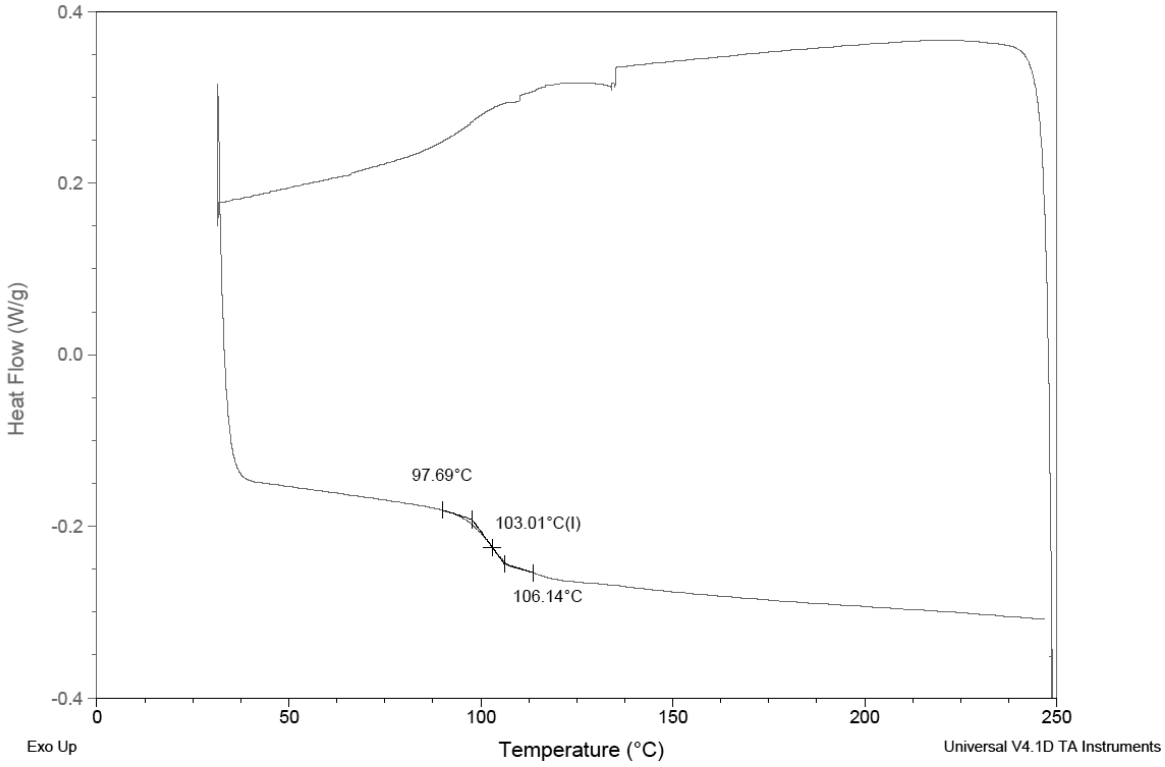

Figure 3-9. DSC curve of **P4** with a T_g of 103 ºC.

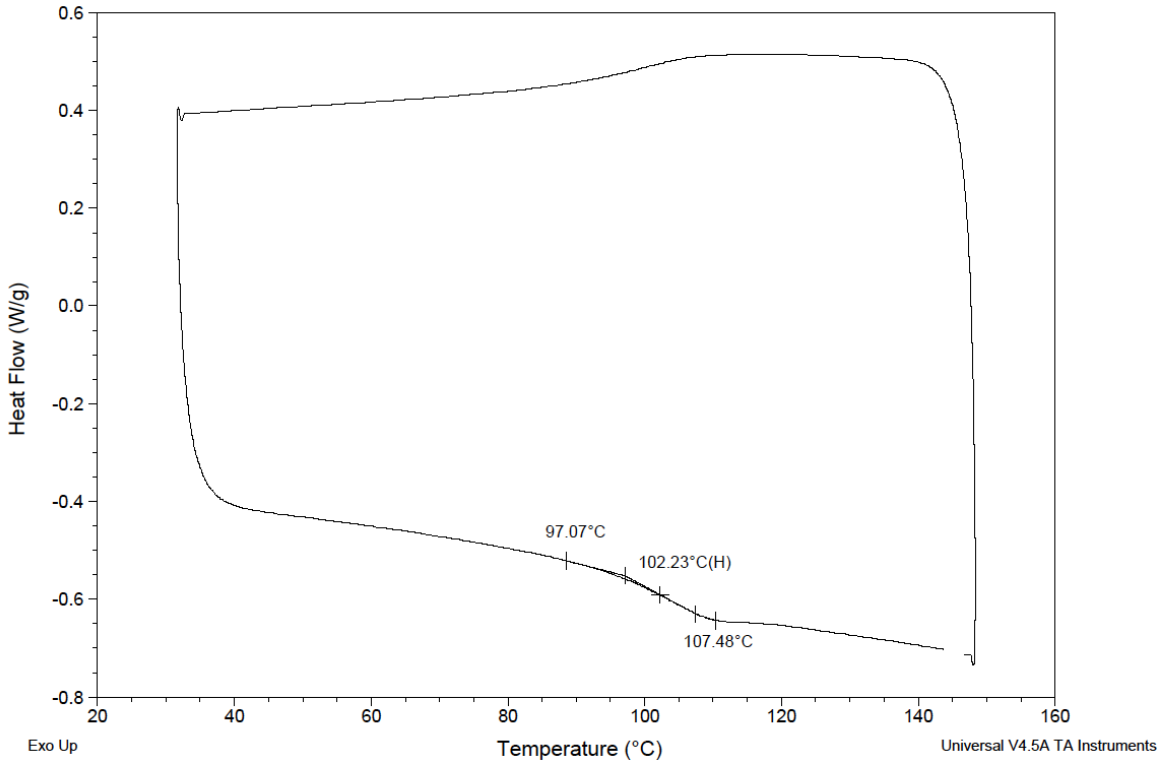

Figure 3-10. DSC curve of **P5** with a T_g of 102 ºC.

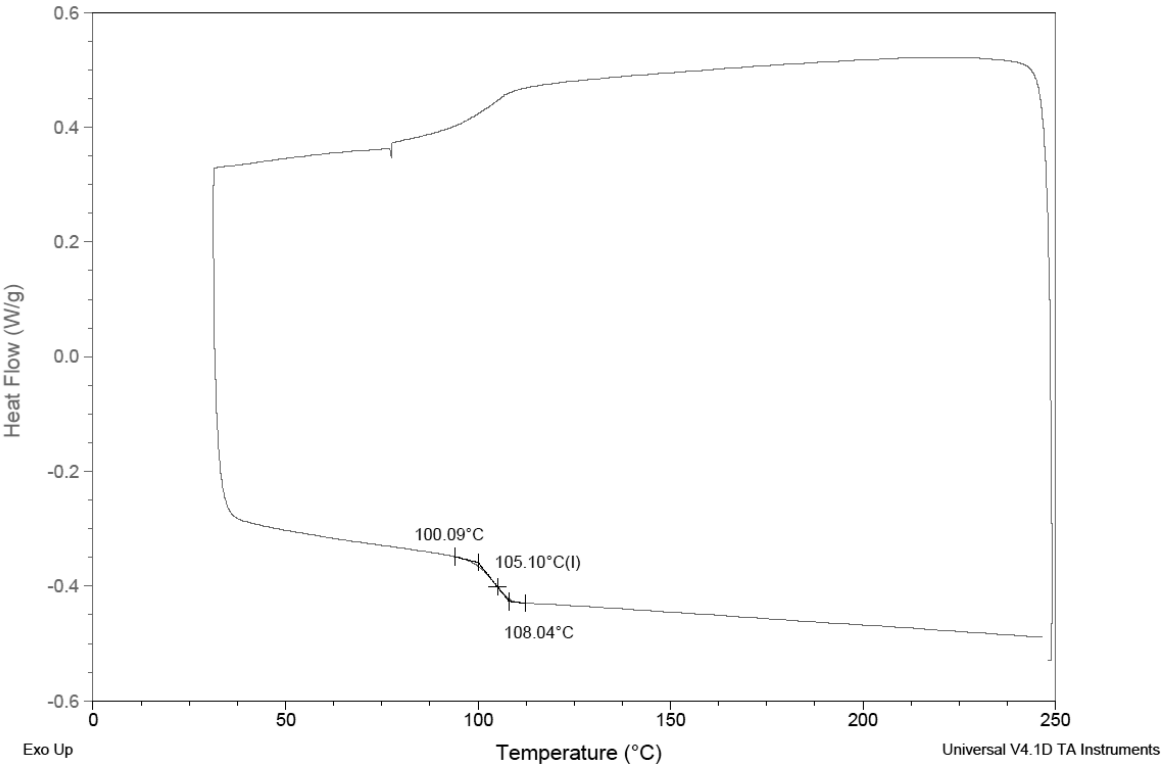

Figure 3-11. DSC curve of **P6** with a T_g of 105 ºC.

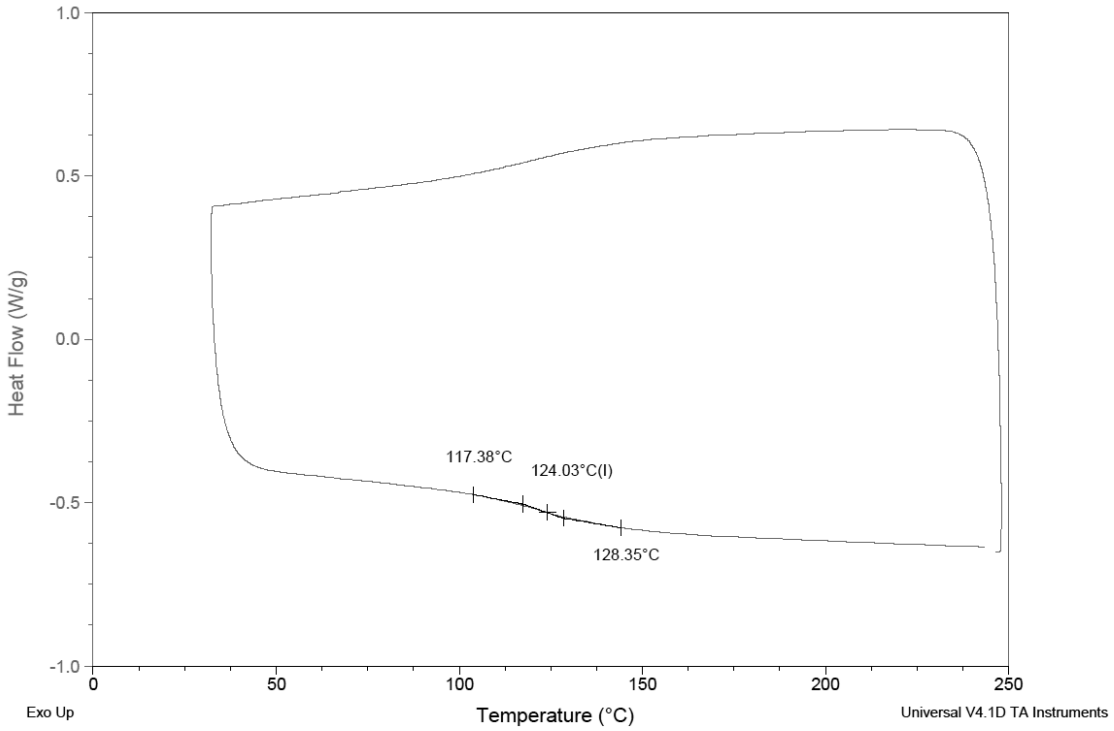

Figure 3-12. DSC curve of **P7** with a T_g of 124 ºC.

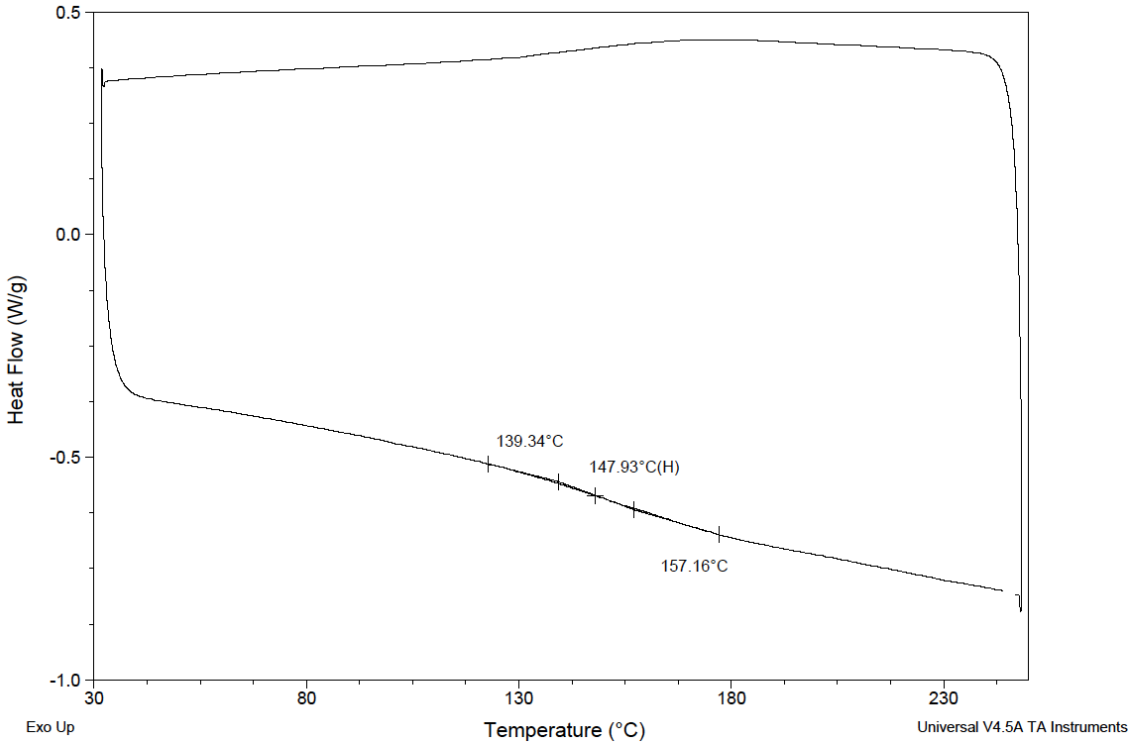

Figure 3-13. DSC curve of **P8** with a T_g of 148 ºC.

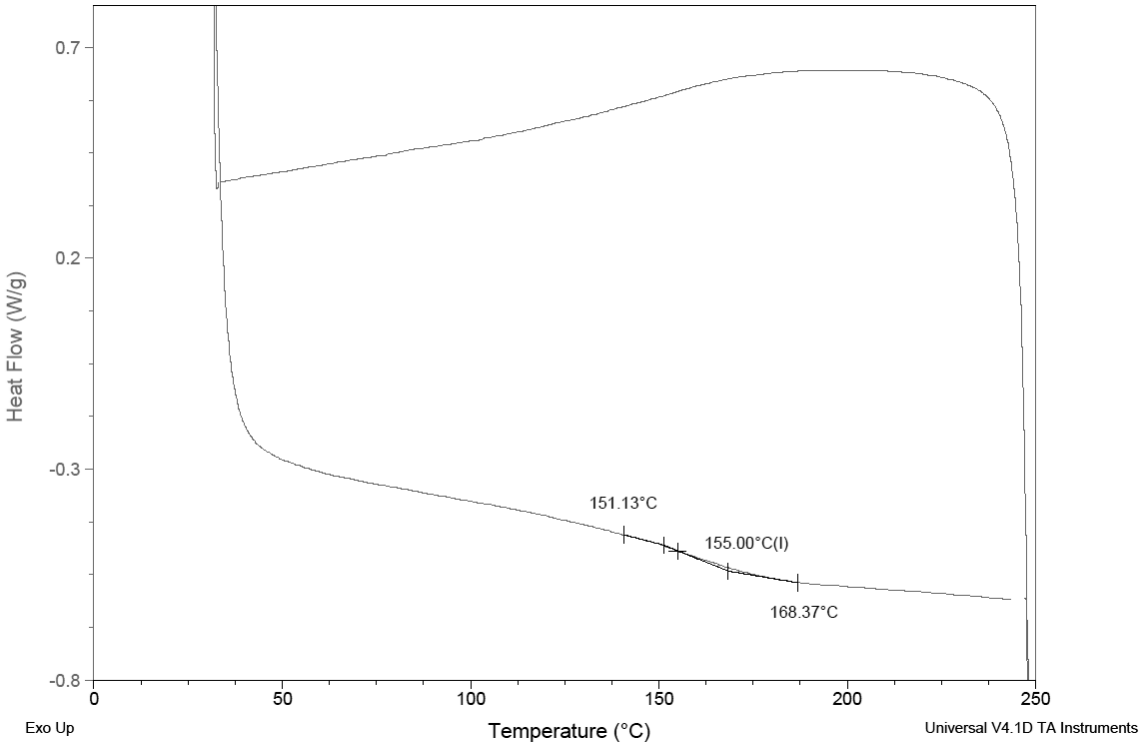

Figure 3-14. DSC curve of **P9** with a T_g of 155 ºC.

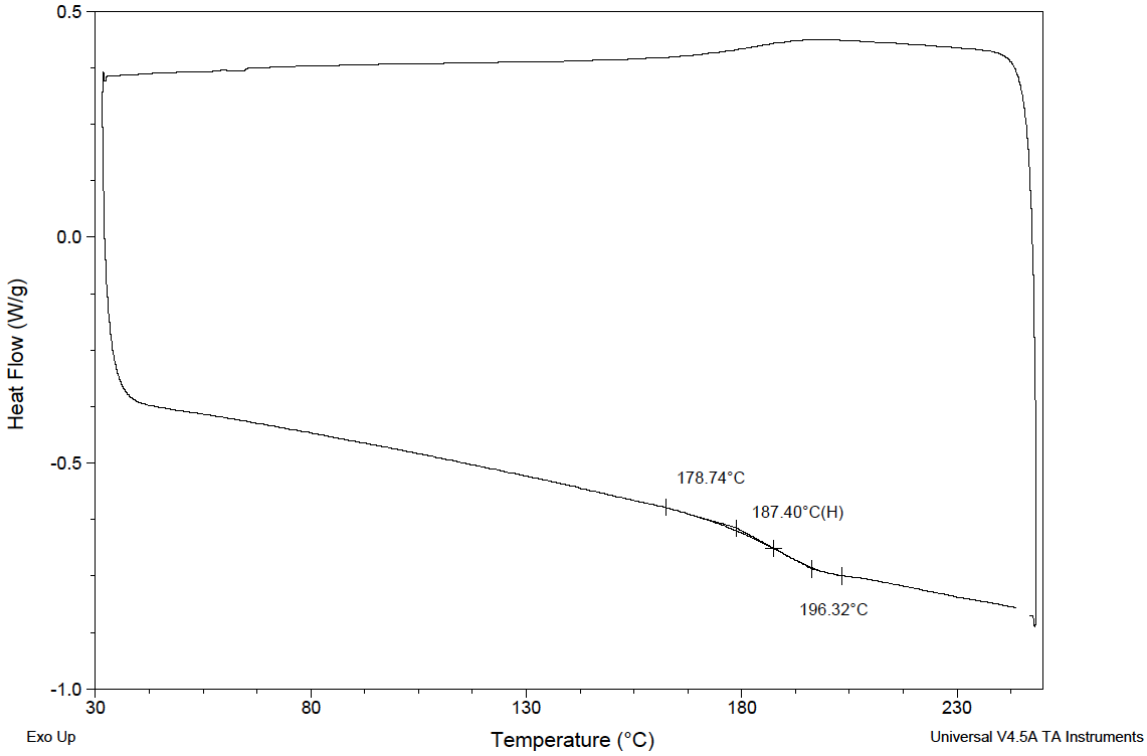

Figure 3-15. DSC curve of **P10** with a T_g of 187 ºC.

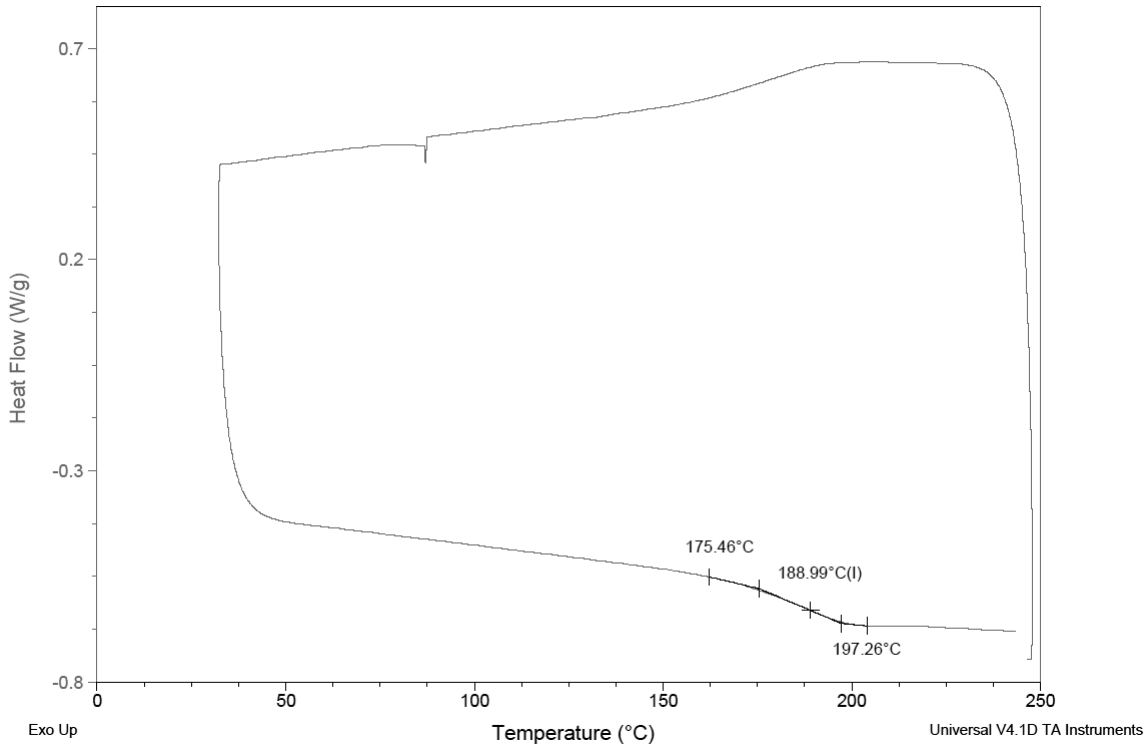

Figure 3-16. DSC curve of **P11** with a T_g of 189 ºC.

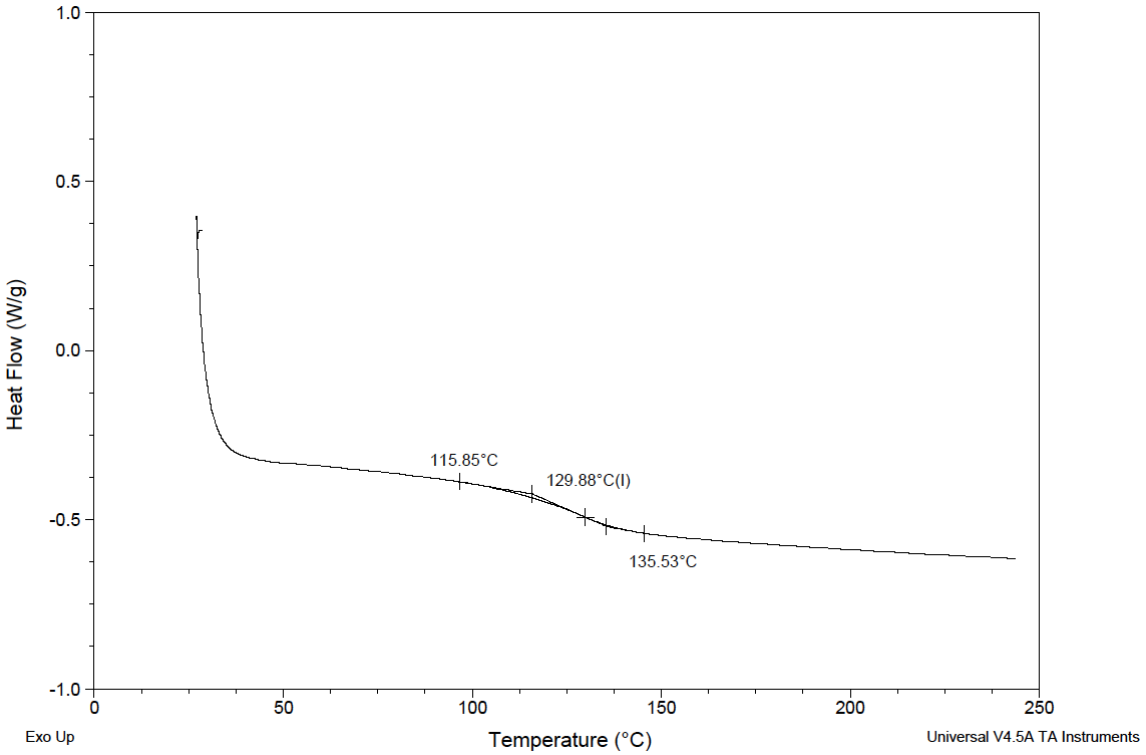

Figure 3-17. DSC curve of **P12** with a T_g of 130 ºC.

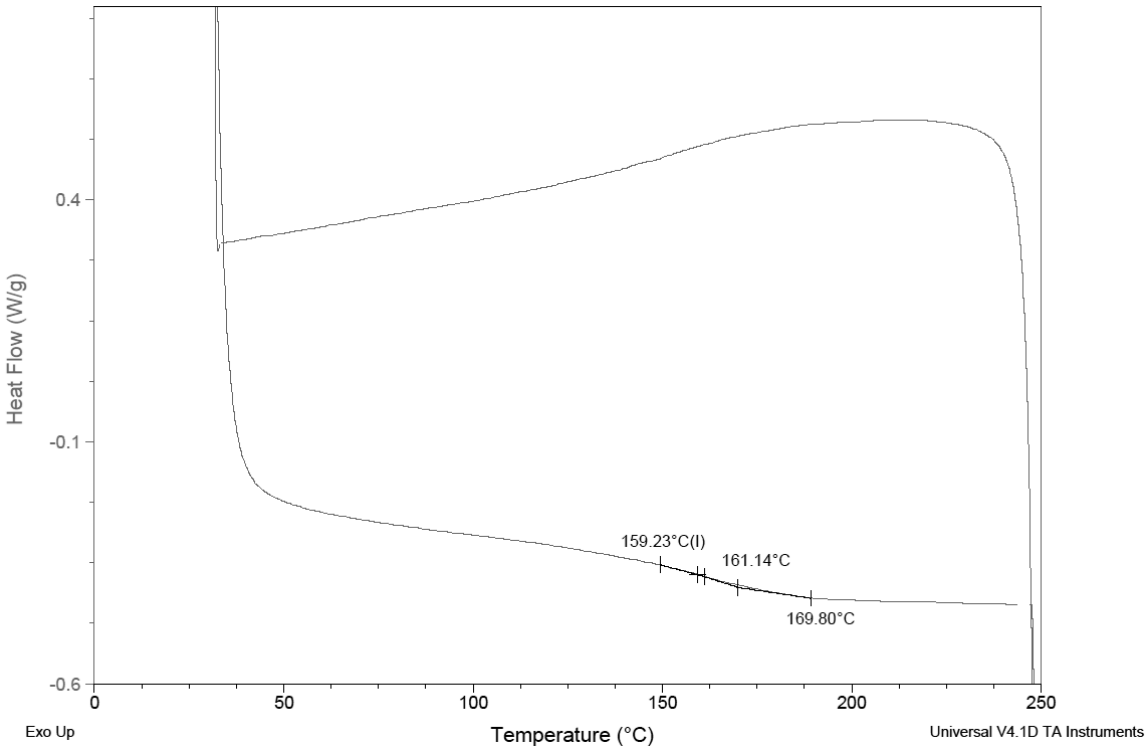

Figure 3-18. DSC curve of **P13** with a T_g of 161 ºC.

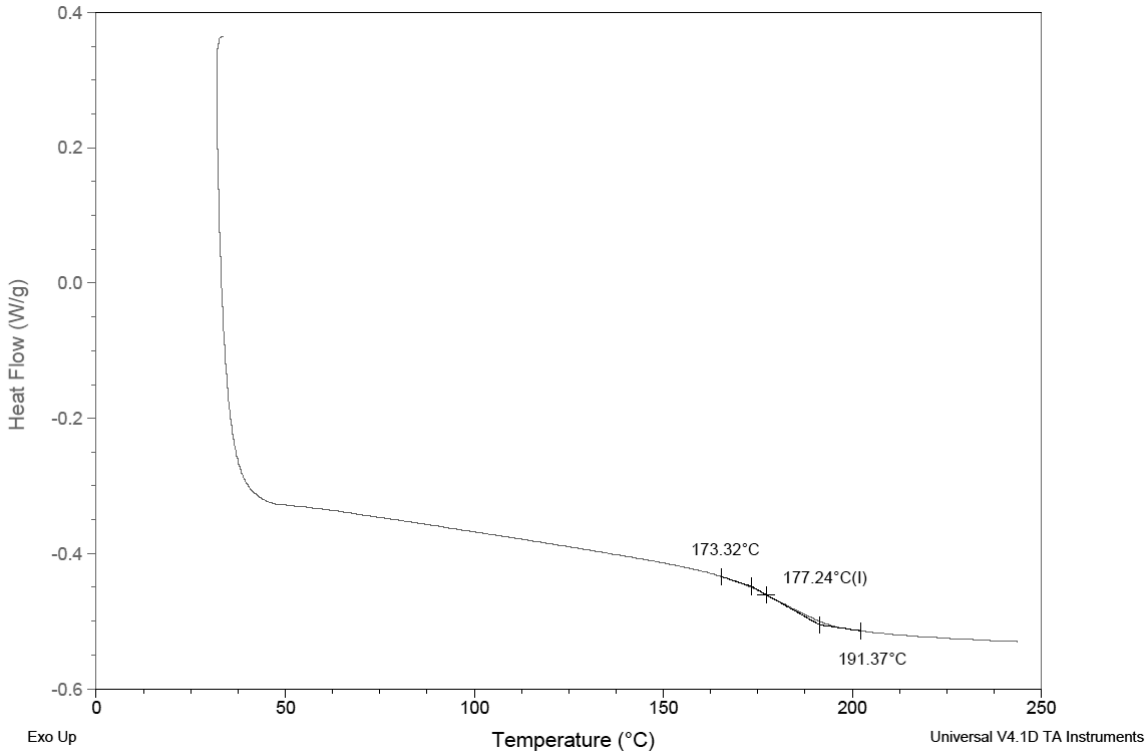

Figure 3-19. DSC curve of **P14** with a T_g of 177 ºC.

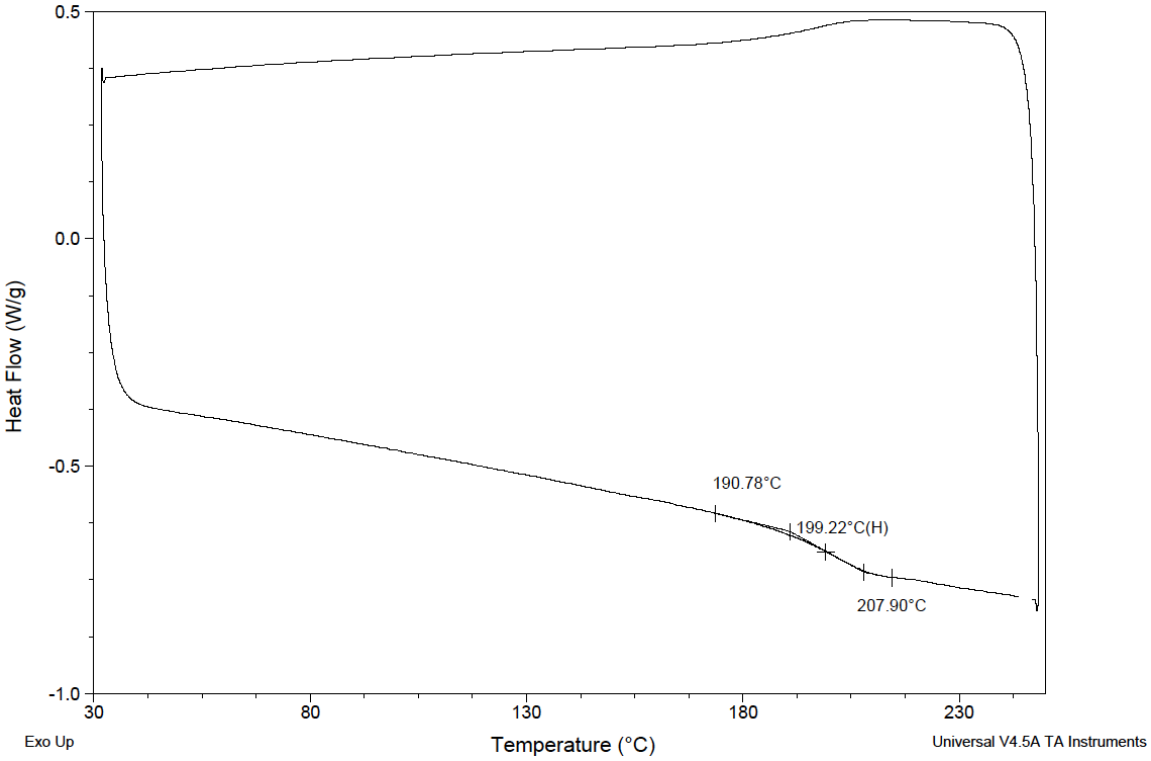

Figure 3-20. DSC curve of **P15** with a T_g of 199 ºC.

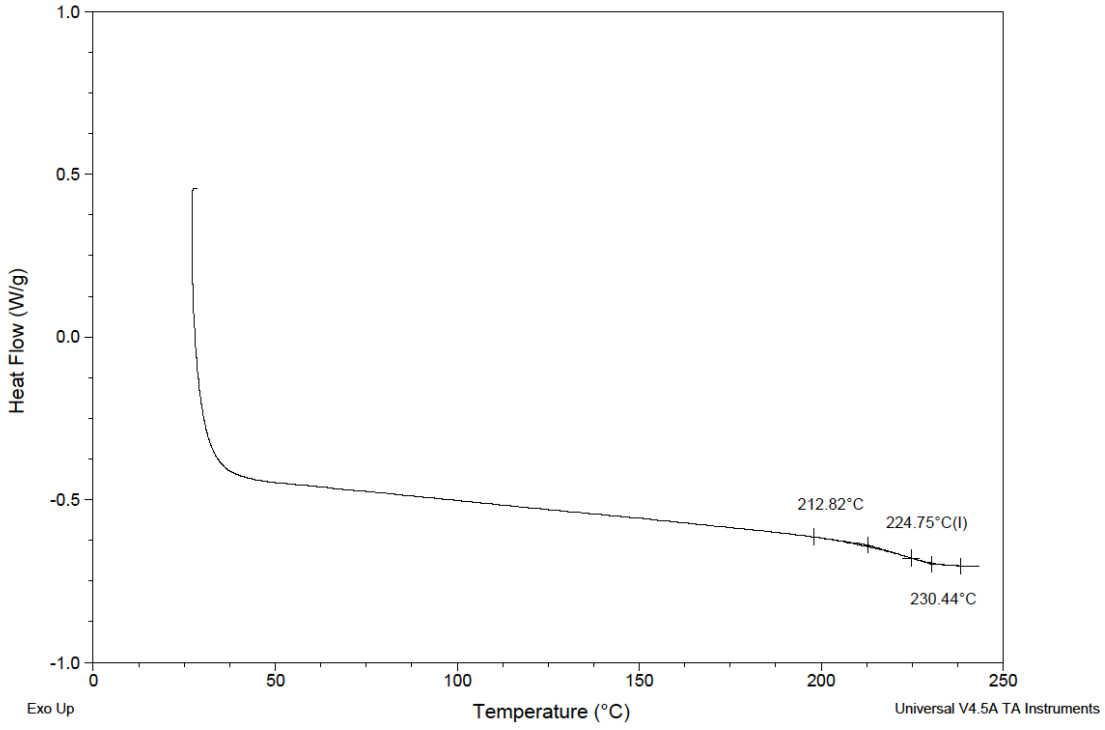

Figure 3-21. DSC curve of **P16** with a T_g of 225 ºC.

Sample Calculation of BET Surface Area

As mentioned in **§1.3.5** (**Chapter 1**), for the calculation of surface area by the BET method, the selection of the relative pressure range of the linear region in a BET plot is important. This section presents a sample calculation of BET surface area of HCP13. Nitrogen adsorption/desorption isotherm of HCP13 (**Figure 3-3**) was transformed into a BET plot (**Figure 3-22**) using the BET equation (**Equation 1-1**, **Chapter 1**). **Figure 3-2** shows a region of the BET plot at low relative pressure. The linear region were selected at P/P_0 =0.05-0.25 by the data processing software (TriStar II 3020 Windows by Micromeritics) to give a BET surface area of 737 m^2/g. The reported data, which were generated by the software, are summarized in **Table 3-2**. Both intercept and C value were found negative, which would be meaningless (see **§1.3.5** for the definition of C value). Therefore a more careful selection on the relative pressure range for the linear region is needed.

Rouquerol and coworkers suggested several criteria for the selection of appropriate relative pressure range: positive intercept, positive C value, and a continuous increase in the term n(P/P_0) with P/P_0.[35] A plot of the term n(P/P_0) versus P/P_0 of HCP13 was generated and is shown in **Figure 3-23**. In order to ensure the term n(P/P_0) increase together with P/P_0 in the linear region, the selected relative pressure range should be kept below 0.16. The data after reselection of relative pressure range for linear region are summarized in **Table 3-3**. Both intercept and C value are positive and the linear region has a higher correlation coefficient compared to the value before reselection (reported value).

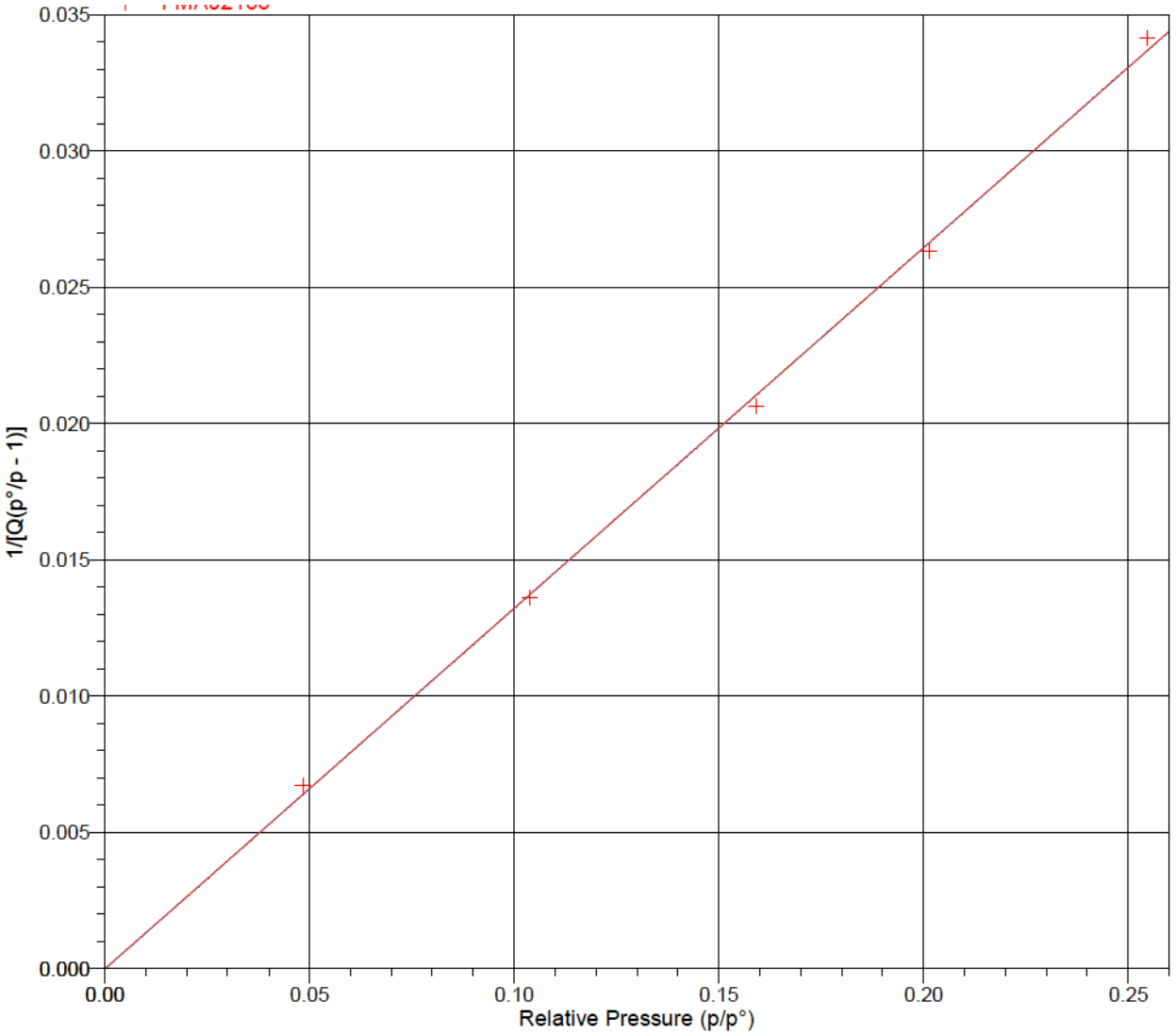

Figure 3-22. The BET plot of HCP13 before reselection of relative pressure range.

Table 3-2. Data for BET surface area calculation before and after reselection of the relative pressure range for the linear region of BET plot.

	Surface area (m^2/g)	Slope (s) (g/mmol)	Intercept (i) (g/mmol)	C	n_m (mmol/g)	Correlation coefficient
Reported value	737	0.1323	-0.000015	-8752	7.56	0.99933
Corrected value	774	0.1255	0.00064	197	7.93	0.99995

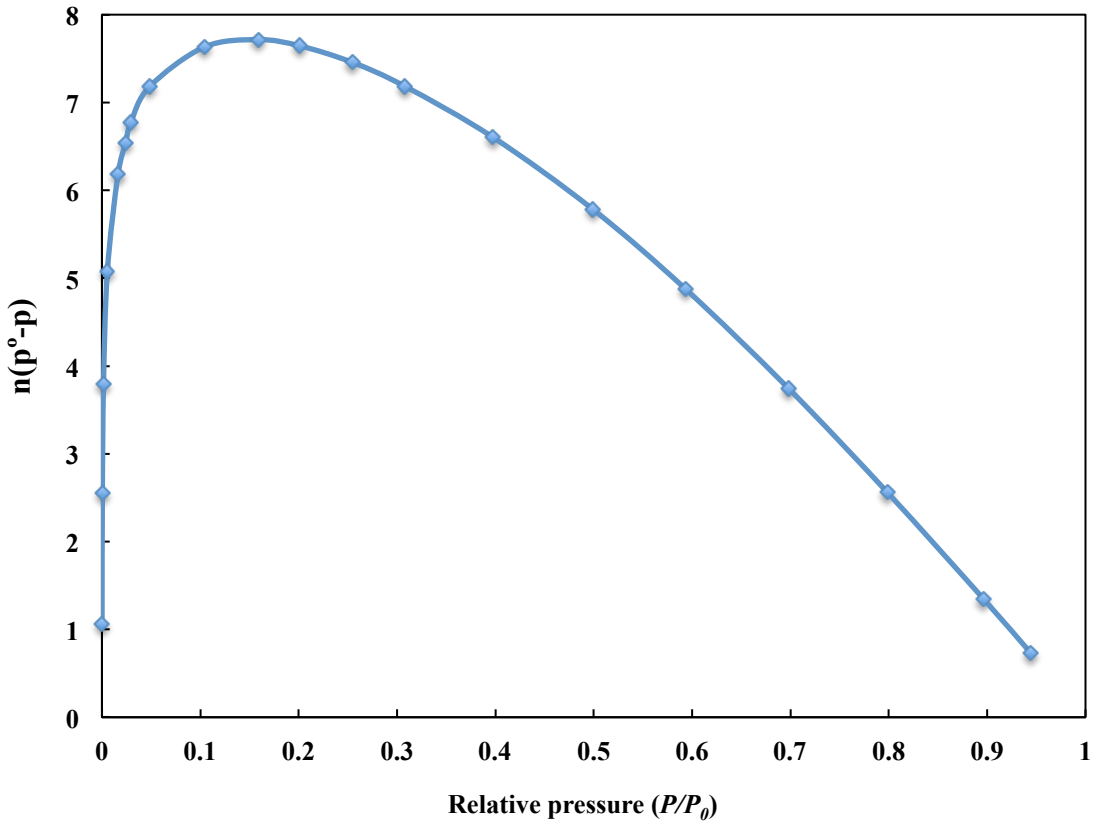

Figure 3-23. Plot of the term n(P_0-P) versus P/P_0.

Chapter 4. Dry Sorbents for Carbon Capture

4.1. Abstract

Amine-functionalized styrene/stilbene-containing polymers and amine-containing silica-based sorbents were prepared. The CO_2 sorption properties of these materials were tested using TGA. The amine-containing polymers, which had low surface areas, showed insignificant CO_2 uptake. Silica-based amine sorbents showed CO_2 uptake up to 12 wt% (at 30 ºC, 1 bar) and amine efficiency up to 0.55 (CO_2/N, mol/mol). The effects of surface area and amine concentration on CO_2 uptake of these materials were discussed in this chapter.

4.2. Introduction

To control CO_2 emissions from coal-fired power plants, carbon capture and sequestration (CCS) technologies, which involve sequestration of CO_2 from large point sources, transportation, and long-term storage, are being developed.[1] Three approaches to capture CO_2 from fossil fuel power plants include pre-, post-, and oxy-combustion (see **§1.1.3**). The current state-of-art technology used in post-combustion processes uses 20-30 wt% aqueous monoethanolamine (MEA) to remove CO_2 from the flue gas.[2] However, this process is too costly and entails issues concerning water treatment, corrosion, etc.[3-5] A more promising method would be to use dry sorbents, which have a high surface area and capture units to selectively adsorb CO_2 and desorb (or release) it at a higher temperature for reuse. Compared to aqueous amines, solid sorbents for CO_2 capture have advantages of better thermal stability, lower regeneration energy, lower heat capacity, and wider range of operation temperature.[6,7] A number of solid sorbents, such as carbon-based sorbents,[8-10] zeolites,[11,12] amine-based sorbents,[13,14] and metal organic frameworks,[15-17] have been studied for CO_2 capture applications. However, designing and

building sorbents with high CO_2 adsorption capability, high CO_2 selectivity, fast adsorption/desorption kinetics, low cost, and robust durability remain a current challenge.

In this chapter, we report the synthesis of a series of amine-based linear/lightly crosslinked polymers via polymerization or post-modification and a series of amine-based porous silica via impregnation methods. CO_2 sorption properties of these materials were tested using thermogravimetric analysis (TGA). The effects of amine content and surface area of these sorbents are discussed. The efficiency of the impregnation method, effect of pore size, and amine efficiency of the silica-based sorbents are discussed.

4.3. Experimental Section

4.3.1. Materials

Vinylbenzyl chloride (mixture of 3- and 4-isomers, Aldrich, 97%), diethanolamine (DEA, J.T.Baker, 99.5%), potassium carbonate (K_2CO_3, anhydrous, Fisher, ≥99.0%), sodium bicarbonate ($NaHCO_3$, Acros Organics, ≥99.7%), triethylamine (TEA, Aldrich, ≥99.0%), magnesium sulfate ($MgSO_4$, Aldrich, anhydrous, 99%), sodium chloride (NaCl, BDH, ≥99.0%), pyridine (Adrich, 99.8%), phosphorus tribromide (PBr_3, Aldrich, 97%), dimethylamine (Aldrich, 40 wt% solution in water), potassium iodide (KI, Aldrich, ≥99.0%), 3,3'-iminobis(*N*,*N*-dimethylpropylamine) (DMPA, Aldrich, 97%), sodium thiosulfate ($Na_2S_2O_3$, Aldrich, ≥98%), *N*-bromosuccinimide (NBS, Aldrich, 99%), *p*-tolualdehyde (Aldrich, 97%), pottassium *tert*-butoxide (^{t}BuOK, Aldrich, 1.0M solution in tetrahydrofuran), 4-methylbenzyl chloride (Aldrich, 98%), 3-methylbenzyl chloride (Aldrich, 98%), *m*-toluidine (Aldrich, 99%), *m*-tolualdehyde (Aldrich, 97%), styrene (STR, Aldrich, ≥99%), maleic anhydride (MAH, Aldrich, ≥99.0%), divinylbenzene (DVB, mixture of isomers, Aldrich, 80%), and 1,4-diaminobutane (DAB,

Aldrich, 99%) were used without further purification. Acetonitrile (MeCN, Fisher, HPLC grade), chloroform ($CHCl_3$, Fisher, Optima), hexanes (Fisher, HPLC grade), ethyl acetate (EtOAc, Fisher, HPLC grade), diethyl ether (Fisher, HPLC grade), methanol (MeOH, Fisher, HPLC grade), methylene chloride (CH_2Cl_2, Fisher, HPLC grade), carbon tetrachloride (CCl_4, Aldrich, anhydrous, ≥99.5%), triethyl phosphite (Aldrich, 98%), benzene (Aldrich, anhydrous, 99.8%), and *N*-methyl-2-pyrrolidone (NMP, J.T.Baker, bio-analyzed reagent) were used as received. Water was deionized before use. 3,3'-Iminodipropoinitrile (Aldrich, 90%) was distilled at 150 ºC and 0.7 Torr to afford a colorless liquid before use. 2,2'-Azobisisobutyronitrile (AIBN, Aldrich, 98%) was recrystallized from methanol. Pentaethylenehexamine (PEHA, technical grade) was distilled before use. SBA-15 was provided by the Mineral Processing & Enviroment Processing (MPEP) Laboratory, Hanyang University, Seoul, Korea. CARiACT G10 (Fuji Silysia) was provided by the National Energy Technology Laboratory (NETL), Pittsburgh, PA. Solutions were concentrated by rotary evaporation unless noted otherwise. Reactions were conducted in a round bottom flasks (RBF) unless noted otherwise.

4.3.2. Synthesis

4.3.2.1. Monomer Synthesis

Preparation of 2,2'-((vinylbenzyl)azanediyl)diethanol (M1) (Scheme 4-1).[18] A mixture of diethanolamine (DEA) (4.17 g, 0.039 mol), vinylbenzyl chloride (VBC) (5.0 g, 0.033 mol), and K_2CO_3 (9.12 g, 0.066 mol) in MeCN (66 mL) was stirred and heated at 50 °C for 24 h. The reaction was monitored by thin layer chromatography (TLC) (eluent 2:1:1 drop hexane/EtOAc/TEA); VBC (R_f, 0.9), product (R_f, 0.1). After cooling, the yellow solution with white solid was vacuum filtered and the filtrate was concentrated to give a yellow viscous liquid.

$NaHCO_3$ saturated solution (100 mL) was added until the aqueous layer reached pH 8. The biphasic mixture was poured into a beaker. The reaction flask was rinsed with $CHCl_3$ (3×200 mL) and poured into a beaker. After separation of the biphasic solution using a separatory funnel, the organic layer was washed with brine (150 mL), dried over $MgSO_4$ at 4 °C overnight and filtered. The filtrate was concentrated and dried under high vacuum to give a yellow liquid (8.4 g, > 100%), which was used in the next step without further purification. ^{1}H NMR (400 MHz, $CDCl_3$) δ 7.1–7.4 (m, 4H), 6.7 (m, 1H), 5.7 (dd, J_{app} = 17.6, 8.1 Hz, 1H), 5.2 (dd, J_{app} = 10.9, 7.9 Hz, 1H), 3.5–3.7 (m, 6H), 2.6–2.8 (m, 4H), 2.5 (s, 1H). (lit.[18] 300 MHz ^{1}H NMR, IR)

Preparation of *N*-(vinylbenzyl)-2-bromo-*N*-(2-bromoethyl)ethanamine (M2). A mixture of **M1** (3.54 g, 0.016 mol) and pyridine (1.01 g, 0.013 mol) in dry $CHCl_3$ (65 mL) was stirred in a round bottom flask, which was cooled in an ice bath. Phosphorus tribromide (PBr_3) (4.33 g, 0.016 mol) was added dropwise. The yellow liquid in the flask began to turn dark orange and gave off heat. After addition of PBr_3 was completed, the mixture was heated at 50 °C for 7 h. The reaction was monitored by TLC (eluent 2:1:1 drop hexane/EtOAc/TEA); **M1** (R_f, 0.1), product (R_f, 0.9). The mixture was poured into a beaker with ice water (150 mL). $NaHCO_3$ saturated solution was added into the beaker with constant stirring until the pH of the solution was 8 (confirmed with pH paper). The mixture was extracted with chloroform (3×100 mL) using a separatory funnel. The combined organic phase was dried over $MgSO_4$ overnight and filtered. The filtrate was concentrated and dried under high vacuum, purified by silica column chromatography (eluent 1:1:1 drop hexane/EtOAc/TEA) to give a yellow oil (1.04 g, 19%), which was used in the next step without further characterization. ^{1}H NMR (400 MHz, $CDCl_3$) δ 7.1–7.4 (m, 4H), 6.7 (m, 1H), 5.8 (dd, J_{app} = 17.6, 9.4 Hz, 1H), 5.3 (dd, J_{app} = 10.9, 7.5 Hz, 1H), 3.7 (2 s, 2H), 3.2–3.4 (m, 4H), 2.9–3.1 (m, 4H).

Preparation of 2,2',2'',2'''-(((vinylbenzylazanediyl)bis(ethane-2,1-diyl))bis(azanetriyl))tetraethanol (M3). A mixture of DEA (0.49 g, 1.4 mmol), **M2** (0.33 g, 3.2 mmol), and K_2CO_3 (0.40 g, 2.9 mmol) in MeCN (3 mL) was stirred in a round bottom flask and heated at 60 °C for 24 h. After cooling, the yellow solution with white solid was vacuum filtered. The filtrate was concentrated to give a yellow viscous liquid. The biphasic mixture was poured into a beaker. The reaction flask was rinsed with $CHCl_3$ (3×5 mL) and poured into the beaker. After the separation of the biphasic solution using a separatory funnel, the combined organic phase was dried over $MgSO_4$ overnight and filtered. The filtrate was concentrated and dried under high vacuum to afford a yellow liquid (0.08 g, 14%). The low yield is probably due to the steric hindrance in preparing dendritic monomer and small-scale of this synthesis. ^{1}H NMR (400 MHz, $CDCl_3$) δ 7.1–7.4 (m, 4H), 6.6–6.8 (m, 1H), 5.6–5.8 (m, 1H), 5.2–5.3 (m, 1H), 3.5–3.7 (m, 10H), 2.7 (m, 1H), 2.3–2.5 (m, 16H). ^{13}C NMR (500 MHz, CD_3OD) δ 138.0, 137.4, 136.6, 136.5, 136.3, 130.0, 129.1, 128.4, 127.4, 126.1, 125.5, 113.3, 113.1, 58.5, 57.4, 56.0, 51.1, 49.5. HR-ESIMS: calculated for $[M + H]^+$: 396.2872, found: *m/z*, 396.2867 $[M + H]^+$, error: -1 ppm.

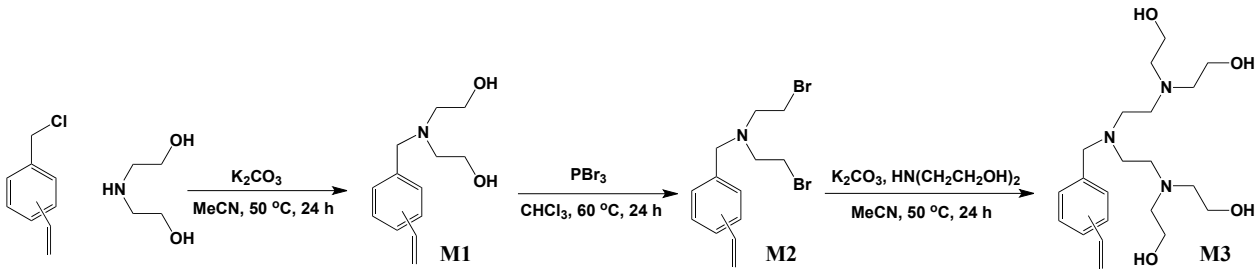

Scheme 4-1. Preparation of **M1**, **M2**, and **M3**.

Preparation of *N*,*N*-dimethyl-1-(vinylphenyl)methanamine (M4) (Scheme 4-2). M4 was prepared using a modified method from literature.[19] A mixture of VBC (2.00 g, 0.013 mol), diethyl ether (15 mL, 1M), and 40 wt% aqueous dimethylamine solution (8.3 mL) was stirred at room temperature for 16 h. The reaction was monitored by TLC (eluent 2:1:1 drop

hexane/EtOAc/TEA); VBC (R_f, 0.9), product (R_f, 0.4). The organic phase was separated from aqueous phase using a separatory funnel, dried over $MgSO_4$ overnight and filtered. The filtrate was concentrated and purified by silica column chromatography (eluent 10:1:1 drop hexane/EtOAc/TEA). A light yellow liquid was obtained (1.32 g, 62 %). (lit.[20] clear liquid). ^{1}H NMR (400 MHz, $CDCl_3$) δ 7.2–7.4 (m, 4H), 6.7 (m, 1H), 5.7–5.8 (m, 1H), 5.2–5.3 (m, 1H), 3.4 (2 s, 2H), 2.2–2.3 (m, 6H). (lit.[20] 400 MHz ^{1}H NMR)

Scheme 4-2. Preparation of **M4**.

Preparation of N^1-(3-(dimethylamino)propyl)-N^3,N^3-dimethyl-N^1-(vinylbenzyl)propane-1,3-diamine (M5) (Scheme 4-3). A mixture of VBC (6 g, 0.04 mol), KI (0.27 g, 0.002 mol), and K_2CO_3 (0.74 g, 0.005 mol) in MeOH (50 mL) was stirred in a three-neck round bottom flask, which was cooled in an ice bath. The flask was purged with N_2. 3,3'-Iminobis(*N*,*N*-dimethylpropylamine) (DMPA) (6 mL, 0.03 mol) was added dropwise to the flask. After 30 min, the mixture was heated at 60 ºC for 24 h. The reaction was monitored by TLC (eluent 2:1:1 drop hexane/EtOAc/TEA); VBC (R_f, 0.9), product (R_f, 0.1). After cooling the brown mixture was filtered. The filtrate was concentrated and purified by silica column chromatography (eluent 1:1 drop EtOH/TEA) to afford a yellow liquid (3.49 g, 43%). ^{1}H NMR showed the product contained both desired compound and DMPA, probably due to the unsuccessful purification. Further purification, such as using column chromatography with optimum developing solvent, is needed.

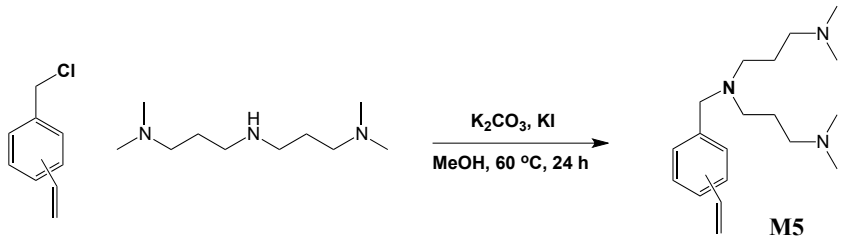

Scheme 4-3. Preparation of **M5**.

Preparation of 3,3'-((vinylbenzyl)azanediyl)dipropanenitrile (M6) (Scheme 4-4).[21] A mixture of 3,3'-iminodipropoinitrile (2.03 g, 0.017 mol), VBC (3.77 g, 0.025 mol), KI (0.047 g, 0.0003 mol), and K_2CO_3 (1.14 g, 0.008 mol) in MeCN (10 mL) was stirred and heated at 85 °C for 24 h under N_2. The reaction was monitored by TLC (eluent 2:1:1 drop hexane/EtOAc/TEA); VBC (R_f, 0.9), product (R_f, 0.4). After cooling, the yellow solution with white solid was vacuum filtered. The filtrate was concentrated to give a brown viscous liquid. The liquid was dissolved in CH_2Cl_2, washed with $Na_2S_2O_3$ aq solution and NaCl aq solution using a separatory funnel. The collected organic phase was dried over $MgSO_4$ at 4 °C overnight and filtered. The filtrate was concentrated and purified by silica column chromatography (eluent 10:1:1 drop hexane/EtOAc/TEA) to afford a colorless liquid (1.97 g, 50 %). (lit.[22] viscous yellow oil) ^{1}H NMR (500 MHz, $CDCl_3$) δ 7.2–7.4 (m, 4H), 6.7 (m, 1H), 5.8 (dd, J = 17.4, 16.3 Hz, 1H), 5.3 (dd, J_{app} = 10.7, 9.3 Hz, 1H), 3.7 (2 s, 2H), 2.9 (m, 4H), 2.5 (m, 4H). ^{13}C NMR ($CDCl_3$, δ) 138.2, 138.0, 137.5, 137.1, 136.7, 136.5, 136.4, 129.0, 128.9, 128.1, 126.6, 126.4, 125.7, 118.8, 114.5, 60.5, 58.1, 58.0, 49.6, 49.5, 16.9. HR-ESIMS: calculated for $[M + H]^+$: 240.1495, found: *m/z*, 240.1493 $[M + H]^+$, error: -0.8 ppm. Elemental analysis: calculated C, 75.30; H, 7.11; N, 17.57. Found C, 75.10; H, 7.30; N, 17.32.

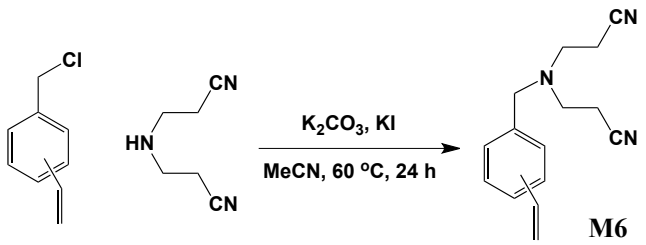

Scheme 4-4. Preparation of **M6**.

Preparation of 4-bromomethylstilbene (M7) (Scheme 4-5).[23] A mixture of 4-methyl-stilbene (4MSTB) (see **Chapter 3** for detailed preparation, 3.88 g, 0.020 mmol), NBS (3.92 g, 0.022 mol), and AIBN (0.08 g) in CCl_4 (100 mL) was stirred at 90 °C under Ar for 4 h. After cooling the mixture was vacuum filtered and the solid was washed with benzene (20 mL). The filtrate was concentrated and dried under vacuum to afford a white solid. The crude product (3.00 g) was purified by silica column chromatography (eluent 50:1 hexane/EtOAc) to afford a white solid (0.88 g, 15 %). mp: 115 ºC (lit.[24] mp 117-118 ºC). ^{1}H NMR (400 MHz, $CDCl_3$) δ 7.0–7.5 (m, 11H), 4.5 (s, 2H). (lit.[24] elemental analysis)

Preparation of (*E*)-2,2'-((4-styrylbenzyl)azanediyl)diethanol (M8) (Scheme 4-5). A mixture of diethanolamine (DEA) (2.29 g, 0.022 mol), **M7** (2.99 g, 0.011 mol), K_2CO_3 (3.04 g, 0.022 mol), and KI (1.46 g, 0.09 mol) in benzene (22 mL) was stirred and heated at 60 °C for 20 h. The reaction was monitored by thin layer chromatography (TLC) (eluent 2:1:1 drop hexane/EtOAc/TEA); M7 (R_f, 0.9), product (R_f, 0.1). After cooling, the yellow solution with solid was vacuum filtered and the filtrate was concentrated to give a yellow solid, which was purified by silica column chromatography (eluent 1:1 Acetone/EtOAc) to afford a yellow solid (1.06 g, 33 %). mp: 104-105 ºC (lit.[25] mp: 102-103 ºC). ^{1}H NMR (400 MHz, $CDCl_3$) δ 7.1–7.4 (m, 4H), 3.7 (s, 4H), 3.6 (m, 4H), 2.7-2.8 (m, 8H), 1.9-2.2 (bs, 2H).

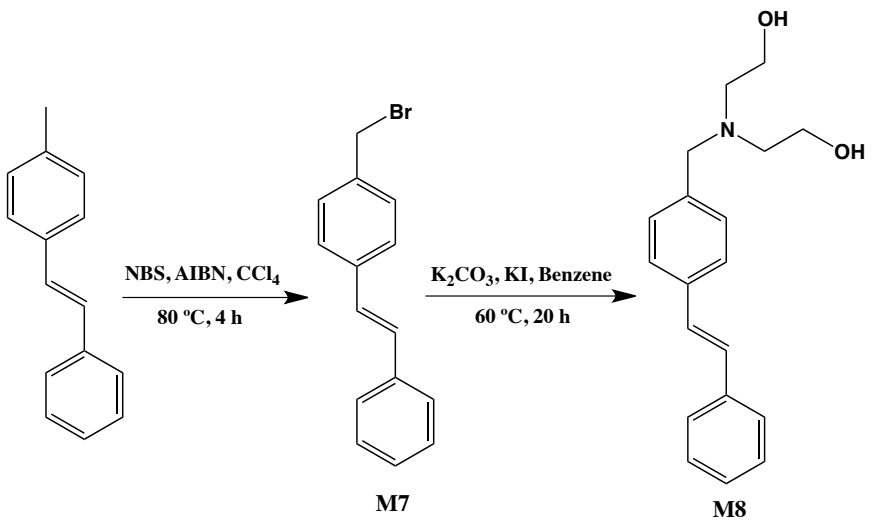

Scheme 4-5. Preparation of **M7** and **M8**.

Preparation of (*E*)-4,4-dimethylstilbene (M9). **M9** was synthesized via the Wittig-Horner reaction using 4-methylbenzyl(diethylphosphonate) and *p*-tolualdehyde (**Scheme 4-6**).[26] To synthesize 4-methylbenzyl(diethylphosphonate), 4-methylbenzyl chloride (30.0 mL, 0.227 mol) and triethyl phosphite (150 mL) were stirred in a 250 ml flask and heated at 160 ºC for 24 h. The remaining triethyl phosphite was removed by vacuum distillation at 80 ºC under 0.2 mmHg to leave a colorless liquid (43.02 g, 78%). 4-Methylbenzyl(diethylphosphonate) (20.00 g, 0.082 mol) and *p*-tolualdehyde (9.80 g, 0.082 mol) in dry THF (75 mL) were stirred in a 250 ml round bottom flask cooled in an ice bath. ^{t}BuOK (1.0 M in THF, 60 mL) was then added dropwise. The solution was stirred at room temperature for 24 h after which it was poured into water (500 mL). The product was precipitated from the solution, filtered, washed with water, and vacuum dried overnight to yield a white crystalline solid (11.1 g, 64%). mp: 182-183 ºC. (lit.[27] mp: 179-181 ºC). ^{1}H NMR (500 MHz, $CDCl_3$,) δ 7.3–7.4 (m, 4H), 7.1–7.2 (m, 4H), 7.0 (s, 2H), 2.3 (s, 6H).

Preparation of 4,4'-dibromomethylstilbene (M10) (Scheme 4-6).[23,28] A mixture of 4,4'-dimethylstilbene (1.48 g, 0.007 mmol), NBS (2.79 g, 0.016 mol), and AIBN (0.12 g) in CCl_4 (35 mL) was stirred at 80 °C under Ar for 4 h. After cooling, the yellow solution with solid was

vacuum filtered and the solid was washed with benzene (20 mL). The filtrate was washed with H_2O (3×20 mL) using a separatory funnel, dried over $MgSO_4$ overnight and filtered. The filtrate was concentrated, purified with silica column chromatography (eluent 10:1 hexane/EtOAc), and dried under high vacuum to afford a yellow solid (1.14 g, 44%). mp: 179-181 ºC (lit.[23] mp: 176-178 ºC). ^{1}H NMR (500 MHz, $CDCl_3$) δ 7.0–7.5 (m, 10H), 4.5 (s, 4H). Due to the time limit of the project, this monomer was not used for further synthesis.

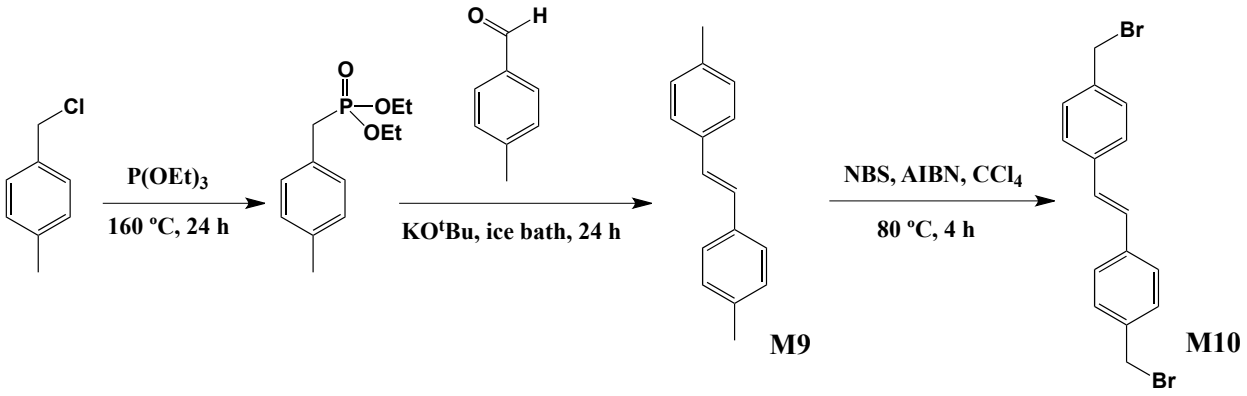

Scheme 4-6. Preparation of **M9** and **M10**.

Preparation of (*E*)-3,3'-dimethylstilbene (M11). **M11** was synthesized via the Wittig-Horner reaction using 3-methylbenzyl(diethylphosphonate) and *m*-tolualdehyde (**Scheme 4-7**).[26] To synthesize 3-methylbenzyl(diethylphosphonate), 3-methylbenzyl chloride (15 mL, 0.114 mol) and triethyl phosphite (75 mL) were stirred in a 250 ml flask and heated at 160 ºC for 24 h. The remaining triethyl phosphite was removed by vacuum distillation at 80 ºC under 0.2 mmHg to leave a colorless liquid (19.66 g, 72%). 3-Methylbenzyl(diethylphosphonate) (5.00 g, 0.021 mol) and *m*-tolualdehyde (2.48 g, 0.021 mol) in dry THF (15 mL) were stirred in a 100 mL round bottom flask cooled in an ice bath. ^{t}BuOK (1.0 M in THF, 22 mL) was then added dropwise. The solution formed was stirred at room temperature for an additional 24 h after which it was poured into water (100 mL). The precipitate was filtered, washed with water, and vacuum dried

overnight to yield a white crystalline solid (3.33 g, 77%). mp: 59-60 ºC (lit. mp: 49-51 ºC [29] and 55-56 ºC [30]). ^{1}H NMR ($DMSO_{d6}$) δ 7.0–7.5 (m, 10H), 2.3 (s, 6H).

Preparation of 3,3-dibromomethylstilbene (M12) (Scheme 4-7).[23,28] A mixture of **M11** (0.53 g, 0.007 mmol), NBS (2.79 g, 0.016 mol) and AIBN (0.12 g) in CCl_4 (35 mL) was stirred at 80 °C under Ar for 4 h. After cooling the colorless solution with solid was vacuum filtered and the solid was washed with hexane (10 mL). The filtrate was concentrated and dried under vacuum to afford a white solid. ^{1}H NMR showed the peaks associated with protons from the targeted product and impurity. Further purification such as column chromatography or recrystallization is needed.

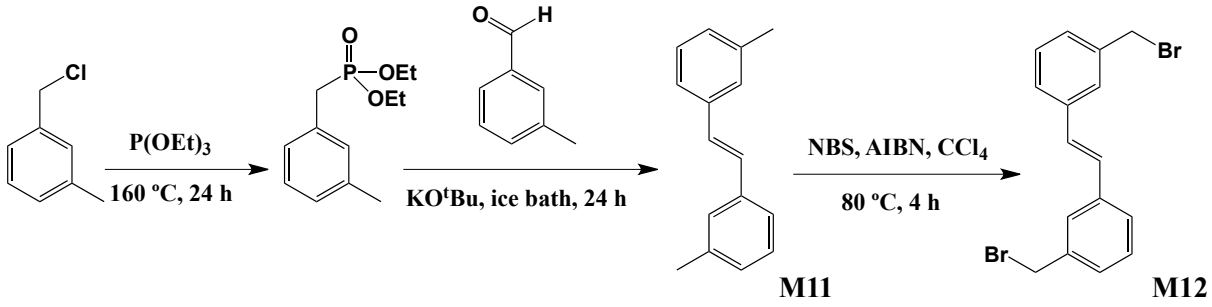

Scheme 4-7. Preparation of **M11** and **M12**.

4.3.2.2. Synthesis of amine-based polymers

Homopolymerization of styrenic monomers. Styrenic monomers were used to prepare polymers via free radical polymerization (**Scheme 4-8**). The reactions were generally initiated by AIBN at 60 ºC in THF (for condition a) or MeOH (for condition b) for 24 h. The initiator concentration was 1.0 wt% based on the monomers and the monomer concentration was 20 wt% based on the solution. Polymers were recovered by precipitating into hexane (for condition a) or diethyl ether (for condition b), filtered, and dried under vacuum at 50 ºC overnight. **Table 4-1** summarizes the reaction conditions and yields of polymers prepared by homopolymerization.

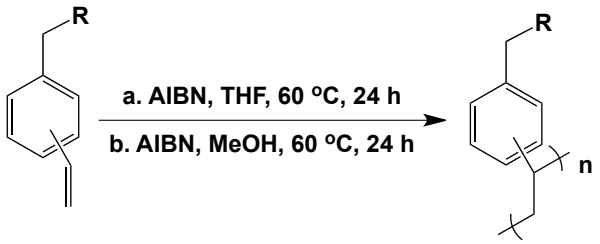

Scheme 4-8. Synthesis of styrenic polymers via homopolymerization (see "R" in **Table 4-1**).

Table 4-1. Polymers prepared from free radical polymerization.

Polymer	R	Condition	Yield (%)
PVBC	Cl	a	58
P1[1]	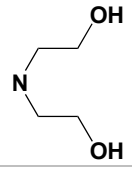	b	14
P2	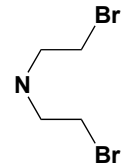	a	32
P3	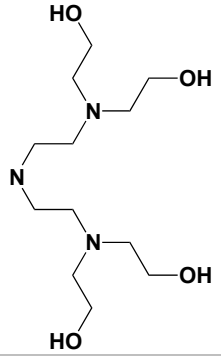	b	4
P4		AIBN, benzene 60 °C, 24 h	5
P5[2]	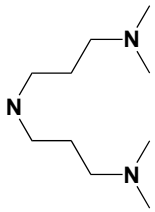	b	55
P6	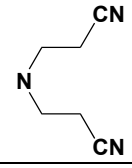	a	46

[1]Mn=8.5 Kg/mol, PDI=3.4 (solvent: NMP); [2]Formed gel after polymerization.

For example, to prepare poly(vinylbenzyl chloride) (**PVBC**), a mixture of uninhibited vinylbenzyl chloride (2.92 g), THF (13.1 mL), and AIBN (0.029 g, 1 wt%) was sealed in a 50 mL, septum sealed glass bottle equipped with a magnetic stirrer. The glass bottle was degassed by purging with N_2 for 20 min using 2 needles, one with N_2 flow and the other to equalize pressure. The glass bottle was heated at 60 °C for 24 h with constant stirring. After the reaction was stopped, the polymer was precipitated in hexane (250 mL). The polymer was filtered and vacuum dried at 50 °C overnight to give a white solid (1.70 g, 58%).

To prepare poly[*N*,*N*-dimethyl-1-(vinylphenyl)methanamine] (**P4**),[31,32] a mixture of **M4** (0.32 g), benzene (1.0 mL), and AIBN (0.016 g) was sealed in a 50 mL, septum sealed glass bottle equipped with a magnetic stirrer. The glass bottle was degassed by purging with N_2 for 20 min and heated at 60 °C for 2 days with constant stirring. After the reaction was stopped, the polymer was added dropwise to MeOH (40 mL) with constant stirring in a 100 mL beaker, which was cooled in an acetone-dry ice bath, to give a white precipitate. The precipitate was filtered and vacuum dried at 50 °C overnight to afford a white solid (0.015 g, 5%).

To prepare poly[3,3'-(vinylbenzylazanediyl)dipropanenitrile] (**P6).** A mixture of 3,3'-(vinylbenzylazanediyl)dipropanenitrile (0.77 g, 0.003 mol), THF (3.4 mL), and AIBN (0.008 g, 1 wt%). was sealed in a 50 mL, septum sealed glass bottle equipped with a magnetic stirrer. The glass bottle was degassed by purging with N_2 for 20 min and heated at 60 °C for 24 h with constant stirring. After the reaction was stopped the polymer was precipitated in hexane (70 mL). The polymer was filtered and vacuum dried at 50 °C overnight to afford a white solid (0.35 g, 46%).

Copolymerization. Copolymerization of monomers via free radical polymerization was generally initiated by AIBN at 60 ºC in THF for 24 h. The initiator concentration was 1.0 wt%

based on the monomers, and the monomer concentration was 20 wt% based on the solution. Polymers were recovered by precipitating into hexane, filtered, and dried under vacuum at 50 ºC overnight. The details of the copolymerization of copolymers, including monomers, mole ratio of monomers, and yield, are summarized in **Table 4-2**.

For example, to prepare $STR_{50}M1_{50}$, a mixture of STR (1.50 g, 0.014 mol), **M1** (3.20 g, 0.014 mol), THF (21.3 mL), and AIBN (0.047 g, 1 wt%) was sealed in a 50 mL, septum sealed glass bottle equipped with a magnetic stirrer. The glass bottle was degassed by purging with N_2 for 20 min and heated at 60 °C for 24 h with constant stirring. After the reaction was stopped the polymer was precipitated in hexane (500 mL). The polymer was filtered and vacuum dried at 50 °C overnight to afford a yellow solid (1.52 g, 32%). Elemental analysis results of copolymers prepared from varying STR and M1 composition are shown in **Table 4-3**. The actual polymer compositions in **Table 4-3** were calculated from N wt%. The large deviations of the elemental analyses suggest that these samples contain impurities.

Table 4-2. Preparation of copolymers including monomers, monomer ratio, and yield.

Polymer	Monomers (see **Figure 4-1**)		Monomer ratio (A:B)	Yield (%)
	A	**B**		
$STR_{25}M1_{75}$			1:3	20
$STR_{50}M1_{50}$	STR	M1	1:1	32
$STR_{75}M1_{25}$			3:1	25
STR-VBC	STR	VBC	1:1	98
VBC-MAH	VBC	MAH	1:1	100
STR-MAH	STR	MAH	1:1	100
4MSTB-MAH	4MSTB	MAH	1:1	65
M4-MAH	M4	MAH	1:1	*
M4-TBMIB[1]	M4	TBMIB	1:1	82

*Formed a mixture of black solution and dark red solid.
[1]M_n=2.2 Kg/mol, PDI=1.59 (solvent: THF)

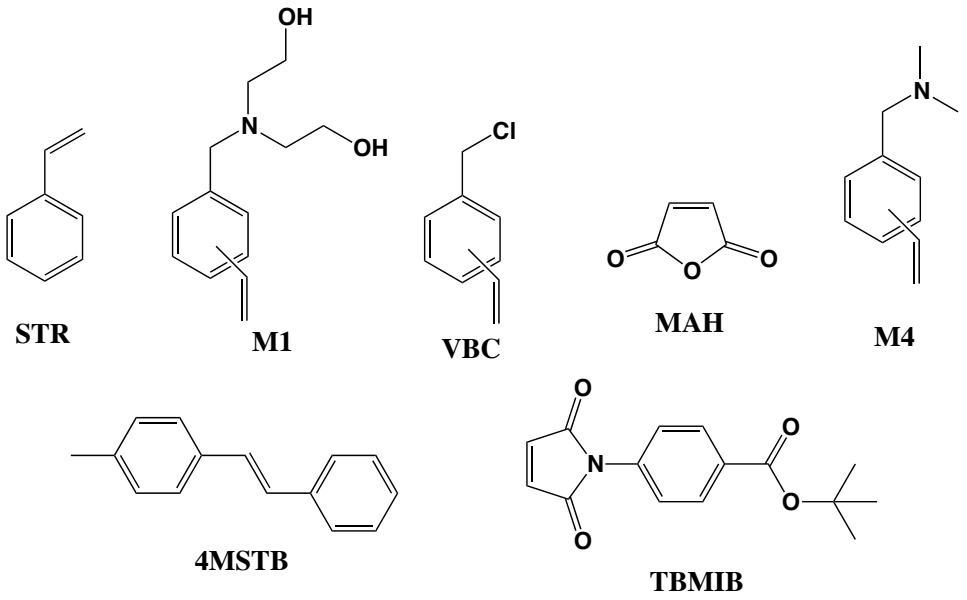

Figure 4-1. Monomers used to prepare copolymers via free radical polymerization.

Table 4-3. Elemental analysis results of poly(STR-*co*-M1).

Polymer	Element	Theory	Found		Actual composition	Calculated (from actual composition)
	C	74.30	69.55	69.83		75.66
$STR_{25}M1_{75}$	H	8.56	8.19	8.25	**$STR_{34}M1_{66}$**	7.40
	N	5.53	5.14	5.06		5.16
	C	78.50	78.89	74.75		79.75
$STR_{50}M1_{50}$	H	8.41	8.03	7.98	**$STR_{56}M1_{44}$**	7.06
	N	4.36	3.96	3.94		4.01
	C	84.57	79.53	79.55		83.43
$STR_{75}M1_{25}$	H	8.19	7.74	7.91	**$STR_{71}M1_{29}$**	6.76
	N	2.67	2.90	2.91		2.99

Crosslinked polymers, **MAH-DVB** and **$(MAH\text{-}STR)_{90}(DVB)_{10}$**, were prepared via free radical suspension polymerization. To prepare **MAH-DVB**,[33] DI H_2O (40 mL), poly(vinyl alcohol) (0.60 g), and sodium chloride (1.00 g) were added to a three-neck, 250 mL round

bottom flask equipped with a mechanical stirrer, gas inlet, and condenser. The mixture was stirred for 2 h at 80 ºC under N_2. A mixture of maleic anhydride (MAH) (1.33 g, 0.014 mol), divinylbenzene (DVB) (2.21 g, 0.014 mol), AIBN (0.041 g), and toluene (6 mL) was stirred under N_2 at room temperature in a 20 mL vial. The organic phase was then added into the aqueous phase in the round bottom flask. The mixture was stirred under N_2 at 80 ºC for 20 h. The polymer beads were filtered, washed with hot H_2O, Soxhlet extracted with a mixture of acetone, MeOH and toluene for 24 h, and dried under vacuum at 50 ºC for 24 h to afford white beads (2.56 g, 72 %).

To prepare (**MAH-STR)$_{90}$(DVB)$_{10}$**,[34] DI H_2O (20 mL), poly(vinyl alcohol) (0.40 g), and sodium chloride (0.67 g) were added to a three-neck, 100 mL round bottom flask equipped with a mechanical stirrer, gas inlet, and condenser. The mixture was stirred for 3 h at 80 ºC under N_2. A mixture of styrene (STR) (0.69 g, 0.007 mol), MAH (1.33 g, 0.011 mol), DVB (0.25 g, 0.002 mol), AIBN (0.027 g), and benzene (5 mL) were stirred under N_2 at room temperature in a 20 mL vial. The organic phase was then added into the aqueous phase in the round bottom flask. The mixture was stirred under N_2 at 80 ºC for 20 h. The polymer beads were filtered, washed with hot H_2O, Soxhlet extracted with a mixture of acetone, MeOH, and toluene for 24 h, and dried under vacuum at 50 ºC for 24 h to afford white beads (0.51 g, 26 %).

Post-modification. PVBC was modified using secondary amines via S_N2 reaction (**Scheme 4-9**). The reaction conditions and yields are summarized in **Table 4-4**. For example, to prepare **P6-m**, a mixture of PVBC (0.51 g), 3,3'-iminodipropoinitrile (0.42 g, 0.003 mol), KI (0.010 g, 0.058 mmol), and K_2CO_3 (0.031 g, 0.224 mmol) in THF (1 mL) was stirred and heated at 60 °C for 48 h under nitrogen. The resulting turbid yellow liquid was filtered. The filtrate was added into hexane (20 mL) dropwise with constant stirring to afford a yellow precipitate. The polymer

was filtered, washed with H_2O, and dried under vacuum at 50 ºC overnight to afford a yellow solid (0.51 g, 63 % yield).

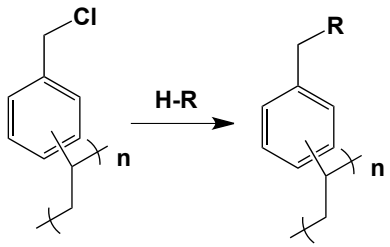

Scheme 4-9. Post-modification of PVBC.

Table 4-4. Polymers prepared from post-modification of PVBC.

Polymer	R	Condition	Yield (%)
P1-m	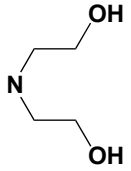	KI, K_2CO_3, THF, 60 ºC, 24 h	57
P4-m		THF, 60 ºC, 2 days	81
P5-m	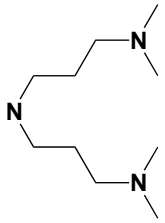	KI, K_2CO_3, THF, 60 ºC, 2 days	>100
P6-m	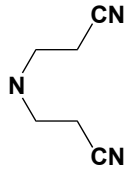	KI, K_2CO_3, THF, 60 ºC, 48 h	63

M1-DVB-m and **M5-DVB-m** were prepared by modification (**Scheme 4-10**) of (VBC)98(DVB)2, which was prepared from suspension polymerization (see Chapter 3). For example, to prepare **M1-DVB-m**, a mixture of (VBC)98(DVB)2 (0.98 g), DEA (1.32 g, 0.013 mol), KI (0.84 g, 0.005 mol), and K_2CO_3 (1.76 g, 0.013 mol) in toluene (35 mL) was stirred and

heated at 80 °C for 48 h. The polymer was filtered, washed with H_2O, MeOH, and diethyl ether, dried under vacuum at 50 ºC overnight to afford white solid (1.32 g, 82%). Elemental analysis results with calculated conversion of polymer modification are shown in **Table 4-5**. Elemental analyses suggest that the post modifications did not occur at the expected levels. The samples are not pure and have to be refined.

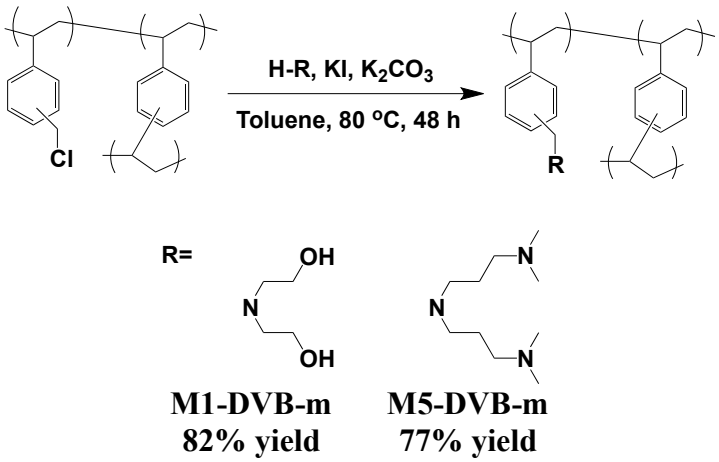

Scheme 4-10. Preparation of **M1-DVB-m** and **M5-DVB-m** via post-modification of (VBC)98(DVB)2.

Table 4-5. Elemental analysis results for **M1-DVB-m** and **M5-DVB-m**.

Polymer	Element	Theory	Found		Conversion	Calculated (from conversion)
M1-DVB-m	C	71.35	69.52	69.42	81.2%	71.63
	H	7.71	8.43	8.32		7.31
	N	6.30	5.45	5.45		5.45
M5-DVB-m	C	71.88	61.73	61.88	25.9%	73.84
	H	9.57	8.40	8.22		6.96
	N	13.79	5.75	5.61		5.67

Crosslinking reaction of MAH containing polymers. Polymers which contain MAH units were crosslinked with diamines in order to incorporate amine groups into the polymers and

increase their surface areas (**Scheme 4-11**).[35,36] To prepare crosslinked polymers, a mixture of MAH containing polymer and diamine (10-20 wt% based on the polymers) in THF was heated at 60 ºC with constant stirring overnight. The resulting polymers were filtered, washed with THF, and dried under vacuum at 50 ºC overnight. The crosslinked polymers were then heated under vacuum at 150 ºC for 12 h, 180 ºC for 6 h, and 200 ºC for 1 h to afford polymers with cyclic imide units. The compositions of polymers crosslinked with diamines are summarized in **Table 4-6**.

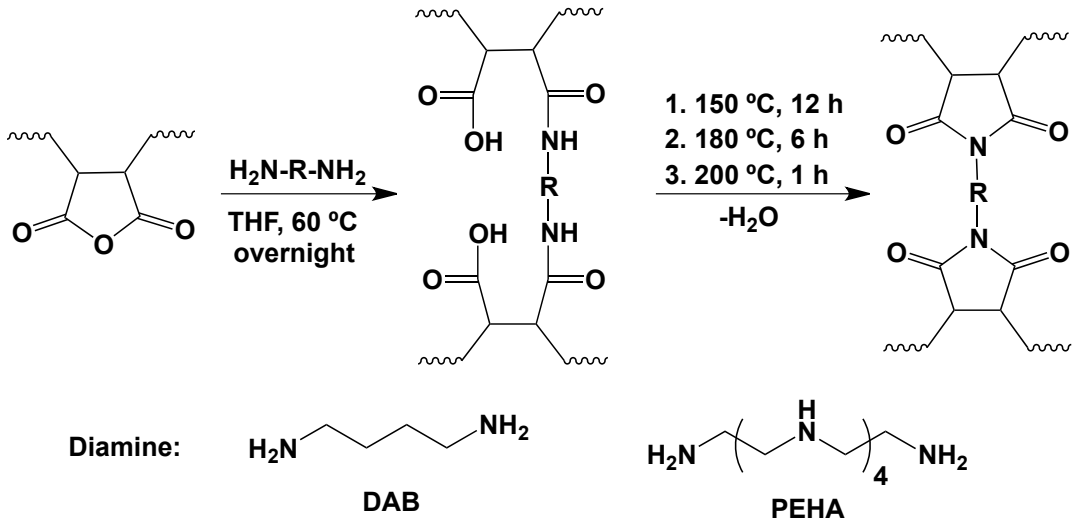

Scheme 4-11. Crosslinking reaction of MAH containing polymers using diamines.

Table 4-6. Polymers modified by crosslinking reaction using diamines.

Polymer	Polymer used for crosslinking reaction	Diamine	Diamine content (wt %)
MAH-DVB-10%DAB	MAH-DVB	DAB	10
MAH-DVB-10%PEHA	MAH-DVB	PEHA	10
STR-MAH-10%DAB	STR-MAH	DAB	10
STR-MAH-20%DAB	STR-MAH	DAB	20
4MSTB-MAH-10%DAB	4MSTB-MAH	DAB	10

4.3.2.3. Preparation of silica-supported amine sorbents

Silica-supported amine sorbents were prepared using the impregnation method.[37,38] For example, to prepare $DMPA_{50}$-SBA15, DMPA (0.11 g) in MeOH (5 mL) was stirred in a 50 mL round bottom flask at room temperature for 1 h. SBA-15 (0.11 g) was added into the solution with constant stirring. The mixture was stirred overnight. The solvent was removed by heating at 40 ºC under vacuum on a rotovapor. The resulting solid was dried under vacuum at 50 ºC overnight to afford a white solid (0.17 g).

4.3.2.4. Casting film

A solution of **P1** (0.08 g) in NMP (1.5 mL) was added slowly into a Teflon® mold (**Figure 4-2** (a)). The solution was heated using an IR light overnight and dried under vacuum at 60 ºC overnight to give a yellow film (**Figure 4-2** (b)).

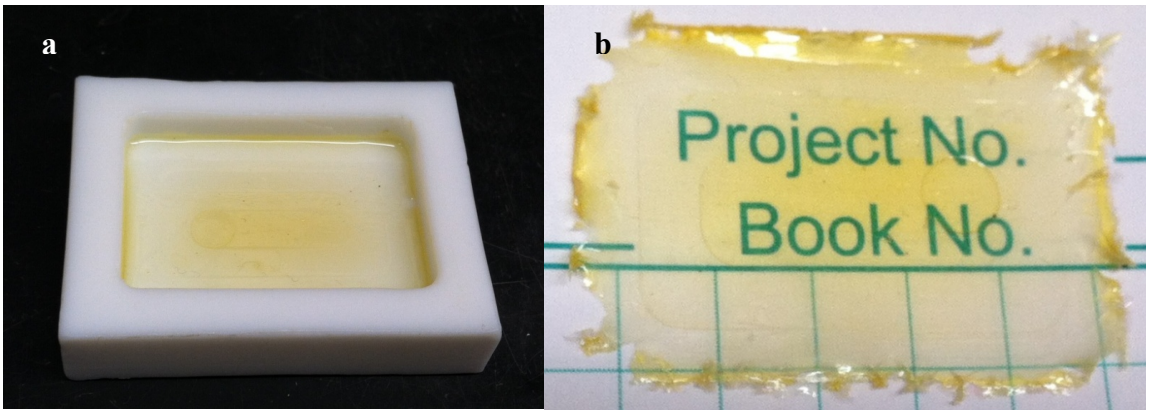

Figure 4-2. P1 solution in a Teflon® mold (a) and a film of **P1** (b).

4.3.3. Characterization

4.3.3.1. General

^{1}H NMR and ^{13}C NMR spectra of monomers were determined in $CDCl_3$ or DMSO-d_6 on Varian Utility 400 MHz, Inova 400 MHz or JOEL EclipsePlus 500 MHz spectrometers at 25 ºC.

Elemental analyses were done by Atlantic Microlab, Inc (Norcross, GA). Mass spectra were obtained using Agilent 6220 Accurate-Mass time of flight (TOF) liquid chromatography/mass spectrometry (LC/MS) system. The surface areas were calculated using the Brunauer-Emmett-Teller (BET) equation and data from nitrogen adsorption/desorption isotherms at 77 K were obtained with a TriStar II 3020 surface area analyzer (Micromeritics, Norcross, GA). Prior to analysis, the samples were heated at 140 °C under N_2 overnight. SEM micrographs were obtained using a LEO (Zeiss) 1550 field emission scanning electron microscope. FTIR data were obtained on a Varian 670-IR spectrometer (DTGS detector); the spectra were collected at a resolution of 4 cm^{-1} at room temperature, and 32 scans were averaged. Molecular weights and molecular distributions were determined in *N*-methyl-2-pyrrolidone (NMP) using a Waters Alliance model 2690 size exclusion chromatograph (SEC) equipped with a Viscotek refractive index detector and a viscometer or in THF using a Waters size exclusion chromatograph equipped with a Water 2414 differential refractive index detector and a Wyatt miniDAWN multiangle laser light scattering (MALLS) detector.

4.3.3.2. CO_2 sorption/desorption measurements

CO_2 sorption/desorption measurements were performed using a TA Instruments Hi-Res TGA 2950 Thermogravimetric Analyzer. **Figure 4-3** shows a schematic setup for the CO_2 sorption/desorption measurements. This setup allows the gas purge into TGA chamber to be switched between N_2 and CO_2 with a controllable flow rate. Before measurements, samples were heated from room temperature to 120 ºC at a heating rate of 20 ºC/min and kept at 110 ºC for 30 min under nitrogen. The adsorption experiment was conducted at 30 ºC under CO_2 gas. The

desorption experiment was carried out at 30 ºC under N_2. The purge gas flow rate to the sample chamber was kept at 25 mL/min.

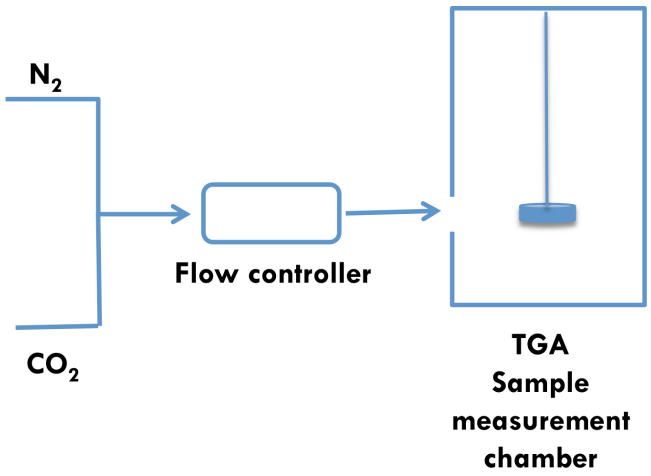

Figure 4-3. Experimental setup for CO_2 adsorption/desorption study.

4.4. Results and Discussion

4.4.1. Synthesis of Amine-Containing Linear Polymers via Polymerization or Post-Modification

Linear polymers were prepared by free radical polymerization of styrenic monomers and/or maleic anhydride/maleimide. The yields in some of the polymerizations are quite low (e.g. **P4**). This may due to the steric hindrance from the bulky pendent groups in some cases. Other possible reasons are the solubility of the polymers in the precipitation solvent and the nature of the polymers (e.g., low T_g), resulting in a lower percentage of polymers recovered from precipitation. In future, NMR studies and elemental analysis of reaction mixtures after polymerization can be used to determine the conversion of the polymerizations. The solvent for precipitation needs to be carefully chosen.

Post-modification of linear polymers was used to prepare amine-containing polymers. Solubilities of some of the modified polymers are very poor in common organic solvents,

making the characterization extremely difficult. Since **P6-m**, modified from **P6**, is soluble in chloroform, the conversion of this modification reaction was found to be 73%, which was calculated using the integrals (labeled a and b) of the ^{1}H NMR spectrum (**Figure 4-4**).

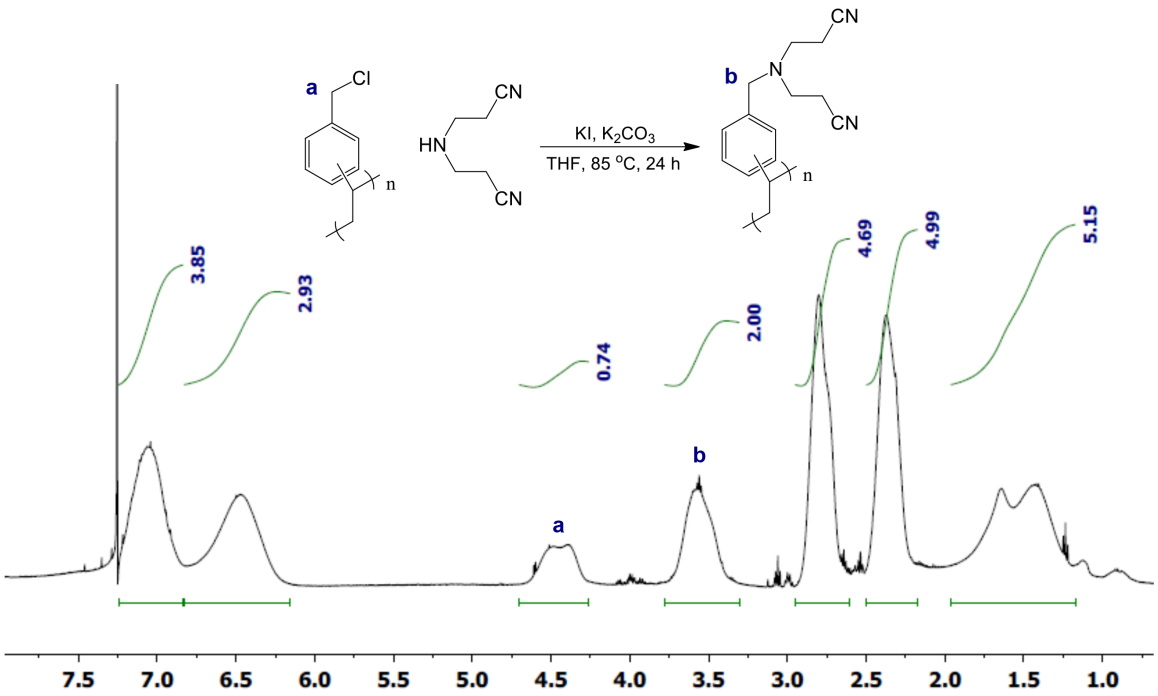

Figure 4-4. ^{1}H NMR of **P6-m** in $CDCl_3$ showing 73% conversion of the modification reaction, which was calculated from the integrals of protons from PVBC and P6-m (labeled).

4.4.2. Preparation and Porosity Characterization of MAH-Containing Crosslinked Polymers

Many groups have reported synthesis of MAH-containing polymers via suspension polymerization.[33,34,39,40] The incorporation of MAH units allows post modification of polymers by reaction with amines.[35,41-43] In suspension polymerization, monomer droplets which contain monomers and initiator are suspended in the presence of a stabilizer with continuous agitation. Polymerization occurs in each monomer droplet to afford spherical particles (**Figure 4-5**). Compared to bulk, solution, and emulsion polymerization, suspension polymerization has the

following advantages: easier temperature control, lower viscosity, milder reaction conditions, and lower separation cost.[44,45]

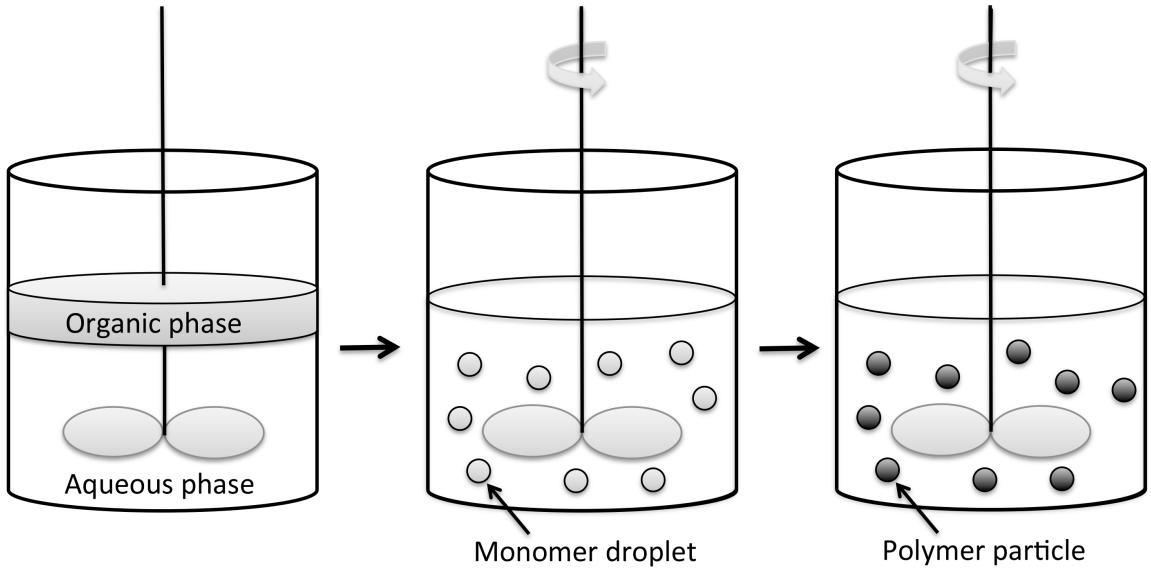

Figure 4-5. Schematic representation of a suspension polymerization.[46]

MAH-DVB was synthesized via free radical suspension polymerization by following a modified literature method.[33] Since MAH units can easily hydrolyze and form carboxylic acids, it is important to dissolve the MAH in the organic solvent before mixing with the aqueous phase for suspension polymerization. In these experiments, we used toluene as a solvent to dissolve MAH. The toluene also serves as a porogen to facilitate the formation of porous structures. From SEM pictures of **MAH-DVB** (**Figure 4-6**), we observed spherical structures under low magnification, which are typical for products from suspension polymerization, with sizes in the range of 10-300 μm. Under higher magnification, rough surfaces were observed, indicating large porosity of **MAH-DVB**.

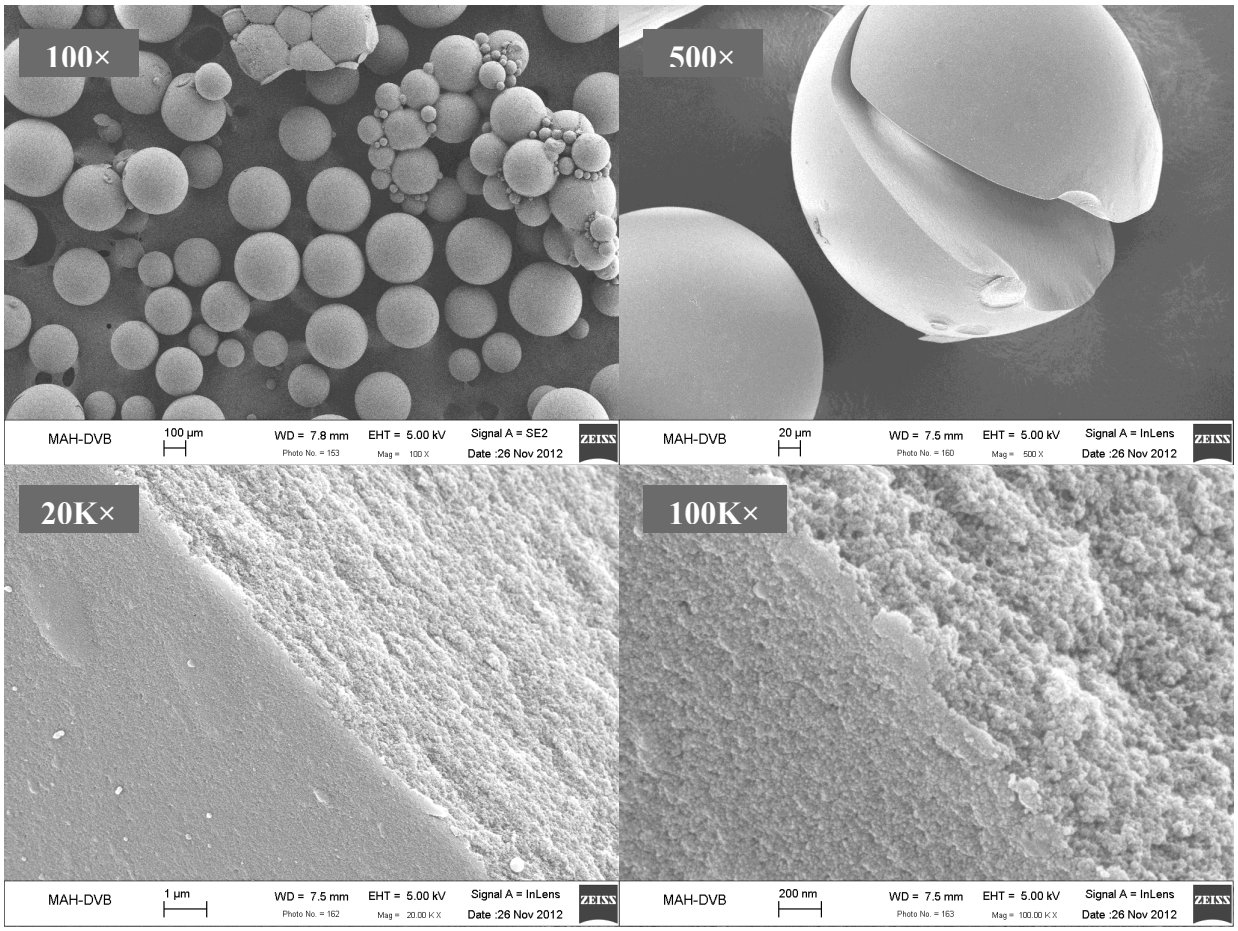

Figure 4-6. SEM pictures of MAH-DVB.

N_2 adsorption/desorption isotherms of **MAH-DVB** and **(MAH-STR)$_{90}$(DVB)$_{10}$** were measured at 77K. Isotherms of **MAH-DVB** are shown in **Figure 4-7**. However, (**MAH-STR)$_{90}$(DVB)$_{10}$** has no gas uptake under the measurement conditions, indicating that it has no porosity, possibly due to its low crosslinking density. According to the classification given by IUPAC, isotherms of **MAH-DVB** are type IV isotherms, which are usually associated with mesoporous materials.[47] Type H2 hysteresis was observed; this is often associated with porous materials with large pore size distribution and non-uniform pore structures.[47] The BET surface area of **MAH-DVB** was found to be 554 m^2/g, which was calculated from N_2 isotherms using the

Brunauer-Emmett-Teller (BET) equation.[48] This result is consistent with the literature value reported by Maciejewska et al. (460 m^2/g).[33]

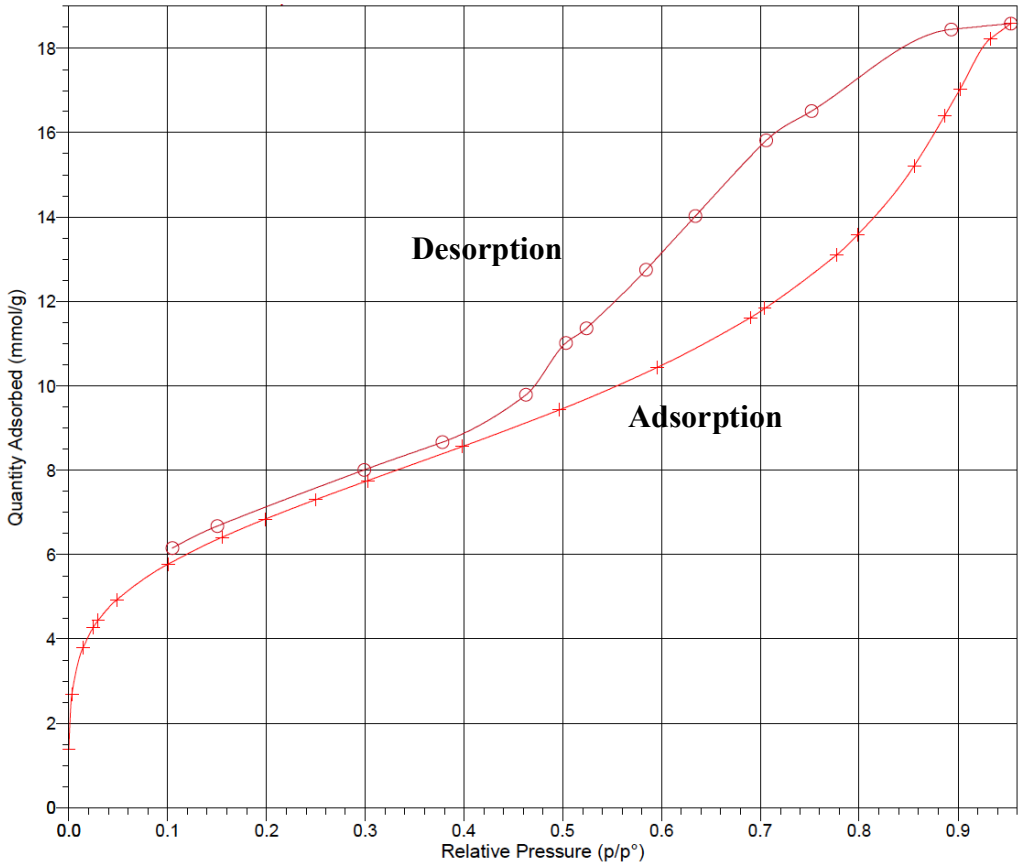

Figure 4-7. N_2 adsorption/desorption isotherms of **MAH-DVB** at 77K.

4.4.3. Modification of MAH-Containing Polymers Using Diamines.

The modification of MAH-containing polymers consisted of two steps: 1) the crosslinking reaction using diamines as crosslinkers; 2) imidization of the crosslinked polymers. Sample mass increased after the crosslinking reaction and decreased after imidization. In order to study the modification process, FTIR spectra were obtained for MAH-containing polymers before and after the crosslinking reaction, and after imdization. The characteristic IR adsorption peaks for amide and imide were previously assigned.[49-54] Two peaks near 1850 and 1780 cm^{-1} associated with the C=O groups from anhydride units were observed for all MAH containing polymers.

Peak near 1704 cm^{-1} and broad peak at 2500-3300 cm^{-1} are associated with the C=O groups and O-H groups from carboxylic acids, respectively. These two peaks indicated the hydrolysis of MAH units in these MAH containing polymers occurred.

Figure 4-8 shows the FTIR spectra of STR-MAH before and after the crosslinking reaction and the STR-MAH-20%DAB after imidization. After the crosslinking reaction, the N-H stretch at 2900-3200 cm^{-1} and peaks at 1500-1670 cm^{-1}, including the C=O stretch of the amide I mode around 1665 cm^{-1} and 1540-1565 cm^{-1} amide II mode, indicated the successful formation of amide units. After imidization, the absence of peaks near 1550 and 1665 cm^{-1} indicated that amide groups were converted into imide groups. Also, the C=O stretch (imide I) peak at 1776 cm^{-1}, the C-N stretch (imide II) peak at 1357 cm^{-1}, the C-H bend (imide III) absorption band at around 1160 cm^{-1}, and the C=O bend (imide IV) absorption band at 755 cm^{-1} confirmed the formation of imide groups.

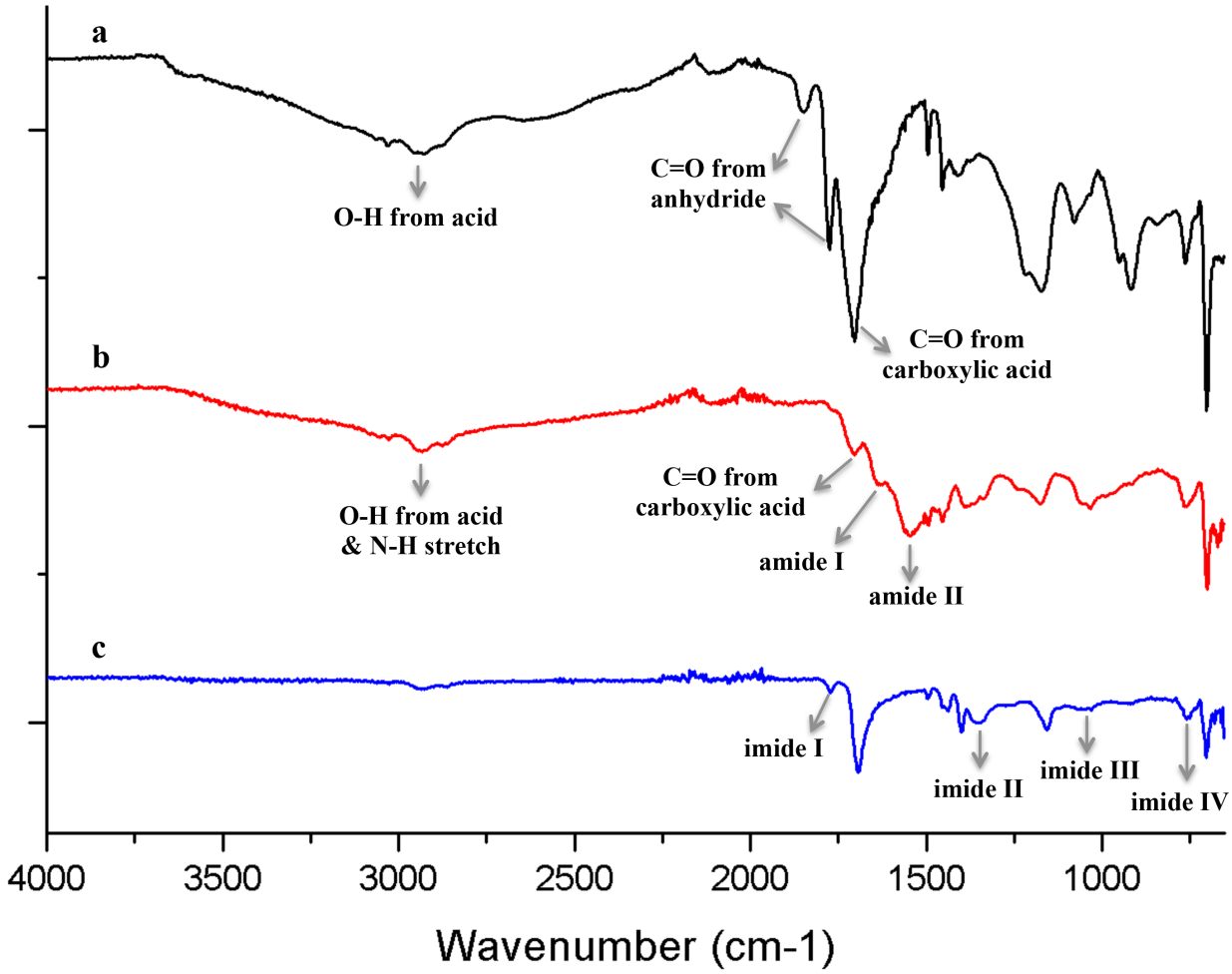

Figure 4-8. FTIR spectrum of STR-MAH (a), STR-MAH-20%DAB (b), and STR-MAH-20%DAB after imidization (c).

4.4.4. Preparation of Amine-Based Silica Using the Impregnation Method

In impregnation, the amine was physically adsorbed in the silica support. Two amines were used to prepare sorbents, and their structures and are summarized in **Table 4-7**. Two mesoporous silica support were used; their physical properties are summarized in **Table 4-8**.

Table 4-7. Chemical structures and boiling points of amines used in impregnation.

Amine	Chemical structure	bp (ºC)
DEA	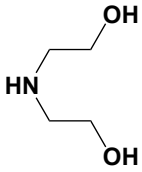	268[55]
DMPA	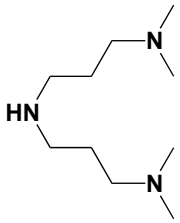	128-131[56]

Table 4-8. Physical properties of silica supports.

Silica supports	Surface area (m^2/g)	Average pore size (μm)
SBA-15	800	8
CARiACT G10	300	200-400

A series of silica supported amine sorbents was prepared. Their N contents were obtained from elemental analyses and compared with target N contents, which were calculated from the amine content loaded into the silica substrate (**Table 4-9** and **4-10**). The efficiency of the impregnation can be estimated by comparing the values of actual N content and target N content. The closer the two values, the higher the efficiency of impregnation. Three series of sorbents, DEA-SBA15, DMPA-SBA15, and DEA-G10, showed high efficiency of impregnation. However, the efficiency of impregnation of the DMPA-G10 series is considerably lower than the other three series. This is probably due to the lower boiling point of DMPA compared to DEA. The large pore size and/or lower surface area of G10 may increase the evaporation rate of DMPA during the impregnation, resulting in lower efficiency.

Table 4-9. SBA-15 supported amine sorbents.

Solid sorbents	Amine	Amine content (wt%)	Target N (wt%)	Actual N (wt%)
DEA20-SBA15	DEA	20	2.69	2.53
DEA30-SBA15		30	4.04	3.57
DEA40-SBA15		40	5.38	4.18
DEA50-SBA15		50	6.73	5.79
DMPA50-SBA15	DMPA	50	8.03	6.88

Table 4-10. CARiACT G10 supported amine sorbents.

Solid sorbents	Amine	Amine content (wt%)	Target N (wt%)	Actual N (wt%)
DEA20-G10	DEA	20	2.69	2.48
DEA30-G10		30	4.04	3.75
DEA40-G10		40	5.38	4.61
DEA50-G10		50	6.73	5.76
DEA60-G10		60	8.08	6.86
DEA70-G10		70	9.42	8.56
DMPA20-G10	DMPA	20	4.48	4.15
DMPA30-G10		30	6.73	3.75
DMPA40-G10		40	8.97	4.61
DMPA50-G10		50	11.21	5.76

4.4.5. CO_2 Capture Study

Control experiments. Several samples were used as controls and their CO_2 uptakes are summarized in **Table 4-11**. PSTR and (VBC)98(DVB)2 are "blank" samples which have low surface area and no amine. The PEI sample, which is linear polyethylenimine (M_w = 2500 g/mol), contains high N content but has low surface area. SBA-15 exhibits high surface area and contains no amine. NETL1 and NETL2 are PEI impregnated on silica substrates, and have high

surface areas (200-300 m^2/g) and high N content (12-14 wt%). TGA curves of PSTR, (VBC)98(DVB)2 and NETL1 are shown in **Figure 4-9** and **4-10**. Spikes in the curves were observed between each step; they are likely attributed to the change in gas flow rate during gas switching between CO_2 and N_2. Blank samples have a mass increase of 0.1-0.3 mg during adsorption. Both PEI and SBA-15 have low CO_2 uptakes during sorption measurements at 30 ºC. NETL samples exhibit 9-12 wt% CO_2 uptakes. Therefore, it is important for a sorbent to have both high surface area and high N content in order to have high CO_2 sorption capability.

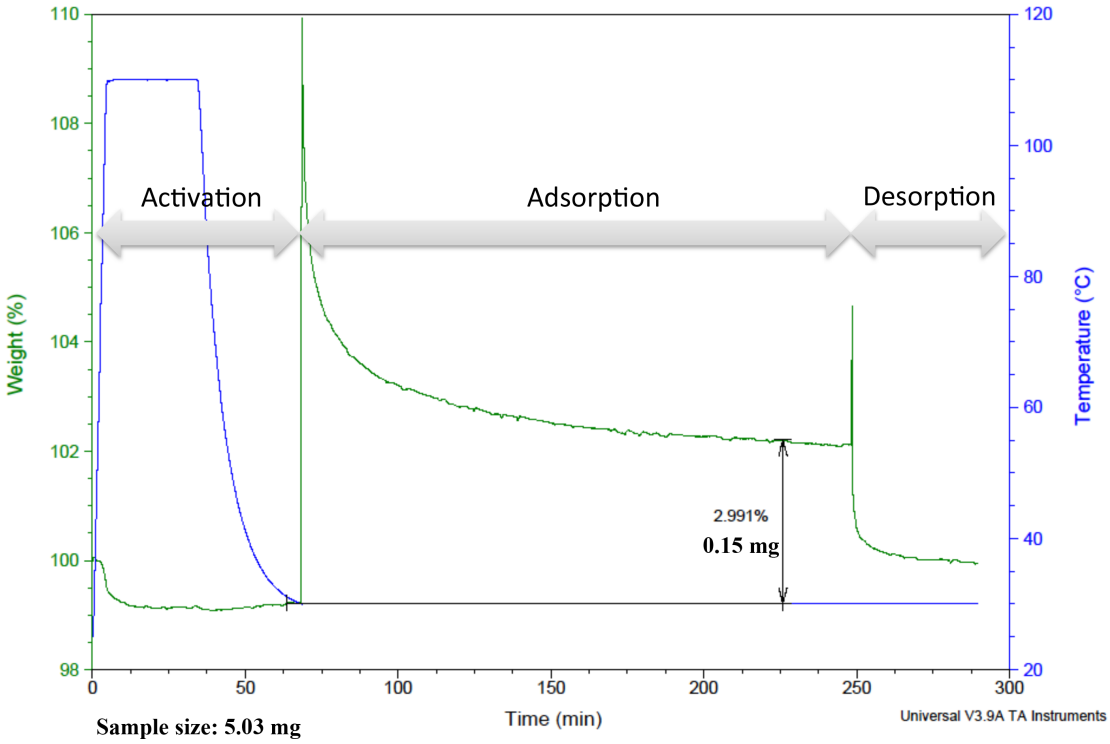

Figure 4-9. CO_2 capture and release behaviors of linear polystyrene (PSTR).

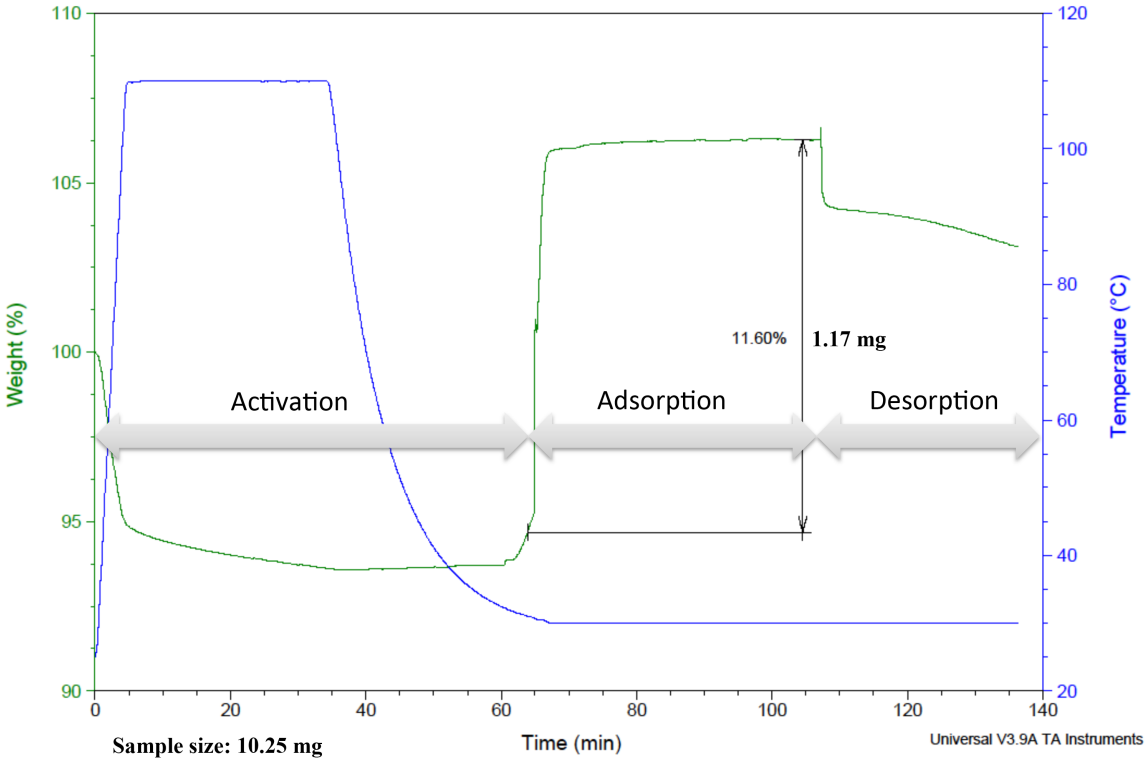

Figure 4-10. CO_2 capture and release behaviors of NETL1 (see **Table 4-11**).

Table 4-11. CO_2 uptakes for control experiments

Sample	N content (wt%)	Sample mass (mg)	CO_2 uptake (mg)	CO_2 uptake[c] (wt%)	CO_2/N (mol/mol)
PSTR	0	5.03	0.15	2.94	N/A
		10.02	0.23	2.28	N/A
		20.58	0.29	1.40	N/A
(VBC)98(DVB)2	0	5.09	0.11	2.21	N/A
PEI	34.15	9.98	0.26	3.56	0.02
		10.17	0.28	3.83	0.03
SBA-15	0	9.46	0.15	1.77	N/A
NETL1[a]	12.15	10.25	1.17	12.01	0.30
		20.30	2.17	11.23	0.28
		29.97	2.72	9.40	0.24
NETL2[b]	14.43	9.50	1.19	12.50	0.28

[a]PEI 423 on CARiACT G10 silica substrate coated with 3-aminopropyltriethoxysilane. [b]PEI 423 on CARiACT G10 silica substrate. [c]CO_2 uptakes measured at different sample mass have 10-29% standard deviation; CO_2 uptakes measured at similar sample mass have ±4% error.

In order to probe the effect of sample size on the CO_2 uptake, samples sizes were varied for CO_2 capture measurements of PSTR and NETL1. For both materials, CO_2 uptake increased as sample size increases. CO_2 uptake in wt % decreased as the sample size increased. Due to the limited size of TGA pan used for measurement, samples with large sample size may not be exposed to CO_2 gas entirely during adsorption, resulting in the decrease in CO_2 uptake in wt%. Therefore, sample size should be kept relatively constant in order to have a meaningful comparison among samples.

Amine-containing polymers. CO_2 adsorption properties of amine-containing polymers were measured and are summarized in **Table 4-12**. These polymers, which contain 3-7 wt% of amine, have low CO_2 uptakes. This result is consistent with the control measurements, where a certain level of surface area of sorbents is a prerequisite for sorbents with high CO_2 uptakes.

Table 4-12. CO_2 uptakes of polymeric sorbents.

Sample	N content (wt%)	Sample mass (mg)	CO_2 uptake (mg)	CO_2 uptake (wt%)
P1	6.39	17.69	0.11	0.01
		6.60	0.13	0.02
		4.94	0.18	0.04
P2	3.56	5.10	0.00	0.00
P3	N/A	31.70	0.23	0.16
M5-DVB-m	5.68	49.69	0.21	0.46

Silica supported amine sorbents. CO_2 uptakes of silica supported amine sorbents were measured and are shown in **Table 4-13**. Typical CO_2 capture and release behaviors of these

sorbents are shown in **Figure 4-11**. The silica based sorbents showed much larger CO_2 uptakes compared to polymeric sorbents. Some of the sorbents from DEA-G10 series have CO_2 sorption capacity comparable with the NETL samples under our testing conditions.

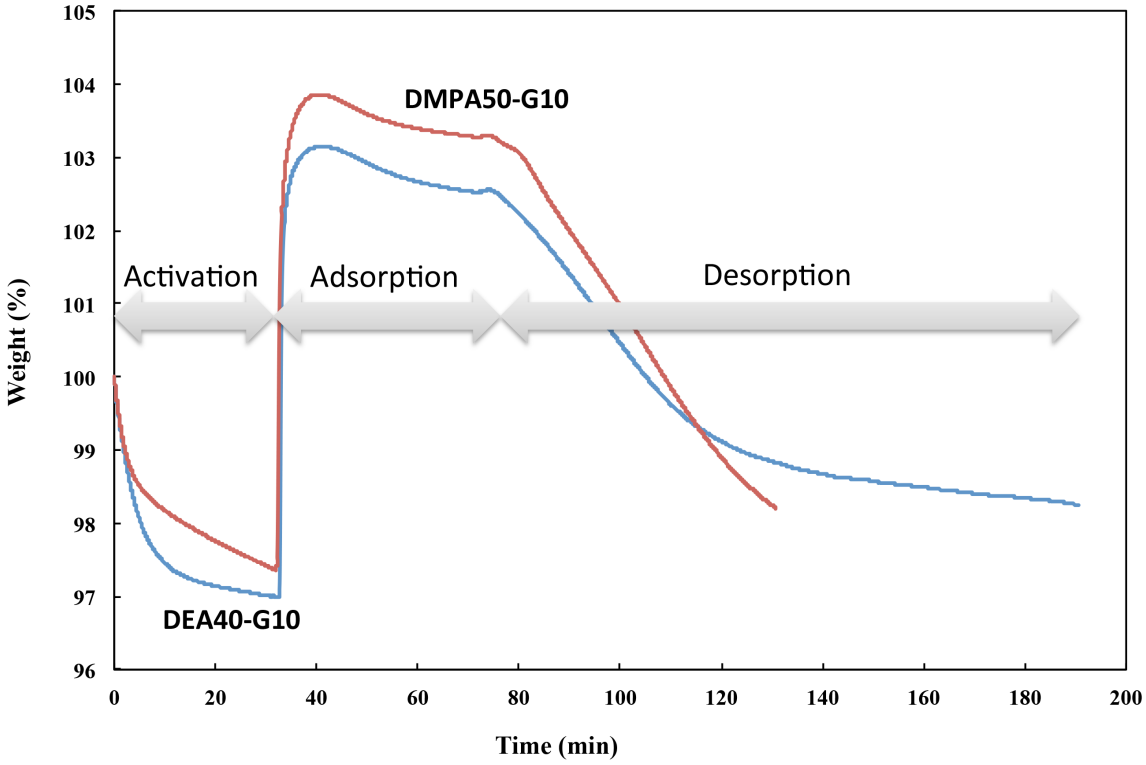

Figure 4-11. CO_2 capture and release behaviors of DEA40-G10 and DMPA50-G10.

Table 4-13. CO_2 uptakes of silica supported amine sorbents.

Sample	N content (wt%)	Sample mass (mg)	CO_2 uptake (mg)	CO_2 uptake[a] (wt%)	CO_2/N[b] (mol/mol)
DEA20-SBA15	2.53	10.77	0.22	2.07	0.25
DEA30-SBA15	3.57	9.88	0.17	1.82	0.15
DEA40-SBA15	4.18	10.41	0.50	5.28	0.37
DEA50-SBA15	5.79	9.61	0.56	6.05	0.32
		10.53	0.72	7.38	0.38
DMPA50-SBA15	6.88	10.07	0.48	5.00	0.22
DEA20-G10	2.48	10.11	0.29	2.92	0.36
DEA30-G10	3.75	10.27	0.47	4.85	0.39
DEA40-G10	4.61	9.61	0.58	6.38	0.42
DEA50-G10	5.76	9.66	0.81	8.59	0.46
		9.94	0.89	9.39	0.49
DEA60-G10	6.86	9.47	1.13	12.25	0.55
		10.16	0.91	9.55	0.42
		10.07	0.81	8.48	0.37
DEA70-G10	8.56	10.26	0.56	5.56	0.20
		9.97	0.56	5.54	0.21
DMPA20-G10	4.15	9.92	0.33	3.46	0.26
DMPA30-G10	3.75	10.31	0.42	4.16	0.34
DMPA40-G10	4.61	9.74	0.60	6.30	0.42
DMPA50-G10	5.76	9.77	0.62	6.68	0.35

[a]DEA60-G10 has 16% standard deviation; DEA50-SBA15, DEA50-G10, and DEA70-G10 have ±10% error. [b]DEA60-G10 has 17% standard deviation; DEA50-SBA15, DEA50-G10, and DEA70-G10 have ±9% error.

In order to probe the effect of N content on CO_2 capture capacity, CO_2 uptakes of silica based amine sorbents were plotted against N wt% (by elemental analysis) (**Figure 4-12**). Here, the sample mass for CO_2 capture experiments was kept at around 10 mg. In **Figure 4-12**, all four

series of sorbents showed a general increase in CO_2 uptake as the N % increased. This result indicates that high N content is very important to a high CO_2 uptake in these sorbents. However, for the DEA-SBA15 series, a decrease in CO_2 uptake was observed when N % passed 7 wt%. A similar trend has also been observed for a series sorbents prepared from impregnation of PEI into silica substrate by Song and coworkers.[13]

Figure 4-13 illustrates the pores in silica substrates with different levels of amine loading.[13] For a silica substrate that contains no amine (A in **Figure 4-13**), the CO_2 adsorption is governed by physisorption. Our control experiments showed that porous silica has a low CO_2 uptake under our testing condition. At low amine loading (B), amines are likely absorbed on the wall of the pores, and the pore size decreases. A higher CO_2 uptake is expected since both physisorption in silica and chemisorption in amine occur in this case. At high amine loading (C), the pores in silica are saturated with amines. Therefore, the pore size is expected to decrease further. In this case, CO_2 adsorption is governed by chemisorption, and the contribution from physisorption becomes insignificant. With extremely high amine loading (D), some amines are absorbed at the external surface of the silica substrate. During adsorption, some of the amines are inaccessible to CO_2 gas and thus result in lower CO_2 uptake.

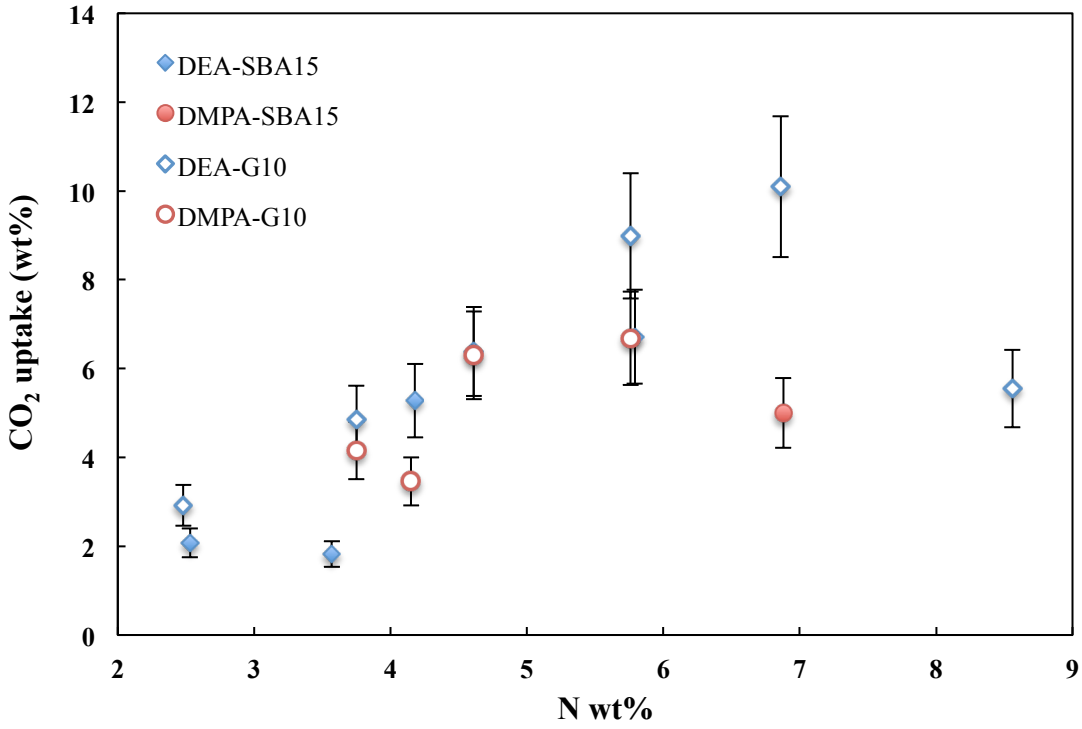

Figure 4-12. CO_2 uptake as a function of N wt%.

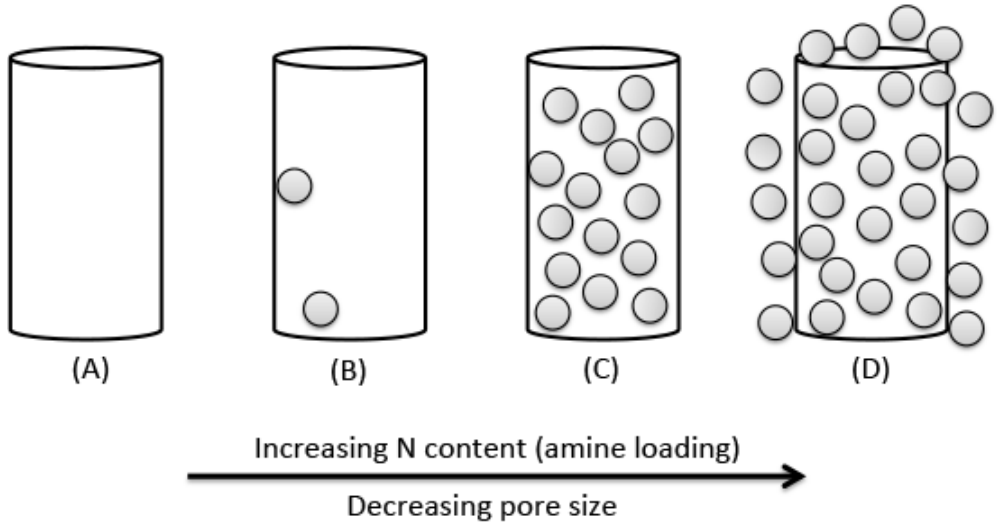

Figure 4-13. Schematic illustration of porous structure in the silica (cylinder) impregnated with various levels of amines (round): (A) silica support, no amine (B) silica support with low amine loading, (C) high amine loading, and (D) extremely high amine loading.[13]

The CO_2 adsorption efficiency of amine (CO_2/N) can be calculated using the following equation:

$$\frac{CO_2\ (mol)}{N\ (mol)} = \frac{CO_2\ uptake\ (mg) \times atomic\ mass\ of\ N\ (\frac{g}{mol})}{Sample\ mass\ (mg) \times \%\ N \times molar\ mass\ of\ CO_2\ (\frac{g}{mol})}$$

The values of CO_2/N of the NETL samples and amine-based silica sorbents were calculated and summarized in **Table 4-11** and **4-13**. CO_2/N values of these samples are in the range of 0.15-0.5 and are compared in **Figure 4-14**. NETL1 and NETL2 show very similar amine efficiency. Generally, efficiencies of the silica sorbents with low amine loading are lower than the NETL samples. As the amine loading gets higher, CO_2/N values increase and some of them exceed the NETL values.

DEA-containing sorbents show higher amine efficiency than their DMPA analogs when comparing DEA-SBA15 with DMPA-SBA15 and DEA-G10 with DMPA-G10. DEA is a 2º amine while DMPA contains 33% 2º amine and 67% 3º amine. The 2º amine is believed to have much higher CO_2 adsorption efficiency compared to the 3º amine.[57] Therefore, DEA showed higher amine efficiency, compared to DMPA.

Also, G10 based sorbents show higher amine efficiency than their SBA15 based analogs when comparing DEA-G10 with DEA-SBA15 and DMPA-G10 with DMPA-SBA15. This is likely due to the much larger pore size of G10 (200-400 μm) compared to SBA-15 (8 μm). The large pores in G10 allow the amines to be accessible to CO_2 during adsorption at high amine loadings, resulting in higher amine efficiency.

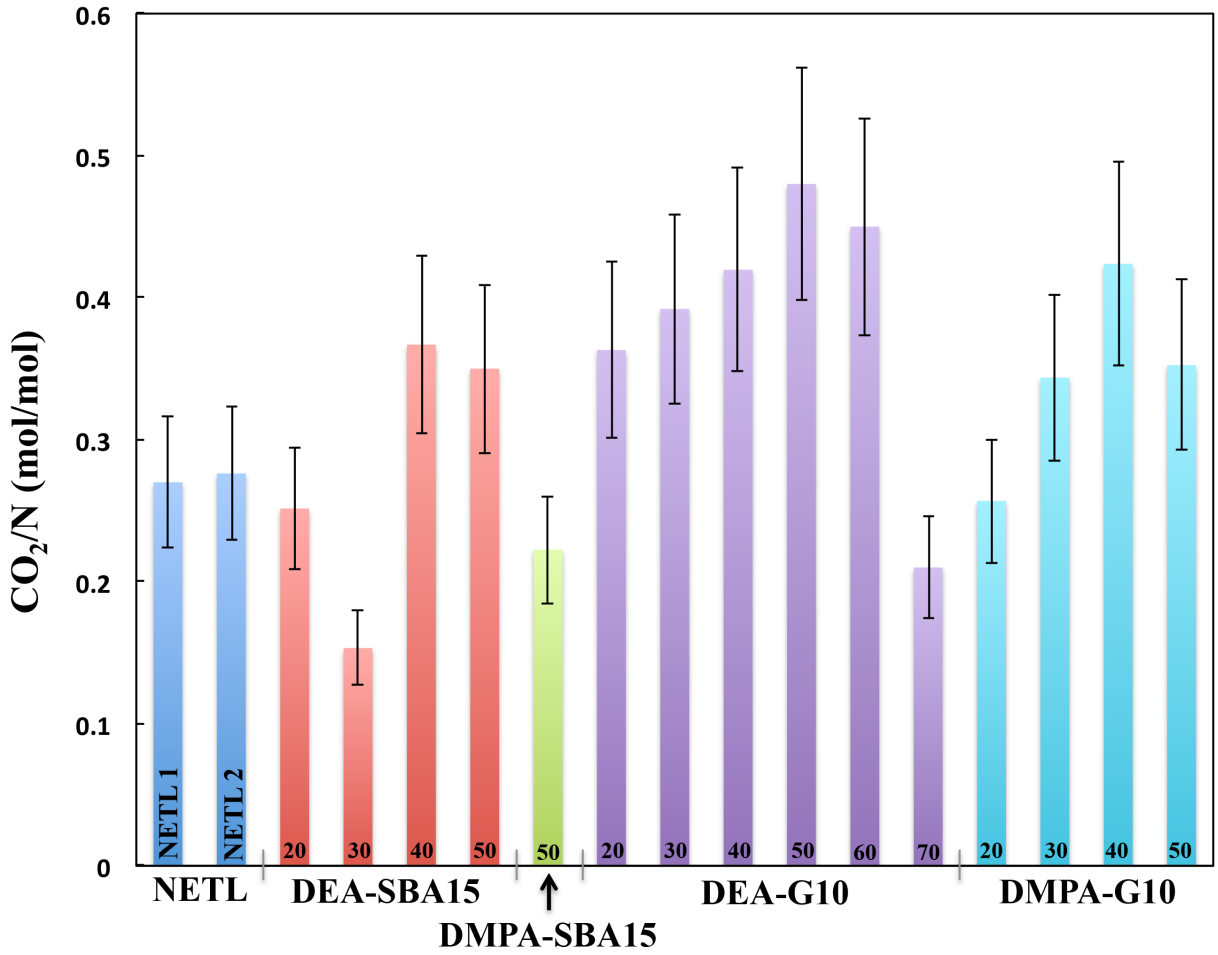

Figure 4-14. Schematic Amine efficiencies (CO_2/N) of NETL samples (blue, NETL1: left; NETL2: right), DEA-SBA15 (red), DMPA-SBA15 (green), DEA-G10 (purple), and DMPA-G10 (aqua). The numbers at the bottom of the column are the amine loading (wt%) in silica support.

4.5. Conclusions

This chapter presents the synthesis of amine-containing styrene/stilbene monomers and amine-containing polymers via polymerization and post-modification. The preparation of amine-containing silica-based sorbents via impregnation is also reported. The CO_2 sorption properties of these materials and control samples were tested using TGA. In control experiments, we found that both high amine content and high surface area are important for a sorbent to achieve high CO_2 uptake. Generally, amine-containing polymers, which have low surface areas, have low CO_2

uptake under our testing condition. Amine-containing silica sorbents show CO_2 uptake up to 12 wt%, some of which are comparable with the NETL samples. We also found that the CO_2 uptakes of these silica sorbents increase and then decrease as the amine loading increases. The reason for the decrease in CO_2 uptake at high amine loading may due to the inaccessibility of amines to the CO_2 gas during adsorption measurement. The amine efficiency is found to be higher in DEA-G10 series because DEA is a 2º amine and G10 has large pore size.

References

(1) *IPCC Special Report on Carbon Dioxide Capture and Storage*, 2005. In http://www.ipcc.ch/pdf/special-reports/srccs/srccs_wholereport.pdf.

(2) Rochelle, G. T. *Science* **2009**, *325*, 1652.

(3) D'alessandro, D. M.; Smit, B.; Long, J. R. *Angew. Chem. Int. Ed.* **2010**, *49*, 6058.

(4) D'alessandro, D. M.; McDonald, T. *Pure Appl. Chem.* **2011**, *83*, 57.

(5) Olajire, A. A. *Energy* **2010**, *35*, 2610.

(6) Samanta, A.; Zhao, A.; Shimizu, G. K. H.; Sarkar, P.; Gupta, R. *Ind. Eng. Chem. Res.* **2012**, *51*, 1438.

(7) Wang, Q. A.; Luo, J. Z.; Zhong, Z. Y.; Borgna, A. *Energ. Environ. Sci.* **2011**, *4*, 42.

(8) Pevida, C.; Plaza, M. G.; Arias, B.; Fermoso, J.; Rubiera, F.; Pis, J. J. *Appl. Surf. Sci.* **2008**, *254*, 7165.

(9) Plaza, M. G.; Pevida, C.; Arenillas, A.; Rubiera, F.; Pis, J. J. *Fuel* **2007**, *86*, 2204.

(10) Su, F. S.; Lu, C. S.; Cnen, W. F.; Bai, H. L.; Hwang, J. F. *Sci. Total Environ.* **2009**, *407*, 3017.

(11) Zhang, J.; Singh, R.; Webley, P. A. *Micropor. Mesopor. Mat.* **2008**, *111*, 478.

(12) Xiao, P.; Zhang, J.; Webley, P.; Li, G.; Singh, R.; Todd, R. *Adsorption* **2008**, *14*, 575.

(13) Xu, X. C.; Song, C. S.; Andresen, J. M.; Miller, B. G.; Scaroni, A. W. *Micropor. Mesopor. Mat.* **2003**, *62*, 29.

(14) Zhao, H. L.; Hu, J.; Wang, J. J.; Zhou, L. H.; Liu, H. L. *Acta Phys. Chim. Sin.* **2007**, *23*, 801.

(15) Britt, D.; Furukawa, H.; Wang, B.; Glover, T. G.; Yaghi, O. M. *Proc. Natl. Acad. Sci. USA* **2009**, *106*, 20637.

(16) Liu, J.; Thallapally, P. K.; McGrail, B. P.; Brown, D. R.; Liu, J. *Chem. Soc. Rev.* **2012**, *41*, 2308.

(17) Sumida, K.; Horike, S.; Kaye, S. S.; Herm, Z. R.; Queen, W. L.; Brown, C. M.; Grandjean, F.; Long, G. J.; Dailly, A.; Long, J. R. *Chem. Sci.* **2010**, *1*, 184.

(18) Jin, L. Y.; Hou, R. B.; Chen, T.; Fang, M. H.; Mah, S.; Yin, B. Z. *Fiber. Polym.* **2007**, *8*, 143.

(19) Tayama, E.; Kimura, H. *Angew. Chem. Int. Ed.* **2007**, *46*, 8869.

(20) Dan, M. H.; Su, Y.; Xiao, X.; Li, S. T.; Zhang, W. Q. *Macromolecules* **2013**, *46*, 3137.

(21) Bell, T. W.; Anugu, S.; Bailey, P.; Catalano, V.; Dey, K.; Drew, M. G. B.; Duffy, N. H.; Jin, Q.; Samala, M. F.; Sodoma, A.; Welch, W. H.; Schols, D.; Vermeire, K. *J. Med. Chem.* **2006**, *49*, 1291.

(22) Bai, F.; Jones, T. D.; Lewandowski, K. M.; Lee, T. K.; Muyres, D. V.; Kelley, T. W.; U.S. Pat. Appl. Publ. 20040222412 A1 20041111.

(23) Soomro, S. A.; Benmouna, R.; Berger, R.; Meier, H. *Eur. J. Org. Chem.* **2005**, 3586.

(24) Kon, G. A. R. *J. Chem. Soc.* **1949**, 224.

(25) Ganushchak, N. I.; Zolotukhina, K. G.; Tashchuk, K. G. *Zh. Obshch. Khim.* **1966**, *2*, 2032.

(26) Li, Y.; Turner, S. R. *Eur. Polym. J.* **2010**, *46*, 821.

(27) Cram, D. J.; Bauer, R. H. *J. Am. Chem. Soc.* **1959**, *81*, 5983.

(28) Horhold, H. H.; Muller, A.; Ozegowski, R. *J. Prakt. Chem.* **1975**, *317*, 877.

(29) Xiao, X. H.; Lin, D. Q.; Tong, S. T.; Luo, H.; He, Y. F.; Mo, H. L. *Synlett* **2011**, 1731.

(30) Newkome, G. R.; Roper, J. M.; Robinson, J. M. *J. Org. Chem.* **1980**, *45*, 4380.

(31) Oh, T. J.; Smets, G. *J. Polym. Sci. Pol. Lett.* **1986**, *24*, 229.

(32) Gelman, M. A.; Weisblum, B.; Lynn, D. M.; Gellman, S. H. *Org. Lett.* **2004**, *6*, 557.

(33) Maciejewska, M.; Szajnecki, L.; Gawdzik, B. *J. Appl. Polym. Sci.* **2012**, *125*, 300.

(34) Gonte, R.; Balasubramanian, K.; Deb, P. C.; Singh, P. *Int. J. Polym. Mater.* **2012**, *61*, 919.

(35) Schmidt-Naake, G.; Becker, H. G.; Klak, M. *Macromol. Symp.* **2001**, *163*, 213.

(36) Lu, J.; Kim, S. G.; Lee, S.; Oh, I. K. *Adv. Funct. Mater.* **2008**, *18*, 1290.

(37) Gray, M. L.; Hoffman, J. S.; Hreha, D. C.; Fauth, D. J.; Hedges, S. W.; Champagne, K. J.; Pennline, H. W. *Energ. Fuel* **2009**, *23*, 4840.

(38) Li, W.; Choi, S.; Drese, J. H.; Hornbostel, M.; Krishnan, G.; Eisenberger, P. M.; Jones, C. W. *ChemSusChem* **2010**, *3*, 899.

(39) Shulkin, A.; Stover, H. D. H. *J. Membrane Sci.* **2002**, *209*, 433.

(40) Mathew, A.; Deb, P. C. *J. Polym. Sci. Pol. Chem.* **1996**, *34*, 1605.

(41) Shulkin, A.; Stover, H. D. H. *J. Membrane Sci.* **2002**, *209*, 421.

(42) Padwa, A. R.; Sasaki, Y.; Wolske, K. A.; Macosko, C. W. *J. Polym. Sci. Pol. Chem.* **1995**, *33*, 2165.

(43) Schmidt, U.; Zschoche, S.; Werner, C. *J. Appl. Polym. Sci.* **2003**, *87*, 1255.

(44) Asua, J. M. *Polymer Reaction Engineering*; Wiley-Blackwell, 2007.

(45) VivaldoLima, E.; Wood, P. E.; Hamielec, A. E.; Penlidis, A. *Ind. Eng. Chem. Res.* **1997**, *36*, 939.

(46) In *http://otech7.tuwien.ac.at/susppoly_sk_e.html*.

(47) Sing, K. S. W.; Everett, D. H.; Haul, R. A. W.; Moscou, L.; Pierotti, R. A.; Rouquerol, J.; Siemieniewska, T. *Pure Appl. Chem.* **1985**, *57*, 603.

(48) Brunauer, S.; Emmett, P. H.; Teller, E. *J. Am. Chem. Soc.* **1938**, *60*.

(49) Chen, K. M.; Wang, T. H.; King, J. S.; Hung, A. *J. Appl. Polym. Sci.* **1993**, *48*, 291.

(50) Saeed, M. B.; Zhan, M. S. *Eur. Polym. J.* **2006**, *42*, 1844.

(51) Pryde, C. A. *J. Polym. Sci. Polym. Chem.* **1993**, *31*, 1045.

(52) Pramoda, K. P.; Liu, S. L.; Chung, T. S. *Macromol. Mater. Eng.* **2002**, *287*, 931.

(53) Abadie, M. J. M. *High Performance Polymers - Polyimides Based - From Chemistry to Applications*; InTech, 2012.

(54) Hu, G. H.; Lindt, J. T. *Polym. Bull.* **1992**, *29*, 357.

(55) Zenkevich, I. G. *J. Anal. Chem.* **2010**, *65*, 267.

(56) Terentev, A. P.; Kost, A. N. *Zh. Org. Khim.* **1947**, *17*, 1632.

(57) Ko, Y. G.; Shin, S. S.; Choi, U. S. *J. Colloid Interf. Sci.* **2011**, *361*, 594.

Chapter 5. Suggested Future Work

5.1. Introduction

Based on the literature review (**Chapter 1**) and findings from this work (**Chapter 2-4**), several research directions are worth further investigating. Large porosity (high surface area) and functionality are two important characteristics of porous materials for gas separation and storage applications. Understanding the structure-porous property relationship is required in order to prepare porous materials with controlled (or large) porosity. Developing new synthetic approaches offers more possibilities for preparation of materials with high surface area and/or new functionality. At the same time, many examples show that functionality enhances the performance of porous materials in gas separation and/or storage. Therefore, incorporating various functional groups with controlled density of functionality into porous materials would make them strong candidates in potential gas storage and separation applications.

This chapter suggests some future work to explore the structure-porous property relationship (**§5.2**), new strategies to porous polymers with high surface area (**§5.3**, **5.4**, and **5.6**), improved synthetic method (**§5.5**), and functionalization of polymers or silica for CO_2 capture (**§5.7**, **5.8**, and **5.9**).

5.2. Incorporation of Bulky Groups into Semi-Rigid Alternating Copolymers

In **Chapter 2**, *tert*-butyl carboxylate-functionalized alternating copolymers were found to have surface areas up to 40 m^2/g. The steric crowding along the polymer backbone in these alternating copolymers leads to inefficient chain packing and results in porosity. Based on the previous finding, we propose to incorporate functionalized monomers with bulky groups into

alternating copolymers in order to interfere with efficient chain packing and thus increase surface area and porosity. **Schemes 5-1** and **5-2** illustrate the preparation of two maleimides, which contain bulky groups. Both maleimides, *N*-(1-naphthyl)maleimide[1] (**Scheme 5-1**) and *N*-(1-adamantyl)maleimide[2,3] (**Scheme 5-2**), can be prepared by the reaction of amines with maleic anhydride followed by imidization with acetic anhydride and sodium acetate based on the methods reported in literature.

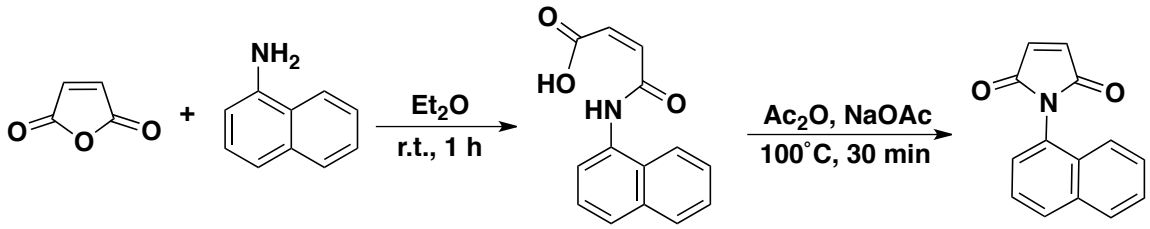

Scheme 5-1. Synthesis of *N*-(1-naphthyl)maleimide.[1]

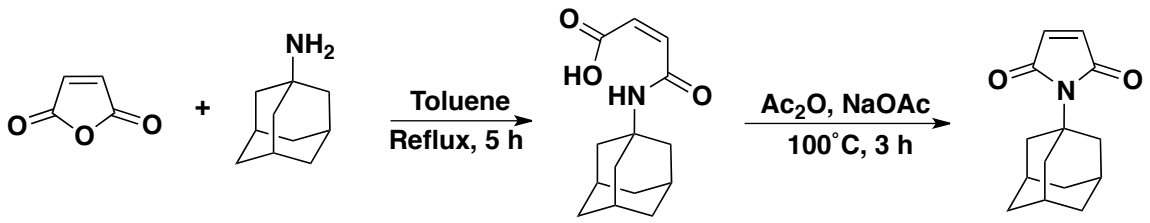

Scheme 5-2. Synthesis of *N*-(1-adamantyl)maleimide.[11,12]

Although copolymerizations of bulky maleimides and styrenes have been reported,[3] copolymerization of stilbene and these bulky maleimides may be difficult due to the steric crowding of the extra phenyl group from stilbene and the bulky group from maleimide. Therefore, electron-donating groups in stilbene maybe are needed in order to facilitate the copolymerization (**Scheme 5-3**).

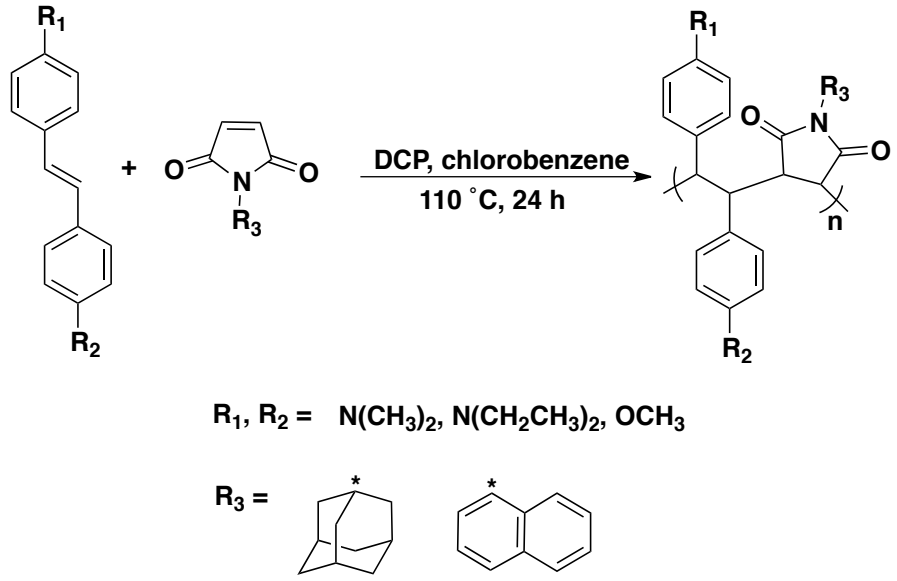

Scheme 5-3. Copolymerization of electron-donating group containing stilbene and bulky maleimide.

5.3. Crosslinking Reaction Using Formaldehyde Dimethyl Acetal

In **Chapter 3**, hypercrosslinked polymers containing T_g enhancing comonomers were prepared by Friedel-Crafts alkylation. Chloromethyl groups from VBC serve as internal crosslinkers in the crosslinking reaction. The incorporation of stiffening units within polymer backbones was found to decrease the surface areas of the resulting hypercrosslinked polymers compared to the controls (polystyrene analogs). The rigid polymer backbones in lightly crosslinked polymer likely inhibit the expansion of polymer networks in the swollen state and/or decrease the crosslinking efficiency during the post-crosslinking reaction, thus affecting the porosity of the resulting hypercrosslinking networks. In order to systematically explore the effect of chain rigidity on crosslinking efficiency while eliminating the effect of chain rigidity on swelling capabilities, hypercrosslinked polymers can be prepared by crosslinking linear polymers.

Tan and coworker reported a "knitting" approach, which involves crosslinking reactions of rigid aromatic monomers using formaldehyde dimethyl acetal (FDA) as an external crosslinker to afford HCPs with high surface areas (see **§1.2.2**).[4-7] We propose to prepare a series of HCPs by crosslinking semi-rigid alternating copolymers using FDA (**Scheme 5-4 b**). The surface areas of these HCPs with varying crosslinking density will be compared with the surface areas of their styrenic analogs (controls) (**Scheme 5-4 a**).

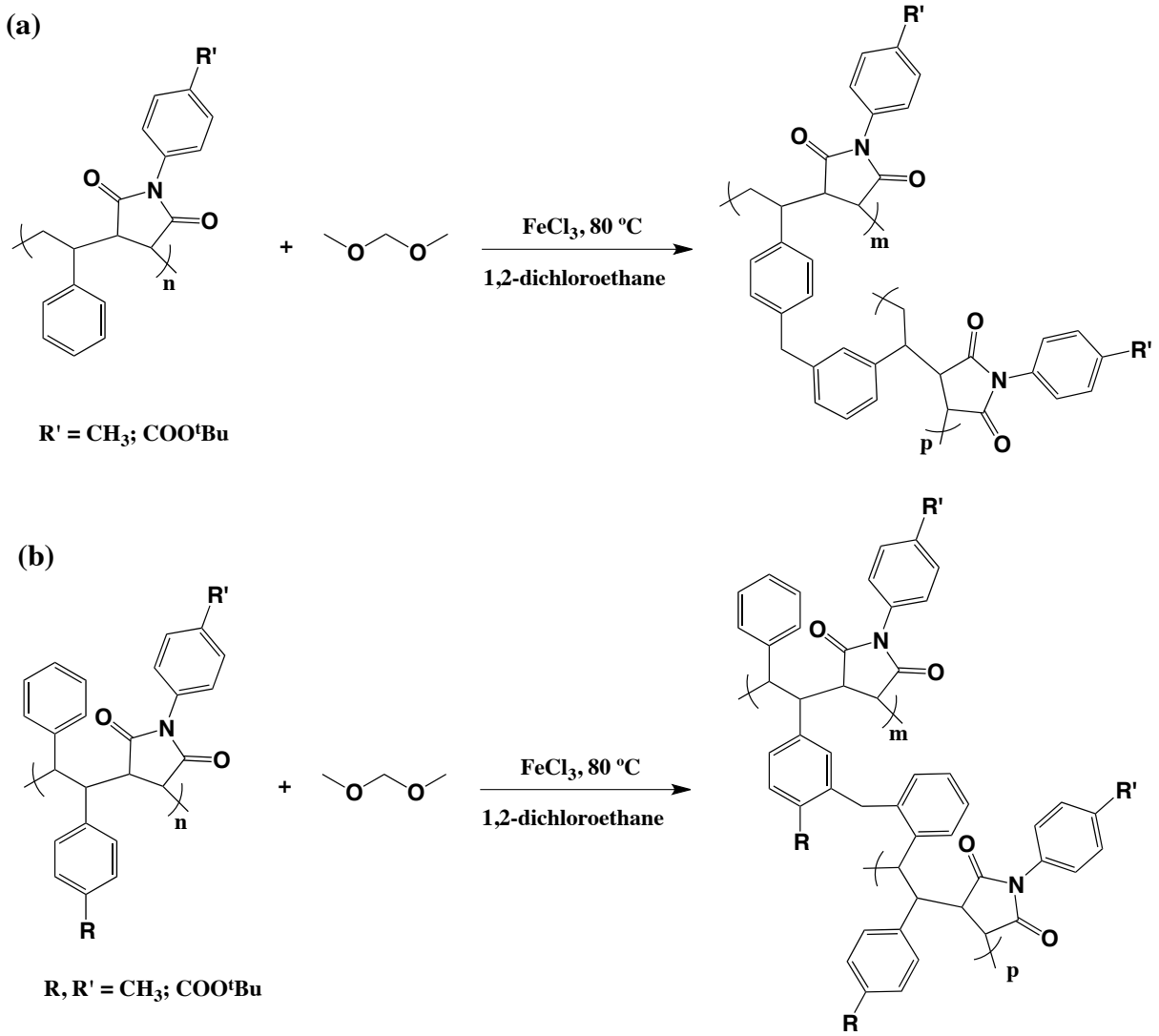

Scheme 5-4. Preparation of HCPs using FDA.

5.4. Crosslinking Reactions of the MAH Moiety via Friedel-Crafts Acylation

The anhydride group from maleic anhydride (MAH) can react with aromatic rings via Friedel-Crafts acylation.[8,9] The proposed work involves a crosslinking reactions of MAH-containing aromatic copolymers (e.g., poly(STR-*co*-MAH)) via Friedel-Crafts acylation (**Scheme 5-5**). The new synthetic method may lead to polymers with high surface areas and high levels of -COOH groups. The materials may find applications as sorption materials where the –COOH might be the sorption site or as porous particles with tunable hydrophobicity/hydrophilicity.

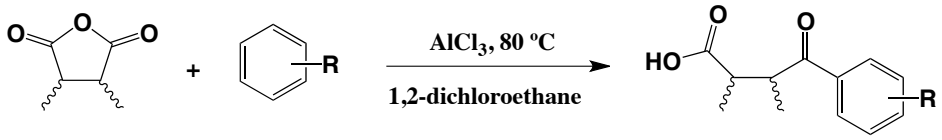

Scheme 5-5. Crosslinking reaction of MAH units via Friedel-Crafts acylation.

5.5. Controlling Particle Size in Suspension Polymerization

In **Chapter 3**, lightly crosslinked precursors were prepared via free radical suspension polymerization. The synthetic parameters including the concentrations of monomer, initiator, stabilizer, and stirring rate were kept constant for all reactions. However, due to the limitations of the apparatus and other factors, we do not have control of the size of these particles, which may have some effects on the porosity/surface area of the final product (hypercrosslinked polymers). Therefore, possible future work includes the study of controlling particle size in suspension polymerization and the effect of particle size on surface area of hypercrosslinked polymers.

In general, particle size of products from suspension polymerization is in the range of 20 μm-2 mm.[10] Particle size can be controlled by various parameters, such as type of stirrer, stirring rate, monomer concentration, stabilizer concentration, etc.[11,12] Empirical relationships between

average particle size and these parameters has been reported[13,14] and can be represented by the following equation:[10]

$$\bar{d} = k\frac{D_v \cdot R \cdot v_d \cdot \varepsilon}{D_s \cdot N \cdot v_m \cdot C_s}$$

where $\bar{d}$ is the average particle size, k is the parameters such as apparatus design, type of stirrer, stabilization, etc., D_v is the diameter of vessel, D_s = diameter of stirrer; R= volume ratio of the droplet phase to suspension medium, N is the stirring speed (or power of mixing), v_d is the viscosity of the droplet phase, v_m is the viscosity of the suspension medium, ε is the interfacial tension between the two immiscible phases, and C_s is the stabilizer concentration. Among these parameters, varying the stirring speed (N) is the most convenient way to control particle size.[10] Therefore, stirring rate will be varied in our system and the particle size of the product will be measured. The techniques to determine particle size distribution include the bulk separation method (sieving), sedimentation, particle size analyzer, photon correlation spectroscopy, electron microscopy, light-scattering particle size analyzer, etc.[15]

5.6. Deprotection of *tert*-Butyl Carboxylate-Functionalized Polymers for Larger Porosity

Previous work in our group showed that the *tert*-butyl carboxylate group could be incorporated into alternating copolymers with controlled density of functionality.[16] The *tert*-butyl carboxylate protecting groups can be de-blocked by reaction with trifloroacetic acid (TFA)[16] or heating at 120 ºC[17] to afford carboxylic acid groups (**Scheme 5-6**).

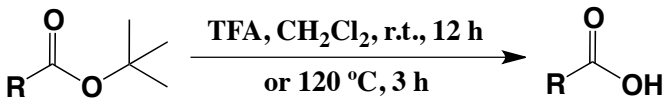

Scheme 5-6. Deprotection of *tert*-butyl carboxylate group functionalized polymers.

Taking advantage of the deprotection reaction, we propose to cleave the *tert*-butyl group in order to generate porosity and achieve high surface areas. Several criteria should be considered in terms of generating porosity. The *tert*-butyl carboxylate-functionalized precursors should have low chain mobility, which can be achieved by a rigid polymer backbone or high crosslinking density, in order to prevent rearrangement of polymer chains after deprotection. Therefore, deprotection by heating in the solid state is preferable compared to deprotection using TFA in solvent.

The heating process to cleave *tert*-butyl groups is similar to calcination in catalyst preparation, which involves thermal treatment of catalyst in air to decompose and volatilize undesired catalyst precursors. During this process, rapid heating of samples should be avoided, because H_2O trapped in the micropores may build up pressure to crack the samples and lead to a decrease in surface area.[18] Therefore, a slow heating rate should be used in deprotection in order to generate larger porosity.

5.7. Modification of MAH-Containing Polymers with Diamines

In **Chapter 4**, MAH containing polymers were modified with 10-20 wt% diamines. In order to achieve high surface area, a higher crosslinking density is required. Therefore, in future, it is interesting to investigate surface area and CO_2 uptake of a series of copolymers prepared by crosslinking copolymers with various amounts of diamines. Both surface area and amine content are expected to increase as amine loading increases. In this study, surface area, CO_2 uptake, and amine content will be obtained using surface area analyzer, TGA, and elemental analysis, respectively. FT-IR will be used to characterize C=O groups before and after modification.

5.8. Polymers Containing Amidine Moieties for CO_2 Capture.

In 2004 and 2008, Endo and coworkers reported the synthesis and CO_2 capture properties of polymers containing amidine moieties (**Scheme 5-7**).[19,20] They found that these polymers could capture CO_2 under atmospheric pressure. In 2010, Gray et al. reported the study of CO_2 capture in tertiary amidine containing activated carbon.[21] It has been reported that the presence of water or alcohol can facilitate CO_2 capture.[22,23] Park and coworker reported a series of hydroxylated amidines that can capture, store, and release CO_2 under dry conditions at low temperature.[23] Based on previous work on amidines, we propose to incorporate hydroxylated amidines into nanoporous polymers including semi-rigid alternating copolymers (**Chapter 2**) and hypercrosslinked polymer networks (**Chapter 3**) to enhance CO_2 capture properties of these polymers.

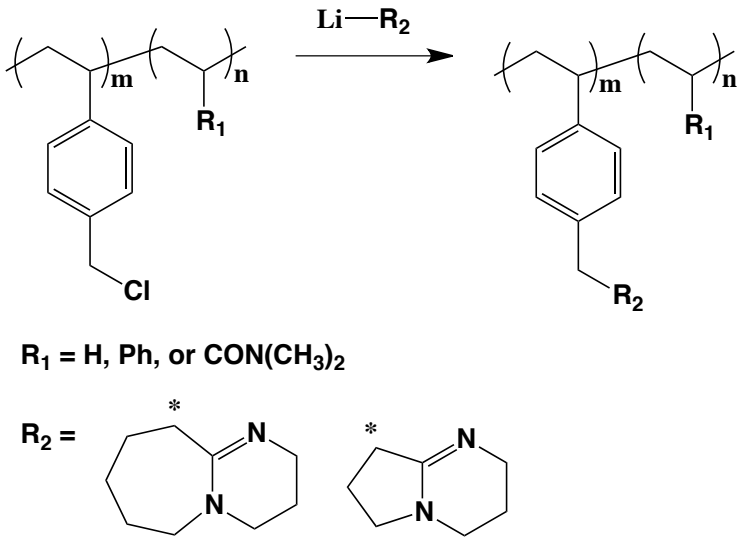

Scheme 5-7. Preparation of copolymers containing amidine groups for CO_2 capture.[20]

Recently, Yavuz and coworker have modified PIM-1 into an amidoxime functionalized polymer with improved CO_2 uptake, surface area, and porosity (**Scheme 5-8**).[24] Taking advantage of the modification method reported by Yavuz et al., the hydroxylated amidine group

can be introduced into –CN containing monomers or polymers prepared previously (**Chapter 4**) in order to enhance CO_2 uptake. Examples of possible monomers are shown in **Figure 5-1**.

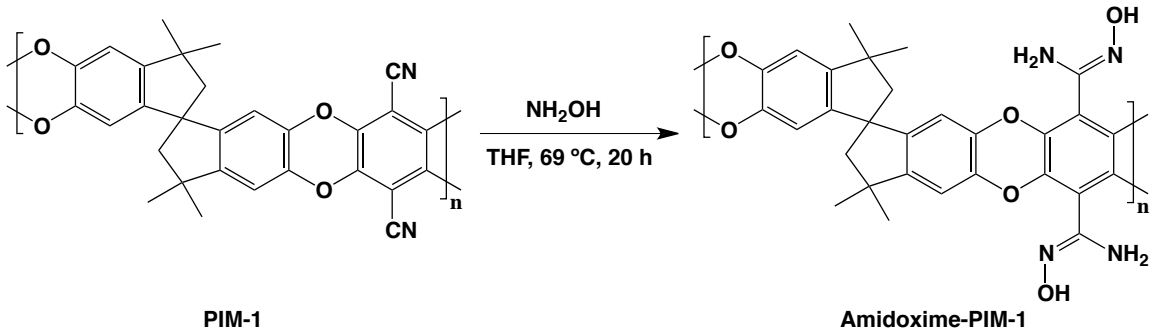

Scheme 5-8. Post-modification of PIM-1 for enhanced CO_2 capture.[24]

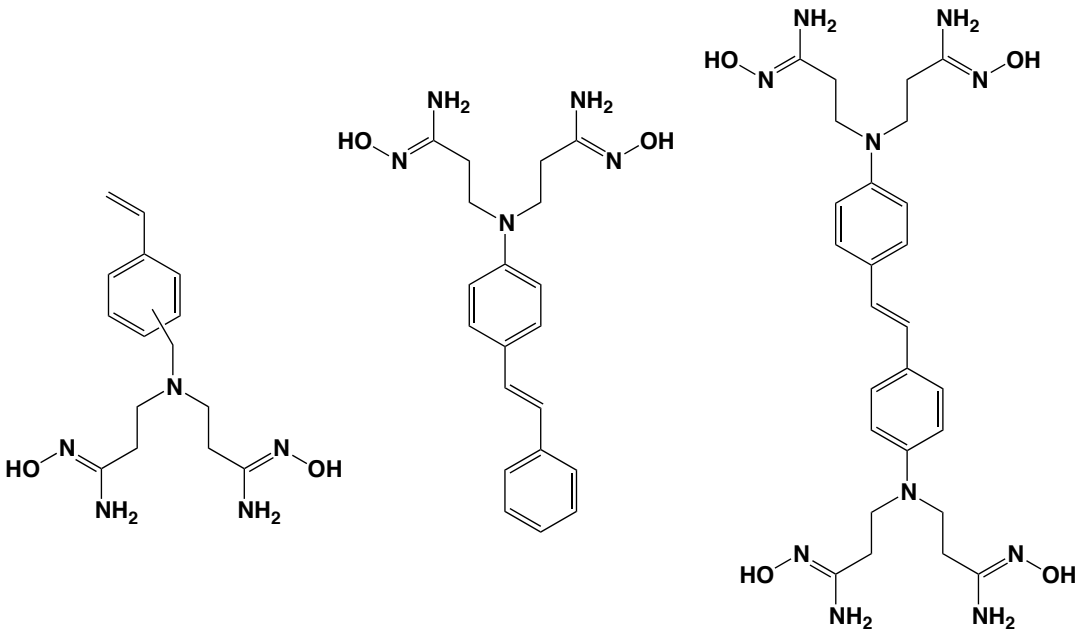

Figure 5-1. Proposed hydroxylated amidine containing monomers.

Styryl amidines (**Figure 5-2**) can be homopolymerized and copolymerized with many comonomers such as styrene or methyl methacrylate.[25] We propose to synthesize amidine-functionalized monomers (**Scheme 5-9**)[26,27] and incorporate these monomers into polymers for CO_2 capture.

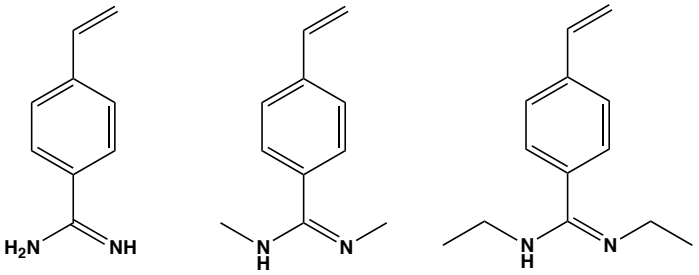

Figure 5-2. Examples of styryl amidines.[25]

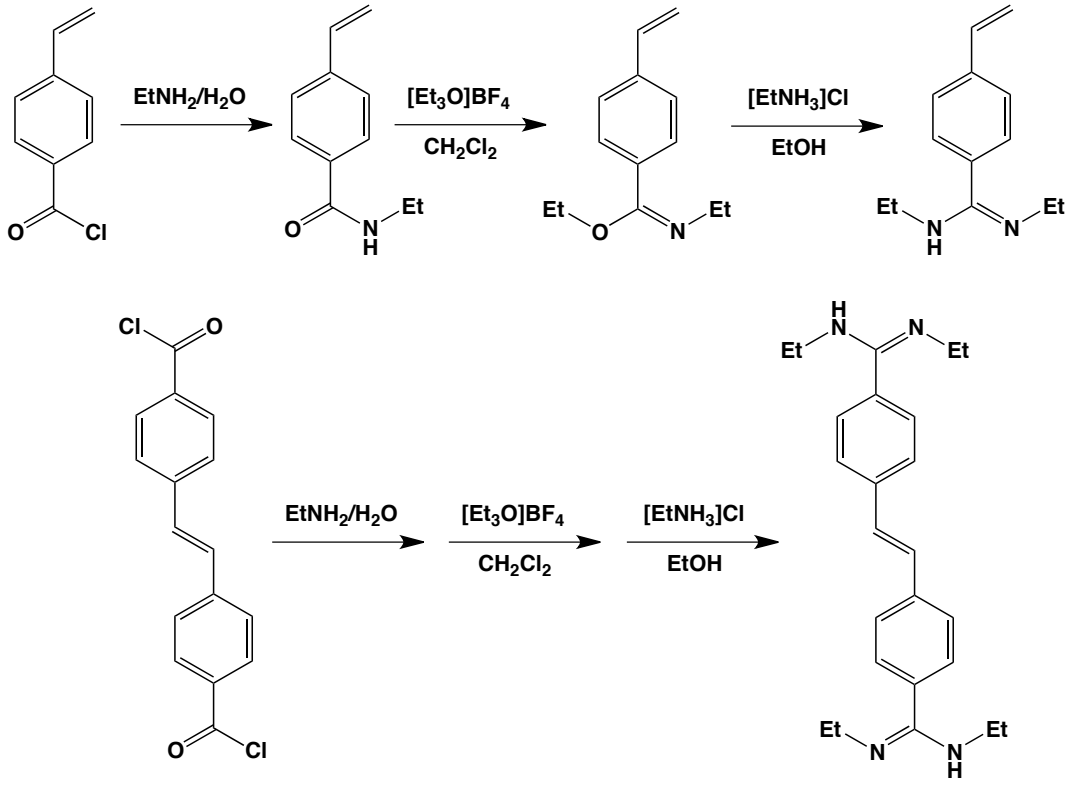

Scheme 5-9. Proposed synthesis of amidine-functionalized monomers.

References

(1) Wang, B. B.; Zhang, X.; Jia, X. R.; Li, Z. C.; Ji, Y.; Yang, L.; Wei, Y. *J. Am. Chem. Soc.* **2004**, *126*, 15180.

(2) Wang, J. E.; Chern, Y. T.; Chung, M. A. *J. Polym. Sci., Part A: Polym. Chem.* **1996**, *34*, 3345.

(3) Chern, Y. T. *Polym. Bull.* **1996**, *36*, 59.

(4) Li, B. Y.; Gong, R. N.; Wang, W.; Huang, X.; Zhang, W.; Li, H. M.; Hu, C. X.; Tan, B. E. *Macromolecules* **2011**, *44*, 2410.

(5) Luo, Y. L.; Li, B. Y.; Wang, W.; Wu, K. B.; Tan, B. *Adv. Mater.* **2012**, *24*, 5703.

(6) Luo, Y. L.; Zhang, S. C.; Ma, Y. X.; Wang, W.; Tan, B. *Polym. Chem.* **2013**, *4*, 1126.

(7) Xu, S.; Luo, Y.; Tan, B. *Macromol. Rapid Commun.* **2013**, *34*, 471.

(8) Xiao, Y.; Malhotra, S. V. *J. Organomet. Chem.* **2005**, *690*, 3609.

(9) Kameo, K.; Ogawa, K.; Takeshita, K.; Nakaike, S.; Tomisawa, K.; Sota, K. *Chem. Pharm. Bull.* **1988**, *36*, 2050.

(10) Arshady, R. *Colloid Polym. Sci.* **1992**, *270*, 717.

(11) Lok, K. P.; Ober, C. K. *Can. J. Chem.* **1985**, *63*, 209.

(12) Kichatov, B. V.; Korshunov, A. M.; Assorova, P. V. *Theor. Found. Chem. Eng.* **2003**, *37*, 306.

(13) Arshady, R.; Ledwith, A. *React. Polym.* **1983**, *1*, 159.

(14) Scully, D. B. *J. Appl. Polym. Sci.* **1976**, *20*, 2299.

(15) VivaldoLima, E.; Wood, P. E.; Hamielec, A. E.; Penlidis, A. *Ind. Eng. Chem. Res.* **1997**, *36*, 939.

(16) Li, Y.; Mao, M.; Matolyak, L. E.; Turner, S. R. *ACS Macro Lett.* **2012**, *1*, 257.

(17) Park, D. H.; Park, J. H. *B. Korean Chem. Soc.* **2009**, *30*, 230.

(18) Bartholomew, C. H.; Farrauto, R. J. *Fundamentals of Industrial Catalytic Process*; 2nd ed.; Wiley: Hoboken, 2006.

(19) Endo, T.; Nagai, D.; Monma, T.; Yamaguchi, H.; Ochiai, B. *Macromolecules* **2004**, *37*, 2007.

(20) Ochiai, B.; Yokota, K.; Fujii, A.; Nagai, D.; Endo, T. *Macromolecules* **2008**, *41*, 1229.

(21) Alesi, W. R.; Gray, M.; Kitchin, J. R. *ChemSusChem* **2010**, *3*, 948.

(22) Heldebrant, D. J.; Yonker, C. R.; Jessop, P. G.; Phan, L. *Energ. Environ. Sci.* **2008**, *1*, 487.

(23) Kim, M.; Park, J. W. *Chem. Commun.* **2010**, *46*, 2507.

(24) Patel, H. A.; Yavuz, C. T. *Chem. Commun.* **2012**, *48*, 9989.

(25) Wulff, G.; Schonfeld, R. *Adv. Mater.* **1998**, *10*, 957.

(26) Peters, L.; Frohlich, R.; Boyd, A. S. F.; Kraft, A. *J. Org. Chem.* **2001**, *66*, 3291.

(27) Kraft, A.; Peters, L.; Powell, H. R. *Tetrahedron* **2002**, *58*, 3499.